

Double-curved precast concrete elements

Research into technical viability of the flexible mould method

H.R. Schipper

September 2015

Double-curved precast concrete elements

Research into technical viability of the flexible mould method

Proefschrift

Ter verkrijging van de graad van doctor
aan de Technische Universiteit Delft,
op gezag van de Rector Magnificus prof. ir. K.C.A.M. Luyben,
voorzitter van het College van Promoties

in het openbaar te verdedigen
op
14 september 2015 om 12:30 uur

door

Hugo Raoul SCHIPPER

Civil ingenieur
geboren te Oud-Beijerland

Dit proefschrift is goedgekeurd door de promotoren:

Prof. dipl.-ing. J.N.J.A. Vamberský

Prof. dr. ir. K. van Breugel

Samenstelling promotiecommissie:

Rector Magnificus

voorzitter

Prof. dipl.-ing. J.N.J.A. Vamberský

Technische Universiteit Delft, promotor

Prof. dr. ir. K. van Breugel

Technische Universiteit Delft, promotor

Onafhankelijke leden:

Prof. ing. M. Menegotto

Sapienza University of Rome, Italy

Prof. dr. ing. O.H. Wallevik

Reykjavik University, Iceland

Prof. dr. ir. T.A.M. Salet

Technische Universiteit Eindhoven

Prof. dr. ing. U. Knaack

Technische Universiteit Delft

Dipl. ing. A. Piber, Msc

UNStudio, Amsterdam

Prof. ir. R. Nijssse

Technische Universiteit Delft (reservelid)

ISBN 978-94-6299-154-5

Printed by Ridderprint, The Netherlands

Cover design by Robert Schipper

L^AT_EX was used to write and typeset this book.

© H.R. Schipper. All rights reserved. No part of this publication may be reproduced or utilized in any form or by any means, electronic or mechanical, including photocopying, recording, or by any information storage and retrieval system, without the prior consent of the author.

SUMMARY

The production of precast, concrete elements with complex, double-curved geometry is expensive due to the high cost of the necessary moulds and the limited possibilities for mould reuse. Currently, CNC-milled foam moulds are the solution applied mostly in projects, offering good aesthetic performance, but also resulting in waste of material, relatively low production speed and fairly high costs per element. The flexible mould method aims to offer an economic alternative for this state of art technology by allowing repeated reuse of the same mould, and if necessary, reuse in adapted shape.

A patent and literature review and comparison of state-of-art formwork methods reveals that, although the idea of a flexible formwork already dates from the mid-20th century, in building industry it has not yet found widespread application, and is still experimental to a large extent. In other industries, such as aerospace and automotive, flexible moulds are occasionally used for rapid prototyping purposes, mostly for the forming of thin metal sheets. The understanding of the flexible mould principle in terms of mechanics is still in development. In combination with concrete, the flexible mould has been industrially applied only on occasion. Deliberately imposed deformation of concrete after casting allows the use of only one single-sided flexible mould, but - being a method quite alien to normal precast concrete production - has hardly been investigated. Therefore, models are needed both for the flexible layer as well as its use in combination with concrete.

By analysing a number of architectural cases in terms of geometrical aspects, more information is gathered about building size, element thickness, curvature radius and number and type of elements. This information is used to define the type of shapes for which the flexible mould method would be suitable. Through the last 80 years, the shape of curved architecture has changed; whereas the early famous shell designers such as Isler and Torroja aimed for structurally optimized and material-efficient shapes, nowadays these shapes have mostly made place for free-form curves, in which parametric design or sculptural influences are leading. For larger projects, several hundreds to even thousands of uniquely curved elements are manufactured, varying in curvature radius in a range between 0.75 m and 45 m. Furthermore the contours and edge position can vary from element to element. Prediction of each element's edge position is non-trivial for the flexible mould method, especially not for elements with strong curvature.

The deformation process can be described mathematically by analysing the curvature parameters. An important and meaningful parameter is the Gaussian curvature. Depending on the change in Gaussian curvature, the imposed deformation of the mould surface and the concrete results in certain amounts of bending action (B) and in-plane surface stretching (S). Bending tensile strains in the still plastic concrete can be in the range of 25 to 50 % for an element with 50 mm thickness, which is far more than the values normally encountered in concrete after casting. The application of in-plane shear deformation appears to be helpful to deform the mould from flat to double-curved. The exact positioning of the element edges can

be determined from this in-plane shear deformation. The shape of the mould, in the present research, is controlled by a grid of actuators - extendible support points that follow the intended architectural shape. As mould surface, a thin rubber layer can be used, that, however, has to be supported by a material that is capable of carrying the weight of the concrete without visible deflection between the actuators. Various solutions are investigated for this support material, of which the strip mould offers the most accurate results and predictability.

As said, the concrete in this method is deliberately deformed after casting in an open, single-sided mould. This requires control over both the fluidity and strain capacity of the fresh concrete: if the concrete is too fluid, it will flow out of the mould after deformation due to the slope of the mould, if it is already too stiff, cracks may occur. Various experiments are conducted to investigate the viability of the principle as well as the parameters that influence the risk of either flow or cracking. It appears that the use of a self-compacting concrete with thixotropic properties reduces both the risks: as a result of quick stabilisation after casting, the yield strength build-up will prevent flow once the mould is deformed and put at a certain slope. Thanks to its plastic strain capacity, this type of concrete will be able to undergo the imposed deformation without cracking. An important measure to prevent this cracking is the curing of the concrete directly after casting and a deformation that takes place before initial setting time. Thin steel rebar, glass-fibre textiles or mixed fibres are all applicable as reinforcement, the latter two giving the best results.

For the measurement of yield strength development of the concrete mixture before and after casting, various methods are investigated. Literature research and experiments demonstrate that, once the rheological behaviour of a mixture has been determined with a viscometer accompanied with slump (flow) tests, the correct moment of deformation of the flexible mould can later be determined from repeated slump (flow) tests with sufficient reliability. However, as soon as the mixture constituents will be adapted, new viscometer measurements have to be carried out again.

The flexible mould method has been successfully tested on single- and double-curved precast concrete elements with a radius down to 1.50 m and an element thickness up to 50 mm. Until this moment, the maximum element size tested was approximately $2 \times 1 \text{ m}^2$, but larger elements are expected to be feasible. An integrated design-to-production process is required: due to the complex geometry and the impact of this geometry on all aspects of the manufacturing, all parties involved should cooperate to make the use of this method possible. Computational skills are needed to determine design parameters and control the manufacturing process.

Several new questions were identified during the research, but at this moment, implementation of the flexible mould method in an industrial environment in cooperation with a concrete product manufacturer is the best way to determine the priorities for further research. From the full research it is concluded that the flexible mould method is viable for the production of double-curved concrete elements.

SAMENVATTING

De productie van prefab-betonnen elementen met complexe, dubbelgekromde geometrie is duur vanwege de hoge kosten van de benodigde mallen en beperkte mogelijkheden deze mallen te hergebruiken. Momenteel vormen CNC-gefreesde mallen de oplossing die in tal van projecten wordt toegepast, met goede esthetische resultaten, maar ook resulterend in verspilling van materiaal, relatief lage productiesnelheid en vrij hoge kosten per element. De flexibele mal-methode is erop gericht een economisch alternatief te bieden doordat hergebruik van dezelfde mal mogelijk wordt gemaakt, waarvan de vorm telkens kan worden aangepast.

Uit octrooi- en literatuuronderzoek en vergelijking van bekistingsmethoden blijkt dat, hoewel het concept van de flexibele mal al dateert van midden-twintigste eeuw, in de bouw nog altijd geen wijdverbreide toepassing ervan voorkomt; de techniek is nog experimenteel. In andere sectoren, zoals ruimtevaart en auto-industrie, worden flexibele mallen al wel af en toe gebruikt voor *rapid prototyping*, vooral voor het vormen van dunne metalen platen. Het begrip van de flexibele mal qua mechanica is nog in ontwikkeling. Het opzettelijk opleggen van vervorming aan betonelementen *na* het storten is weliswaar gunstig omdat ze het gebruik van een enkelzijdige mal mogelijk maakt, toch is dit principe - als methode ongebruikelijk voor normale prefab productie - nog nauwelijks onderzocht. Daarom zijn modellen nodig voor zowel de flexibele mal als het gebruik ervan in combinatie met beton.

Door het analyseren van een aantal architectonische *cases* met het oog op hun geometrische aspecten, is meer informatie verkregen over gebouwafmetingen, elementdikte, kromtestraal en het aantal en het type van de elementen. Deze informatie is gebruikt om het type vormen te definiëren waarvoor de flexibele mal geschikt moet zijn. De laatste 80 jaar is het gebruik van gekromde vormen in architectuur veranderd. Terwijl beroemde schaaldak-ontwerpers als Isler of Torroja vaak streefden naar constructief geoptimaliseerde en materiaal-efficiënte vormen, zijn het nu de *free-form* gebouwen waarin parametrisch ontwerpen of sculpturale overwegingen leidend zijn. Voor grotere projecten worden soms tot zelfs duizenden unieke gekromde elementen vervaardigd, variërend in kromtestraal van circa 0,75 tot 45 m. De contouren en de randpositie variëren van element tot element. Positionering van de rand is niet triviaal, zeker niet voor elementen met sterke kromming.

Het vervormingsproces kan wiskundig worden beschreven door analyse van de krommingsparameters. Een belangrijke parameter hierbij is de zogenaamde Gaussiaanse kromming. Afhankelijk van de verandering van deze parameter zal tijdens de opgelegde vervorming van het maloppervlak en van het beton een bepaalde hoeveelheid buiging optreden loodrecht op het malvlak (B) en rek in het malvlak (S). De benodigde buigrek in de nog plastische beton kan hierbij oplopen tot een ordegrootte van 25 tot 50 ‰ voor een element van 50 mm dikte, wat veel hoger is dan de waarden zoals die gewoonlijk in beton optreden. De toepassing van schuifvervorming in het vlak blijkt een behulpzame vrijheidsgraad om de mal van vlak tot dubbelgekromd te vervormen. De exacte positionering van de elementranden kan bovendien worden afgeleid uit deze afschuifvervorming. De vorm van de mal wordt in dit onderzoek

gestuurd door een raster van actuatoren - uitschuifbare steunpunten die de beoogde architectonische vorm volgen. Als maloppervlak kan een dunne rubberlaag worden gebruikt, die echter dient te worden ondersteund door een materiaal dat in staat is het gewicht van het beton op te nemen zonder zichtbare vervorming tussen de actuatoren. Verschillende oplossingen zijn onderzocht voor dit dragermateriaal, waarvan de strippen-mal de meest nauwkeurige resultaten biedt.

Zoals gezegd, wordt het beton bewust vervormd na het storten in een open, enkelzijdige mal. Dit vereist controle over zowel de vloeibaarheid als de rekcapaciteit van het verse beton: indien het beton te vloeibaar is, zal het, als gevolg van de hellingshoek, uit de mal lopen na vervorming; als het al te stijf is kunnen scheurtjes ontstaan. Verschillende experimenten zijn uitgevoerd om zowel de haalbaarheid van het principe als de parameters die het proces beïnvloeden te onderzoeken. Het blijkt dat het gebruik van een zelfverdichtende beton met thixotrope eigenschappen beide risico's beperkt: als gevolg van snelle stabilisatie na het storten wordt voorkomen dat beton wegstroomt uit de mal wanneer deze wordt vervormd en onder een bepaalde helling wordt gebracht. Vanwege de dan nog wel aanwezige plastische rekbaarheid zal dit type beton de opgelegde vervorming goed kunnen ondergaan zonder te scheuren. Een belangrijke maatregel om scheurvorming te voorkomen is het afdekken van het beton direct na het storten en het vervormen voordat chemische binding intreedt. Dunne stalen wapening, glasvezeltextiel of meegemengde korte vezels zijn alle drie mogelijk als wapening; de laatste twee geven de beste resultaten.

Voor het meten van de vloeibaarheid van het betonmengsel en de ontwikkeling hiervan in de tijd na het storten zijn verschillende methoden onderzocht. Zowel literatuuronderzoek als experimenten tonen aan dat, wanneer het rheologische gedrag van een mengsel eenmaal is vastgesteld met een viscometer in combinatie met zetmaat- of vloeimaatproeven, in de productielijn genoemde proeven voldoende betrouwbaarheid bieden om het juiste moment van vervormen van de flexibele mal te kiezen. Zodra echter de samenstelling van het mengsel wordt aangepast zullen opnieuw viscometer-metingen moeten worden uitgevoerd.

De flexibele mal methode is succesvol getest op enkel- en dubbelgekromde geprefabriceerde betonnen elementen met een straal vanaf 1,50 m of groter en met een dikte tot 50 mm. Op dit moment is de maximale geteste elementgrootte ongeveer $2 \times 1 \text{ m}^2$, maar naar verwachting is productie van grotere elementen haalbaar.

Een geïntegreerd ontwerp- en productieproces is een vereiste: vanwege de complexe geometrie en de invloed hiervan op alle aspecten van de productie, moeten alle partijen intensief samenwerken om de toepassing van deze methode mogelijk te maken. Computervaardigheden zijn nodig om de ontwerpparameters bepalen en het productieproces te controleren.

Hoewel verschillende nieuwe vragen zijn gerezen tijdens het onderzoek, is op dit moment de toepassing van de flexibele mal methode in een industriële omgeving in samenwerking met een betonproducten-fabrikant de beste manier om prioriteiten voor verder onderzoek vast te stellen. Uit het volledige onderzoek wordt geconcludeerd dat de flexibele mal methode een haalbare techniek is voor de productie van dubbelgekromde betonelementen.

Contents

I	Introduction to the research	1
1	Introduction	3
1.1	Realization of architecture using curved shapes	3
1.2	Advanced formwork technology	5
1.3	The flexible mould	6
1.4	Objective and scope of the study	7
1.5	Outline	8
2	Present formwork technology and its limitations	11
2.1	Introduction	11
2.2	Available techniques for free-form concrete surfaces	12
2.2.1	Timber falsework and formwork	12
2.2.2	Steel formwork	12
2.2.3	CNC-milling	13
2.2.4	Hotwire-cutting	14
2.2.5	Fabric formwork with air pressure	14
2.2.6	Fabric formwork with concrete pressure	16
2.2.7	3D-printing of concrete	17
2.2.8	Spraying concrete	18
2.2.9	Concrete cloth	19
2.2.10	Discussion of available formwork methods	20
2.3	General need for a flexible mould principle	20
2.4	Early example: free-form plastic by Renzo Piano	22
3	Patent review of flexible formworks	25
3.1	Introduction	25
3.2	Search method	25
3.3	Classification	27
3.4	Single-curved moulds formed by bending	29
3.5	Wax milling and inflatables	30
3.6	Draping and deforming after casting	31
3.7	Pin-beds	33
3.8	Patented product types	37

3.9	Patent study by Munro and Walczyk (2007)	38
3.10	Discussion of patent review	39
4	Literature review of flexible formworks	41
4.1	Introduction	41
4.2	Forming of thin sheets of material	41
4.3	Various master's thesis projects at TU Delft (2000-2011)	45
4.4	Tests of Huyghe and Schoofs	48
4.5	Other research worldwide	50
4.6	Discussion of literature review	53
4.7	Conclusions of part I	55
II	Double-curved elements for architectural applications	57
5	Architectural examples and cases	59
5.1	Introduction	59
5.2	Architectural designs using curvature	59
5.3	Overview of cases	63
5.3.1	Case 1 - Spencer Dock Bridge, Dublin, Northern Ireland	63
5.3.2	Case 2 - EPFL Rolex Learning Centre, Lausanne	65
5.3.3	Case 3 - Precast concrete shell, Mysore, India	67
5.3.4	Case 4 - Heydar Aliyev Cultural Centre, Baku	69
5.3.5	Case 5 - Metro stations for new Crossrail-line London	71
5.4	Discussion	72
6	CAD, CAM and complex geometry	75
6.1	Introduction	75
6.2	Principles	75
6.2.1	Shape description	75
6.2.2	Splines	76
6.2.3	NURBS-curves, point control and NURBS-surfaces	77
6.2.4	Curvature of surfaces	78
6.3	Recent developments in software algorithms	79
6.3.1	Surface subdivision or panelling	79
6.3.2	Mould depots and rationalisation	80
6.4	Towards a full mass-customized production	82
6.4.1	Large scale free-form asks for mass-customisation	82
6.4.2	Sketch of the proposed method	83
6.5	Geometrical issues in this method	85
6.5.1	Introduction	85
6.5.2	Developable or non-developable surfaces	85
6.5.3	Imposed strain distribution	87
6.5.4	Effects in z-direction	93
6.5.5	Total strain - order of magnitude estimation	94

6.5.6	Geometrical aspects of edge positioning	94
6.6	Discussion	95

III Mechanical engineering of the machine **97**

7	Modelling the mould behaviour	99
7.1	General approach	99
7.1.1	Introduction	99
7.1.2	Elasticity of the flexible formwork	99
7.1.3	Stepwise approach	101
7.2	Strip mould, single-curved	101
7.2.1	Approximation with beam theory	101
7.2.2	Large displacements neglected	103
7.2.3	Smallest possible bending radius	103
7.2.4	Maple model for single-curved mould with n support points	104
7.2.5	Influence of mould stiffness and actuator spacing	106
7.2.6	Influence of curvature	107
7.2.7	Complexity of shape versus number of actuators	108
7.2.8	Reaction forces	109
7.2.9	Horizontal displacements	110
7.2.10	Experimental set-up	110
7.2.11	Discussion of the strip model	110
7.3	Plate mould, double-curved	111
7.3.1	Introduction	111
7.3.2	Mechanical model	111
7.3.3	Local buckling	113
7.3.4	Discussion of plate model	114
7.4	Crossing-strips mould, double-curved	114
7.4.1	Introduction	114
7.4.2	Mechanical model	114
7.4.3	Limitations of the strip mould	115
7.4.4	Kine-Mould: an improved crossing-strips mould	116
7.5	Work-flow	116
7.6	Discussion	118

IV Concrete Technology **119**

8	First flexible mould viability tests	123
8.1	Introduction	123
8.1.1	Description of the flexible mould process	123
8.1.2	Imposed deformation in relation to phase transition	124
8.2	Theory	125
8.2.1	Modelling the fluid phase: Bingham model	125

8.2.2	Strength development in the first hour	127
8.2.3	Concrete under slope	130
8.2.4	Relation between slump and shear yield strength	131
8.2.5	Bending of reinforcement	133
8.2.6	Discussion	135
8.3	Suppositions	135
8.4	Operationalisation	136
8.4.1	Mini-deformation and mini-slump tests	136
8.4.2	Concrete mixtures	137
8.4.3	Single-curved deformation tests	137
8.4.4	Double-curved deformation tests	139
8.5	Observations	141
8.5.1	Mini-deformation and mini-slump tests	141
8.5.2	Single-curved deformation tests	144
8.5.3	Double-curved deformation tests	146
8.5.4	Geometry research	156
8.5.5	Position of reinforcement after deformation	157
8.6	Data analysis	159
8.6.1	Mini-slump tests	159
8.6.2	Mini-deformation tests	160
8.6.3	Deformation tests	160
8.7	Empirical generalisations and testing of suppositions	161
8.8	Theory development	162
8.9	Concluding remarks	164
9	Parameter variation study	167
9.1	Introduction	167
9.2	Rheology	168
9.2.1	Comparison between Newtonian fluids, solids and fresh concrete	168
9.2.2	Differences between solids and fluids according to Bingham	168
9.2.3	Measuring rheological parameters	171
9.2.4	Determination of yield strength with slump (flow) tests	172
9.2.5	Direct measuring with a viscometer	177
9.3	Yield criterions from theory of plasticity	177
9.3.1	Introduction	177
9.3.2	Strain capacity $\epsilon_{allowable}$	177
9.4	Reinforcement	181
9.5	Discussion of section 9.1 to 9.4	182
9.6	Suppositions	183
9.7	Operationalisation	184
9.7.1	Research variables	184
9.7.2	Test set-up for unreinforced elements	194
9.8	Observations	194

9.8.1	Measuring rheological properties with BML viscometer	194
9.8.2	Deformation tests - plain concrete - summarized report	197
9.8.3	Deformation tests - plain concrete - detailed report	197
9.9	Additional tests: textile reinforcement	216
9.10	Additional tests: microscopy	217
9.11	Data analysis	220
9.11.1	Introduction	220
9.11.2	Development of yield stress to find t_1	220
9.11.3	Development of strain capacity - finding t_2	223
9.11.4	Effect of concrete mixture on t_1 and t_2	227
9.12	Empirical generalisations and suppositions testing	228
9.13	Theory development	230
9.14	Concluding remarks	231
V	Final remarks	235
10	Conclusions and Recommendations	237
10.1	Introduction	237
10.2	Conclusions	238
10.3	Practical recommendations	240
10.4	Recommendations for further research	242
	Bibliography	244
A	Patents related to the flexible mould	265
B	Maple model for single strip	271
C	Geometry double-curved elements viability research	277
D	Research variables parameter variation study	287
E	General procedure casting, deformation and hardening	289
F	Casting and deformation tests	295
G	Set-up of BML Viscometer	333
H	Brief review of theory of elasticity and plasticity	337

Part I

Introduction to the research

Chapter 1

Introduction

1.1 Realization of architecture using curved shapes

Curvature offers a beautiful shape language for architecture, a language that would not exist if only straight lines and rectangular, flat surfaces made up the architect's vocabulary. The use of curvature results in expressive designs, as illustrated, for example, by the building of Zaha Hadid Architects shown in Figure 1.1 on the following page. Even though the use of curvature is not a new phenomenon, in contemporary architecture it is still mainly restricted to high profile projects or iconic architecture, often with above-average budgets. This limited use is caused by the higher costs of curved buildings due to both the extra effort needed for handling complex geometry during the design stage and the need for unconventional construction methods on the building site or in the factory. The famous builder-architect-engineer Heinz Isler already stated two decades ago (Isler, 1994):

"There is a general trend today in the design of buildings to break out of the boring uniformity of cubic architecture. Many new buildings are decorated with some form of curved elements, imposed for aesthetic reasons to interrupt the monotony of the box-like structural forms. Shell forms can provide a remedy for design monotony, offering a real alternative".

The cultural appreciation for free-form architecture is still growing: submissions for international design contests and conferences show an increasing use of and interest in complex geometry. Curved shapes inspire project developers and clients with taste for aesthetics and beauty. Today, in many large cities worldwide, iconic projects have been realized that illustrate this appreciation. Although complex geometry has been an issue of continuous interest since decades, the new generation of architects that have completed their study have now learned to use 3D-software such as Catia, Maya, Rhinoceros 3D and others, that allow these complex shapes to be dealt with in a powerful manner already from the design stage. Computational methods now enable the detailed analysis and optimisation of the flow of forces through complex



Figure 1.1: Example of the use of curvature in architecture: Heydar Aliyev Cultural Centre in Baku, Azerbaijan, Zaha Hadid Architects, 2012 (www.skyscrapercity.com)

designs, which was not possible before. The structural efficiency of curved shapes can already be evaluated in the early design stage. Driven by these developments in design possibilities and by the wishes of clients, more experience is gained in realizing curved shapes in buildings.

This thesis will cover a specific part of this new and emerging field of expertise: the manufacturing of *double-curved elements in precast concrete*. Being the most widely used building material, concrete seems to form a perfect match with free-form architecture: the structural strength and aesthetic quality allow freedom of form, and during its liquid stage, concrete can fill almost any shape of formwork.

It is this same formwork however, that, to a large extent, determines the total costs of concrete buildings: percentages between 35 and 60% are found in literature, expressing formwork costs as part of total construction costs. Casting concrete in-situ basically requires the free-form building to be manufactured *twice*: once as a formwork, and once in concrete. Although this is common practice for all buildings in concrete, a formwork with complex shape is expensive and often hardly reusable, as opposed to the formwork for orthogonal buildings. Precasting techniques reduce these costs only for a part, as complex geometry often leads to very limited repetition possibilities of similar concrete formwork-shapes. This thesis therefore addresses the question of how to optimize the use of precast concrete in free-form architecture.

1.2 Advanced formwork technology

For one-off buildings in which the shape shows little or no repetitive parts, the formwork can be used only once. Free-form shapes, by definition, differ from mathematically described primitives such as spheres, cylinders, and cones, making it hard to find repetitive elements. For free-form shapes, one might fall back on traditional formwork techniques, or, as has been done in a number of occasions, use the possibilities of CNC-milling. A formwork material, e.g. polystyrene foam, is milled from a digital model of the building element, and then used to cast concrete in. One of the first projects in which this technique was applied at large scale was Der Neue Zollhoff in Düsseldorf, by architect Frank O' Gehry. In this project a load bearing concrete façade with a double-curved shape was used (see Figure 1.2). The foam moulds were not reusable in another way than just recycling the material.

In situations where similar shapes can be identified, reuse of the moulds is possible. Elements with similar edge-contours, but with the curvature varying per element, can be cast in a flexible rubber box. This flexible box, containing fibre-reinforced concrete, still in unhardened condition, is then positioned on a polystyrene foam layer that has been given the desired curvature in advance by CNC-milling or hotwire-cutting. This technique has been used for - among others - the façade cladding of the Fondation Louis Vuitton pour la Création in Paris, also from architect Frank O' Gehry (see Figure 1.3 on the following page). The foam counter-mould afterwards is disposed of in a similar way as after normal CNC-milling and casting as described above. The rubber box can be reused for other curvatures.

The difficulty stays that for panels with more varying edge contours (e.g. triangular, differing angles per element or with curved edges) in combination with varying curvature a unique mould is necessary for each individual element. A next step towards mass-customization should be made in order to reduce labour and material costs for realizing free-form architecture in concrete. In this study this is done by the design of a versatile and reusable formwork system that allows the casting of free-form concrete elements: *the flexible mould*.

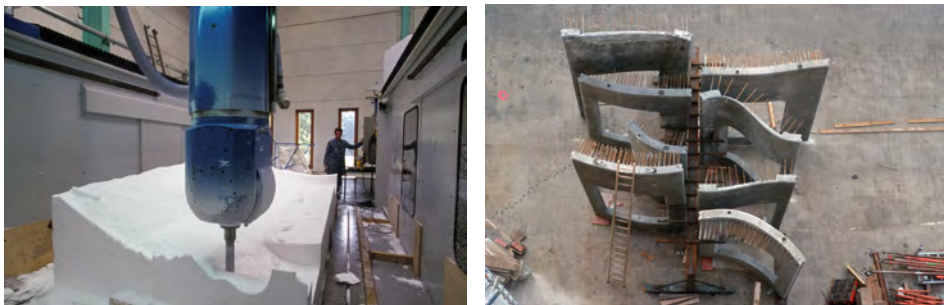


Figure 1.2: Der Neue Zollhoff in Düsseldorf, architect Frank O' Gehry - left: CNC-milling of Styrofoam formwork, right: precast façade elements (Thomas Mayer)



Figure 1.3: Complex and curved façade cladding used in the new building for Fondation Louis Vuitton pour la Création in Paris, architect Frank O' Gehry

1.3 The flexible mould

Mass-customized production of double-curved free-form elements is generally regarded only possible after the realization of a flexible mould system: an adjustable formwork consisting of an elastic material that can be formed into any curved surface by the use of pistons, actuators, pin beds or the like. On this elastic formwork the actual building element can be shaped, either by casting a hardening material such as concrete on the formwork, or by depositing a material that can be softened, such as a sheet of heated thermoplastic or glass. After the building material has taken the form of the formwork and is hardened or solidified, e.g. by hydration or cooling down, the shaped building element is ready for use, and the flexible mould can be reused for another element, possibly with a different shape.

Several prototypes for a flexible mould system have been designed and in some cases also been built by other researchers and architects over the years. One of the first to design, construct and operate a flexible mould for architectural purposes was the renowned architect Renzo Piano, that already built one around 1966 (shown left in Figure 1.4 on page 7). Piano's diagram shows how a part of a scale model of a curved shape is enlarged into an element at full scale, using an ingenious pneumatic device. In an article in the Italian journal *Casabella* the term *stampo deformabile* or, translated, *flexible mould* is used:

"Diagram of the machine for the moulding of the membrane elements, starting from a 1:10 scale model. The pattern is read by means of a device that transmits the data to a deformable mould, which automatically takes the shape read from the model (Piano, 1969, translation RS)".

The machine was realized and has actually been used for the production of a number of plastic shell elements for a number of sphere-shaped and free-form pavilions. A machine with similar concept is shown in the middle image of Figure 1.4 on page 7.

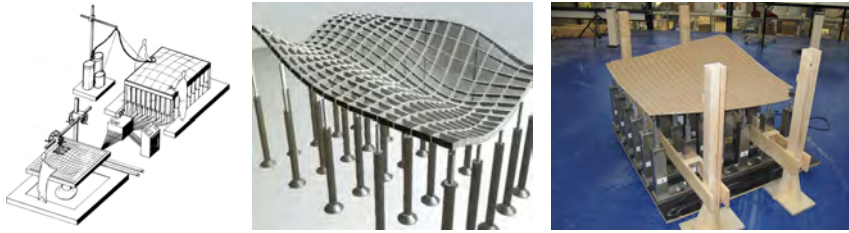


Figure 1.4: Three concepts of a flexible mould, by Piano (1969, left), Spuybroek (2004, middle) and a prototype by Vollers and Rietbergen (2009, right)

In a discussion of various computer-controlled machining techniques architect Lars Spuybroek (2004) imagined an elastic material as intermediate layer between mechanical actuators and the building element's material -plastic or concrete, for example- so that the casting of plastic or concrete is possible with a smooth surface, whilst protecting the mechanism of vulnerable moving parts.

One of the first recent prototypes of a flexible mould system for the material concrete was built by Vollers and Rietbergen (see Figure 1.4, right image). This system comprised a computer-driven set of vertical actuators, which were controlled by coordinates read from an architectural design in the computer. The actuators deformed a flexible layer, which was in turn used as a formwork for concrete. This advanced and promising prototype demonstrated that it is possible to manufacture precast concrete elements, using the flexible mould principle.

However, the system showed a number of imperfections, and aspects of it needed further elaboration. One of the main unsolved issues was that the shape of the flexible layer could not be controlled accurately. As a result of large deflections, inherent to the principle, horizontal displacements occur in the control points of the flexible layer. Furthermore a model for exact description of the elastic behaviour lacked, making it impossible to predict the shape after deformation accurately (Huyghe and Schoofs, 2009).

1.4 Objective and scope of the study

The objective of the present study was to develop and improve the flexible mould method for the manufacture of double-curved precast concrete elements. These elements will be applicable during the construction of buildings with complex geometry. In this thesis, presently available production methods will be discussed and compared to the flexible mould principle. A simplified production process with industrial potential can form a valuable addition to these available techniques. This study therefore will build further on the already existing concepts for a flexible mould system as described in the previous section, and try to overcome shortcomings and unsolved problems of these earlier designs after studying these designs.

The main research question of this thesis is:

How can the flexible mould concept be effectively used to manufacture double-curved precast concrete elements?

Although many other building materials are used in architecture, the scope of this study is limited to the material concrete, partly as a result of the personal interest of the author for concrete, partly because concrete by its nature is a suitable material for casting in different shapes, and therefore particularly fit for use in combination with the flexible mould concept. The research is further delimited by the choice to only investigate and develop precasting methods, rather than extending to both precasting and casting in-situ.

1.5 Outline

The thesis consists of five parts (see Figure 1.5 on the next page):

Part I Introduction to the research starts in *Chapter 1* (the present chapter) with giving a brief introduction into the topic of this study and a description of its objective and scope. The subsequent chapters then will identify what the state of the art is (*Chapter 2*), give a patent review (*Chapter 3*) and literature review (*Chapter 4*) and point out where further research and development is necessary.

Part II Double curved elements for architectural applications will, starting with *Chapter 5*, provide the proper border conditions for parts III and IV of the research, by analysing a number of cases of free-form architecture, that will be discussed and analysed in terms of geometrical aspects, e.g. building size, element thickness, curvature, radius, type of elements and potential for application of a flexible mould method. This analysis will result in control parameters for the type of shapes for which the flexible mould method should be suitable. *Chapter 6* will be a qualitative study that discusses the mathematical aspects of the drafting and manufacturing process. This is done by reviewing closely the methods of shape definition in current CAD software, and by discussing a number of recent developments in the panelisation (distribution) of curved surfaces into discrete elements. This study is partially done by referring to literature, and partially by demonstrating a number of issues in an example. In this thesis, a delimitation will be made to two specific categories of elements: cladding and stay-in-place formwork panels.

Part III Mechanical engineering of the machine addresses the machine beneath the mould surface that deforms it into the accurate shape. This study is described in *Chapter 7*. Although more mechanical than civil engineering, the understanding and description of the kinematics of several parts of this machine form a necessary step to produce accurately shaped concrete elements.

Part IV Concrete technology forms the core of the experimental work with the deformation of concrete after casting into curved shapes, and is split in *Chapter 8*, describing first viability tests, and *Chapter 9*, describing a parameter variation study. Part IV aims to describe the behaviour of fresh and hardening concrete under deliberately imposed deformation.

Part V Final remarks concludes this thesis with *Chapter 10*, a review of the most important findings, theoretical conclusions and recommendations for both practical application of the work as well as for further research.

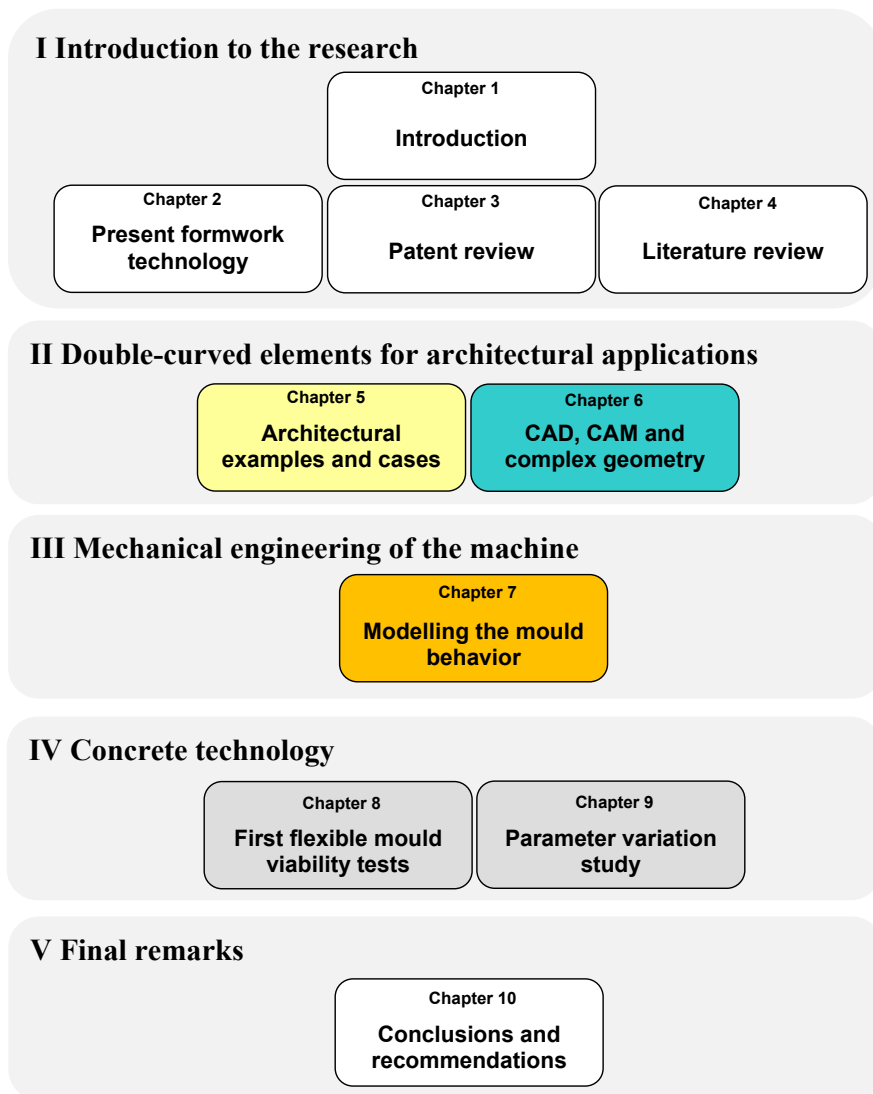


Figure 1.5: Main outline of this thesis

Chapter 2

Present formwork technology and its limitations

2.1 Introduction

In this chapter, the state of the art in the field of manufacturing free-form concrete elements will be discussed by carrying out a review of earlier work. Although the main focus is on concrete, a few sidesteps will be made to the forming of other materials, and to manufacturing techniques stemming from other industries, offering possibly useful solutions for the material concrete.



Figure 2.1: Timber formwork construction and casting of Isler shells (taken from Bösigler, 2011)

2.2 Available techniques for free-form concrete surfaces

2.2.1 Timber falsework and formwork

Placing timber falsework and formwork with wooden shuttering historically was the traditional and most commonly used way of forming arches, shells and domes. The materials could sometimes be reused, depending on the degree of customization and the wear during the building process. In the shells structures designed by Heinz Isler, for instance, lost formwork and partially reusable shuttering were used (see Figure on the preceding page). This depended on the function of the building in question: acoustic or thermal insulation layers were used as lost formwork panels to improve building physics, but for buildings without demands on acoustics or insulation, simple timber shuttering was reused. The methods described here, even when allowing partial reuse of the material, require highly qualified carpenters working on site (Bösiger, 2011, p165), and take a significant amount of time. Isler for example, only worked with specialized contractors, and was very keen on quality control. The reuse was possible only due to the fact that more than one shell with similar shape was realized, leading to repetition. An example of a shell structure with repeatedly used formwork can be found in Pöggeler (1982).

2.2.2 Steel formwork

To enhance stiffness and strength and reduce wear, steel formwork has also come into use, leading to an increase of material cost which could be compensated by the possibility of reusing the formwork multiple times. The use of steel modular formwork systems has therefore, understandably, boomed only for orthogonal building shapes. For orthogonal and flat formwork systems, a high degree of automated customisation is already possible, especially in the placement of mould edges, inserts, window frames and the like. This can be done using magnetic systems, shuttering robots, plotters and laser projectors (Kuch et al., 2010, p216). For curved

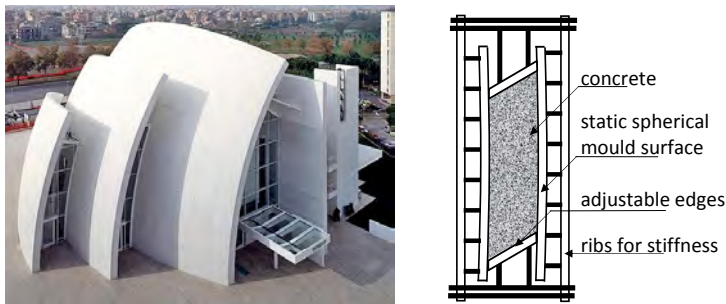


Figure 2.2: Jubilee Church in Rome (2000), architect Richard Meier - left: the building, right: cross section of formwork for precast façade elements (RS, after Italcementi / Lamaro Appalti S.p.A.)

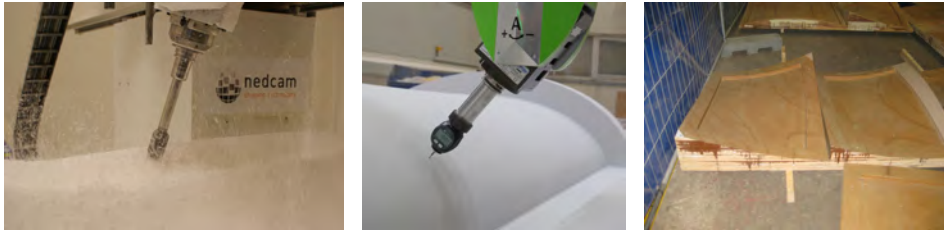


Figure 2.3: CNC milling (left and middle images used with permission of Nedcam, right image Bull, 2011)

shapes, this is much less the case. The companies that offer steel systems in some cases have single-curved shuttering available. Double-curved formwork in steel, however, is hardly available, and mostly custom-made for a specific project, as it is only economically viable if sufficient repetitive use is possible. An example building in which a bespoke steel formwork for precasting was applied, is the Jubilee Church in Rome of architect Richard Meier. Three large and partially overlapping double-curved surfaces together form an impressive architectural gesture, not only due to their geometry, but also due to their material and colour: all elements were constructed through the connection of precast concrete elements in brightly white, self-cleaning concrete. These elements were cast in a partially adjustable steel mould (see Figure 2.2 on the preceding page).

2.2.3 CNC-milling

The use of high-speed Computer Numerically Controlled milling (also known as CNC-routing) has found a wide-spread use in the production of 'plugs' for ships, as complex double-curved shapes are daily practice in ship building. A fast-spinning tool head is moved along multiple axis to machine wood, foams, synthetic materials or soft metals. In case foam is used as basis material, for obtaining a smooth surface, the moulds after milling are normally coated with a hot-sprayed poly-urea which is sanded and polished afterwards. Large building projects realized using CNC foam-milling are Der Neue Zollhoff in Düsseldorf (Kolarevic, 2001, p277), Germany of architect Frank O' Gehry (PS foam moulds, see Figure 1.2 on page 5) and the Rolex Learning Centre in Lausanne, Switzerland of architect SANAA (CNC-milled timber moulds, Scheurer, 2010).

Nedcam, a spin-off company of MARIN (Maritime Research Institute Netherlands), that has shown interest in the developments of the present thesis work, mainly uses CNC-milling as shaping technique for architectural objects (see Figure 2.3). Well-known examples of constructions milled by Nedcam are the Spencer Dock Bridge in Dublin (Ireland, Garcia, 2010) and the roof of the Yitzhak Rabin Centre in Tel Aviv (Israel, Menges, 2006). The Spencer Dock Bridge will be discussed in more detail later (see page 63).



Figure 2.4: Hotwire-cutting (Fangyuan Plastics Machinery Co., Ltd)

2.2.4 Hotwire-cutting

Drawing a hot-wire through polystyrene or other foams allows the creating of ruled surfaces. Due to the necessary tension in the hot wire, the cutting front always has a linear geometry. Single-curved surfaces in any chosen curvature can be made, either convex or concave. Convex double-curved surfaces can be made as soon as the workpiece and the wire-arm are rotated after initial cutting. Concave surfaces cannot be made with a wire-cutter (Brooks and Aitchison, 2010). CNC-machines are available to automate the cutting (see Figure 2.4). Although the surfaces that are cut with a wire are already smoother than the ones that are cut by CNC-milling, a post-processing with poly-urea spray and polishing is possible to even further enhance the surface quality.

In hotwire-cutting, developments are in progress in implementing robotics (Ruttico and Lorusso, 2013). The technique described in the reference is to achieve double-curved shapes by discretization of the surface in small single-curved parts, and glued together after wire-cutting. This, however, still results in a slightly faceted double-curved surface. , The Louis Vuitton Foundation in Paris, a building in which the technique of hot wire cutting of foam shapes was applied in combination with rubber moulds, was shown in Figure 1.3 in the previous chapter.

2.2.5 Fabric formwork with air pressure

Concrete can be cast in or on a formwork of fabric, foil or textile, leading to distinct and remarkable shapes. In the early 1960s the use of inflatable formwork of fabric was introduced by Bini (Mungan and Abel, 2011, p42). On top of these inflated formworks, reinforcement steel and concrete were placed, so that after Hardening a shell structure ("Binishells") was realized. The Binishells formed a dome-shaped shell structure with a regular and symmetrical shape. The creation of free-form shells at that moment was not possible, as the design of the textile required computational effort. A recent demonstration of pneumatic formwork was given in an Austrian



Figure 2.5: Thin concrete elements lifted by inflation of a pneumatic formwork (TU Wien, 2014)

project, conducted by TU Vienna (Aigner, 2014). In this project, wedge-shaped thin concrete elements were lifted by a pneumatic formwork and fixed in their final position (see Figure 2.5).

Research of Pronk and Houtman (2005); Ströbel and Singer (2008) showed that computation of the textile strains and stresses has become more feasible by the use of advanced computational methods, allowing more complex shapes. In Hennik and Houtman (2008), the authors conclude that pneumatic formwork is suitable for the construction of thin curved shells. However, only if repetitive use is possible, the cost of the formwork, which are still considerable, can be spread over projects.

This viewpoint is confirmed in the interview of a structural engineer that recently completed the design of a dome-shape fuel-station for Green Planet in The Netherlands. After looking into the possibilities for using an inflatable formwork, it was concluded that the costs would be too high compared to other methods [interview with ing. Van Vliet, ABT, august 2013]. The dome is now realized with intermediate support points and a system of glulam timber beams en steel roof panels.

Another way to use air pressure is the creation of vacuum in closed textile or plastic 'bags' filled with particles. The atmospheric pressure will create a stiff formwork that can be used for concrete. Recently Huijben (2014) completed his research on the use of so called 'vacuumatics'. By selecting various particle types, experimenting with different pressure-differences and foils, it was demonstrated that the use of the vacuumatics-principle is a feasible method for the support of freshly cast concrete, and that both the interesting textures in the concrete surface can be obtained. Also, under the proper circumstances the formworks are strong enough to support larger structures in the stage when the concrete is still curing. A question that remains is how to bring the vacuumatics formwork in the desired shape if a specific pre-defined curvature for precast elements is required. Furthermore the stiffness of these formworks is relatively limited for larger spans. This can, however, be overcome by using an additional scaffolding system.



Figure 2.6: Concrete cast using fabric formwork (taken from Veenendaal et al., 2011)

2.2.6 Fabric formwork with concrete pressure

Instead of using air-pressure, it is also possible to let the concrete pressure in combination with the elasticity of the plastic foil, fabric or membrane determine the final concrete shape prior to hardening. Manipulation of the fabric formwork is possible to control the shape before, during and after casting. One of the groups active in this field is the CAST-laboratory led by prof. Mark West at the University of Manitoba (West, 2001; West and Araya, 2009, 2012). An extensive overview of the history and present use of fabric and membrane formwork was provided in a publication of Veenendaal et al. (2011). The article provided a taxonomy of the various ways in which fabric can be used, making a distinction between the method of pre-stressing (no pre-stress, mechanical pre-stress and pneumatic pre-stress) on one hand, and the distinction between thin layers cast under self weight and thicker elements formed under self weight and concrete fluid pressure. Veenendaal et al. concluded that the recent work at CAST has led to a renewed international attention to an already existing technology, and that the development of engineering and analysis tools, along with this attention is expected to deliver new developments in the near future. Illustrating this, in 2008 and 2012 International Conferences on Flexible Formwork (ICFF) have been held at University of Manitoba and University of Bath, respectively.

An interesting characteristic of using plastic foils as formwork, is the extremely smooth and shiny quality of the resulting concrete surface. This is due to the absence of water absorption by the mould surface in combination with the reflection of the foil surface within the concrete. Both the shape control and prevention of wrinkling of the foils however, remain difficult.

Based on work presented at the last IFCC2012, it must be concluded that the use of fluid pressures in combination with the large deformations impose a certain restriction on the shapes that can be efficiently and accurately realized using fabric formwork. When compared to the more or less complete freedom of form and high accuracy of CNC-milling, and the considerably limited freedom, but yet high accur-



Figure 2.7: left: 3D printer 'D-Shape' using sand and fluid binder of manufacturer Monolite; right: plans for a 3D-printed house with this printer (website ESA / Universe Architecture)

acy of hot wire cutting, fabric formwork, looking at present state of art, seems most suitable for organically shaped concrete surfaces for which the shape accuracy is not the first and highest concern. Slight deviations in form in many of the cases where fabric formwork was used even seemed an advantage, making the designs more playful and organic. If, however, one thinks of the large numbers of cladding panels of a free-form building that need to be quickly manufactured with many varying edge shapes, varying curvature coupled with high required accuracy (within few mm), fabric formwork seems less suitable.

2.2.7 3D-printing of concrete

One of the techniques nowadays directly associated with the term 'rapid prototyping' is 3D-printing (also known as stereo-lithography or additive manufacturing). The technology of depositing thin layers of a hardening powder or fluid on top of each other allows the quick build-up of an accurate three-dimensional object, based on a digitally available model. In the early years (mid 1990s) the development was still received with cautious optimism (Hull et al., 1995). At present in many fields, such as medical science, art, food, weapons, design and mechanical engineering the technology is applied to a greater extent (Chhabra and Singh, 2011). The resolution of the recent generation of printers is already comparable with that of traditional ink jet printers (600 DPI). The materials from which the models are printed are many: metals, gypsum, bioplastics, polyurethane, epoxy, ceramics, etc.

Although in architecture the use of 3D-printing until recently has mainly stayed restricted to smaller models, the printing of full-scale buildings or building parts gradually becomes within reach. In a research project for ESA, Foster + Partners have even investigated the possibility to use a 3D-printer to produce buildings on the moon (Leach et al., 2012). A development in direct relation to concrete-like building materials is the work of the Italian engineer Dini (Soar and Andreen, 2012; Tissink, 2013). He designed a full-scale printer with the name D-Shape (see Figure 2.7, left

image), using sand as basic material, and spraying an ecological binder on the sand. The present resolution is limited to layers of a few mm each (equal to around 10 DPI), resulting in a rather coarse surface that needs extensive polishing after printing. It is however possible to print moulds, in which concrete can be cast later. An example of this was the work on the Sagrada Familia in Barcelona, Spain, where scale models of Gaudi's details were printed in wax, to be later transformed into flat sections that could be used by stonemasons (Beesley et al., 2004). Other full-scale 3D printing of cement-based materials has been investigated and carried out by Khoshnevis et al. (2001) under the name 'Contour Crafting'.

At present, the material quality and aesthetics produced by the printer are still not comparable to what is possible using other techniques, but given the high pace at which developments are proceeding, it can be safely assumed that within a number of years the technology could offer solutions for specific niche-market applications. A recent attempt to print a house at full scale is undertaken by Dini in collaboration with the Dutch architect Universe Architecture (see Figure 2.7, right image).

2.2.8 Spraying concrete

Sprayed concrete, also known as shotcrete, is used for many years in situations where the application of formwork is not or hardly possible or not desirable, for example in situations where the surface that needs to be finished with concrete is of irregular shape and a thin layer of concrete is required. The lining of traffic or railway tunnels and structural support of mining activities are important fields of application of sprayed concrete. Also the stabilisation of excavated areas in road construction and the creation of rough and natural-looking artificial rock formations in zoo's and aquariums are often carried out with the use of shotcrete.



Figure 2.8: Spraying concrete on curved surface (confuzine.com)

Shotcrete is applied pneumatically, by conveying the dry or wet ingredients through a hose and nozzle and blowing them at high velocity towards the surface that needs to be covered. By adding short fibres of steel, glass or synthetic materials, the structural performance and workability of the sprayed concrete can be influenced. Also traditional steel reinforcement can be applied (see Figure 2.8), leading to a concrete with similar structural performance as normal reinforced concrete.

As the mixtures are generally designed and suitable for application in situations where the receiving surface is under a slope, vertical or even overhead, application for free-form structures is an obvious possibility. It is known that for some of his shell structures Heinz Isler also made use of sprayed concrete (Balz, 2011, p3), (Bösiger, 2011, p168). In those cases, a traditional timber formwork was constructed first. Even in the work of Prof. Mark West at the University of Manitoba, where fabric formwork is used, spraying is suggested as a suitable method for concrete application (West, 2008). In situations where formwork is available, either in a non-deforming (timber) or a flexible (fabric) shape, the method can prove useful, especially with regards to its ability to cover sloping surfaces. For the formwork itself, however, the method does not offer an alternative. A possibility could be to use the flexible and configurable mould in combination with sprayed concrete.

2.2.9 Concrete cloth

Concrete Canvas, also on the market under license as Concrete Cloth, is a flexible sandwich of fabric and foil, filled with a non-set premix of fine-grained concrete and a three-dimensional matrix of fibres. After erection or deployment in the desired final shape from a roll, the construction is sprayed with water after which the concrete mixture sets. After hardening, temporary support structures can be removed. The thickness of the sandwich is typically 5 to 13 mm, and rolls have a width of around 1 m. Applications mentioned by the manufacturer are a.o. canal lining, slope protection, mining, protection of water outfalls and sheltering.



Figure 2.9: Concrete Cloth; left image: sealed rolls; middle image: inflated shelter; right image: build-up of the material (Nuna Innovations Inc. / Concrete Canvas)

Although the thickness and flexibility of the material are probably useful in combination with a flexible mould, the aesthetic quality at this moment is more suitable for civil and military engineering purposes than for architecture. The principle however, is probably transferable without fundamental problems to an architecturally more attractive appearance. For truly free-form shapes, the material then not only needs to be able to cover developable surfaces, but also double-curved, non-developable surfaces. For this it needs to allow in-plane stretching, shearing or a combination of both which is only possible to some extent with the present product due to the backing of PVC foil.

2.2.10 Discussion of available formwork methods

In the previous subsections an overview was given of available methods for arriving at a free-form shape in concrete. In Table 2.1 on the facing page a comparison is made between the various techniques. From this comparison it is concluded that a flexible formwork method, as studied in the present thesis, could form a valuable addition to the state of art. This is mainly the result of the form-changing ability of the flexible mould that allows manifold reuse. This characteristic is especially beneficial in free-form architecture, where repetition of shapes is limited. This will be discussed further in the next section.

2.3 General need for a flexible mould principle

Prefabricated concrete elements stand for a growing market share in the total European building construction volume, both in high and low rise buildings (Vamberský and Schipper, 2010). Precast concrete elements have the advantage of combining high quality with relatively high strength and stiffness and heat accumulation properties. Usually, these precast concrete elements are flat or prismatic in shape, that is, without curves, and the repetition of these elements (achieved mostly by the use of the “master mould” principle in the manufacturing) makes it possible to reuse a single mould many times during the same project. Precast concrete offers many of the desired qualities required in our (environment conscious) human society: production by skilled workers in labour-friendly off-site environment, freedom of shape, high aesthetic value, high load bearing strength, small size tolerances and safe and fast assembly on-site (Vamberský and Schipper, 2010).

New developments related to computer aided manufacturing (CAM) such as file-2-factory and mass-customization have been adapted into a large degree by precast manufacturers, reducing failure costs, enabling flexibility in the production process whilst maintaining efficiency, economy and accuracy. From this point of view, precast concrete technology seems a very suitable construction technology for free-form architecture.

Due to the complexity of the free-form shapes, however, it is often not possible to distinguish any repetition between elements in the building at all (Iwamoto, 2009). Furthermore, most free-form building designs consist of many single- or double curved surfaces which require complex shapes for the mould and element edges (Pottmann et al., 2007). As the costs of the moulds (formwork) for precast concrete make up a significant percentage of the final price per element or per square meter, the feasibility of free-form buildings in precast concrete is still far from optimal. A flexible mould system that combines complex and adaptable geometry with the advantages of precasting can be seen as a key-enabler for concrete in the market of free-form construction. An early adopter of this idea was Renzo Piano, which is illustrated by an ingenious device designed by this architect, discussed in the next section.

Table 2.1: Comparison of various formwork methods

method	amount of manual labour needed	machining and tooling	costs	speed of shaping	freedom of form	surface quality	reuse of shaped elements	recycling of raw material
timber formwork	large, usually on-site	high-tech only if complex shape	high	low	large, but complex shapes require CNC	medium (shuttering generally visible)	limited, and if same shape	yes
steel formwork	limited, due to repetition	high-tech only if complex shape	high	low	limited (double-curved is expensive)	high	often, if same shape	yes
CNC-milling	average, mainly finishing	high-tech	high	medium	practically unlimited	high, if finished properly	only in mould banks	partially
hot-wire-cutting	average, mainly finishing	medium-tech	medium	medium	only ruled surfaces	high, if finished properly	only in mould banks	partially
fabric formwork (air)	limited, during erection of inflatable shape	cutting patterns / sewing	medium	high	limited to controllable pneumatics	high, depending on fabric	yes, if same shape	partially
fabric formwork (concrete)	limited, during preparation	cutting patterns / sewing	low	high	limited to controllable form-finding	high, depending on fabric	limited, if same or similar shape	partially
3D-printing	limited, set-up of installation	high-tech, presently not on full building scale	high	low	large, but limited resolution	low (at present, but improving rapidly)	not applicable	not applicable
flexible mould	limited, edge positioning	medium-tech	unknown	high	large, but less than CNC	high	formwork is reshape-able	possible

2.4 Early example: free-form plastic by Renzo Piano

One of the firsts to carry out comprehensive research and development on the flexible mould in relation to the manufacturing of *architectural elements* was Renzo Piano (1969). A flexible mould for the production of double-curved fibre-reinforced plastic (FRP) elements was described, built and used by Piano in the years prior to the publication. Piano did not refer to the material concrete in his article, but Makowsky, who studied Piano's work (Makowsky, 1969; Oosterhoff, 1969), stated that the mould could also be used for the construction of reinforced concrete shells. Piano's work will be discussed here, as it gives a good illustration of many issues involved in producing free-form elements, forming a reference for the discussion in the further literature review.

Piano was experimenting with blob-like shapes, pavilions and free-form domes in plastic, and realized that the production of these shapes and material required new manufacturing techniques. The prototype of a flexible mould that Piano built, consisted of a grid of plungers (or "actuators") and a flexible mat on top of those plungers, to shape three-dimensionally curved elements of plastic segments, that would together be assembled into free-form pavilions. The position of the plungers was ingeniously controlled by a measuring device that 'read' the vertical height from a scale model, and translated this to the real element by multiplying the measured height and transferring this height to the correct x-y coordinates electronically. Figure 2.10 on the next page shows a scheme of the mould, including a number of clarifying photographs and sketches of details. Aspects that are important to note for the further research are:

- the pneumatic or hydraulic plungers were positioned in a rectangular grid of 9x9 plungers (in other images a 10x10 square grid) on a typical distance of between 10 and 20 cm in both directions;
- the flexible surface was formed by a 'mat', which was able to follow the desired curvature and is suitable to cast a plastic element on;
- the tops of each plunger were connected to the mat in such a way that rotation was made possible;
- the prototype suggested a highly automated, or at least mechanized, manufacturing process;
- the process required a panellization or subdivision of a continuous building shape into smaller elements that could be manufactured in the workshop and assembled later on the building site;
- Piano used square, rectangular as well as triangular meshes for subdivision (not visible in figure);
- Piano, in the accompanying text, spoke of "printing individual elements", which places the present development of 3D-printing in an interesting historic perspective;

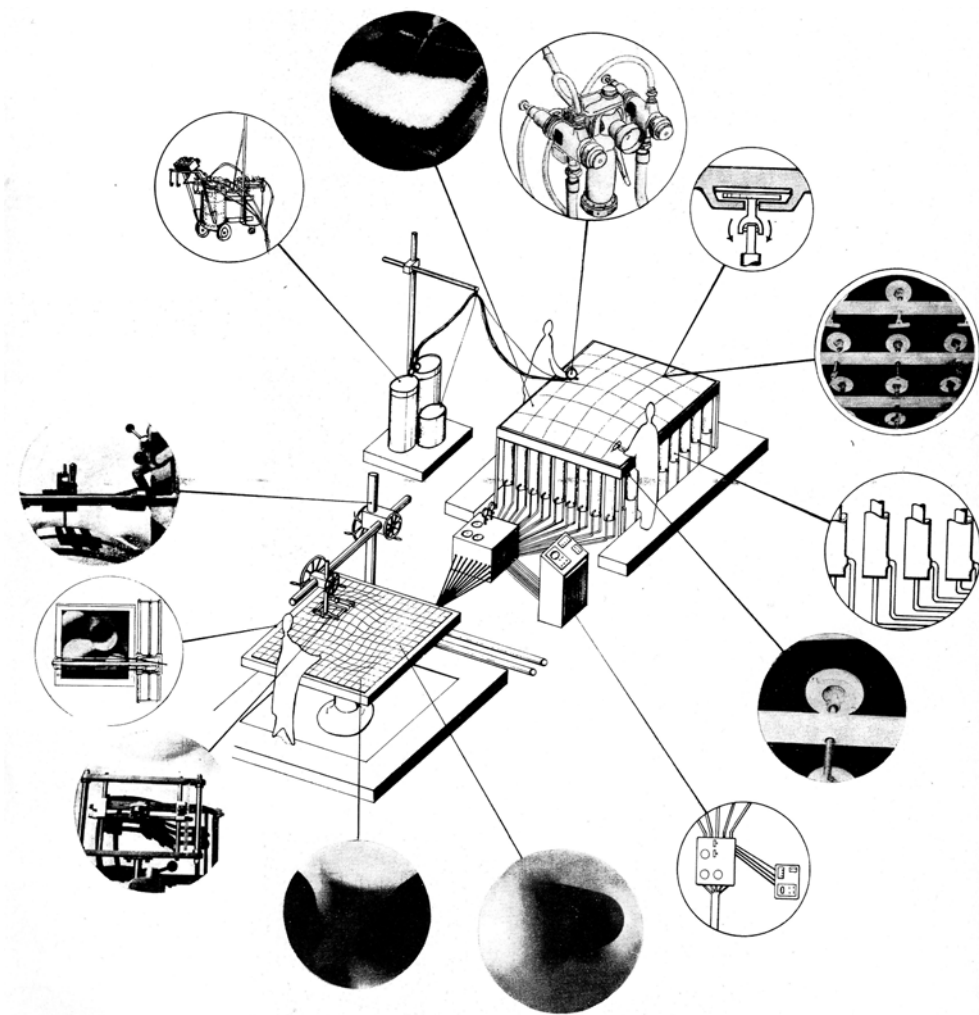




Figure 2.11: Two ways of connecting the triangular elements together, during assembly (left two images) and in the final stage (right) (Piano, 1969)

- Piano also stated that “industrial production does not necessarily mean production of standard elements with constant dimensions”, suggesting that the mould was meant for *mass-customization*.

The articles also showed a solution (see Figure 2.11) for connecting the thus manufactured elements together during the assembly and further lifetime of the building: a temporary connection to keep the elements in place during the construction stage and a gluing system, realized by injecting polyurethane in a rather wide joint that provided for the required tolerances during manufacturing and assembly. A reinforced polyester part was used to ensure structural continuity.

Chapter 3

Patent review of flexible formworks

3.1 Introduction

Patents generally give a good idea of the developments and state of the art of certain technical inventions over time. Although not every patent is always applied in practice, the filing of a patent demonstrates that a specific line of thought was investigated and a problem was solved in some manner, which was apparently puzzling people at that time. Combined with a review of scientific literature, such as journal and conference papers, insight can be obtained into both the developments of the flexible mould over the years, as well as the present state of art. A classification of patents can furthermore help understanding the general principles and give a clue regarding necessary further developments.

3.2 Search method

Espacenet, the database of the European patent office, was searched for filed patents related to flexible moulds for concrete. As the database contains more than a million patents from all over the world, the following search strategy was applied to narrow down the number of hits: most of the patents have a long and descriptive title, a short abstract in English describing the content, and a separate file with images giving an impression of the finding. Table 3.1 on the following page gives a schematic overview of the keywords and search method.

Search (1) lead to a collection of around 1000 patents, related to various industries, including, but not limited to, building industry and also related to various materials, including those normally used in construction. These 1000 patents were related to a wide range of topics, such as the forming of air plane fuselages, wind turbine blades, optical lenses, marine vessel and automotive sheet metal, foam con-

tainers, laminated glass windscreens, products in food industry, antenna dishes, LCD displays and touch screens, other electronic parts, 3D-surface polishers, vehicle seats and foam cushions, bottles, footwear and orthopaedics, medical, dental or surgical auxiliaries, clothing and personal protection, agriculture, furniture, insulation elements, tubes and pipes, and others.

Table 3.1: Search method used for finding relevant patents in Espacenet

search (1)	Title and abstract, selection on keywords: [(<i>die</i> OR <i>mould</i> OR <i>mold</i> OR <i>formwork</i> OR <i>shuttering</i>) AND (<i>flexible</i> OR <i>reconfigurable</i> OR <i>adjustable</i>) AND (<i>curved</i> OR <i>double-curved</i>)] resulting circa 1000 patents
>1973	selection on last 40 years, resulting in circa 450 patents browsing titles and images resulting in circa 25 relevant patents
search (2)	above subset of 1000 patents, selection on keywords: (<i>concrete</i> OR <i>gypsum</i> OR <i>cement</i> OR <i>ferrocement</i>)
cross-ref	also adding relevant cross-referenced patents resulting in 75 relevant patents manually browsing, reading and selecting relevant
selection	selection of around 60 patents, shown in Appendix A

After a restriction of these findings to the ones filed in the last 40 years (thus starting 1973), a selection of around 450 patents remained. By browsing titles and visually scanning the images in these 450 patents, a further selection was carried out. Patents that did obviously not relate to the research question were deselected. Among these last category were many patents concerning general reconfigurable formwork systems for prismatic and flat shapes of cast in-situ concrete, and a large number of patents related to slip-form, jump-form and other climbing or sliding formwork systems with adaptation over the length of the structures (e.g. pipes and towers). Around 25 patents appeared to offer useful information for this thesis work.

In search (2), the first 1000 titles, not restricted to year of invention, were again narrowed down, this time to select those mentioning specifically cement- or gypsum-based materials. This yielded another 75 patents that were not already in the first selection of 25. The collection of around 100 patents then was read more thoroughly, also the cited and citing patents were checked for additional relevant material. Out of these 100 and adding the mentioned cross-referenced patents, a total subset of around 60 patents resulted, that needed further detailed analysis to get a good idea of previously patented work.

3.3 Classification

The above-mentioned subset of around 60 patents was analysed in more detail. Keeping in mind the research question of this thesis (page 8), various criteria were used to determine the relevance for this research and classify the patents. The patents were skimmed, looking for techniques, ideas, procedures or explanations that could offer solutions for the production of double-curved precast concrete elements. The table in Appendix A (starting page 265) gives a complete overview of the classification. The following criteria for classification were used:

- *Reconfigurable*: Is the mould surface reconfigurable, can it be used repeatedly and for various shapes? For any economically acceptable system, this is an important issue.
- *Actuation method* and actuator distance: in what way is the flexible mould surface manipulated to take the correct position corresponding to the desired shape? Also it was examined whether this is done manually or mechanically and whether controlled is numerically (NC), computer-numerically (CNC) or otherwise. At what intervals are the actuators positioned? Many tools from metal industry use closely packed actuators, tools e.g. stemming from glass industry on the other hand use actuators at several cm intervals. Two main categories can be distinguished: (1) pin-beds with directly adjacent pins, or (2) pin-beds with distant pins at regular intervals.
- *Reduction to practice*: Is a practical implementation known of the described invention? Often the patents do not give a clue about this, so if 'yes' is filled in, this information is generally coming from other sources. In some cases the name of the company holding the patent gives a clue in this direction (e.g. Eternit, Lafarge or North Sails).
- *Apparatus, product or method*: Does the patent describe an apparatus, a production method, a product or a combination of these? Some patents merely describe the mechanical engineering invention or solution, others also give an extensive description of a production process or product for which the patent is meant.
- *Curvature*: Can the patent be used for single-curved or double-curved elements or both? Generally double-curvature is harder to achieve due to elastic phenomena. Some patents use ruled surfaces or segmented surfaces as basic form, which is not what we are looking for. A single-curvature formwork is fundamentally easier to achieve than one with double-curvature, as only elastic *bending* stresses in the formwork material have to be dealt with, as opposed to the situation with double-curvature, where large in-plane *shear and normal stresses* will result from the deformation, introducing elastic resistance opposed to the desired deformation and instability through buckling.

Table 3.2: Patents within selection filed per decade, showing a clear increase after 1990 [RS]

year	patents filed
<1940	1
1940 - 1950	1
1950 - 1960	2
1960 - 1970	4
1970 - 1980	2
1980 - 1990	8
1990 - 2000	13
2000 - 2010	11
>2010	13

- *Edge solution*: If discrete elements are produced, how is the configuration of the edge of the element dealt with? Not only is the shape of elements out of plane important, but also the shape of the element edges. Some patents describe only the first.
- *Radius and element size and thickness*: Does the patent mention any specific radius or can it be roughly estimated from the description? What element length, width and thickness is intended with the method? Some patents describe the forming of continuously curved strips with parallel edges of thin material (e.g. long corrugated roof elements from sheets of concrete or metal), others describe elements of a limited size (e.g. automotive wind screen). Many patents do not give a clue about the dimensional possibilities; in such cases a rough estimation is made by the author based on the images in the patent and scale and shape of the apparatus described.
- *Single- or double-sided mould*: Is the cast material completely surrounded by mould surfaces; is only a bottom mould present or is a double-sided mould applied?
- *Formed product*: Which material is formed? e.g. concrete, gypsum, glass, metal, etc.
- *Mould surface material*: What material is used as mould interpolator surface between actuators and formed product? Generally it is necessary to have an intermediate layer smoothing the actuator tips, in order for these tips not to show in the final product.
- *Deformation after casting*: If the material of which the product is formed is cast, is it deformed after casting or is the mould shape configured before casting?
- *Application*: For what type of products is the patent intended?

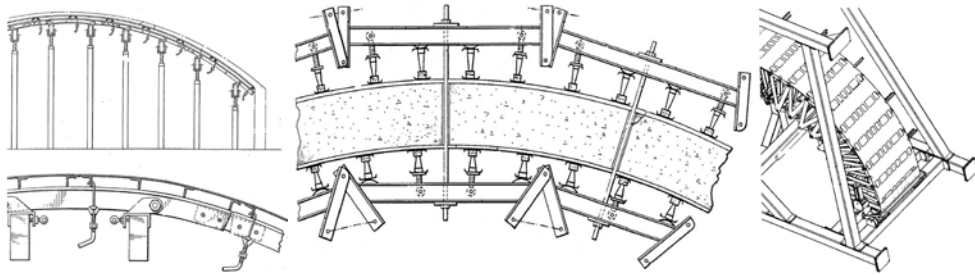


Figure 3.1: Three examples of single-curved mould or formwork systems, from left to right Hawes (1952), Jones and Brown (1993), Glorieux (2012) (Espacenet)

The selected patents were filed in 12 different countries, plus a number of Worldwide and European patents, and were filed between the years 1928 and 2013. Except the 1928 patent, all are filed after 1945. Table 3.2 on the preceding page gives the distribution over the decades, illustrating a clear increase of the number of patents filed starting from 1990. It was not investigated how this increase can be explained, but a possible explanation for this might be the use of complex geometry CAD software, resulting in a growing need for production of curved elements. Evaluating and examining the results of the classification shows that a large variety of combinations is found, making a classification in strict classes somewhat arbitrary. Therefore, a number of groups and trends are discussed in the following subsections.

3.4 Single-curved moulds formed by bending

A first and important group of patents are those describing *variable single-curved moulds or formworks* (see examples in Figure 3.1). Around 20 single-curved moulds in the list all boil down to some form of configurable formwork systems for arches, barrel-vaults, tunnel liners, silo's and tanks. As, often in practice, a different radius is necessary for each new project, many systems are patented allowing easy change of radius, reusing the same formwork materials. Examples are Hawes (1952, Figure on this page left) and Vidal (1987), both showing a single-sided formwork for use in erecting arched roofs, floors, ceilings and similar arched structures formed in concrete, Jones and Brown (1993, Figure 3.1 middle), describing an adjustable formwork systems for walls with variable curvature and Glorieux (2012, Figure 3.1 right), describing a device for manufacturing an arched element, arched element and roof assembly in precast concrete following a continuous moulding process. The patent of Alweg Forschung (1960) used twisted and single-curved steel plates as variable formwork for the production of curved rail-beams for monorail systems. Jump-form systems for cooling towers are described in Parry (1928) and Mygind (1983). Although the hyperbolic shape of a cooling tower is double-curved, these towers are made by using single-curved systems, as the radius of a vertical section

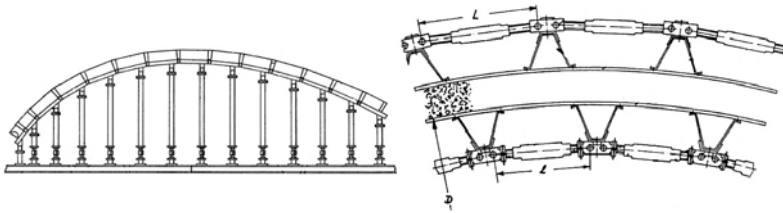


Figure 3.2: left: pivoting actuators, Vidal (1987); right: varying radius by actuators in offset to plane parallel to mould, Maier (1985) (Espacenet)

is so large that it can be approximated with single-curved segments.

As discussed in the previous subsection, a single-curvature formwork is fundamentally easier to achieve than one with double-curvature. However, from the patents concerning single-curvature, some useful lessons can be learned: it can be observed that large required deformations require solutions for the horizontal displacements and rotation of the actuator tips, Hawes (1952), and rotation of the actuator feet, Vidal (1987, see Figure 3.2 left). Many of the solutions describe adjustable horizontal positioning, an important phenomenon that will be observed in our own research later in this thesis as well. An interesting way to achieve a variable radius is by creating a layer of actuators in the same direction as the formwork, but with a certain offset, see Maier (1985), Figure 3.2 right. Change of length of the actuators leads to a change in curvature of the formwork.

3.5 Wax milling and inflatables

A second but small group found in the patent database are systems that use alternative principles to obtain reconfigurability. The first is a system which recently has found renewed interest, the *CNC-milling of wax*. A CNC-router is used to mill a predefined shape from a block of hardened wax. In this open space that is formed after the removal of wax, concrete is cast. After the hardening of the concrete, the elements are demoulded and the remaining wax mould is heated to its melting point, after which the process can be repeated with the milling of a different form. The advantage of this principle is that it ideally leads to a zero-waste situation. A disadvantage is the time necessary for the milling, since for a large building with many varying elements essentially the whole building might need to be milled, all scale 1:1. Examples of wax-milling in the patent database are the inventions filed by Ahonen (1986) and Dittmann (1989), see Figure 3.3). It is known that these systems have been used in practice, e.g. by the Finnish precast-company Partek, that has had a broad interest in robotising and automating production of precast concrete elements (Van Acker, 1996). Recently, the use of wax was mentioned in work that will be discussed below (Oesterle et al., 2012).

Matthews and Matthews (1962) and Liron (2006) use air-pressure to form concrete. Matthews and Matthews described the use of an *inflatable formwork* for syn-

thetic resin or asbestos-reinforced concrete to create dome-shaped elements. Liron uses a similar method to produce double-curved sails. In the literature review below, a number of other alternative ways of shaping will be discussed, not present in this patent list due to the chosen keywords.

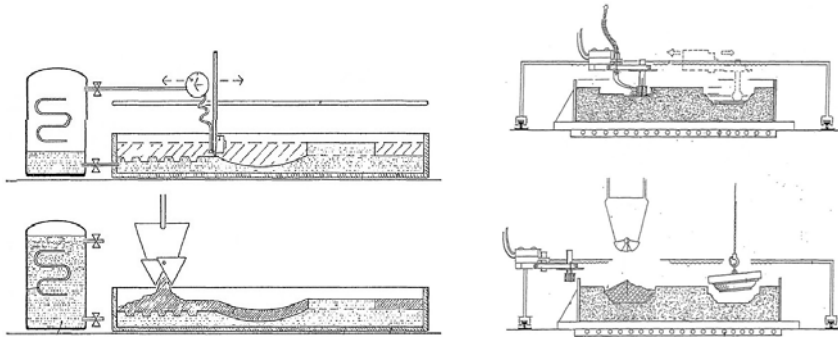


Figure 3.3: Two examples of CNC-milling and casting of concrete in a meltable wax, left Ahonen (1986), right Dittmann (1989) (Espacenet)

3.6 Draping and deforming after casting

A third group are the patents describing the *draping* of an extruded layer of concrete or other materials over a pre-formed die or formwork. Although in the described patents the formwork is not always reconfigurable, the technique of draping or *deforming after casting* is interesting, and will play a central role in this further thesis. Examples are the patents of Kasahara Natsue (2006, see Figure 3.4 top left), which described the extrusion of a layer of concrete on a sort of conveyor belt, after which the top of the layer of yet plastic concrete is impressed with a pattern, and the concrete is draped over a formwork. Finally, the hardening takes place and the concrete can be demoulded in the pre-formed shape. Deformation after casting was also used by Liu Nong (1997) and Oohi Kunio (2002, Figure 3.4 top right), that deformed a layer of yet plastic FRC in a curved shape, after which the hardening took place. A further step of applying these curved elements is using them as lost formwork, like Oohi Kunio proposed and can be seen in Figure 3.4 top right. Oesterheld (1965) and Eternit (1967) described a method for the production of the bending of corrugated asbestos cement panels, also in the stage when the concrete is still plastic.

It is also possible to deform a product that is already hardened. Imura Hiroyuki (1996) described this for thin concrete panels that have been made flexible by cutting grooves in it. Rietbergen and Vollers (2007, see Figure 3.4, bottom left) described a method for deforming glass panes over a pre-formed mould after heating the glass. The patents of Krug (1993, see Figure 3.4 bottom right) and Sykes (1996) discussed a similar production method, used for curved automotive wind screens from a precast flat sheet of laminated glass. In another patent, Vollers and Rietbergen

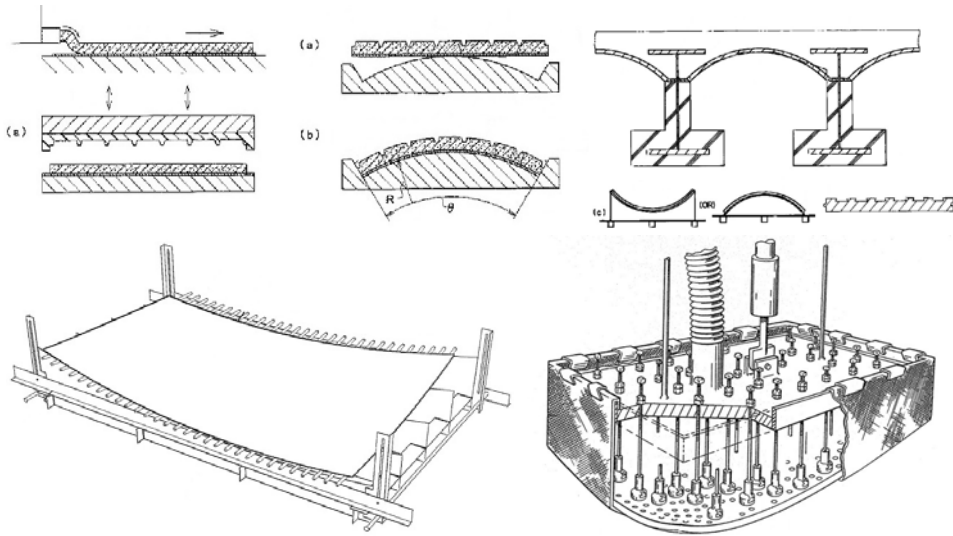


Figure 3.4: Draping or deforming after casting, top left Kasahara (2006), top right Oohi (2002), lower left: double-curved glass, Rietbergen and Vollers (2007); lower right: wind screen production, Krug (1993) (Espacenet)

(2008) described this process using a configurable mould, and also extended the application to concrete or other curing materials.

The vacuum moulding process patented by Lafarge in 2008, mentioned in Martin-Saint-Léon et al. (2011), was investigated (see Figure 3.5). The principle of casting and then deforming is mentioned by Behloul and Quidant (2008, 2011). In this patent, a similar principle is described, to deform a closed flexible mould, containing a ultra high performance (possibly fibre-reinforced) concrete mixture (UHPC), into a predefined shape by means of actuators (“organes de déformation”), which are connected to the mould using ball joints, thus allowing rotation around three axes. The authors describe that the mould is initially on a table in horizontal position to allow easy filling and closing of the mould. The lower and top part of the mould are kept together by means of a vacuum system. As soon as the mould is filled and the vacuum is applied, the actuators lift the mould from the horizontal table into its deformed shape. The mould is kept in this shape until the concrete has hardened sufficiently. The method is meant to manufacture 3D single- or double-curved thin (5 to 50 mm) concrete elements, preferably without discontinuities. The elements have a size of preferably 5 m², but possibly up to 20 m². A similar process is described by Jaques and Lagrange (2010), also from Lafarge. The vacuum-part of this patent was actually applied in practice for the manufacturing of the façade panels for the Frank O’ Gehry building “Fondation Louis Vuitton pour la Création” in Paris. Instead of actuators, however, wire-cut PS-foam was used for shaping the flexible moulds (see right image in Figure 3.5).

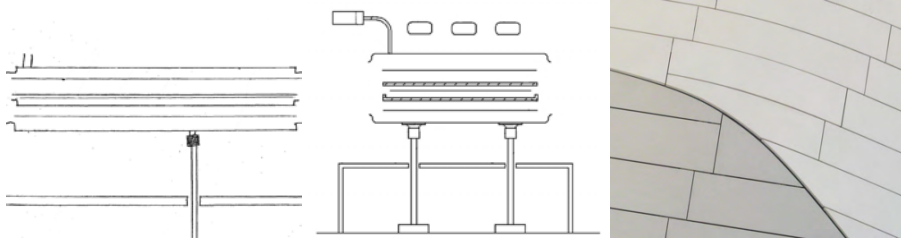


Figure 3.5: Left and middle: Images from patents of Behloul (2008, 2011) and Jacques (2010), describing a vacuum-based system, all filed by Lafarge [source: Espacenet] - Right: Ductal panels of Fondation Louis Vuitton pour la Création in Paris

The method of deformation by actuators brings us to the fourth group of patents, the pin-beds, which will be described in the next subsection.

3.7 Pin-beds

The fourth and final group are the patents in which *pin-beds* are used. A pin-bed is a set of configurable actuators placed on a regular grid, with their tips together forming the contours of a double-curved shape. Two categories can be distinguished: (1) adjacent actuators and (2) distant actuators. On top of this contour of actuator tips, a flexible mat of e.g. rubber, often called an 'interpolator', is placed to form a smooth surface. The interpolator transfers the concentrated forces from the tips to the actual material that is deformed by pressing or stretching, much like in the earlier described work of Renzo Piano. Obtaining a smooth surface is not simple, as will be discussed later.

The patent of Behloul and Quidant (2008, 2011) in the previous subsection also uses a pin-bed, and discusses the visibility of the actuators in the workpiece of concrete:

"If one member of deformation is implemented" ... "the surface may have a single hump, if several members of deformation are used, then the surface may comprise a plurality of bumps more or less high and separated by valleys" ... "The workpiece surface is similar to the surface of a rough sea".

This is an issue that is addressed by others and will also play an important role in this thesis. The oldest patent found using *actuators* to define a flexible and adjustable shape in concrete is from Eisel (1979) (Figure 3.6). Eisel described an upper and lower formwork that could be used for precast elements with a variable architectural appearance. The example of precasting parts of spherical shell structures was mentioned. The shape of the formwork could be adjusted by modifying the height of a large number of pins that were covered with a plastic foil to prevent contact between concrete and mechanism.

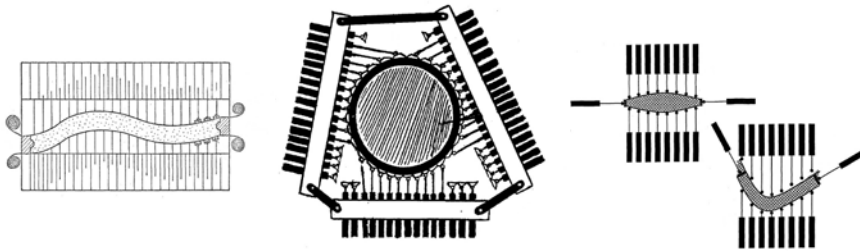


Figure 3.6: left: earliest patent found using a pin-bed for concrete elements, Eisel (1979); middle and right: large degree of shape freedom, Laloux (1988) and Gould (2006) (Espacenet)

Laloux (1988) and Gould (2006, see Figure 3.6) described a reusable formwork modules making it possible to form a large variety of architectural shapes. Remarkable in these patents is the large freedom of form that was envisioned, allowing fabrication of spheres, walls, roofs and other free-form shapes, using actuators from all directions. This is more or less similar to the sketches of a flexible mould drafted by Spuybroek (2004), whose work will be discussed later (see Figure 4.8 on page 51). It is questionable, however, whether this freedom of form is possible in reality, due to various practical issues, also to be discussed later.

Most patents aim for much simpler, slightly and gradually curved shapes, for example those patents covering metal stretching: Chen Yueming et al. (2013) and Zhongyi Cai et al. (2011) described a continuous process using stretch forming of metal over a reconfigurable pin-bed die for the production of gently curved plates, that can be used e.g. in façades. The stretching method of Zhongyi Cai is illustrated in Figure 3.7, top left. Mingzhe Li et al. (2011) also described a system with closely packed pins that support the material (see Figure 3.7, top right). Yamahada described a general-purpose platform in which parts can be formed in a specific shape (see Figure 3.7, bottom). Guangjun Li (2009) describes the use of a pin-bed for rapid prototyping of double-curved aluminium aircraft wing parts.

One of the first to give an extensive description of the possible use, scientific background and suggestions for practical application for creating free-form structures in concrete is Kosche (1999) in his patent *"Integriertes rechnergestütztes Entwurfs-Konstruktions- und Fertigungsverfahren unter Verwendung eines Schaltisches für frei geformte Bauteile und erhaltende Materialien"* (Kosche, 1999). Kosche envisioned a flexible formwork, adjustable in shape by computer-controlled actuators, and stated that, although the calculation of free-form structures becomes more feasible through the use of finite element software, the manufacturing of these structures still is a problem. Kosche did not consider the use of CNC-milling to be a practical solution for large-scale buildings, for much the same reasons as those against wax-milling described above. He suggests that the use of precast elements made in a reusable mould is a better way to reach an accurate, fast and economically feasible production technique. He comes with two solutions: (1) the use of an actuator-controlled system

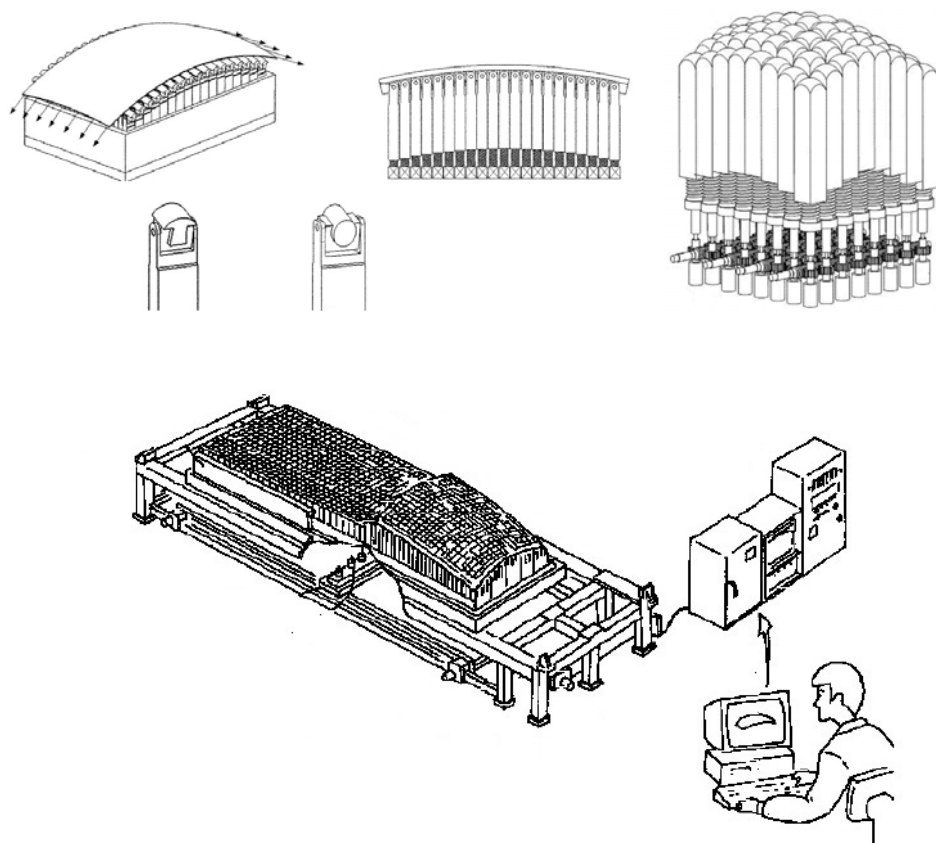


Figure 3.7: Various pin-bed moulds, top left Zhongyi (2011), top right Mingzhe Li (2011), bottom Yamahada (2002) (Espacenet)

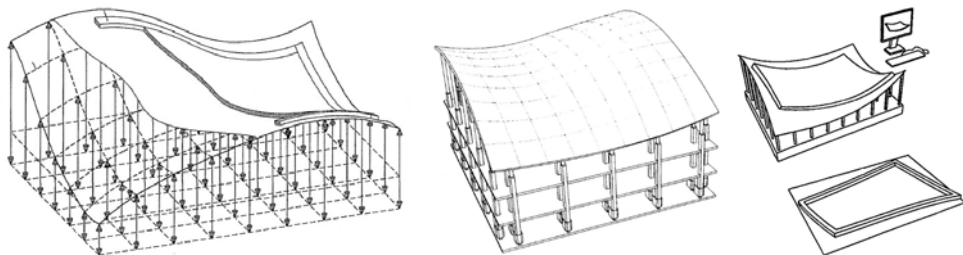


Figure 3.8: Similar principles patented by Kosche (1999, left), Kristensen and Raun (2010, middle) and Vollers and Rietbergen (2010, right) (Espacenet)

and (2) the use of computer-shaped sand, both as alternative undergrounds for a flexible formwork. To the author's knowledge, Kosche's patent was never applied in practice by himself. The patent, however, is referred to in the patents of Vollers and Rietbergen (2007, 2008) and Kristensen and Raun (2010), that have actually built flexible moulds for concrete.

The firm Adapa from Denmark has described (Kristensen and Raun, 2011) and patented (Kristensen and Raun, 2010 and Raun, 2013) a quite advanced combination of actuators, flexible mats and vacuum-technique to obtain the required shape with a smooth surface that can be used for casting concrete, and also other thermoplastic, hardening or drying materials, such as acrylic plastic, glass, gypsum, polyester or epoxy. This recent patent is also described in (Raun et al., 2010) and was implemented in a prototype. Recently, Raun filed an additional patent on the subsystem of three layers of flexible rods that supports a flexible mat (see Figure 3.9). The shape is controlled by a combination of measuring and correction, and the possibility to exchange the flexible variable rods for others with different stiffness. At present, the company is advertising that the technology can be used in commercial projects. Furthermore a recent patent (Raun and Henriksen, 2014) was filed by Adapa and Waagner-Biro Stahlbau that describes the use of the above-mentioned apparatus to first manufacture a double mould surface in a thermoplastic material, that is in turn used as formwork for a curing material such as concrete. This stepwise approach makes it possible to produce large series of elements without the need for a large set of expensive moulding machines. The thermoplastic material is recycled after use.

Vollers and Rietbergen own two patents (Vollers and Rietbergen, 2008, 2010) on the use of the flexible mould. The first one, invented in 2008 and filed in 2010, describes the application of a "viscous-fluid" material, cast on a flat and horizontal plane. After a certain time of hardening, the plane is deformed in a predefined curved shape, during which process the viscous-fluid material also takes the desired shape. The time necessary for the fluid to gain strength to allow deformation and later the time to harden sufficiently to be demoulded is important in the process. The patents describes several methods for obtaining the predefined shape of the plane and of the edges of the cast element.

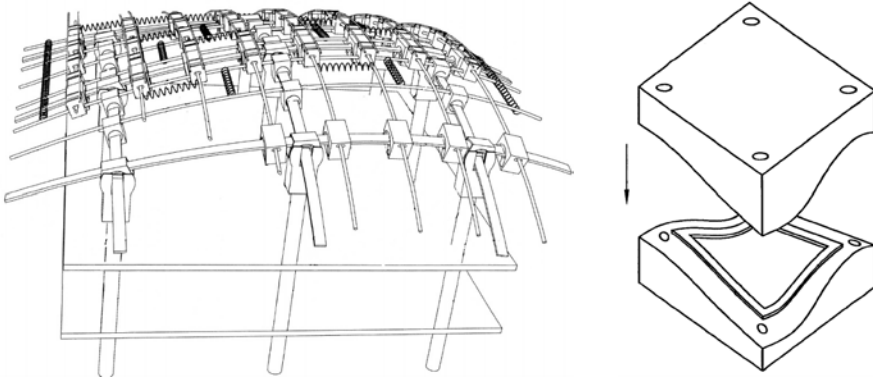


Figure 3.9: left: Raun (2013) patent for subsystem of flexible mat; right: Raun & Henriksen patent (2014) for using intermediate moulded layer (Espacenet)

3.8 Patented product types

Milinkovic and Milinkovic (2010); Nachbauer et al. (2012) have patented not the production system, but the application of precast-elements as stay-in-place formwork for large curved cast in-situ roofs or other curved surfaces, see Figure 3.10. Whereas Nachbauer described the use of variously shaped elements with a reinforced top layer of cast in-situ concrete for free-form shapes such as artificial mountains, but Milinkovic described a more mathematical geometry, like a tunnel arch built of precast ferro-concrete shell elements, also with a cast in-situ top layer.

Milinkovic uses ribs on the elements described in the patents. Haeger (2010) described the use of a flexible mould for the production of precast-concrete Telecom towers with tapered cylindrical shape.

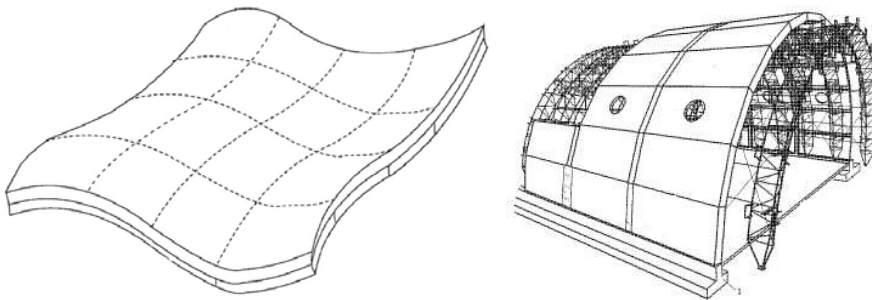


Figure 3.10: Products that could be produced by a flexible mould. Left: concrete elements used as lost formwork for a plank floor (Nachbauer, 2012), right: tunnel liners (Milinkovic, 2010) (Espacenet)

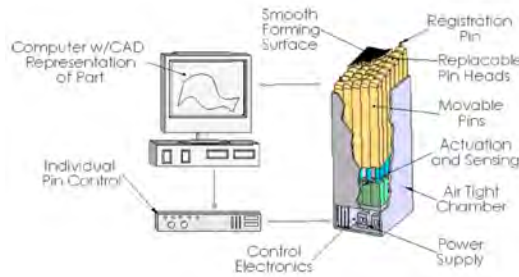


Figure 3.11: Schematic representation of an ideal reconfigurable tool (taken from Munro and Walczyk, 2007)

3.9 Patent study by Munro and Walczyk (2007)

Munro and Walczyk (2007) carried out an extensive patent review of reconfigurable moulds from various industries. The article traced back ideas for using pin-beds as reconfigurable surfaces for forming or moulding materials in various industries as far back as the year 1863, and characterized and compared 35 patents filed until 2004, partially overlapping with the patents described above. Also academic research and realized-in-practice work were investigated. All reconfigurable moulds were given a score by comparing them to an imaginary and ideal reconfigurable tool (see Figure 3.11), based on nine preferable characteristics. Many of these nine characteristics would be desirable properties of concrete moulds as well, making the article a useful basis for scoring possible developments made later in this thesis. The authors concluded that, despite the long history of the topic, there still was considerable and continued interest in developing reconfigurable pin-type tooling. Progress however was limited: the same basic design features kept reappearing in many patents filed in the last century. The introduction of computer control re-boosted developments, especially regarding the configuration speed.

Remarkably enough, the authors conclude that, when measured along the mentioned nine characteristics, the current reconfigurable tools have almost matched the ideal configurable tool. Yet, the use in practice in general industry has remained limited to only two commercial versions. The authors therefore analysed factors that explain this limited interest of industry, identifying three factors: 1) the market for the reconfigurable tool is too limited in relation to the costs, 2) the advent of rapid CNC tooling has reduced immediate need, 3) the material needed as flexible, interpolating layer between the pins and the moulding material gives several concerns. The authors finally gave recommendations to help facilitate successful commercialisation: develop an economical tool consisting of individually actuated, close-packed pins with sufficient size and resolution (small pins, large elements), do research into more efficient control schemes, and pursue application in other industries than the aerospace market, where most of the earlier commercial attempts were done.

For architecture, it was observed by the authors that the use of reconfigurable tooling would be 'ideal', since the repetition of parts is generally low. In the discussed patents, the material concrete, however, is not mentioned. The authors mention curved sheeting of metal and drape-forming of glass as examples.

3.10 Discussion of patent review

The patent research has revealed several interesting points:

- The flexible mould principle has puzzled many inventors from various branches of industry for almost a century, basically for the same reason: creating freely formed elements in a quick and affordable manner. The oldest patent discussed in this study stems from 1928, the most recent one from 2014. Earlier reviews, as discussed in the previous subsection, even discussed patents from 1863. Yet, practical application was only found in few projects, as will be discussed later in the present study.
- Different methods are used to reach the deformed shape: pressurized air (inflation or vacuum), actuators, pins, bending, wax milling and shaping. The pin-bed reconfigurable mould types are the mould types offering a large degree of freedom and reconfigurability. In many cases the pins are actuated mechanically, and in the most recent patents controlled by computer.
- On top of the pins generally an interpolating layer is necessary. As interpolating layer, some inventors use a soft, rubber-like formwork, others use timber or steel plating that is elastically deformed by force, without however reaching the plastic stage, so that reconfiguration for other shapes is possible.
- Many materials can be used for the cast elements. Patents from automotive or aerospace industry are describing the forming of thin metal sheets. Other materials found in the patents are characterized by a typical two-phase working: fluid but viscous at first, then hardening, e.g. concrete, gypsum or synthetic resin. In some patents the addition of reinforcement is described. Some patents describe the use of thermoplastic materials, which are heated prior to deformation.
- Any method needs to be accurate, fast and reusable in order to be economically more attractive than in-situ formwork. The reuse of the formwork also has environmental advantages in terms of limited material and energy use.

A number of ideas or solutions were *not* found in the patents:

- The use of a single (open) mould in combination with concrete is mentioned, but there are clues given neither for the proper type of concrete nor the type of reinforcement that could be used in combination with the deformation process; the only patent that gives a quite detailed concrete recipe uses a double (closed) and vacuumised mould.
- The exact displacement- and elastic behaviour of the mould surface is touched by some patents, but never described in detail; some patents mention measurement methods for checking the form. Further literature study must show whether the exact shape control was investigated and solved or not.
- The exact placement of the edges in relation to the subdivision of the complex geometry of the curved building into smaller elements is touched, but not described in detail in any of the patents.

In the further literature review these ideas and open questions will be investigated further.

Chapter 4

Literature review of flexible formworks

4.1 Introduction

As already stated in the introduction of the patent review, a patent review needs to be combined with the review of literature, such as journal articles and conference papers to acquire a complete idea of developments and prior art. In this chapter, an overall review of the relevant material will be provided.

4.2 Forming of thin sheets of material

For forming thin and flat sheets of material, such as metal or plastic, into three-dimensional shapes, solid *dies* are often used. These pre-formed solid dies have the negative shape of the desired product, and are used as backing for the sheet of the actual product that is force-pressed into the die. For each new shape, a new die is necessary, making this particular process mostly feasible for large series of similar products. For small series or for rapid prototyping, a reconfigurable mould would be a better solution. In various industries other than building industry this similar problem occurs: marine, aerospace, automotive, transportation and energy industry are all confronted with situations in which low-repetition, dedicated shapes have to be manufactured, making tooling costs very high due to low quantities, required accuracy and high variety. It is for this reason that research on reconfigurable tools has been done in the past.

The Japanese pioneer Nakajima (1969) in the late 1960s worked on the idea to use bundled small diameter pins or wires to form a reconfigurable shape to stamp thin sheet metal into double-curved shapes. He protected the sheet metal from being scratched by the sharp ends of the pins by using rubber sheets as interpolator in between. Nakajima showed that his method could also be applied for vacuum

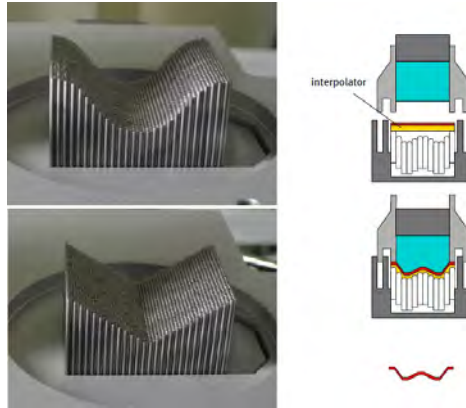


Figure 4.1: FlexiMold system (taken from Boers, 2006)

forming, die-casting or compression moulding of plastics. The work of various academic researchers in the 1970s and 1980s using the same principle for creating double-curved shapes for aerospace industry is discussed in Munro and Walczyk (2007). Most of the work described presents configurations of large numbers of closely packed pins with small diameters.

A principle quite similar to Renzo Piano's prototype, analysed in more detail from a mechanical engineering point of view, was described by Kleespies and Crawford (1998). The authors used a rubber membrane 'interpolating' between the position of discrete pins (actuators) to form a sheet of styrene thermoplastic. As in Piano's design, the pins are at a relatively large distance from each other. In contrast to Piano's principle, a vacuum pressure is used to maintain contact between interpolator and rubber membrane. The authors investigated the relation between the thickness and Young's modulus of the interpolating material, the *dimpling* or *waviness*, the vacuum pressure and the radius of the formed shape. They investigated this by using and comparing three approaches: 1) Timoshenko's plate theory 2) FEM analysis to account for in-plane membrane forces and large displacements and 3) measuring of experimentally formed plastic sheets. One interesting conclusion of their work (Kleespies and Crawford, 1998, p336) was, "the surface geometry of the formed parts is limited, however, to a compromise between the surface waviness and radius of compound curvature", an observation also done later in our own research: looking at free-form shapes, one has to restrict the radius to a certain minimum if a feasible flexible mould system is to be designed.

Boers (2006) developed the FlexiMold-system, another example of a reconfigurable mould. In his PhD thesis, mechanical engineer Boers (2006) described a reconfigurable die using a matrix of pins (see Figure 4.1) that could be reconfigured in short time in any shape, allowing rapid prototyping and small series of uniquely shaped sheet metal elements. The method could also be used for forming of other materials, such as thermoplastics. The elasticity and plasticity of the deformed ma-



Figure 4.2: Pin-bed mould and sheet of thin metal pressed into saddle shape (taken from Song et al., 2010)

terial and the supporting rubber sheets ('interpolators') were researched by the author for a number of NURBS-curves, in order to come to a smooth surface quality without visibility of the pins in the final product ('dimpling'). The author also aimed at application of the reconfigurable die in the field of architecture and building construction materials. Although the size of the machine at the time of the above publications was still small ($40 \times 50 \times 25 \text{ mm}^3$), larger prototypes were under development, with effective working volumes of $1000 \times 1000 \times 500 \text{ mm}^3$ (Pronk and Moncrieff, 2009). These prototypes could potentially be used for production of concrete elements.

A well-illustrated description of the process of pressing thin metal sheet using a similar method was found in Song et al. (2010). Figure 4.2 shows the upper half of a mould and a produced saddle-shaped metal piece.

In contrast to using a double-sided die, the deformation of flat sheet metal into a pre-formed die can also be executed using a single-sided die and explosion forming (Groeneveld, 2008; Pronk and Moncrieff, 2009). The sheet metal is placed on the die which has been milled in the required shape in a prior step. After that, the die cavity is vacuumised and the assembly is placed under water. An explosive charge is detonated to press the metal in the die within a few milliseconds. The method offers



Figure 4.3: Explosion-formed stainless steel cladding, booster pump station Amsterdam, Group A architects, 2006 (image courtesy of flickr-jpmm)

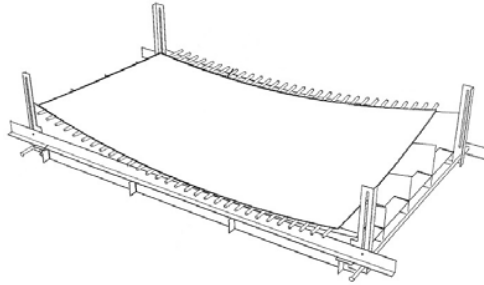
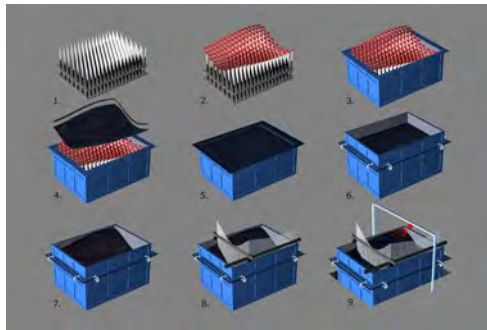


Figure 4.4: 'flex-rod' system (taken from Vollers and Rietbergen, 2008)

a larger freedom of shape than the FlexiMold process, allowing large plates (up to 10 x 2 m) in various thicknesses (0.3 - 60 mm) and is suitable for various metals. The method is not likely to be suitable for concrete, since the explosion forming principle makes use of the plasticity of metals, a material property typically not present in concrete, at least not to the same extent.

Similarly, it is possible to bend glass over a mould, addressed by Vollers and Rietbergen (2007) by the realisation of a 'flex-rod system' and a 'Free-D' surface for the manufacturing of double-curved glass panels (see Figure 4.4). The system was made of CNC-cut timber sheets with curved upper edges and thin and flexible metal rods across these edges to carry the glass pane. The glass pane was cut to the correct edge sizes prior to deformation. After this, the glass pane was slid in an oven, where the glass temperature would rise to the annealing temperature, and the glass pane would sag over the predefined shape of the flex-rod system. Upon cooling down, a curved glass pane would be obtained. In the paper (Vollers and Rietbergen, 2007), two outlooks are given: 1) a computer-driven set of actuators for the above mentioned flex-rod system to replace the CNC-cut timber parts, and 2) the use of a flexible mould with a freely curving working surface for the production of plastic and concrete panes. The paper already shows an image of an early prototype, which was later successfully used for concrete by Schoofs and Huyghe Huyghe and Schoofs (2009).



(a) pin-bed membrane mould



(b) Flexible mould from two layers of strips



(c) with carved fibreboard surface, left: actuators, right: mock-up panels

Figure 4.5: Various ideas conceived during master's thesis projects at TU Delft in the years 2000-2011: (a) Quack (2000); (b) Jansen (2004); (c) Huyghe and Schoofs (2009)

4.3 Various master's thesis projects at TU Delft (2000-2011)

In the last decade, the work of a.o. Vollers and Rietbergen at the Faculty of Architecture and the Structural Design Lab at the Faculty of Civil Engineering resulted in a constant interest of master-students at TU Delft in the topic. A brief overview of MSc-thesis work is presented here.

Quack, in her master's thesis research (Quack, 2000; Eekhout et al., 2004), supervised by Vollers et al., does the preposition that free-form or 'fluid' designs can only be accurately manufactured if the panels that make up the desired curved design are curved themselves. According to Quack, prefabrication is a suitable method for such accurate manufacturing. She denotes that subdivision of the fluid shape into flat panels would lead to less attractive buildings, that differ from the original conceptual design. Since building industry is still mainly used for serial production of large numbers of similar elements, there is a contrast to the variability of shape in free-form designs. Prefabrication, in the eyes of Quack, can therefore be only cost-effective when founded on a flexible serial production method. In such

a method, the computer is not only playing a role in the design stage, but also in the manufacturing stage. Quack proposed the use of a flexible mould system (see (a) in Figure 4.5), consisting of a pin-bed carrying a flexible rubber surface for the manufacturing of double-curved façade elements constructed from GFRC. Quack's design builds further on the work of Piano, also featuring an automatically adjustable pin-bed, controlled by a CAM-system. The exact shape of the rubber surface is checked by measuring through a mechanical gauge, following the surface in an x-y-grid, or remotely by using a laser measuring device.

Jansen (2004), supervised by Vollers et al., investigated new production methods for the realisation of free-form buildings. According to Jansen, these buildings can be characterized by the use of three-dimensional curved surfaces without repetition. Using Maya and Rhinoceros, that - at the time of publication - were still mainly applied for surface modelling, Jansen recognized the need to model volumes instead of surfaces, in order to be able to design proper detailing for concrete elements. Jansen built a prototype of a strip-mould supported by a pin-bed (see (b) in Figure 4.5), and cast a number of curved concrete elements on this mould.

Although Diks (2005) focusses on sandwich systems in translucent plastic for double-curved complex geometries in her master's thesis, some valuable conclusions are drawn in her master's thesis report, supervised by Vollers et al., conclusions that are relevant for free-form concrete structures as well: 1) special moulding techniques using a flexible mould are necessary to realize geometrically complex shapes, 2) in these moulding techniques special attention should be paid to the rules for shape description of the element edges, 3) integration of architectural shaping, structural design, production method and assembly is a necessary condition for success and 4) in this integration the computer plays a central role to achieve sufficient fitting accuracy.

Van Roosbroeck (2006), supervised by Wagemans et al., observed that the construction of concrete shells had stagnated, after a flourishing period roughly around the 1950's and 1960's. This stagnation is mainly due to the high labour costs and the inefficient use of formwork materials. The scope of the thesis was limited to load-bearing precast concrete shells, not considering curved cladding panels. Van Roosbroeck stated that, despite the developments in concrete technology and renewed attention for both free-form and form-finding-based structures in recent years, a re-flourishing was still hindered due to lack of an integral and optimal design-construction process for precast concrete shells. She implicitly suggested that precasting in this respect has more future than in-situ casting. Van Roosbroeck's master's thesis aimed to make a step towards optimisation of this design to production process, by mapping the aspects and relationships within both the design and production process and defining a new and integral process by linking the design, the segmentation and the production. After research, Van Roosbroeck concluded that this linking is possible through the utilisation of innovative options of design tools, concrete compositions, production methods and surface segmentation techniques. The process, according to Van Roosbroeck, is very much depending on the building project itself: in situations where morphology is leading, she recommends to start the process by

defining morphology, then defining concrete composition and performing structural calculations. After this, the next steps are surface segmentation, choice of production method and defining a connection system, in an order suiting the project, and with feedback after each step to the results of earlier steps.

Van Roosbroeck recommends that 1) more research is needed on the flexible pin-bed mould, especially regarding the heads of the pins to improve smoothness of the concrete surface, 2) the flexible mould system should be considered a vulnerable system in which non-functioning of one pin can possibly block the entire system, 3) integration between the segmentation and the structural calculation is necessary to prevent the segmentation to be done on locations where the forces are too high, 4) a fully automated process from design to production is necessary, 5) the construction method needs to be taken into consideration and 6) the price of the flexible mould should be investigated, since it might become too high compared to use of milled formwork.

Den Hartog (2008), supervised by Wagemans et al., carried out a master's thesis research in which the aim was to find the difficulties and possibilities of the design and production of prefabricated concrete shells, and to come with possible solutions for these problems and make production more feasible. Like Van Roosbroeck, Den Hartog emphasises the need for an integral approach from architectural design, via structural analysis, to production and assembly, since all steps are interrelated to great extent. In her work, a broad spectrum of aspects are studied: 1) structural mechanics of prefabricated shells, 2) grid generation and element subdivision and the influence of these on element connections and structural behaviour, 3) concrete composites, 4) the adjustable formwork and element edges and 5) the design process. Den Hartog finalized her research with the development of a geometry design tool to facilitate this process and a case study. Conclusions of the work were, among others, that research on the connections between shell elements is necessary, that high-performance FRC is a suitable material for precast shell elements, at least when valid design codes will be available, that an adjustable formwork needs to be developed first, and that the best way of proceeding with further research is the construction of a real prefabricated concrete shell.

Ter Maten (2011) investigated the possibilities for constructing a 150 meter span dome structure using 35 mm thin precast shell elements in UHPC. The findings are applied in a case study involving plans for a free-form sports-dome in The Netherlands, and demonstrate a high potential for this solution. The issue of moulds is also addressed. Ter Maten deems the development of reconfigurable or flexible moulds still not proven in practice sufficiently, and therefore chooses a reusable static steel mould with adjustable edge positions to accommodate different element edge contours. The curvature is kept constant for each mould, but due to change in curvature over the dome shape, multiple steel moulds are necessary.

Janssen (2011), Kok (2013) and Eigenraam (2013) also carried out master's thesis research on the topic, but their work is done within the framework of this PhD thesis and will be discussed later.

4.4 Tests of Huyghe and Schoofs

Huyghe and Schoofs (2009) did a research on the production of double-curved concrete panels under supervision of Vollers, Rietbergen and Grünewald, and, for some aspects, were given consultation by the author of the present thesis. The research contained various experiments with the principle to first cast concrete in a horizontal, flat position, and then, after an initial setting period, deform the concrete into its finally required curved shape. The further hardening then took place with the element in this deformed shape. Demoulding was done when the concrete had sufficiently hardened. Finding the right moment of deformation appeared to require a concrete composition with predictable and optimized development of fluidity. Slump tests were executed to find out the right moment of deformation. In discussion with the author of the present thesis it was also found that the deformation itself may cause strain in the fresh concrete mixture, depending on the thickness of the element and the radius of the curvature. This possible effect was already denoted earlier by Hartog (2008) on page 95-96. In the research of Schoofs and Huyghe, some initial theoretical assumptions were worked out with respect to strain ϵ , curvature κ , thickness d and radius R , leading to at least one important conclusion, that the experiments were not scalable with respect to the behaviour of the concrete in relation to the deformation after casting.

After several experiments with concrete mixtures and programming control scripts in Rhinoceros 3D® and Grasshopper®, the automated version of the flexible mould constructed by Vollers and Rietbergen (2007) was used to cast a number of panels. Much attention was paid to choose the right type of flexible surface on top of the grid of actuators. An expert involved in a large Dutch precast concrete manufacturing firm strongly advised to use timber as basis, mainly due to economical reasons and because of the fact that the concrete industry is very much used to application of wood. It was observed that the automated movement of the actuators was obstructed by the horizontal reaction forces on the tips of the actuators holding the curved surface. Here another important notion was understood: the flexible surface will show significant horizontal displacements, which need to be taken into consideration if the system is to work in a controlled fashion. Various materials were tested for the flexible surface: reinforced polyurethane rubber, reinforced silicone rubber, stiff rubber and timber in the form of a carved medium density fibre-board panel (see (c) in Figure 4.5 on page 45), of which the last material gave satisfying results. It was also concluded that a calculation model for the flexible surface is an absolute must to get rid of unforeseen inaccuracies in the final shape of the panels. Finally it was also recommended to investigate the control of the edge positioning. With respect to concrete technology, three different concrete mixtures were tried:

1. a basic recipe consisting only of sand 0.125-2.0 mm, cement CEM 1 52,5 R and water;
2. a more advanced FRC mixture ('Holcim') consisting of CEM 1 52,5 LA, micro silica, Poraver 0.1-2.0 mm (expanded glass aggregate), plastic fibres, water and

various admixtures;

3. an ECC mixture consisting of cement CEM 1 52,5 R, fly-ash, quartz sand, 0.125-0.25 mm sand, PVA fibres, water and admixtures.

Due to the unknown rheological (=flow) properties of the mixtures it appeared quite difficult to estimate and control the moment in time appropriate for deformation, but it was expected by Schoofs and Huyghe that this could be controlled easily after more research. By varying the amount of admixtures, such as plasticizers or retarders, the moment of deformation was expected to be controllable, aiming for rheological properties that would be convenient in a manufacturing process. A second test by Huyghe and Schoofs was carried out in opposite order: first deformation of the mould, then casting. Due to the slope of the mould, a certain minimal yield strength was necessary during casting (> 40 Pa, see p84 of their thesis). For these tests an undisclosed mixture of Hurks Beton was used. The following conclusions were drawn (a.o.):

1. self-compacting concrete is preferred, this makes it possible to embed complex edge profiles or surface textures in the mould; vibration is not desirable on the fragile set-up;
2. *first deforming the mould and then casting* concrete makes it difficult to control the exact thickness of the element; since a relatively large yield strength is necessary, the compaction of the mixture is problematic;
3. *first casting and then deforming* therefore is the preferred order of working.

In discussion with the author of this thesis the hypothesis was raised (Huyghe and Schoofs, 2009, pp51-52) that the developed strain ε in the deformed concrete is proportional to the thickness of the concrete element and to the reciprocal of the radius of curvature over which the element is deformed, similar to a bending problem in a linear elastic material (see Figure 4.6, second left graph). Perhaps, this makes scaling of experiments impossible: if e.g. the thickness of the concrete element is scaled

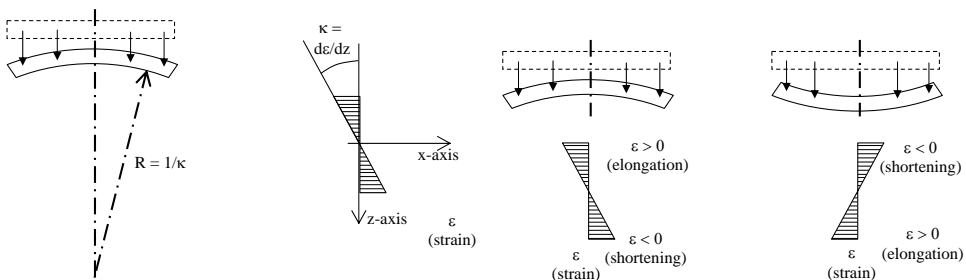


Figure 4.6: First assumption regarding the relation between curvature radius and strain, 2009

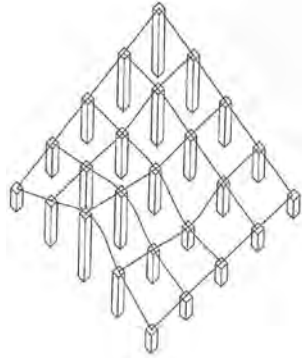


Figure 4.7: Shaping a doubly-curved surface with an array of numerically-controlled pins (Mitchell and McCullough, 1994)

with a factor 2, the expected strain under a certain radius of deformation is also scaled with a factor 2, making the findings of a scaled experiment not representative for a full-scale situation. If deformation would not lead to cracks in the scaled experiment, this would not offer any guarantee that the same would result in the full-scale situation¹.

4.5 Other research worldwide

Mitchell and McCullough (1994), MIT and Harvard professors, give an early theoretical framework behind the world of computer-aided design and manufacturing. In a discussion of several prototyping methods, also a system very much alike the idea of Piano is mentioned: “Shaping of a double-curved surface with an array of numerically controlled pins”. In the subsections “Reshaping” and “Reproducing Moulds and Dies” the possibilities are mentioned to “reshape a material through the application of force, heat, steam, and so on”. No further details are given as how such a system would work in practice, but a simple schematic figure is offered (see Figure 4.7).

Architect Lars Spuybroek, in his book *NOX: machining architecture* (Spuybroek, 2004), discussed several methods of shaping. Spuybroek has realized several free-form objects, both architectural and sculptural, and recognizes the manufacturing as an integral part of the design. In his book, Spuybroek envisions a fully automated file-to-factory manufacturing system: a house can be ordered ‘over the internet’ and automatically manufactured. He stated that a shift from standardized to vari-

¹During the research of Huyghe and Schoofs it did not become clear whether there really is strain possible directly adjacent to the mould surface. In fluid dynamics, it is usually assumed that at the surface a no-slip situation is present. At the interface surface between concrete and mould, this would imply that the strain of the concrete is equal to the strain of the mould. For an oiled mould however, this might be different. Also, the stretching of the mould itself due to the deformation from flat to double-curved may result in strains in the concrete. These aspects will need further investigation.

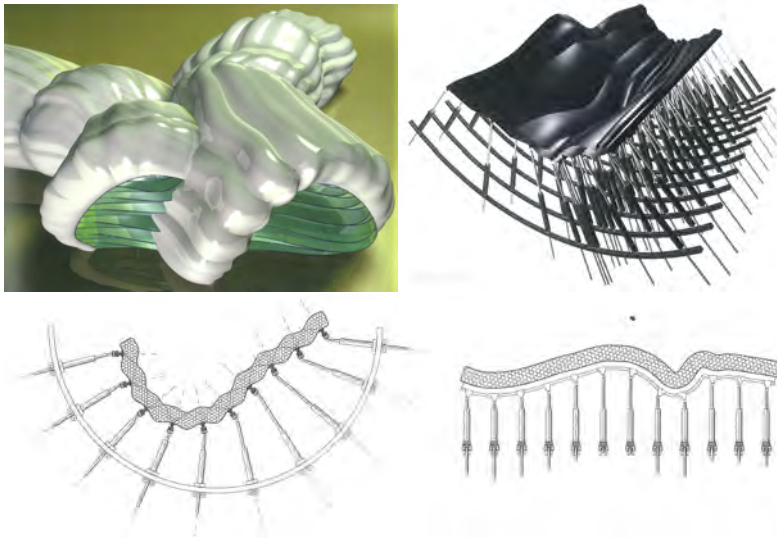


Figure 4.8: A building with various double-curved surfaces (top left) and a flexible mould (other images) to manufacture the building elements, according to Spuybroek (2004)

able and non-standard elements would change building technology considerably. A formwork-table that could be adjusted numerically into a double-curved shape could be used as a mould to make concrete elements. The author also recognized the possibly conflicting requirements: flexibility to take any free-form shape, and stiffness to carry the weight of concrete. Spuybroek suggested that variable flexibility could be obtained by application of vacuum-forming, but describes no further attempt to find specific design rules for a flexible mould system or for the behaviour of the mould surface. Figure 4.8 shows a mould consisting of a flexible surface controlled by hydraulic or pneumatic actuators, apparently capable of small-radius deflections. Apart from using the material concrete, Spuybroek also imagined that large corrugated rubber-polyurethane sandwiches could be used as self-supporting building envelope.

Raun et al. in 2010 and 2012 reported on a reconfigurable mould for double-curved surfaces in Raun et al. (2010); Raun and Kirkegaard (2012). Some parts of the technical system were not described in detail, but more information was found in patent (Kristensen and Raun, 2011), discussed above. The authors saw a market for a flexible and reconfigurable mould for cladding panels in concrete or other hardening materials such as gypsum or thermoplastic, possibly reinforced with glass-fibre (FRC, FRG, FRP). They described a number of available manufacturing methods for curved panels, among which the 'milled foam method', system-based traditional formworks, air-pressure-controlled membrane moulds, and actuator-controlled moulds. The authors considered the latter to be a valuable addition, positioned between the relatively fine detailed, small-radius 5-axis CNC-milling tech-

nique and the large-scale, limited detail, large-radius traditional formwork systems. The described mould was made up of a $1.20 \times 1.20 \text{ m}^2$ membrane controlled by a 5×5 grid of Arduino-controlled electric actuators. The authors stated the elasticity of the mould surface is something that can only be known from testing the prototype. The edge-continuity was controlled by an angle-restraining device around the outer contours of the mould. The radius that could be formed was 1.50 m or larger, the deviations between the CAD-shape and the realized panels were between 2 and 3 mm. The panels had a thickness of around 10 mm. The principle described was to put the material on the mould when this mould was still in horizontal position, and after a waiting period deform it in the desired shape. The described system was build in a prototype, and several mockup-panels were successfully cast. The positioning of the mould edge prior to deformation is performed by a laser projector. A potential disadvantage of the technology presented by Adapa might be the complex mould surface and subsystem in relation to the curing time of the concrete: to obtain an acceptable cycle speed for larger numbers of elements in a full scale project (typically 100++ panels), either very-fast-hardening concrete needs to be applied or multiple costly set-ups of the mould system will be needed in parallel.

Oesterle et al. described the use of hot wax, shaped on a mould surface that was deformed by a flexible 5×5 robotised actuator system (Oesterle et al., 2012). The research was embedded in the EU-FP7 project TailorCrete (www.tailorcrete.com). The wax, after solidifying, was used as smooth surface for casting concrete on. A double-sided wax mould can be used for walls, a single-sided mould for floors. After removal, the wax could be fully reused waste-free, reducing the costs of the system. Special attention was necessary for the melting point of the wax in relation to surface temperatures due to solar radiation and hydration heat. Also the hardness of the material required a specific wax in order not to be damaged by the application process of the steel reinforcement. The method differs from the earlier discussed patents of Ahonen (1986) and Dittmann (1989), in which an actuated mould is used to form the wax instead of CNC-milling.

Michel (2012) reports on a model to electronically control an adaptive wall formwork for free-form concrete walls and shells. As part of his PhD research Michel targets to understand and model the complex geometric and kinetic behaviour of a two-surface formwork, controlled by an array of actuators. Perhaps, Michel is the first to recognize that this behaviour is non-linear and that a simulation is required to accurately predict and control the position of actuators and mould surfaces. By coupling a geometrical model in Rhino and a numerical solver Michel succeeded in doing so. A physical prototype has yet to be made.

Another target of Michel's work is to find a mould surface that can accurately follow the required deformation. As we will see later in the present thesis, for this deformation in-plane strains (longitudinal and/or shear strain) are necessary to form a double-curved surface. Michel and Knaack (2014) for this purpose propose a clever system of rotating elements that can undergo these strains.

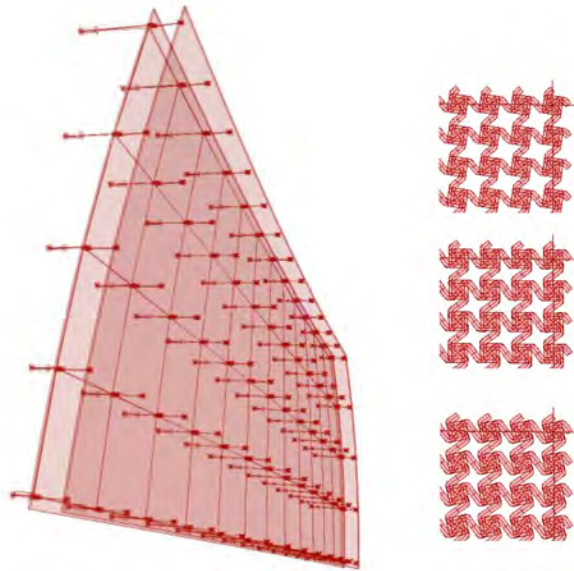


Figure 4.9: Model of a surface as free-form wall formwork (Michel and Knaack, 2014)

4.6 Discussion of literature review

In this subsection, the present state of art will be discussed and summarized, based on the findings the literature review:

- A flexible mould system is believed to be potentially cost effective by various authors, limiting both labour and material costs. If however the technology in the flexible mould system becomes too delicate, high-tech or advanced, its costs might become higher than other presently available technology (Quack, Van Roosbroeck). One author clearly states the flexible mould principle is still not proven technology (Ter Maten). In terms of possible level of detail, the flexible mould is positioned between CNC-milled formwork and traditional curved timber or steel formwork (Raun et al).
- The flexible mould is considered applicable for the manufacturing of precast rather than in-situ concrete elements, both for load-bearing and for architectural (cladding) elements (Quack, Van Roosbroeck, Den Hartog). In case of precasting, the assembly during the construction stage requires special attention due to the complex geometry and fitting.
- An integrated design-to-production 'file-to-factory' process using innovative tools for parametric design, panellization, structural analysis and construction stage are deemed essential, tailored on the project requirements (Diks, Van Roosbroeck, Den Hartog).

- New cement-based materials are mentioned as possibly very suitable in combination with the flexible mould: ECC, SCC, FRC, UHPC, concrete composites (Van Roosbroeck, Den Hartog, Ter Maten, Huyghe and Schoofs). Some sources mention that compaction through vibration of the concrete is not desirable in combination with the delicate system. Deformation after casting (Mitchell and McCullough, Huyghe and Schoofs, Raun) presumably gives better thickness control and reduces need for compaction. Prediction of the development of concrete fluidity then becomes important to choose the right moment of deformation (Huyghe and Schoofs). Also a first assumption regarding the parameters determining the strain in the fresh concrete is done (Huyghe and Schoofs). Other building materials, such as corrugated rubber-polyurethane sandwiches (Spuybroek) or fibre-reinforced gypsum or thermoplastics, (Raun et al, Mitchell and McCullough) are also mentioned.
- Various authors claim that the geometry and placing of the element edges need special attention; furthermore, surface segmentation is considered important, especially for load-bearing structures (Diks, Van Roosbroeck, Den Hartog, Huyghe and Schoofs, Raun). The accuracy of the shape needs to be measured and controlled mechanically or with laser (Quack).
- Most authors use the principle of an automatically adjustable pin-bed with a rubber-like interpolation surface. The adjustment is done by hydraulic or pneumatic actuators. Some authors discuss the characteristics of the interpolation layer on top of the pins (Mitchell and McCullough, Quack, Diks, Van Roosbroeck, Huyghe and Schoofs, Spuybroek, Raun), but no mathematical or mechanical models are found. Both the continuous surfaces, strips and more advanced layered systems are discussed as possible interpolation surface. Obviously, all sources agree that the tool should be reconfigurable after use. Multiple sources describe the need for accurate prediction of the mould elastic behaviour and kinetic behaviour and/or horizontal displacements (Huyghe and Schoofs), possibly leading to contradicting demands (Spuybroek). Dimpling or waviness is considered a potential risk of any system using a pin-bed, meaning that the pins in that case will be visible in the final product.
- As was also concluded from the patent research, some authors suggest the use of an intermediate material that is formed first before casting on that intermediate material. For this intermediate material a recyclable such as wax (Oesterle et al) or thermosetting plastic (Raun and Henriksen, 2014) could be used.
- Among the first to address the computational and kinetic complexity of a flexible mould are Michel and Knaack. They present a solution for these issues by a Rhino-model linked to a numeric solver, and for the mould surface present a clever stretching principle.

Only a limited number of sources could be found in which the use of a prototype of serious dimensions during the research was described in combination with a

cement-like material: Vollers & Rietbergen (and their students Schoofs and Huyghe) did various tests with a real prototype and produced multiple elements in various concrete mixtures. Adapa / Raun show, on their internet-pages, various elements that have been manufactured with their flexible mould. Finally, also Oesterle et al. describe the tests done in the EU-FP7 project TailorCrete. Theoretical underpinning of either the flexible mould mechanism, the deformation of concrete or the mechanics of the interpolation layer could however only be found in the work of Michel.

4.7 Conclusions of part I

The purpose of the chapters 2 to 4 was to obtain an overview of prior art, and identify areas in which progress can be made. Based on the presently available techniques for manufacturing free-form concrete elements, and on the patent and literature review, it is concluded that:

1. the flexible mould technology for application in building industry, and more specifically for precast concrete elements with double-curved geometry, is potentially viable and powerful, but still is experimental to a large extent;
2. the understanding of the flexible mould principle in terms of mechanics is still in development; only one researcher was found describing the principle in terms of validated models or rules;
3. models or rules are needed not only for the interpolating layer, but also for the use of concrete in combination with a flexible mould: deformation after casting is a principle which is quite alien to normal concrete practice.

The objective of the present thesis research as already described in section 1.4 therefore is considered relevant.

Part II

Double-curved elements for architectural applications

Chapter 5

Architectural examples and cases

5.1 Introduction

This chapter will provide border conditions by analysing a number of architectural cases in terms of geometrical aspects, e.g. building size, element thickness, curvature, radius, type of elements and potential to apply the flexible mould method. This analysis will render a bandwidth of control parameters that will be used to define the type of shapes for which the flexible mould method would be suitable.

5.2 Architectural designs using curvature

First, this section will show a selection of projects that clearly illustrate the use of curved concrete in architecture over the past 80 years. For each project a short description is given, e.g. span, type of material use, concrete dimensions or structural system (see Table 4.1 on the following pages). The overview demonstrates that the application of curvature can originate from many different reasons, such as structural, aesthetic or functional, and sometimes combines of all these three. The table could have easily been extended with multiple pages, since an abundant number of examples can be found in literature. From the buildings and their opening years, it is concluded that the application of double-curved concrete surfaces is neither a modern trend nor a trend that has diminished over time. Initially, shell designers sought for optimal structural performance by finding forms that would reduce bending moments and promote shell-action. The form-found shape then was generally also considered to be of aesthetic value.





Table 5.1 Selection of curved concrete structures in the last 80 years

year	project title, city, country (architect / structural engineer)	type of structure	image
1934	Algeciras Market Hall, Algeciras, Spain (arch. Manuel Sánchez Arcas / s.e. Eduardo Torroja)	thin concrete shell dome, diameter 47.6 m; thickness 10+ cm (Clark, 2012)	
1945	Storehouse (arch. / s.e. Pier Luigi Nervi)	18 mm thick ferrocement corrugated elements (Greco, 1995)	
1957	Táchira Club, Caracas, Venezuela (arch. Fruto Vivas / s.e. Eduardo Torroja)	thin free-form concrete shell, locally spans 32 m, thickness 10 cm (Escrig and Sánchez, 2005)	
1958	Chapel Lomas de Cuernavaca, Cuernavaca, Mexico (arch. Guillermo Rosell and Manuel Larrosa / s.e. Félix Candela)	Concrete hypar shell, top height 21 m, span 31 m, locally 4 cm thick (Garlock and Billington, 2008; Holzer et al., 2008)	
1959	Guggenheim Museum (arch. Frank Lloyd Wright)	concrete structure, curved parts consist of shotcrete on vertical formwork (Cohen, 1958)	
1962	TWA building Kennedy airport, New York (arch. Eero Saarinen)	connected free-form concrete shells, thickness 20-110 cm (Boothby and Rosson, 1998; Consiglieri and Consiglieri, 2010)	
1969	Sicli Building, Geneva (arch / s.e. Heinz Isler)	two connected thin shells, span 34.5 m (Schafer, 2012)	
1973	Sidney Opera House (arch. Jørn Utzon / s.e. Ove Arup)	roof cladding in precast 3 cm thick ferro-cement panels with stiffening ribs and ceramic tiles	
1977	Pavilion for Zentralverband Gartenbau, Bonn (arch Hans Luz und Partner / s.e. SBP)	hypar shells of 1.5 cm GRC shotcrete, repeated formwork (Mungan and Abel, 2011)	

Table 5.1 Selection of curved concrete structures in the last 80 years

year	project title, city, country (architect / structural engineer)	type of structure	image
1979	Tennis halls, Bern, Switzerland (arch / s.e. Heinz Isler)	connected thin concrete shells, span 34.5 m, thickness 9-10 cm+ (Isler, 1994; Chilton, 2000)	
1981	Badi Brugg, Switzerland (arch Gross und Hermann / s.e. Heinz Isler)	thin concrete shell spanning 35 x 35 m2, thickness 9 cm (Isler, 1994; Chilton, 2000)	
1987	Air Force Museum, Dübendorf, Switzerland (arch Gross und Hermann / s.e. Heinz Isler)	connected thin concrete shells spanning 51.7x18.6 m2 (Isler, 1994; Chilton, 2000)	
2000	Infosys Campus Bangalore (arch / s.e. Sundaram Architects)	hypar shells on repeated formwork 7.5-20 cm thick, span 20 m (www.builtexpressions.in)	
2003	Casar de Cáceres Bus Station (arch. Justo García Rubio)	curved continuous loop canopy, cast in-situ concrete	
2005	Magma Arte & Congressos, Adeje, Tenerife, Spain (arch. Fernando Menis)	concrete shell structure, folded landscape (Liu, 2007, page 56)	
2005	Kakamigahara Crematorium (arch. Toyo Ito)	concrete shell structure on wooden formwork (Mungan and Abel, 2011, page 22)	
2006	Mercedes-Benz Museum, Stuttgart, Germany (arch. UNStudio)	cast in-situ concrete structure featuring a double helix ramp connecting all floors (Liu, 2007, page 44)	
2008	Het Funen (NLArchitects)	residential building with cast in-situ single curved concrete roof (drawings from architect)	

Table 5.1 Selection of curved concrete structures in the last 80 years

year	project title, city, country (architect / structural engineer)	type of structure	image
2010	EPFL Rolex Learning Centre, Lausanne (arch. SANAA, s.e. Bollinger + Grohmann)	moderately curved concrete floor, cast in-situ on CNC-fabricated formwork (Weilandt et al., 2009)	
2012	Cidade da Cultura, Santiago de Compostella, Spain (arch. Peter Eisenman)	free-form curved landscape (www.cidadedacultura.org)	
2013	Heydar Aliyev Cultural Centre, Baku (arch. Zaha Hadid / s.e. Werner Sobek)	GFRC-panels on steel space-frame substructure	
2014	Fondation Louis Vuitton pour la Création (arch. Frank Gehry, s.e. RFR)	curved FRC tile cladding, by use of rubber moulds on EPS formwork (Martin-Saint-Léon et al., 2011)	

International design competitions such as the FEIDAD awards Liu (2003, 2007); Liu and Lim (2009) demonstrate that aesthetic value is still an important driving aspect in recent flourishing of non-orthogonal architecture. In cases where the concrete is used structurally, sufficient double curvature is required for proper shell-action, in order to transfer normal forces without buckling problems (Isler, 1994). However, the desire to have complete freedom of form can be conflicting with this structural law. This can be clearly observed in buildings that at first glance might seem to profit structurally from their shape, but after further study show to have made concessions like extreme concrete thickness (e.g. Rolex Learning Centre) or a clear division between structure and finishing (e.g. Fondation Louis Vuitton or Heydar Aliyev Cultural Centre). This division was already seen in the Sydney Opera House, and sometimes is a more economical solution than trying to integrate load-bearing and aesthetic function of the concrete. Furthermore, thin concrete shells as built in the middle decades of the last century are not built as frequently now as then, among others due to the changed proportion between labour and material costs in Western countries (see "*Are thin concrete shells dying out?*" in Mungan and Abel, 2011, p41).

In this thesis, both load-bearing elements and cladding elements are taken into consideration, but always based on a *precast* solution. For the cladding, precasting is a natural choice, since joints and seams are generally accepted in cladding. For a load-bearing structure, however, the notion of manufacturing precast parts that need to be assembled on site may conflict with structural issues. For small-span

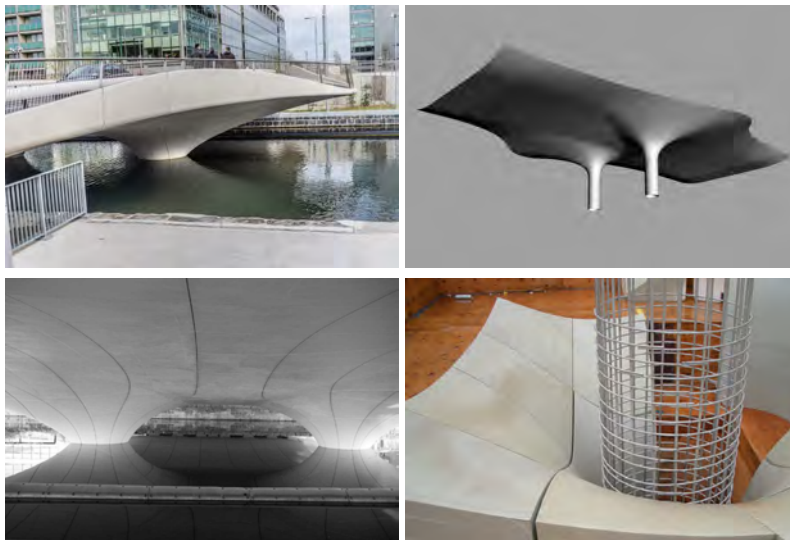


Figure 5.1: Spencer Dock Bridge, Dublin - clockwise, starting top left: overview photo, rendering of soffit surface and pillars, photo of milled formwork set-up with pillar rebar, photo of finished soffit surface with fluid lines accentuating its curvature (informatique / Nedcam)

buildings, such as the 1945 storehouse of Nervi, the use of precast load-bearing elements with repeating shape appeared a good choice. For large-span buildings though, subdivision of a large span in smaller segments might result in structural conflicts due to the thus introduced joints. In the following section, an illustration is given how for both the categories the application of precast double-curved concrete elements may be useful. This is done by looking in detail at a number of cases.

5.3 Overview of cases

5.3.1 Case 1 - Spencer Dock Bridge, Dublin, Northern Ireland

Spencer Dock Bridge: discussion of existing formwork system

The first case is not a building but an infrastructural object. This concrete bridge with a span of 40 m and a width of 25 m was completed around 2009 and built according to a design of Amanda Levete / Future Systems Architects. The bridge for pedestrians, cars and trams spans the Royal Canal in the docklands area and has a very soft and characteristic non-orthogonal shape, which is visible in the 'manta ray' shaped deck edges and the curved soffit of brightly coloured concrete that contrasts with the dark water surface, see Figure 5.1.

The formwork for the double-curved soffit surface was CNC-milled by the Dutch company Nedcam of EPS blocks directly from the 3D geometry files, and after that



Figure 5.2: Suggested use of thin precast concrete formwork planks for the Spencer Dock Bridge - for an impression of the scale: the element that is shifted from its place has a size of around 1.10 m at the shortest edge, 3.75 m at the opposite edge and a longest edge length of 6.40 m. The thickness in the drawing here was (arbitrarily) chosen as 5 cm. The curvature in two directions is visible.

finished with multiple layers of hot-spray poly-urea coating to obtain a smooth and sufficiently strong top surface. The curved formwork surface was divided in separate elements, both for transportation, manufacturing and architectural purposes. The fluid division lines in the surface were chosen in dialogue with the architect, and contribute to the accentuation of the curvature. The coated EPS blocks around the pillars locally had to support relatively high concrete pressures due to the increasing deck thickness at that point, as well as local point loads on the mould surface from the supports of the heavy rebar system.

The bridge's soffit surface has the strongest curvature around both pillars, that have a radius of 0.75 m (diameter 1.5 m) at the circular section leading to the foundation. In the plane perpendicular to these circles, the radius varies from around 1.50 m around the point where the circular section starts widening up to several meters at further distance from the pillars. Around both bank supports, locally a radius of 0.3 m was applied. Most of the soffit surface is double-curved, resulting in a non-zero Gaussian curvature.

Spencer Dock Bridge: alternative formwork system

If the same bridge were to be constructed using an alternative formwork system in which the EPS blocks would be replaced by thin stay-in-place double-curved precast concrete elements, a situation as sketched in Figure 5.2 could be obtained. After divi-

sion of the surface into smaller segments, these segments, given a certain thickness in the same range as traditional flat plank floors, like 5 to 7 cm, and strengthened with sufficient reinforcement, could be used as formwork panels. These formwork panels then at the same time form the aesthetic outer shell of the bridge, and also - as true formwork - provide sufficient strength to carry the full weight of the thick cast in-situ concrete layer of the bridge deck and its reinforcement. The thin precast panels, in their turn, would also need to be supported by a dense scaffolding system, as was the case in the original solution where the EPS blocks also were supported. The use of thin GFRP panels as permanent formwork was investigated earlier by Kim et al. (2010).

5.3.2 Case 2 - EPFL Rolex Learning Centre, Lausanne

Rolex Learning Centre: discussion of existing formwork system

The second case that will be discussed in more detail is the Rolex Learning Centre for the EPFL in Lausanne by architect SANAA, see Figure 5.3. In Weilandt et al. (2009), the structural engineers give a detailed description of the formwork system used:

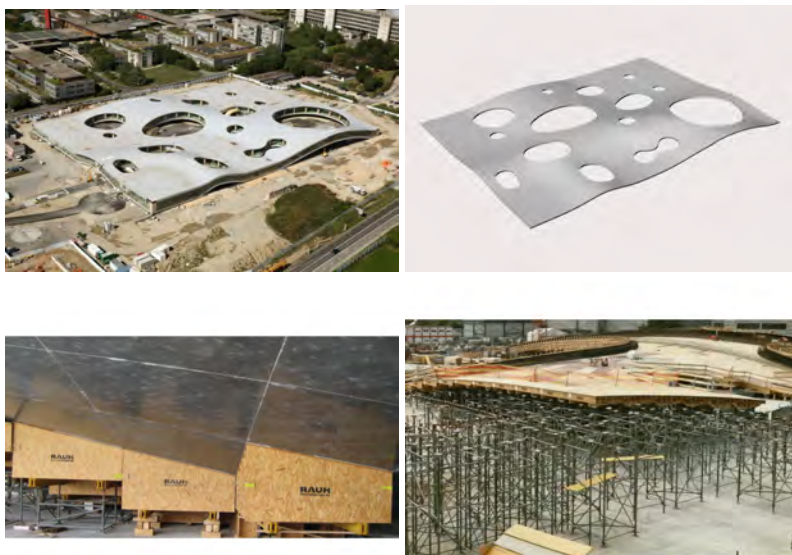


Figure 5.3: Rolex Learning Centre, EPFL, Lausanne - clockwise starting top left: the building as it was under construction around 2010; the curved CAD geometry of the concrete ground floor with a thickness of around 80 cm; the scaffolding system consisting of props and customized timber tables; a detail of the tables and the concrete surface after de-shuttering (images: wikipedia, RS, Weilandt et al., 2009, Dennis Cheung)

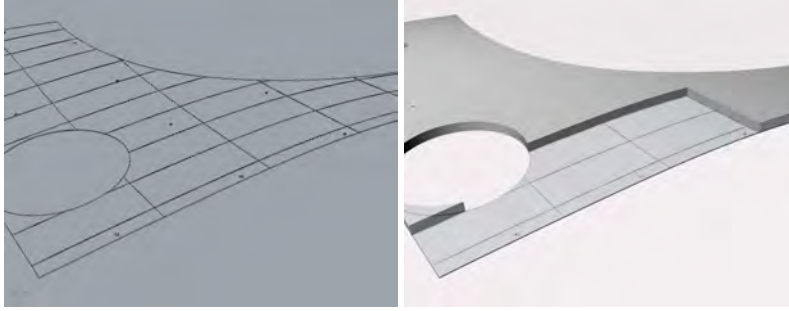


Figure 5.4: Rolex Learning Centre, EPFL, Lausanne - Alternative solution with stay-in-place concrete planks as formwork (left) with cast in-situ top layer (right); shown is a possible panelisation in transportable units of the curved precast formwork planks; each element has a size of around $8 \times 3.4 \text{ m}^2$ (RS, after Moiralis, 2013).

"The formwork was prefabricated in factory by $2.50 \times 2.50 \text{ m}$ formwork tables." ... "Each of these tables consisted of two wooden base beams on which 7 OSB plates were fixed. The lower edge of these plates was horizontal while the upper edge followed the contour lines of the formwork surface. The formwork surface itself consisted of 10 cm wide wooden planks and a laminated chipboard panel subsequently nailed on these plates".

The curvature has a different scale than the Spencer Dock Bridge: for the Rolex Learning Centre the smallest radius is around 45 m. Yet, transformation to flat elements would have visibly resulted in kink angles and loss of aesthetic quality. Therefore, in order to give each of the nearly 1500 formwork tables the correct curvature and to be able to assemble them in the correct order at the building site, the process was programmed to automatically CNC-cut each table. Each of the thus manufactured formwork tables was supported by standard scaffolding towers with different heights (Scheurer, 2010). The tables had to be able to withstand - without unacceptable deformation - a formwork pressure equal to about 80 cm of concrete (around 20 kN/m^2) plus point loads of heavy reinforcement bars. A smooth surface finish was required, although it was allowed to have the pattern of formwork visible in the concrete surface after de-shuttering. After de-shuttering, the customized tables could only be reused as waste or - in the best case - as biomass, although OSB and chip-wood may contain chemical glues. The scaffolding towers, being standard equipment, were completely reusable in other projects.

Rolex Learning Centre: alternative formwork system

An alternative formwork method might have consisted of around 5 cm thick stay-in-place concrete planks with sufficient load-bearing capacity and stiffness to transfer the weight of the cast-in-situ top layer and the reinforcement to the scaffolding

towers. The concrete planks in that case would then have already formed the final soffit surface of the floor and would have formed the basis for placing of reinforcement nets, ducts, etc., much similar to the existing practice of precast plank floors in Europe. Figure 5.4 on the preceding page shows the proposed precast and in-situ layers for a fragment of the floor area, which are slightly double-curved.

The precast elements would always need to have modest dimensions that allow transportation by truck (here chosen 8×3.4 m), which implies that the structural span of the shell for this building would be larger than the length of a single precast element. The consequence of this is that the precast element cannot have a structural function, but will merely be used as replacement of the timber formwork, but with this advantage that it can stay-in-place (reducing waste) and that its surface finish is of high quality. Disadvantages could consist of the reduced height available for the shell reinforcement (namely $80 - 5 = 75$ cm), leading to a lower lever arm, and of the more complex temporary connection between scaffolding towers and the precast concrete planks in comparison to the straight lower edges of the wooden formwork tables that were used in the original solution. These disadvantages and their possible solutions will not be further investigated in this thesis, where the feasibility of manufacturing thin double-curved concrete precast planks is the prime focus.

5.3.3 Case 3 - Precast concrete shell, Mysore, India

Mysore shell: discussion of existing formwork system

The third case is a shell structure. Figure 5.5 shows a sketch-design for this planned shell structure in Mysore (India), having spans of approximately 48×60 m and a height just over 21 m. Since the building has not been constructed yet and is still in an early stage of development, no formwork system has been chosen yet. Generally, for this type of shell structures, the traditional way of scaffolding, shuttering and concreting is applied, as was already discussed in subsection 2.2.1 and is also described in a.o. Isler (1994). For countries such as India where labour costs are still relatively

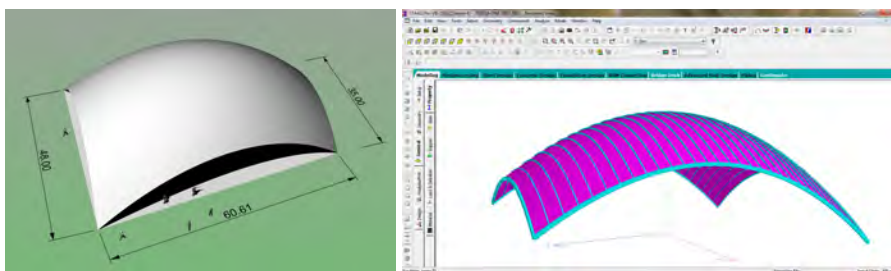


Figure 5.5: left: sketch design for a shell in Mysore, India (RS, after R. Sundaram) - right: possible subdivision in precast elements (R. Sundaram)

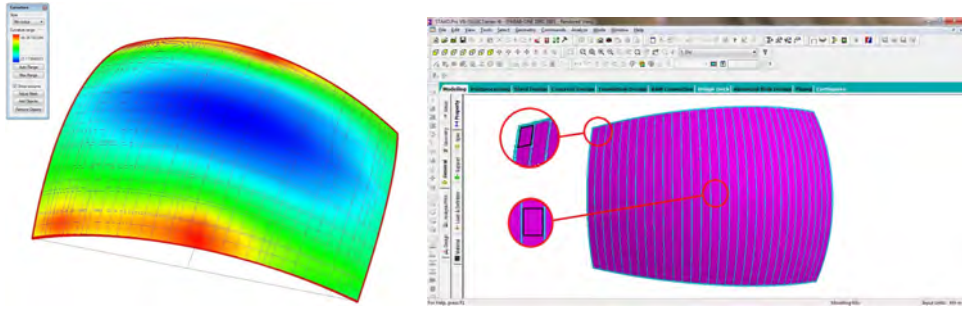


Figure 5.6: Shape of the elements in terms of curvature (left) and contours (right; RS after R. Sundaram)

low in comparison to material costs, this traditional approach will still be feasible. But, as was already stated in subsection 2.2.1, highly skilled carpenters are needed on the site, and also the placing of reinforcement and concrete requires a sufficient amount of craftsmanship. An alternative technology could be the precasting of smaller elements and joining these on site to one structurally integrated shell.

Mysore shell: precast elements as alternative solution

In such an alternative approach, the designers of the shell at Sundaram Architects investigated the possibility to divide the shell into precast segments, as shown in the right image in Figure 5.5. Here the ribs (in blue) form the division of the shell surface (in purple) into lanes of double-curved elements that can be prefabricated. This would require a solution to obtain sufficient coherence in the connections. These connections need to be sufficiently strong and stiff, in order not to disturb the shell-action and introduce new buckling problems. Studying this is outside the scope of the present work. However, Hartog (2008) and Ter Maten (2011) investigated the general possibilities to build shells out of precast elements, and were positive about the idea. Apart from the above-mentioned obstacles, they both identified the limited repetition of the formwork. This could be addressed by the use of a flexible mould system as studied in the present thesis.

The minimal curvature radius of the shell is approximately 43 m in the longest span direction and 23 m in the shortest span direction (curvature analysis in Figure 5.6). Although in some points of the shell the (variation of) curvature is relatively limited, the contour shape of the elements is varying for more or less rectangular in the middle to parallelogram- or diamond-shape near the support points of the shell. The flexible mould would need to accommodate this variation in curvature and edge contours.

5.3.4 Case 4 - Heydar Aliyev Cultural Centre, Baku

Cultural Centre: discussion of existing formwork system

The fourth case to be discussed as example of one where the flexible mould technology could have offered an alternative solution is the recently completed Heydar Aliyev Cultural Centre in Baku, Azerbaijan. The project, designed by Zaha Hadid Architects, was already shown earlier in this thesis in Figure 1.1 on page 4. In this iconic building, the double-curved façade elements do not have a structural function, since a steel space frame underneath the panels is forming the substructure.

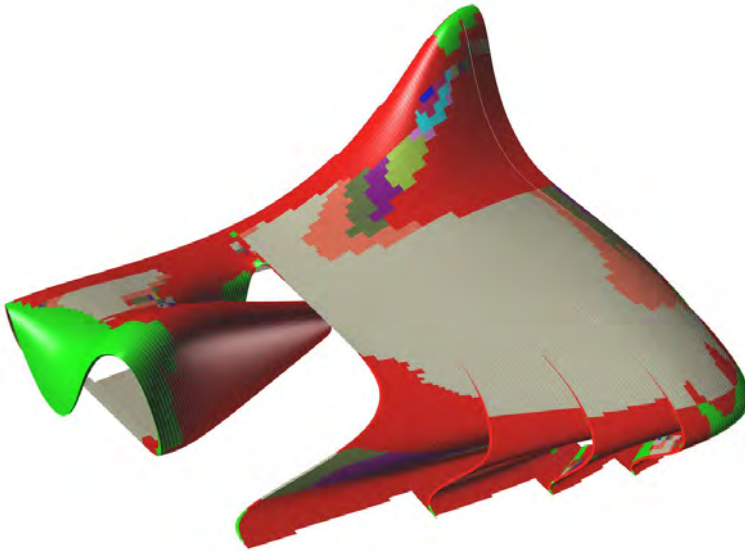


Figure 5.7: Panellisation of Heydar Aliyev Cultural Centre, colours indicating various degrees of curvature such as flat, single-curved, double-curved (Zaha Hadid Architects)

In an interview with the responsible project manager of Werner Sobek, Thomas Winterstetter, the following details are given on the manufacturing and fixing of the cladding panels (Dispenza, 2011):

"Glass fibre reinforced plastics (GFRP) and glass fibre reinforced concrete (GFRC) panels are the predominant materials used in the façade system. The panels are composed of various layers of fine-grain high-performance white cement concrete, reinforced with fibre glass mats. It's a very durable and resistive material¹ which can be made very thin, only a few mm or cm, because there is no concrete cover needed, like for steel reinforcements. By eliminating the need for steel reinforcing, the panels offer a lightweight construction method, and they can be individually

¹some remarks on durability of glass fibre can be found on page 217

moulded to form the curved shapes required by the design². The panels are cast into customized single-use mould. These moulds are partly from CNC-cut 2D ribs (like a boat's hull) and partly from 3D-milled Styrofoam blocks. Werner Sobek had to generate all of the production information associated with the exterior panels, so that they could be manufactured, then shipped to the site for installation by local workers. On site, each panel is lifted by crane, then negotiated into position by hand (which is possible due to the product's light weight). The panels are screwed to fittings on a previously installed metal substructure. There are about 15,000 panels, each with an individual curved geometry, in sizes up to a maximum of 1.5 m wide and 7 m long, none equal to another one. There are 40,000 m of 3D computer-generated substructure metal tubes underneath the panels, no tube equal to another one, perfectly matching the panels and their fixing positions."

Curvature analysis of the model of the building shows that some parts of the envelope surface are strongly double-curved, for example the areas indicated with bright-green in Figure 5.7. As far as could be derived from available drawings, these elements have a smallest radius of approximately 12.5 m in one direction and 2.20 m in the perpendicular direction. Other elements with stronger curvature have a radius of approximately 1.35 m in one direction, but are almost linear in the other direction. Figure 5.7 also indicates that substantial parts of the building could be covered with flat panels (the grey areas) or single-curved panels (the red areas), which are less expensive to manufacture and were acceptable from an architectural point of view.

The position of the seams and the rationalisation of the various categories of panels were a major point of attention during the design. As the subdivision into smaller panels is necessary for manufacturing, transportation and assembly, the seams were intentionally used to emphasize the shape of the building and give a better understanding of the project's scale to visitors. This has made the seams an essential element in the design (Bekiroglu, 2010).

Cultural Centre: alternative formwork solution

The flexible mould method could have been used here to reduce the number of necessary CNC-milled moulds, thus possibly reducing the project costs. The technology of reinforcing with glass-fibre fits well in the flexible mould method, as will be demonstrated later in the present work. It is not to be expected that 100% of the curved elements would or should be made on the flexible mould, as especially the most strongly curved elements impose severe demands on the moulds flexibility. In some cases, CNC-milling of some extremely shaped panels might be less expensive than designing a flexible mould according to these extreme specifications. So even here, a rational approach is always needed. However, a large portion of the single- or moderately double-curved elements could have been manufactured with a flex-

²*water-tightness was reached by a closed foil in a cavity underneath the panels*

ible mould, to our expectation. For now, the radii as described above give a good indication of what the flexible mould should be capable of.

5.3.5 Case 5 - Metro stations for new Crossrail-line London

Crossrail: discussion of existing formwork system

The fifth and final case that will be discussed here are two subway stations for the new Crossrail line in London. For these stations, that are presently under construction in London, a clear idea exists for the desired interior finishing: a smoothly curved cladding that connects the various tubes is shown in the mock-up that was built to communicate the envisioned image (see Figure 5.8). That the elements are double-curved is clearly emphasized by the pattern of the panel seams. The large tube has a radius of 4,48 m; the smaller tube 2,72 m, and the fillet between the tubes 1,25 m. Presently, the idea is to use a CNC-milled formwork system with sprayed concrete (the formwork shown earlier in the utmost right image Figure 2.3 on page 13).

Although the available data of the project is limited, the use of sprayed concrete on CNC-milled formwork is expected to lead to high amounts of waste material, since especially in the areas where the new metro tube is connected to passenger tunnels leading to other tunnels and station buildings, many customized shapes will be present, having limited repetition.

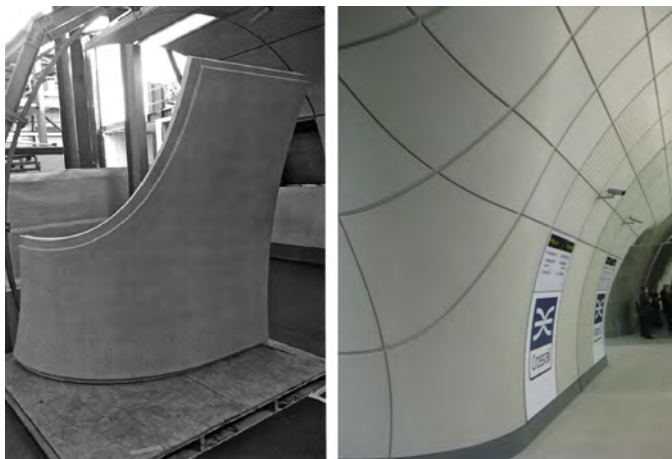


Figure 5.8: Double-curved interior cladding panels in a mock-up for the new Crossrail Line in London (Bull, 2011)

Crossrail: alternative formwork solution

If it would be possible to reduce the amount of CNC-milled formwork, a substantial cost cut-down could possibly be achieved. The flexible mould could be a solution for

this, if it will be able to deliver the sometimes strongly curved shapes with sufficient accuracy and also with the proper concrete quality. Another choice could be, as discussed above, to still manufacture the most extremely curved elements on milled formwork, and use the flexible mould to bridge the production gap between milled formwork and flat or single-curved panels.

5.4 Discussion

The previous sections have given insight in the type of architecture that could benefit from a production method incorporating the flexible mould method. Some preliminary conclusions:

- through the last 80 years, the use of curved architecture has sustained; nowadays, the structurally optimized shapes of the early famous shell designers, however, have mostly, though not exclusively, made place for free-form designs in which parametric design or random shapes are introduced; this is greatly facilitated by the availability of 3D CAD and FEM software;
- whereas traditional concrete shells were mostly constructed using timber formwork, for non-repeating double-curved elements CNC-milled formwork is the method used most nowadays; the material that is milled can be a.o. EPS foam or timber;
- materials that are used for the elements are traditional steel reinforced concrete, ferrocement, sprayed concrete or GFRP; in one case GFRP is mentioned;
- the radius of the curvature in the found examples varies between 0.75 m and 45 m; in many cases curvature in one direction was (much) stronger than in the other direction; this could have implications for the flexible mould; in various projects a curvature analysis was done to categorize the elements in flat, single-curved and double-curved;
- in larger projects, the number of elements that needs to be produced is generally in the order of hundreds to even many thousands; this requires an efficient production strategy and capacity; although not all of these elements have a complex shape, even the high costs of a small percentage of the panels can make a project very expensive;
- the fact that precasting technology requires a subdivision into smaller and transportable elements is not necessarily a disadvantage from an architectural point of view: in various examples the seams between the panels are used by the architect to emphasize the curved shape, and have become an essential part of the design;
- not only the radius offers challenges, also the position of the edges: the contours of many elements are irregular, having curved or diamond-shaped edges; this needs to be addressed by the manufacturing method;

- distinction can be made between
 - load-bearing elements, spanning larger distances, sometimes carrying floors of large live loads
 - (thin) cladding panels, carrying mainly self-weight, wind-load, snow, etc.

this distinction may be gradual, as can be seen in the situation where the thin panel is used as stay-in-place formwork for thicker concrete floors or shells.

These preliminary conclusions will help to get a general idea of the border conditions for the manufacturing method that will be developed. It makes sense to aim for thin cladding panels, precast plank floors and possibly also other products that can be manufactured with a flexible mould.

Chapter 6

CAD, CAM and complex geometry

6.1 Introduction

This chapter will be a qualitative study that discusses the mathematical aspects of the drafting and manufacturing process. This is done by reviewing closely the methods of shape definition in current CAD software, and by discussing a number of recent developments in the panellisation of curved surfaces into discrete elements.

6.2 Principles

6.2.1 Shape description

The production of any curved building element starts with the specification of the three-dimensional geometry of the building. Whereas traditional form-finding methods as applied by for example Antoni Gaudi or Heinz Isler would lead to a physical scale-model that was reproduced on full scale at the building site, nowadays software is used for shape description. Even a modern architect like Frank Gehry, that in the initial sketch design stage still prefers to work with physical models, will have his model transferred to a software environment early in the design process for further shape description, engineering and construction. Generally, a surface model is obtained that describes the envelope surfaces of the building and subdivision in various rooms. An example of such a model that will also be used in the remainder of this thesis is shown in Figure 6.1 on the next page. It was provided by the Austrian firm Evolute, and represents a typical shape of a free-form building comparable to the cases described earlier in section 5.3. Before we discuss the subdivision into smaller elements as shown in the right part of the image, let's first look at the geometrical primitives used to describe free-form shapes.

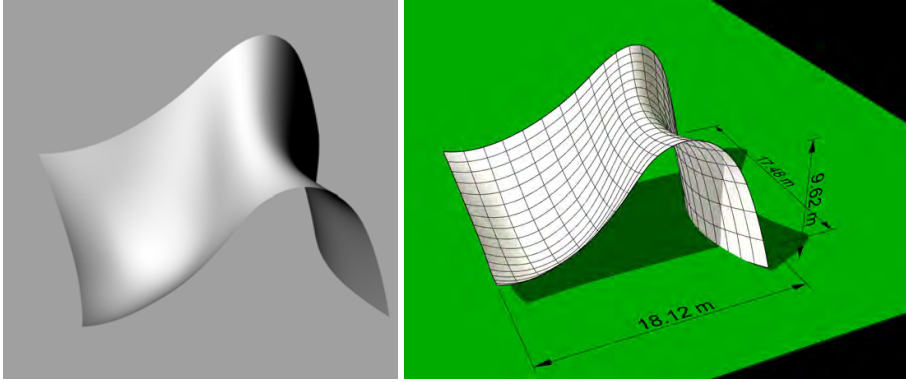


Figure 6.1: Surface model of a virtual building envelope and possible subdivision in smaller elements that can be prefabricated (Evolute)

6.2.2 Splines

The description of the shapes of curves and curved surfaces in CAD drawings is usually performed through the definition of some variant of *splines*. Although nowadays the word is almost directly associated with computer drawing, it is interesting to briefly go back to the use of splines in their original context: the making of hand drawings in e.g. ship, air-plane and automotive engineering.

Splines (see Figure 6.2) are thin flexible rods, fixed in position on the drawing board by small weights connected to these rods. The splines were (and sometimes still are) used by draughtsmen for drawing smooth free-form curves by hand. It is not difficult to understand why the spline was also introduced as a tool in CAD software: some smooth shapes cannot be defined by a circle, ellipse or hyperbola, and require some other sort of a numerically constructed curve. In 1959 and 1962 respectively, the Frenchmen Paul de Casteljau and Pierre Bézier worked independently on the same mathematical algorithm (Pottmann et al., 2007) to construct a curve from a number of control points. With control points we mean that the curve follows a number of predefined points, such as points that define the contour of a road, ship or car: by moving the points, the curve follows. The control points can be compared to the weights in the traditional analogue splines. The analogy between

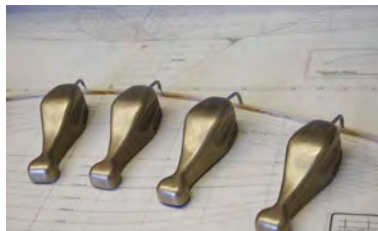


Figure 6.2: Splines for ship design

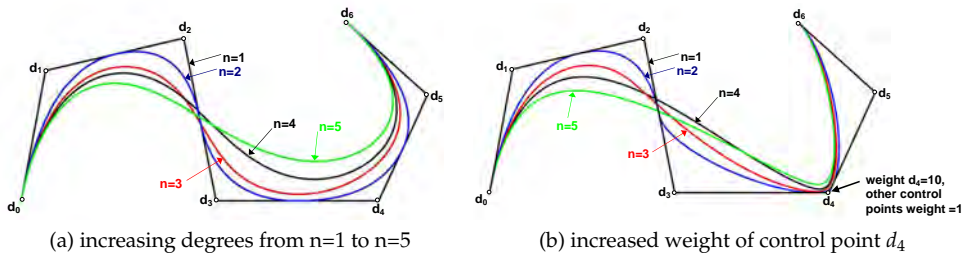


Figure 6.3: NURBS-curves

manipulating a spline and manipulating a flexible mould surface is striking, and will be investigated later in this thesis.

6.2.3 NURBS-curves, point control and NURBS-surfaces

In modern CAD software, curves are usually drawn with a digital and more enhanced version of splines: Non-uniform rational B-splines (abbreviated *NURBS*). These are primitives that can describe virtually any curvature by interpolation and weighing of a number of control points. The higher the *degree* of the NURBS-curve, the more complex and smooth the shape can be (higher order polynomial). NURBS-curves offer far more user control than the traditional spline, since they have the following properties:

1. NURBS are *subdivided* in several shorter curves to allow more complex shapes. The subdivision in smaller segments enables the user to make complex curves with curvature into different directions and radii (also out-of-plane).
2. The *degree* of the curve defines the extent up to which interpolation between control points takes place: the higher the degree, the more control points are included in the calculation of the coordinates of a certain point on the curve. In terms of mathematics: a curve with a degree 2 is defined by a quadratic polynomial (parabola); a curve with a degree 3 is defined by a cubic polynomial, and so on (Figure 6.3a).
3. A *knot vector* is defined to collect the knots where the different curves are joined, allowing for a smooth connection from one curve segment to the following.
4. NURBS offer the possibility to add *weight* to each control point, making some control points “more important” than others (Figure 6.3b).

It is important to notice that these increased control possibilities for digital curves as compared to the traditional spline-tool cause some difficulties as soon as one tries to translate digital shapes back to the analogue shape of a flexible mould: the first simple observation that can be made is that, for example, the control points of the

NURBS-curve in Figure 6.3 are only laying *on* the curve itself in the endpoints and one intermediate point. Whereas the profile of the traditional analogue spline is controlled by a number of small weights that hold it in place on the drawing board, simply translating control points of the curve into position of the actuators of the flexible formwork does not work. Furthermore sharp turns (called “bumps”, “loops” or “cusps”) will be difficult to realize using a flexible formwork: the radius near control point d_4 , for example, is so small that an average elastic formwork would probably break at this point. For the drawing of very sharp curves, it is obvious that the rod of the spline has to be more flexible than for curves with a big radius. This relation is also apparent in the flexible mould: the choice of the stiffness or elasticity depends on the amount of curvature one wants to reach. We will look at the consequences of this observation later.

So far, only linear CAD elements have been discussed. A collection of NURBS-curves or points in 3D space can be used to generate a NURBS-surface. Basically, each point at the surface is determined mathematically by interpolating between the describing curves or points (Béchet et al., 2013, lecture 6). NURBS-surfaces can be used to describe building geometries in an accurate and efficient manner, and due to their mathematical definition make it possible to perform geometrical manipulations, such as determining intersections, extruding, trimming, and so on. This makes NURBS-surfaces the most used primitives in modelling of complex geometries in architecture and other industries.

6.2.4 Curvature of surfaces

The curvature of a surface is a geometrical variable defined by the radii in two directions R_x and R_y (for double-curved elements) or by their reciprocal value κ (kappa), which are defined for the x- and y-direction as

$$\kappa_x = -\frac{d^2w}{dx^2} = \frac{1}{R_x} \quad (6.1)$$

and

$$\kappa_y = -\frac{d^2w}{dy^2} = \frac{1}{R_y}, \quad (6.2)$$

where:	κ_x, κ_y	curvature along x- and y-axis	m^{-1}
	w	coordinate of surface on z-axis	m
	R_x, R_y	radius of curvature along x- and y-axis	m

For double-curved elements also the so-called ‘Gaussian curvature’ Gauss (1827)

$$K = \kappa_1 \cdot \kappa_2 \quad (6.3)$$

is relevant, being the product of the two principle curvatures in perpendicular directions 1 and 2 and having the unit $[m^{-2}]$. A positive Gaussian curvature of a double-curved surface is found at locations where this surface has the centre of the

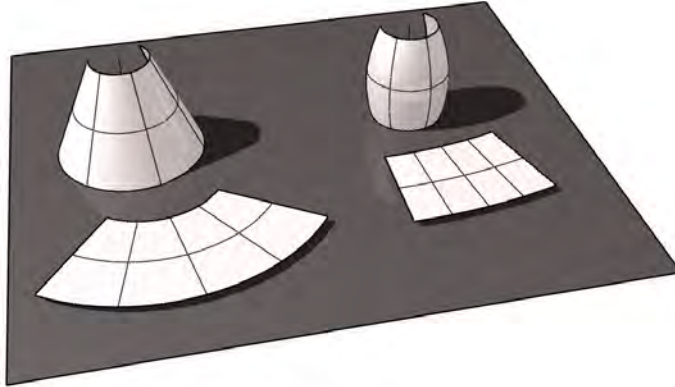


Figure 6.4: Left: Gaussian curvature = 0; right: Gaussian curvature $\neq 0$; the truncated cone in the left image can simply be manufactured by folding a flat piece of material; in the right image however, the flat piece of material will not lead to the barrel-like shape without local in-plane distortion

radii of both principle curvature directions on the same side of the surface (e.g. in a parabolic or sphere-shaped surface). A negative Gaussian curvature is found at a location of a surface where the centres of curvature are at opposite sides of the surface (e.g. in a hyperbolic or saddle-shaped surface). If the Gaussian curvature is zero, the surface is only curved in one direction, a single-curved surface, or it is a flat surface (Pottmann et al., 2007). The Gaussian curvature has great importance for manufacturing processes, as single-curved surfaces can be bent or folded from a flat piece of material without any in-plane strains, whereas double-curved surfaces cannot be formed without in-plane shear-strains and/or normal-strains (see Figure 6.4). In subsection 6.5.2 this will be discussed further.

6.3 Recent developments in software algorithms

6.3.1 Surface subdivision or panelling

The NURBS-surfaces that define the building shape generally will have to be subdivided into smaller elements in order to allow manufacturing. This subdivision process is also referred to as *panelling*. The position and size of the seams between elements is influenced by both technical and architectural considerations, as was already discussed in Chapter 5. Given a chosen pattern of seams, the mathematical subdivision of the larger NURBS-surface into a collection of smaller discrete NURBS-surfaces is done by software. These smaller surfaces will be further called *elements* or *panels* here. After analysis of the curvature of each item in this collection of elements, generally the following types can be discriminated:

- planar (flat, not curved)
- cylindrical (single curved, constant radius)
- parabolic (single curved, variable radius)
- torus (double-curved, two constant radii)
- cubic (double-curved, variable radii)

In the work of Eigensatz et al. (2010), it was recognized that the manufacturing costs per element generally are increasing significantly in the order of the above list, due to the increasingly complex manufacturing method that is needed. Since many building materials are shaped by first making a mould (or *mold*), the manufacturing costs for a series of panels in a specific shape are the summation of the price per individual panel plus the price per mould needed to produce this panel. Depending on the building material, the costs of one mould will, in general, be significantly higher than the cost of an individual panel. This principle is a well-known fact in precast concrete design: steel formworks are relatively expensive, and are only feasible in case of sufficient repetition. For complex geometry, due to the very limited repetition, this results in an optimisation process, also referred to in literature as *rationalisation*. In the next subsection some aspects of this rationalisation are discussed.

6.3.2 Mould depots and rationalisation

In the work of Eigensatz et al. a *mould depot* is defined, in which a reduced number of moulds for each panel type is used, together enough to enable the production of the complete series of panels for a specific building project. Two computational techniques can help to facilitate the process of recognizing similar shapes in a large number of different elements present in a building of reasonable size (typically several hundreds):

1. *finding congruency*: by first grouping elements that are geometrically defined by similar parameters, classes of similar shapes can be defined. Within each class,

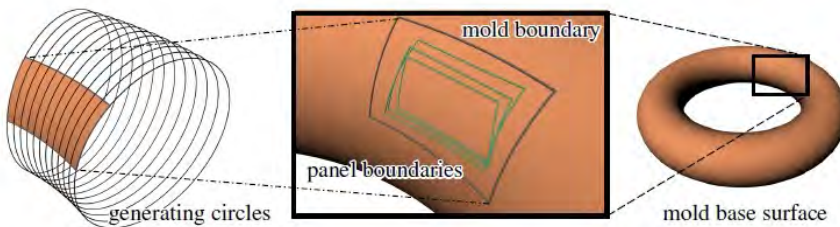


Figure 6.5: image from Eigensatz (2010) showing the grouping of elements with a similar torus-based shape (taken from Ceccato et al., 2010)

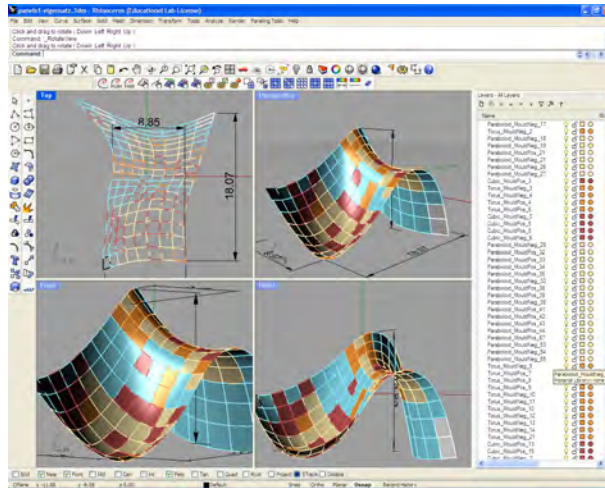


Figure 6.6: Example of panelisation and curvature analysis of the shape shown earlier in Figure 6.1: 144 panels have been assigned to 119 moulds depending on the accepted tolerances, the number of moulds will increase (Evolute)

parameter variation is still allowed, but restricted to a limited number of variations. Although the edge position might differ for each element in the same congruent class and with the same curvature parameters, these elements can still be manufactured on the same mould, by repositioning the edge profiles (see Figure 6.5).

2. *optimizing panel shape if no exact congruency can be found*: since technique 1. could still lead to a large number of classes or instances within classes (all containing 1 unique element), rationalisation is necessary: by building classes of sufficiently distinctive shapes, and for each necessary shape finding the mould that closely approximates the desired shape of the original design, the number of necessary moulds in the bank can be reduced drastically. As long as the divergence between the intended shape and the rationalized approximating shape is sufficiently small, it can hardly be observed by eye, leading to an architecturally acceptable solution for significantly less costs.

Both techniques will be illustrated now, using the virtual building shape shown earlier in Figure 6.1 on page 76, using the proposed division curves between 144 panels shown in the right image in that figure. Assume that these proposed curves are an architectural choice, based on aesthetics. The calculated mould assignment of this shape is shown in Figure 6.6. The colours in the image represent the five types from the list presented above; within each type also the variation in radius parameters is identified. Almost 83% of the panels (119 out of 144) apparently need a unique mould surface, illustrating the very limited repetition.

The question now is, how this large variation in panels can be reduced and repetition increased? Advanced algorithms to guide this computational process have been developed in recent years by various research-groups. Eigensatz et al. worked on advanced mathematical algorithms to help reduce costs by exchanging more expensive panel types for less expensive ones, without unacceptably compromising the aesthetics of the building. In this optimization process a trade-off is made between costs and accuracy, by defining allowable discrepancies between the 'real' surface and the 'approximated' surface. The kink angle between panels, the allowable divergence between panel edges and also the position in the building of a specific panel are taken into account, as well as the manufacturing costs per category. The optimisation algorithm will produce a 'best fit' based on the pre-specified tolerances. This appears to be a very effective strategy to reduce the total panelling costs. This work has been implemented in Evolute Tools, software from the Vienna-based firm Evolute.

Another firm, Gehry Technologies, is working on the software framework 'Euclid' to efficiently deal with the computational tasks related to complex geometry, using cloud computing to enable the processing of large amounts of data (Witt and Boyer, 2013).

6.4 Towards a full mass-customized production

6.4.1 Large scale free-form asks for mass-customisation

The larger the building, and the less repetition the geometry shows, the less milling or hotwire-cutting of moulds become a suitable solution. Scale and size matter (Scheurer, 2009), as can be understood from the path length the milling head or wire has to travel to produce an object: if the size of a three-dimensional object doubles in all directions, the one-way travel distance and production time will at least double, while the amount of waste, the material that is subtracted from the original blocks that are milled, increases with a factor $2^3 = 8$. For this reason, CNC-milling in large buildings can only be used economically after profound simplification and rationalisation, leading to a situation in which moulds can be applied more than once, for example by the use of a mould depot, as was explained earlier. Otherwise, the building will, in the worst case, be manufactured twice: once in foam moulds, and once in concrete.

As was also concluded earlier from literature and patents, a solution fundamentally different from simplification and rationalisation is *reconfigurability* of the moulds: if more panel types could be manufactured with the use of one flexible and reconfigurable mould system, a mould depot would become superfluous. Reconfigurability can lead to a smaller cost difference between different types, leading to lower building costs. Ultimately, the geometrical difference between panel types might become unimportant, which would also take away the constraints in the rationalisation process, ending in a full mass-customized production. However, as

was concluded from the literature review in Chapter 2, to be able to profit from a cost benefit of a reconfigurable mould, the amount of manual labour and materials necessary for the reconfiguration then have to be kept to an *absolute minimum*. Despite all the interesting technical challenges, this consciousness should be present during all steps of the further development of the flexible mould method.

6.4.2 Sketch of the proposed method

Reconfigurability will lead to a number of challenges in terms of geometrical adaptation of the mould: both the mould's surface shape as well as the position and shape of the edges need to be adaptable. Even the position of anchors, cut-outs, desired surface texture, etc. can change from panel to panel. As with CNC-controlled foam mould milling, the proposed reconfigurable mould is expected to be highly dependent on digital technology, such as 3D-computation, laser-projection, CNC-actuators and the like. Yet, keeping in mind the costs, a simple solution should be strived after, in order to arrive at the desired cost cut-down. Figure 6.7 on the next page shows a sketch of a possible manufacturing line: (1) each empty flexible mould is cleaned and oiled (2) controlled digitally, the pins supporting the flexible formwork are set to the proper height for each panel (3) the mould edges are fixed (4) the panel is cast when the panel is still in horizontal position (5) the panel is deformed into the shape prepared in step 2 and 3 (6) each panel needs hardening time (7) the panels are demoulded and (8) packaged.

A number of aspects characterize the proposed method:

1. Multiple flexible moulds will be necessary to allow a sufficiently fast production, as concrete hardening and preparation of each casting session requires time;
2. Each mould has a separate pin-bed and interpolation layer; these two components are kept as simple as possible;
3. In the proposed method, step 2 and 3 are the only steps in the process that are fully or partially supported by CNC-technology, whereas the other steps rely on mechanical steps that can - but not necessarily need to - be automatised or mechanized.

The mechanical engineering of the flexible mould will be discussed later in Chapter 7. At first, some geometrical issues will be discussed that are related to step 5, the deformation from flat to curved, which is a less trivial step than might be expected at first glance.

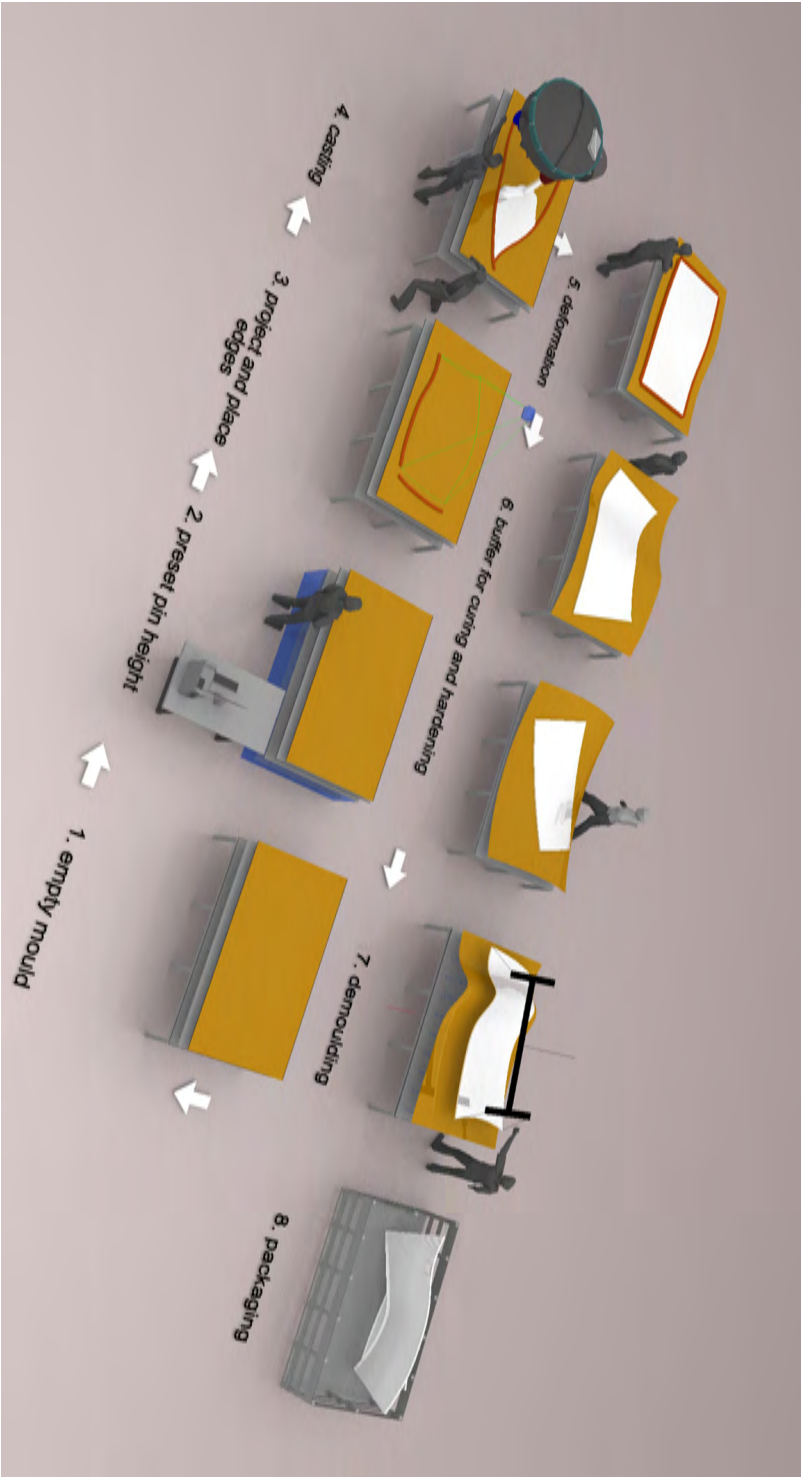


Figure 6.7: Possible manufacturing line for mass-customized production (patent pending) for double-curved precast concrete panels

6.5 Geometrical issues in this method

6.5.1 Introduction

In step 5 of the manufacturing method described above, the concrete is deformed from flat into curved after casting; this has several advantages that were already discussed earlier in Chapter 2 and 3. It was also concluded from these chapters that this transformation needs to be executed following an accurate method that results in exactly the desired shape. In patents and literature, however, no model or calculation method was found to cover this aspect. During the earlier attempts of Rietbergen and Vollers and Schoofs and Huyghe, it was already experienced (see page 48) that without sufficient understanding of this process, it will not be possible to produce accurately shaped elements. Therefore, an attempt is now done to describe this transformation more accurately.

6.5.2 Developable or non-developable surfaces

The transformation of a flat surface into a curved surface, after studying background literature, appears to be fundamentally different for developable curved surfaces and non-developable curved surfaces Pottmann et al. (2007, p533):

Developable curved surfaces

Developable curved surfaces are surfaces that are curved, but can be formed from a flat material without any in-plane strain or compression. For example: a cone shape can be formed from a sheet of paper by simply rolling it, but a barrel shape can not (see Figure 6.4 on page 79). In relation to the flexible mould process this could be understood as a situation in which, with very limited force, the desired shape can be obtained by simply bending or twisting the surface into the final shape. This bending or twisting does not result in any in-plane strains, but only in strains resulting from bending and torsion deformation. Since bending and torsional stiffness of thin surfaces are generally low in comparison to their in-plane tension- or compression-stiffness, only limited external forces need to be exercised. Figure 6.8 shows two examples of flat shapes that are deformed into developable curved surfaces:

The fact that no in-plane strains and stresses are caused by this transformation process was described first by Carl Friedrich Gauss (1827, p21):

“When a surface is regarded, not as the boundary of a solid, but as a flexible, though not extensible solid, one dimension of which is supposed to vanish, then the properties of the surface depend in part upon the form to which we can suppose it reduced, and in part are absolute and remain invariable, whatever may be the form into which the surface is bent”.

Whether a transformation is, or is not possible without stretching can mathematically be tested by calculating the Gaussian curvature before and after. If, during a

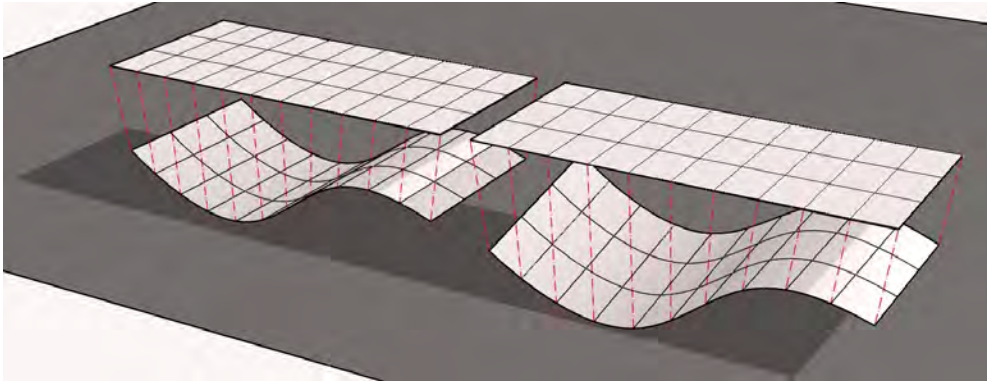


Figure 6.8: Developable surfaces with zero Gaussian curvature in all shown situations (left: only bending, right: bending and torsion)

transformation of a surface from one shape into the other, the Gaussian curvature remains constant (but not necessarily zero), no in-plane strains or stresses will occur due to this transformation.

The flexible mould methods always starts with a flat surface, which has Gaussian curvature $K = 0$. As long as deformation of the flexible mould is only carried out into shapes that are developable surfaces, like the ones shown in Figure 6.8, no extension of the mould or the concrete will take place, only bending and/or torsion. Calladine (1983, section 5.2) gives an example that illustrates this:

“if a triangle is drawn on a piece of paper, the length of the sides of this triangle do not change when the paper is rolled into an arbitrary cylindrical or a conical surface”.

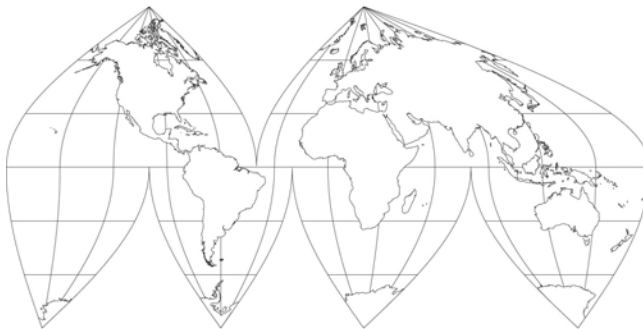


Figure 6.9: Sinusoidal 6 point projection of the world globe on a flat map: example of the strains necessary to project a curved surface on a flat piece of paper

Non-developable surfaces

Non-developable surfaces are surfaces that *cannot* be made from a flat piece of paper without tearing or distortion. Referring to Calladine's triangle again: they cannot be made without changing the length of the triangle's sides when formed from a flat piece of paper. This is illustrated clearly by the projection of the world globe on a flat map (see Figure 6.9): due to differences in arc lengths between two points for the flat and curved shape, strains are necessary, which in case of the globe projection is solved by cutting segmented parts, as with an orange peel. This category of curved surfaces have a Gaussian curvature *unequal* to zero; they are double-curved.

Gauss' observation could - unfairly - be considered an iron rule that implies that it is impossible to deform any flat surface into a double-curved surface. For elastic materials, however, Gauss' condition of being non-extensible is not true, implying the invalidity of the above-mentioned rule under such circumstances. This can be easily imagined by thinking of a rectangular thin rubber sheet, fixed at four edges and loaded with e.g. water or sand: due to stretching, it will transform easily from flat to double-curved. This notion in the flexible mould method will also be used in the rubber interpolating surface of the flexible mould method.

Still, Gauss' rule is helpful in understanding some effects: if materials with a higher Young's modulus than rubber, such as thin steel or timber plates, that are 'almost' non-extensible, are deformed from flat to double-curved, Gauss' observation explains the buckling effects that occur. Initially, in the present research, it was attempted to deform a thin timber plate into a double-curved shape (see section 7.3 and subsection 8.5.3). Although it was indeed possible to obtain roughly the desired deformed shape, internal normal strains were responsible for buckling effects that distorted especially the edges of the plate (see Figure 7.12 on page 113). With a massive plate, the limits of deformation appeared to be set by buckling effects under compression stresses. The division of the plate into an array of narrow strips solved this problem, as we will see later in section 7.4 on page 114. Deformation of flat surfaces into developable surfaces will not demonstrate this behaviour.

6.5.3 Imposed strain distribution

During the process of deforming the - initially flat - flexible mould into a curved surface, several materials possibly have to deform somehow:

- the concrete
- the reinforcement in the concrete
- the rubber mould surface keeping the concrete
- the edges of this rubber mould
- the elastic surface or set of strips that support the rubber mould

The textbook "*Theory of Shell Structures*" of Calladine (1983) appeared very helpful for the further study. To describe the structural behaviour of curved shell surfaces, Calladine separated shells conceptually into two surfaces, labelled the bending surface (B) and the stretching surface (S). Similarly, for the flexible mould process, we distinguish two kinematic effects of any imposed deformation that may or may not occur simultaneously:

- (B)** bending action (when deforming a flat piece of material into a developable or non-developable surface)
- (S)** in-plane stretching (when forming non-developable surfaces out of flat material or when stretching flat material)

Both kinematic effects will be discussed here in more detail now.

(B) Bending action

Assume that a rubber mould, containing still plastic concrete, is curved from a flat into a cylindrical (thus single-curved and developable) surface, without stretching the mould surface by any means: it is basically just rolled (developed) from flat to curved, as if wrapping it around a cylinder. Both the mould and the concrete in the mould will need to undergo a change of shape from linear to curved. At this point we will not go into the possible elastic reaction of the rubber mould or the forces needed to deform the concrete, but we will restrict to trying to understand the kinematic behaviour. The goal is to find a description of the strains that necessarily follow from the deformation.

Let's first look at the concrete, and assume that the plastic concrete completely follows the shape of the deformed mould surface during deformation. We assume that *no slip* occurs between mould and fresh concrete and that neither any gaps will occur between mould and concrete.

Already during the experiments of Huyghe and Schoofs (2009), the imposed curvature was assumed to be governing for the strain in the concrete mixture (see Figure 4.6 on page 49). Strong curvature (= small R = large κ) was expected to result in high strains, although it was not clear which strain distribution occurred over the height of the elements: the kinematic relation between curvature and strain was unknown (see Figure 6.10). We will now try to find this relation.

If the plastic concrete obeys Bernoulli's hypothesis "flat sections remain flat after curvature", the question is where the neutral line due to the curvature is. The neutral line is that height in the cross-section where the strain is equal to zero. Figure 6.10a shows three hypothetical strain distributions, where in the left image of Figure 6.10a it is assumed that the neutral line is in the middle of the element, in which case $\varepsilon_{max} = \pm \frac{1}{2}h \cdot \kappa$, according to simple beam equations from structural mechanics. The *sign* of the strain in all three images depends on the direction of the curvature and the position of the neutral line. The middle image of Figure 6.10a is an example of a possible strain distribution that does not follow Bernoulli's

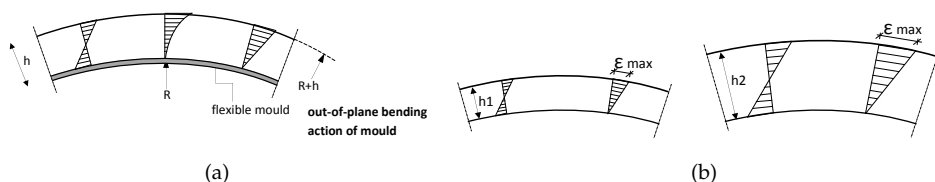


Figure 6.10: (a) possible strain distributions as a result of out-of-plane action of the mould (b) possible influence of thickness on strains

hypothesis ($\partial\epsilon/\partial z \neq \text{constant}$), and is for that reason rejected. In the right part of Figure 6.10a it is assumed that the neutral line is on the mould surface, in which case $\epsilon_{max} = h \cdot \kappa = h/R$. Of the three suggested possible strain distributions, this is the only one that corresponds with the idea of ‘wrapping’ the mould around a cylinder, since the mould surface itself is not stretched, but only curved, and a no-slip situation was assumed. It is concluded that the relation $\epsilon_{max} = h \cdot \kappa = h/R$ fits best to all border conditions.

Apart from the radius R , the element height h then also has influence on the strains resulting from bending action (see Figure 6.10b). Table 6.1 on the following page gives the order of magnitude of the strains necessary for following a certain curvature, depending on the element height. For this table, the relation $\epsilon_{max} = h \cdot \kappa = \pm \frac{h}{R}$ was used, in which the sign follows from the direction of bending. It can be seen that strain values above 25‰ are possible for elements of $h = 0.050$ m or thicker combined with curvatures with $R \leq 2.0$ m. To compare the order of magnitude: in fully hardened and loaded concrete C20/25 the strain generally is between 1.5 and 2.5 ‰ when the compression strength is reached. The much higher strain values in Table 6.1 therefore make clear that imposed deformation can only occur without cracking in a stage that the fresh concrete is still sufficiently plastic.

So far, only the deformation of the concrete was discussed. As pointed out in the beginning of this subsection, also the reinforcement, the mould surface and edges and the supporting strips will have to follow the deformation, and it is important to understand their kinematic behaviour. Furthermore, not only the kinetic behaviour, but also the resulting stresses and reaction forces need to be described. For the reinforcement in the concrete, various options will be discussed later in this thesis, among which are: flexible reinforcement in the form of textiles (see subsection 9.9), and traditional steel reinforcement in small flexible diameters (see subsection 8.2.5).

The effect of bending action on the reinforcement is depending on its distance to the neutral line. In hardened concrete, for reinforcement which is at a non-zero distance from the neutral line, imposed deformation cannot take place without strain of this reinforcement. This is the result of the bond between hardened concrete and reinforcement. In the case of the flexible mould method, in plastic concrete that is just starting to develop initial stiffness, it is not very likely that the imposed deformation at an early stage can lead to an overall *normal strain* of the reinforcement, as bond has hardly developed. It is expected that the reinforcement will *bend*, but also will slip

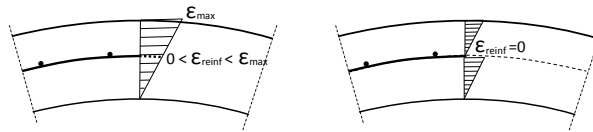


Figure 6.11: Reinforcement laying outside of the neutral line will have to strain (left) or slip (right) - in the latter case, the concrete that is above this layer might also restart with zero strain - later it will be shown that this is the case with a dense 8 mm mesh of textile reinforcement (slip of reinforcement plus concrete). For steel mesh with 100 mm mesh size, the reinforcement will be 'retracted' through the straining section of concrete (slip of only reinforcement)

Table 6.1: Imposed strain due to bending [‰] - The table presents the order of magnitude of maximum strains $\varepsilon_{max} = \frac{h}{R}$ to be expected during deformation for different element radii R .

element radius R [m]	element height h [m]				
	0.010	0.025	0.050	0.075	0.100
1.0	10	25	50	75	100
2.0	5	13	25	38	50
3.0	3.3	8	17	25	33
4.0	2.5	6	19	19	25
5.0	2	5	15	15	20

in the concrete or induce a slipping plane between two layers of concrete (see Figure 6.11).

At the same time, the curvature of the reinforcement will lead to *bending* strains in the reinforcement, that depends on the moment of resistance of the individual bars or fibre bundles. The flexible textiles will appear to be not much affected by this type of bending action, since textiles have small diameters and are consisting of bundles of very flexible fibres. The bundles follow the imposed deformation effectively, as will be shown later. Due to a larger moment of resistance the steel reinforcement will indeed appear to be affected; elastic spring-back could even result in the bars coming out of the concrete. Restricting the diameter in relation to the curvature of the deformation will appear to keep this in control. In the mentioned subsections this will be discussed in detail, and also supported by experiments.

For the mould surface, the effects of bending action are considered negligible, as in the present research it is made of rubber with a low Young's modulus and is very thin (1-2 mm). For the mould edges, effects due to bending action were also neglected in a pragmatical way, as in the experiments a very elastic foam was used that could easily follow any deformation of the mould surface. The edge positioning and edge behaviour however is less predictable and controllable when looking at (S) in-plane stretching, which will be discussed below. Finally, chapter 7 will investigate in depth the deformation of the mould and supporting strips, and also discuss the

elastic effects resulting from this deformation. For all materials however that are subjected to bending action, the same relations between radius R , curvature κ , strain ϵ and element height h will keep reappearing.

(S) In-plane stretching

Since our final goal is to be able to form not only developable curved surfaces, but also non-developable, double-curved surfaces, another necessary type of kinematic behaviour will be discussed now: going from flat to double-curved by changing the Gaussian curvature. Eigenraam (2013) studied the work of Calladine (1983) and found there very useful tools to describe and understand the flexible mould process. Calladine (chapter 6) states that all changes in Gaussian curvature $g = \Delta K$ can be expressed by the following kinematic equation (6.4), formed by the summation of three terms. Each term expresses small changes in 'angular defect': two in-plane normal strain components in orthogonal directions and one in-plane shear strain component:

$$g = -\frac{\partial^2 \epsilon_{xx}}{\partial y^2} - \frac{\partial^2 \epsilon_{yy}}{\partial x^2} + \frac{\partial^2 \gamma_{xy}}{\partial x \cdot \partial y}. \quad (6.4)$$

A formal derivation of this equation is done by Calladine, but intuitively the meaning of each term can be understood. The first term could be understood as follows: suppose a flat surface would get an equal strain ϵ_{xx} for all y -coordinates, this would imply simple in-plane elongation of the original surface in the direction of the x -axis, not leading to any curvature of the surface. If the same flat surface in one section would get a strain ϵ_{xx} increasing linearly for positive y -coordinates (so $\frac{\partial \epsilon_{xx}}{\partial y} = \text{constant}$) this would lead to an in-plane kink of the surface, but still allowing it to stay flat ($z = 0$). If, however, the second partial derivative of ϵ_{xx} along the positive y -axis would yield a constant value, resulting in a curved strain distribution in-plane, then it would no longer be possible for the whole surface to only deform in-plane: a three-dimensional curved surface would be formed as a result of these strains, see e.g. Figure 6.12.

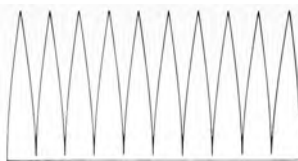
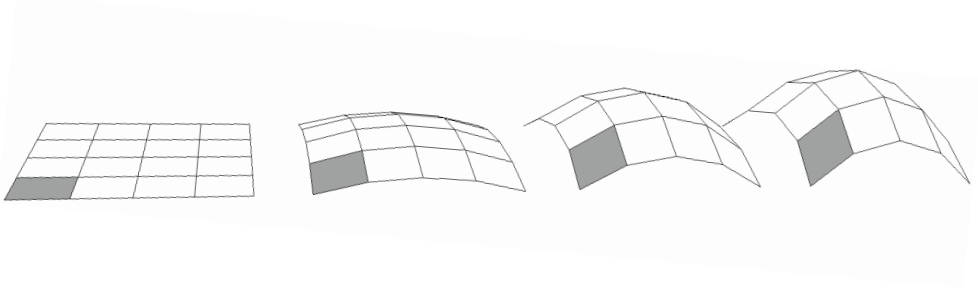
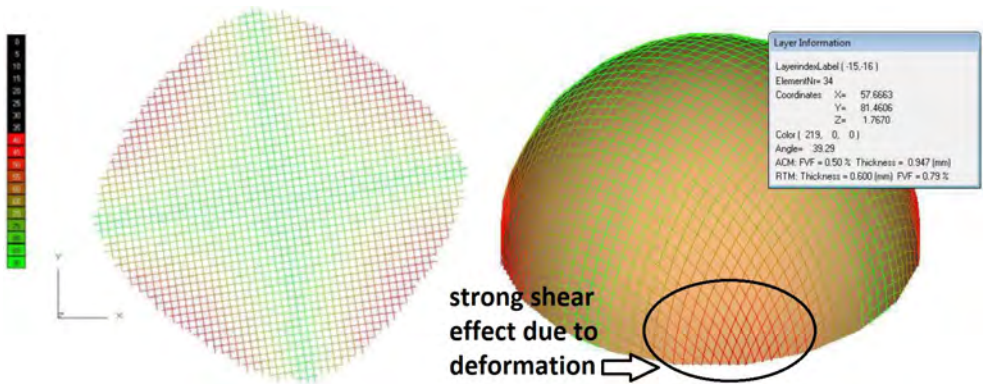


Figure 6.12: Deformation out-of-plane through $\frac{\partial^2 \epsilon_{xx}}{\partial y^2} = \text{constant}$: glueing the flat paper along the edges will lead to a sphere-shaped curved surface (after Calladine, 1983)

The second term in the equation is similar, but then for strains along the y -axis. The first two terms can also be understood by imagining the inflation ('stretching')



- (a) In-plane strains are necessary to deform a surface from flat to double-curved; in the image, only the component $\partial^2 \gamma_{xy} / \partial x \cdot \partial y$ from Equation 6.4 on the previous page is applied (taken from Eigenraam, 2013)



- (b) Calladine's principle is applied to shear-deform a flat and non-stretchable piece of textile into a double-curved shape, using the software Drape; image from Woodington (2014)

Figure 6.13: Shear-deformation allows deformation from flat to double-curved without in-plane normal extension

of a soap bubble: a sphere of which the radius increases. The soap layer will have to stretch equally in the two perpendicular directions. The numerical value of the Gaussian curvature K will reduce, since $K = 1/R^2$; g will get a negative value.

The third term in equation (6.4), representing in-plane shear deformation, is less easy to understand, but proved to be of major importance, both for controlling the supporting strips and for placing of reinforcement textiles. This is illustrated in Figure 6.13a: here a flat frame or ribs is depicted, which is deformed into a double-curved shape. Even without change of the length of the ribs - the first two terms in equation (6.4), shearing will allow deformation. This makes it possible to still deform a non-stretchable material into a double-curved shape (Bergsma, 1995), as can be seen in Figure 6.13b. This is an important finding that will greatly simplify the flexible mould principle.

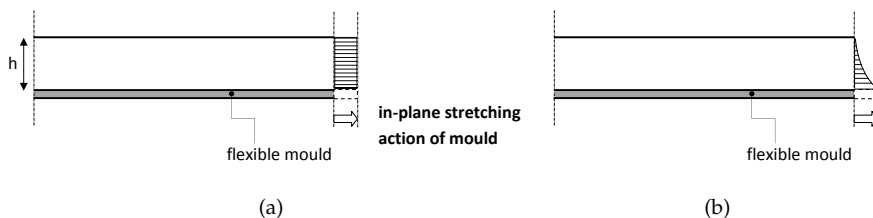


Figure 6.14: (a) constant strain distribution $\partial\epsilon/\partial z = 0$ and $\epsilon = C$ in the concrete layer with height h as result of in-plane stretching action of the mould $\epsilon = C$ of the mould - this implies however that $E = 0$
 (b) varying strain distribution $\partial\epsilon/\partial z \neq 0$ as a result of the elasticity of the mixture $E > 0$

6.5.4 Effects in z-direction

Strain distribution along z-axis due to in-plane deformation

The in-plane normal-strains ϵ_{xx} and ϵ_{yy} of the mould could lead to a subsequent in-plane strain of the concrete. When the friction between concrete and mould is such that no slip occurs, at least plausible two strain distributions along the z-axis (vertically) can be imagined:

1. A constant and linear strain distribution over the height of the element (Figure 6.14a), based on the extreme assumption that Young's modulus $E \approx 0$ and the whole concrete layer follows the elongation of the mould.
2. A non-constant, linear or exponential strain distribution over the height of the element (Figure 6.14b), based on the assumption that $E > 0$ and that, due to elasticity of the concrete, the top part of the cross-section will not be influenced by this stretching (or compression). This, however, would imply an out-of-plane curvature of the cross-section, since $\kappa = \partial\epsilon/\partial z \neq 0$.

At this point it can not be decided which of the two models is correct. However, as we expect that in-plane strains ϵ_{xx} and ϵ_{yy} of the mould may not occur at all, and as the third term of equation (6.4), the shear-deformation γ_{xy} , will take fully care of the stretching effect (S), the discussion might even be more complex (how does the concrete follow shearing of the mould surface?). For now, though, this effect is considered negligible due to the limited shear angles necessary for the deformation, as we will see in the next subsection.

Thickness change due to shear

In his master's thesis, Woodington (2014, p27-28) explains that deformation of a flat volume of concrete to a double-curved volume of concrete by shearing has the effect of thickening the deformed layer, since the volume must remain constant. He

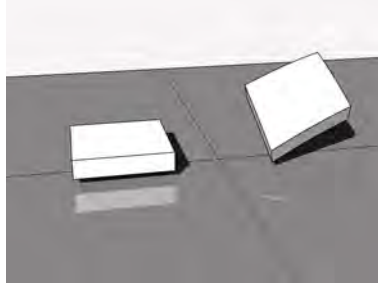


Figure 6.15: Deformation due to combined (B) and (S) effects: the (B) effects results in bending in two perpendicular directions; the (S) effects results in the deformation from rectangular to the sheared diamond-shape

finds the simple relation $h_{new} = h_{original} / \sin(\theta)$, in which θ is the shearing angle. A situation without shearing ($h_{original} = 1$ and $\theta = 90^\circ$) yields $h_{new} = 1$, whereas for a shear angle $\theta = 60^\circ$ (so a deformation of $90 - 60 = 30^\circ$) $h_{new} \approx 1.15$. The thickening effect will be negligible for limited shear deformation. It is expected that this will be the case for the panels that can be formed with the flexible mould method, as from the work of Woodington (2014) it appeared that for deformation of a flat textile into a hemisphere, shear angles of around 38 or less are to be expected. As many of the panels that will be formed with the flexible mould method will be less extremely curved than a hemisphere, the shear angles are also expected to remain restricted to smaller values.

6.5.5 Total strain - order of magnitude estimation

Based on the considerations above, it is concluded that Table 6.1 on page 90 gives a good estimation of the maximal normal strains that will occur in the concrete, depending from the element height h and curvature radius R . Whether the strains are positive or negative depends on the direction of the curvature. Although this table only covers the (B) deformation, we will later see that the stretching deformation (S) can only be realized by the third term from equation (6.4), the shear-term. This implies that at certain points in the concrete, a combination of bending strains and in-plane shear strains will be necessary to deform from flat into double-curved. If the grey rectangle from Figure 6.13a on page 92 is observed closely before and after deformation, this can be seen more clear, see Figure 6.15.

6.5.6 Geometrical aspects of edge positioning

Figure 6.16 shows two possible methods for laser projection of the contours of a random panel's edges on mould surface. In the situation on the left, projection is carried out in the stage that the mould has not yet been deformed. In the situation on the right, the deformed mould is the base for projection. Although the same panel

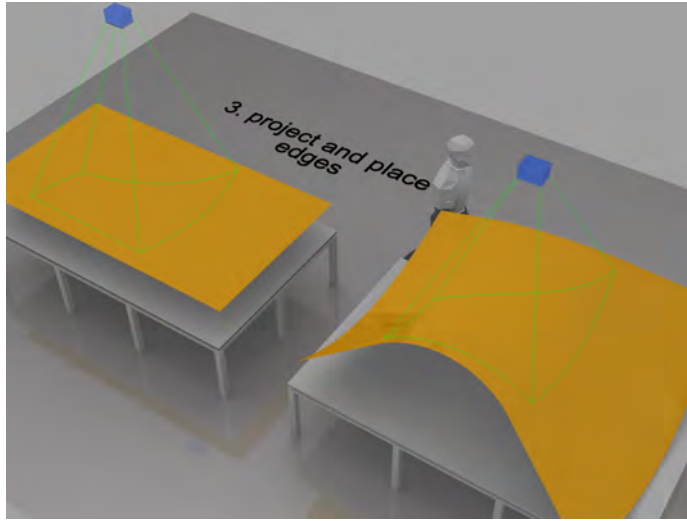


Figure 6.16: Different laser projection of mould edges in flat situation (left) or in deformed situation (right): compensation is necessary.

is projected, the contours need to be different. The shape of the projected pattern for the *deformed* situation can be directly derived from the 3D shape of the desired element. This can be done relatively simply by intersection calculations in CAD software. The projected pattern in the undeformed situation, though, is non-trivial and will be dependent on the expected contribution of the three terms in Calladine's equation 6.4 that result from deformation from flat to double-curved. According to this equation, normal- and/or shear-strains will necessarily occur during the deformation. These strains will lead to distortion of the contours that are projected in the flat situation, as also visible in the clear difference between the projected patterns in left and right part of the image in Figure 6.16. This distortion depends on the deforming strip mechanism under the interpolating material. At this point, this projection algorithm is yet to be developed. For slightly curved elements, an approximation by orthogonal projection might be acceptable, but for elements with stronger curvature, this is likely to result in an error in the edge shapes of the final element. It is recommended to do further research on the accurate projection of the edge position.

6.6 Discussion

In this chapter, we have first reviewed some basic shapes such as splines and NURBS-curves and -surfaces that are used to define shapes in modern CAD software. Moreover we have seen that basically two approaches are possible for a feasible production of double-curved surfaces for architectural purposes: rationalisation or mass-customisation. In recent years, considerable progress has been made in the

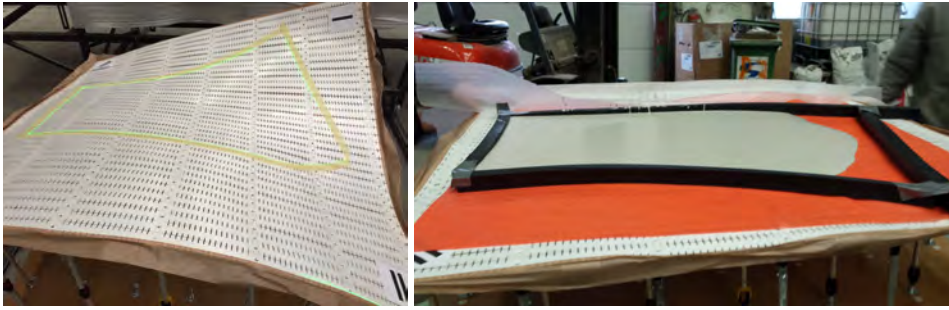


Figure 6.17: Laser-projection of edge positions on a prototype of the flexible mould in the deformed situation (left) and edge position in undeformed situation (right) (Schipper et al., 2015)

development of computer algorithms to facilitate the rationalisation process, leading to significant cost reductions. Yet, rationalisation is an optimisation process that can never reduce costs beyond a certain point where the aesthetics of the building become too much compromised. If for example a curved building shape is visibly flattened and segmented, costs might be low, but the architectural quality is reduced to an unacceptable level.

Mass-customisation, for example by using the flexible mould, can offer an additional solution, provided that the costs of the production method will not surpass the costs of the original mould technology, and preferably will be much lower than that. A conceptual manufacturing line for such mass-customized elements was shown in Figure 6.7 to demonstrate how this promise can eventually be fulfilled.

The flexible mould method relies on deformation of a flat material into a curved surface and using this as mould. This brings along several geometrical issues. The deformation process can be described mathematically by analysing the curvature parameters. An important and meaningful parameter is the Gaussian curvature, that is the product of the principle curvatures in two directions. Curved surfaces with zero Gaussian curvature are easier to manufacture with the flexible mould method than curved surfaces with non-zero Gaussian curvature, as the last category not only is deformed out-of-plane, but also in-plane. The findings of Calladine were discussed, that give clear insight in the necessary separation of bending effects (B) and stretching effects (S). Furthermore the three components of stretching were investigated, of which shear-deformation appears to be sufficient to deform from flat to double-curved. This will later appear to be an important notion for the construction of the flexible mould mechanism. Furthermore, the order of magnitude of strains was estimated, to get a general idea of the effects of the deformation process on the mould and the concrete. These numbers will be used later in the part on the design of the mould and the part on concrete technology. Finally, even the correct positioning of the mould edges in the flat situation seems to depend on the deformation components described by Calladine. This was not worked out any further at this moment.

Part III

Mechanical engineering of the machine

Chapter 7

Modelling the mould behaviour

7.1 General approach

7.1.1 Introduction

In chapter 2, several ideas and attempts to realize an elastic flexible mould surface have been described. Over the years, numerous concepts have been invented and in few cases have also been built, of which the most notable are the work of Renzo Piano, Lars Spuybroek and the patents of Florian-Peter Kosche, Vollers and Rietbergen and quite recently Raun en Kristensen. Most of the mentioned researchers use an elastic material as intermediate layer between a set of actuators and the material that needs to be deformed. Without such an intermediate layer, it is difficult to realize a sufficiently smooth concrete surface. A prototype built under guidance of Rietbergen and Vollers already demonstrated (see page 48) that the proper choice of the elasticity of this intermediate layer is one of the crucial factors to success: using an overly stiff material leads to difficulties in adjusting the formwork into the desired curvature; using an overly flexible material on the other hand leads to a uneven surface which is not acceptable from an aesthetic point of view (see Figure 7.1 on the following page).

As it could be observed, a structural mechanics model of the behaviour of an elastic material under forced displacement for this specific application in a flexible mould was never published. Although a trial-and-error approach could be followed in order to arrive at correctly shaped elements, it is the belief of the author that it is helpful and even necessary to understand and model the behaviour in order to be able to successfully choose the material specifications and shape adjustment method.

7.1.2 Elasticity of the flexible formwork

The concept of the adjustable formwork mechanically does not work very different from that of the spline as discussed in subsection 6.2.2: a flexible material fixed in

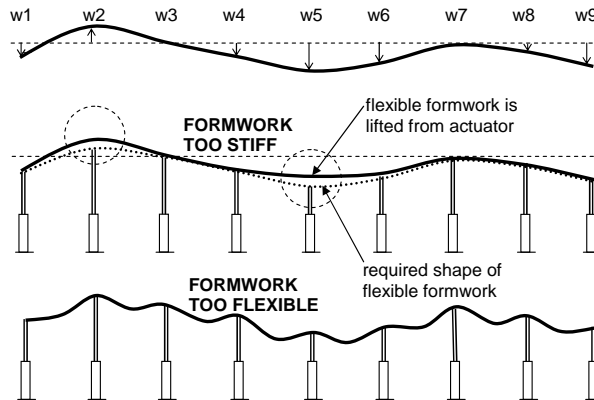


Figure 7.1: Mould surface too stiff - mould surface too flexible: an inherent optimisation problem for each flexible formwork (Schipper and Janssen, 2011a)

a curved position by control points. The control points can be moved by pistons, actuators, worm-screws, or any other adjusting method. In Figure 4.5 on page 45 the prototype built by Daan Rietbergen was already shown, which, for these tests, was finished using a thin intermediate layer of timber. Other materials such as synthetic rubber with varying specifications have also been tested by Huyghe and Schoofs (2009). As said, different from NURBS-curves, in the flexible mould concept the control points are assumed to be *laying on* the curve. It is not always easy, though, for the elastic material to “follow” the position of the actuators, causing the problems sketched earlier and schematically shown in Figure 7.1. In the tests by Schoofs and Huyghe this appeared to cause some unpredictable effects disturbing the smooth adjustment of the actuators and eventually also hindering the accuracy of the resulting panel shape. Let us therefore take a closer look at the elastic effects in the moulds intermediate layer.

Figure 7.2a illustrates, in the most simplified manner, how an elastic layer can be manipulated by actuators (or in terms of structural mechanics: support points) A, B

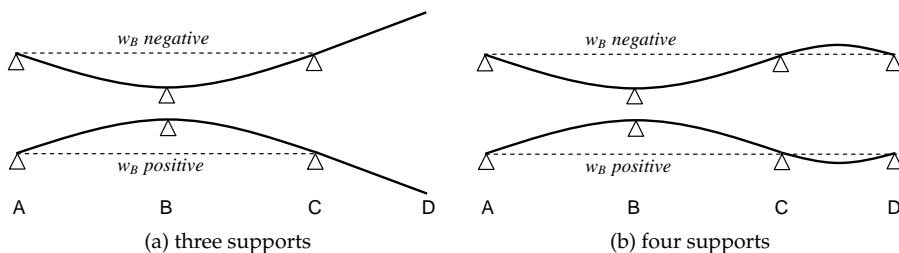


Figure 7.2: Elasticity results in mutual interaction of different parts of a beam

and C. By moving support point B up and down, the shape can be adjusted. Point D in Figure 7.2a is not adjusted by an actuator, but is freely following the rotation of the beam around point C. If point B is adjusted downwards (negative) point D moves up, and the other way around. It is clear that the position of point D is ruled by point B. If, for some reason, one would add an extra support at point D, as is done in figure 7.2b, the forces in support points B and D become 'interconnected' by the elasticity of the material. Not only will the force necessary to move actuator D be influenced by actuator B, but it is also clear that the shape of the mould between point C and D is influenced by the position of actuator B. Actually, the position of all actuators has influence on the situation between C and D. A similar interconnection will occur in a flexible mould set-up with multiple support points, both in 2D and in 3D.

7.1.3 Stepwise approach

In the following sections, a stepwise extension of the modelling and experimental work will be presented. The first step, described in section 7.2, consists of a linear strip mould under bending in one bending direction, using beam theory. This model was used in a number of experiments and proved to be useful to investigate and explain a number of phenomenons that occur both in single-curved moulds as well as in flexible moulds in general. To go from single-curved strips to a double-curved surface, a second model was made and tested experimentally: section 7.3 describes a thin plate mould that is controlled by a grid of actuators that force the thin plate to deform into a double-curved shape. Although the use of a thin plate has several advantages, the elastic behaviour brings along some fundamental limitations, as was demonstrated experimentally. In section 7.4 therefore the strip mould is extended in two directions to obtain a deformable double-curved surface. This is done by grouping sets of perpendicularly crossing small strips and describing the bending behaviour. This crossing strip mould was used successfully in various experiments, allowing stronger curvature than the plate mould. To allow even more accurate shape control of the strip mould, an improved strip model was developed and tested, under the name *Kine-Mould*. This mould is described in section 7.4.4. The chapter is concluded with a discussion of the various mould concepts and an outlook to possible further developments and alternatives in section 7.6.

7.2 Strip mould, single-curved

7.2.1 Approximation with beam theory

This elastic behaviour, which is well known in structural engineering, is described by the Euler-Bernoulli differential equation that describes the bending behaviour of an elastic beam for small displacements:

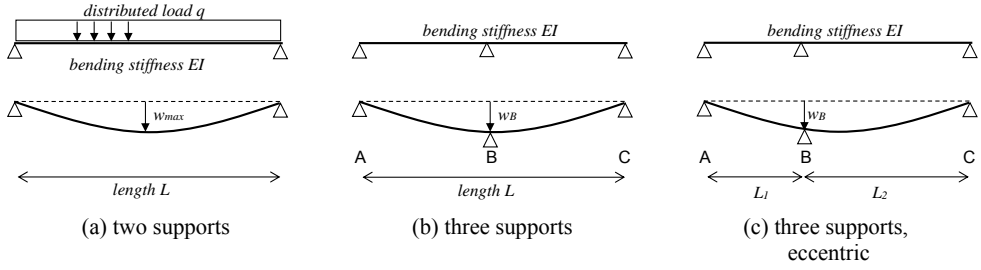


Figure 7.3: Simple beams on bending as start for a mechanical model for the flexible mould

$$EI \frac{\partial^4 w(x)}{\partial x^4} = q \quad (7.1)$$

where x is the position on the beam, EI is the bending stiffness of the beam, $w(x)$ is the deflection of the beam in point x , and q is the load on the beam. This equation relates the bending stiffness and deflection on the left hand side of the equation to vertical forces on the beam, such as external loads, self weight and support reaction forces on the right hand side of the equation. The fourth order, visible in the equation, is responsible for the form of many well-known design solutions used in structural engineering. For many practical cases, the solution of the differential equation is a fourth order polynomial. For example, the solution for a beam on two supports with an equally distributed load q , as shown Figure 7.3a, is:

$$w(x) = \frac{q x}{24EI} (L^3 - 2Lx^2 + x^3) \quad (7.2)$$

In the situation of the flexible mould, the deflection is not only caused by a vertical load q , like in the equation above, but additionally by the deliberate adjustment of the support points, as illustrated in Figure 7.3b. In order to understand what parameters influence the shape of the mould and the forces on the supports we will investigate a simple example first. To lower the support point B in Figure 7.3b over a distance w_B , a force F_B is needed, due to the bending stiffness of the mould EI . Both force F_B and the shape of the mould are governed by equation 7.1. The solutions can be found in most structural engineering handbooks (e.g. ?):

$$F_B = \frac{48EI}{L^3} \cdot w_B \quad (7.3)$$

$$w(x) = \frac{F_B L^3}{48EI} \left(-4 \frac{x^3}{L^3} + 3 \frac{x}{L} \right) = w_B \left(-4 \frac{x^3}{L^3} + 3 \frac{x}{L} \right) \quad (7.4)$$

Equation 7.4 (valid for $0 < x < \frac{L}{2}$) shows that the function for the shape of the curved beam under a forced displacement w_B in $x = \frac{1}{2}L$ is a third-order polynomial,

which is the case for all situations where $q = 0$: equation 7.1 then solves into a third-order polynomial. The flexible mould, if considered in a 2D situation and controlled by multiple actuators, can be modelled using a similar approach. This approach will be worked out after a brief discussion of the effect of large displacements and of the bending radius.

7.2.2 Large displacements neglected

A complication is that, for large displacements, the direction of load q and the support reactions F_i are under a non-negligible angle ϕ with the deformed axis of the beam, introducing a factor $\cos \phi$, for all vertical loads and reaction forces (Beléndez et al., 2002) and causing difficulties in solving the non-linear differential equation. In this thesis however, we will still proceed using the equations as if displacements were not large, under the assumption that a) for a complete description of the mould system a FEM-approach in the end will be necessary anyhow, making the relevance of an accurate analytical solution somewhat smaller, b) for gaining insight in the behaviour of the mould, the accuracy of the model will be of smaller importance than the readability of the equations, and finally c) the effects that will be observed during experiments can be explained and predicted using the simplified approach.

7.2.3 Smallest possible bending radius

The material and thickness of the flexible mould determine its bending stiffness and bending strength. The maximal elastic bending moment M_{max} for a given material with yield strength f_y is $M_{max} = f_y \cdot W_{elast}$. Higher moments will lead to plastic deformation or yielding of the material. Using

$$M = -EI\kappa = -\frac{EI}{R} \text{ and } W = \frac{2 \cdot I}{h} \leftrightarrow I = \frac{W \cdot h}{2} \quad (7.5)$$

the maximum moment for strips with rectangular cross-section can be expressed in Young's modulus E and material thickness h :

$$M_{max} = f_y \cdot W_{elast} = -\frac{EI}{R} = -\frac{E \cdot W_{elast} \cdot h}{2R} \quad (7.6)$$

$$R_{min} = \left| -\frac{E \cdot h}{2 \cdot f_y} \right| \text{ or more general } \sigma = \frac{E \cdot h}{2 \cdot R} \quad (7.7)$$

For example, a timber strip with a thickness $h = 4 \text{ mm}$ and $E = 8000 \text{ N/mm}^2$ and $f_y = 17 \text{ N/mm}^2$ will yield if bent with a radius smaller than:

$$R_{min} = \frac{8000 \cdot 4}{2 \cdot 17} = \frac{32000}{34} = 941 \text{ mm},$$

while e.g. a steel strip with a thickness $h = 4 \text{ mm}$ and $E = 210000 \text{ N/mm}^2$ and $f_y = 235 \text{ N/mm}^2$ can reach only:

$$R_{min} = \frac{210\,000 \cdot 4}{2 \cdot 235} = \frac{840\,000}{470} = 1787 \text{ mm.}$$

Some more results are shown in Table 7.1. It is concluded that, apart from the thickness h , the *proportion* between Young's modulus E and the yield bending strength f_y is determining the smallest possible radius R_{min} that can be applied to a strip of material before it will yield. Furthermore it is concluded that a radius down to $R = 1.00 \text{ m}$ can be realized with a strip thickness of $h = 4 \text{ mm}$ for timber and of $h = 2.2 \text{ mm}$ for steel. For HDPE even strips thicker than $h = 10 \text{ mm}$ can be applied, although creep aspects are not taken into account here and could occur.

Table 7.1: Allowable curvature radius R_{min} for strips in Pure®, HDPE, timber and steel

strip thickness [mm]	R_{min} [mm] for Pure*) ($E/f_y =$ 5000/200=25)	R_{min} [mm] for HDPE**) ($E/f_y =$ 900/16=56)	R_{min} [mm] for timber ($E/f_y =$ 8000/17=471)	R_{min} [mm] for construction steel ($E/f_y =$ 210000/235=894)
1	13	28	235	447
2	25	56	471	894
3	38	84	706	1340
4	50	113	941	1787
5	63	141	1176	2234
10	125	281	2353	4468

*) Lankhorst Pure® composite **) High Density Polyethylene

7.2.4 Maple model for single-curved mould with n support points

A linear flexible mould with n actuators can be considered as a beam for which each actuator $A_{i=1..n}$ forms a support point at location x_i that can exercise a vertical displacement w_i on that point of the beam (Figure 7.4 on the next page). During this displacement w_i a force F_i is developed, which will be determined by the stiffness EI of the beam, the distributed load q on the beam and the forces exercised in the other actuators $A_{j \neq i}$. By considering the displacement of each point of the mould as the superimposed effect of load q and all single actuator loads $F_{i=1..n}$, a system of equations can be formulated and solved.

Both ends $x = 0$ and $x = L$ of the beam are assumed to be kept on vertical position $w = 0$. Then the displacement w_j in a point j due to the point load F_i at position x_i can be described with the third-order equations:

$$w_{F_i;j;left} = \frac{F_i \cdot b \cdot x}{6 \cdot EI \cdot L} \{2L(L - x) - b^2 - (L - x)^2\} \text{ for } j \text{ left of } F_i,$$

$$w_{F_i;j;right} = \frac{F_i \cdot a \cdot (L - x)}{6 \cdot EI \cdot L} \{2L \cdot b - b^2 - (L - x)^2\} \text{ for } j \text{ right of } F_i$$

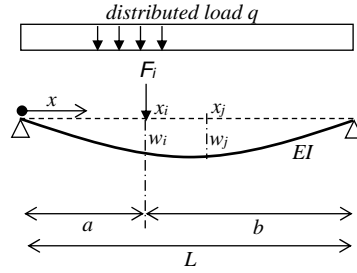


Figure 7.4: Actuator A_i exercising force F_i and displacement w_i at position $x_i = a$

and the displacement due to q as a fourth-order equation:

$$w_q = \frac{qx}{24EI}(L^3 - 2L^2 + x^3). \quad (7.8)$$

Janssen (2011, chapter 5) worked out the system of equations for a 2D single-curved mould supported by 11 actuators similar to the one shown in Figure 7.1 on page 100. The model uses Maple as platform, allowing mostly symbolic maths representation, offering transparency for the user. In the model, a beam on 11 support points at intervals ΔL is described. A user-defined curve can be applied by definition of individual actuator heights w_i . The bending stiffness is determined based on the mould's Young's modulus E and thickness h , which latter can also be evaluated based on user-defined border conditions. A variable concrete load q can be specified, which is taken into account according to the above equations.

Since a symbolic approach is chosen, various border conditions can be defined mathematically, such as ' $R_i > 0$ ' (determine mould height h so that no negative reaction forces occur) or ' $w_q < w_{max}$ ' (relative deflection between actuators is limited to a specified maximum). A range of allowable thicknesses or mould materials can be evaluated by the model, reaction forces are calculated and an accurate diagram of the elastic deflection is plotted. Bending moment, shear forces and maximum stress in the strip are calculated, and curve length and expected horizontal displacements are calculated.

The model was validated both experimentally and numerically and, although it does not take into account the theory of large deformations, it proved useful during the experiments for prediction of the phenomenons that were to be expected due to various parameter modifications. Appendix B shows a part of the model originally described in Schipper and Janssen (2011a) with an improved algorithm by the author that has the same functionality but with shorter notations. In the following subsections, the model is used to demonstrate the influence of the most important parameters. Obtaining a good understanding of these influences will not only prove useful for single-curved strip moulds, but for double-curved surfaces as well.

7.2.5 Influence of mould stiffness and actuator spacing

In an example we will first illustrate the effect of the chosen strip stiffness in relation to the deflections between the actuators. Assume a mould is loaded with a 50 mm thick concrete layer; $q = 23 \cdot 0.05 \cdot 0.20 = 0.23 \text{ kN/m}^1$ (self-weight strip neglected here). The actuator interval $\Delta L = 200 \text{ mm}$. As mould material, a steel strip is chosen with $E = 210\,000 \text{ MPa}$, strip width $b = 200 \text{ mm}$ and strip height $h = 1 \text{ mm}$. The mould is not deliberately deformed by bringing it in a curved shape after casting, but all actuators are kept in their original zero-position for the sake of clarity in this example. Figure 7.5 shows the intended shape (horizontal blue line) and the real shape under influence of the deflection due to the concrete weight (red curve). At the position of each actuator, the deviation between the originally intended and real mould shape is zero, per definition.

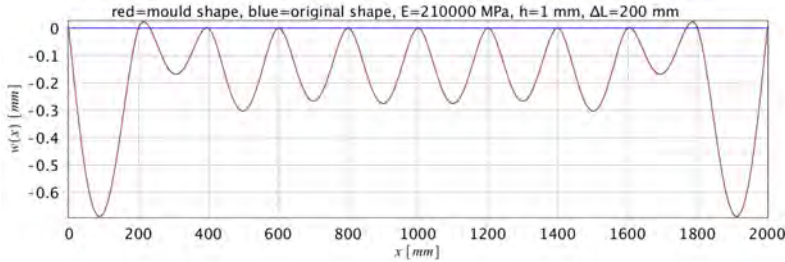


Figure 7.5: Influence of mould thickness, $h=1 \text{ mm}$

From the graph it is observed that the outer two fields show significantly more deflection than the middle fields. This is behaviour that is general for any flexible mould that does not have the outer edge clamped. In the second and ninth field, locally upward deformation occurs due to continuity of the curve. Furthermore it is concluded that - for the chosen parameters in this example - the maximum deflection is approximately $0.28 \text{ mm} = \Delta L/714$ for the middle fields and $0.69 \text{ mm} = \Delta L/290$ for the two outer fields. If the thickness of the steel strip is now doubled to $h = 2 \text{ mm}$, keeping all other parameters constant, all deflections decrease with a factor $2^3 = 8$ due to the increase of the moment of inertia of the strip I . If the actuator spacing is doubled but once again $h = 1 \text{ mm}$, deflection due to the concrete load will increase with a factor $2^4 = 16$ compared to the first situation, due to the power x^4 in equation (7.8). It is concluded that for the straight horizontal mould the same rules apply as for normal beams loaded on bending. This behaviour was also checked and validated during the experiments. Furthermore it is concluded that deflections between actuators are non-negligible and might also be visible in the final product if a too much flexible strip is chosen or if the actuator spacing is too large.

7.2.6 Influence of curvature

Now the effect on the exact shape of the strip mould of moving the actuators is investigated. In order to be able to distinguish this effect from the deflection due to concrete weight in the previous subsection, the load of the concrete is first set to $q = 0$. For the mould shape one half period of a sinus-function with amplitude -300 mm is chosen, see Figure 7.6. The smallest radius of this curve at $x = 1\,000$ mm is $R = 1.35$ m. From the deviation graph it is concluded that the shape can be reproduced accurately with the chosen actuator distance and strip thickness: the largest deviation is 0.008 mm, which is negligible.

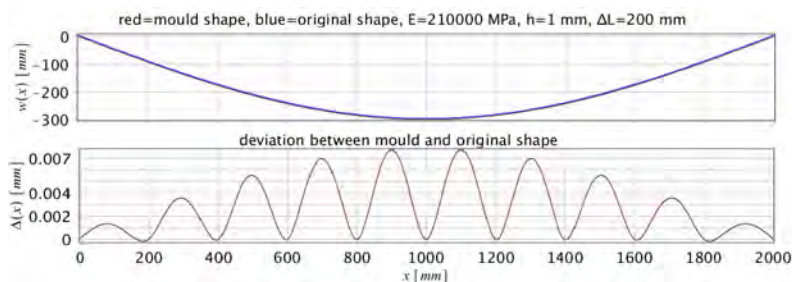


Figure 7.6: Half sinus function without concrete load and amplitude 300 mm - deviations are negligible

Now another sinus-shape is chosen with same amplitude but choosing 3π periods. The smallest radius of this curve is $R = 0.15$ m, which is much less than in the previous example. The concrete load is still kept at $q = 0$. The maximum absolute value of the deviations between realized and intended shape will increase to approximately $0.7\text{ mm} \approx \Delta L/286$, as is visible in Figure 7.7 on the next page. Although this is still considered a very limited deviation which would probably not be visible in the concrete product, this example illustrates that there are minor deviations between intended and realized shape.

As said, the smallest curvature radius is $R = 150$ mm, which results in a bending moment $M = EI/R = 210000 \cdot \frac{1}{12} \cdot 200 \cdot 1^3/150 = 23\,333$ Nmm and a corresponding bending stress $\sigma = E \cdot h/2R = 700$ MPa. This unfortunately is too high for a strip in S235 quality. This conclusion could already have been drawn from Table 7.1 on page 104, which gives a lower boundary for the radius of a 1 mm steel strip of $R_{min} = 447$ mm. As a strip thinner than 1 mm will not be practical in steel, another material has to be chosen. A higher steel grade would be a solution, but for the sake of the example we will now choose a strip of 5 mm HDPE from Table 7.1. With this choice the radius would be allowable. Repeating the calculation with this strip thickness and material yields an almost identical picture as Figure 7.7 on the next page.

However, if now the concrete loads are applied again (see Figure 7.8), we see that choosing such a flexible material will result in larger deviations between the actuators, in this situation an absolute value up to $1.6\text{ mm} = \Delta L/125$, which is probably non-negligible with respect to the concrete product. This illustrates that there

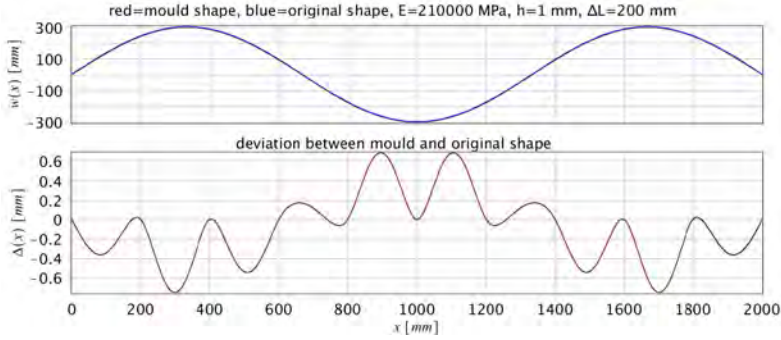


Figure 7.7: 3π sinus function without concrete load and amplitude 300 mm - deviations are perhaps non-negligible any more if they would be visible in the concrete product

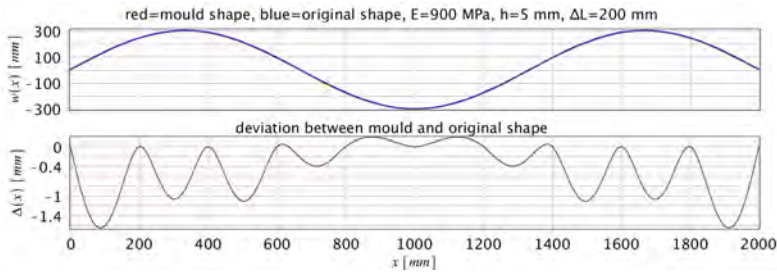
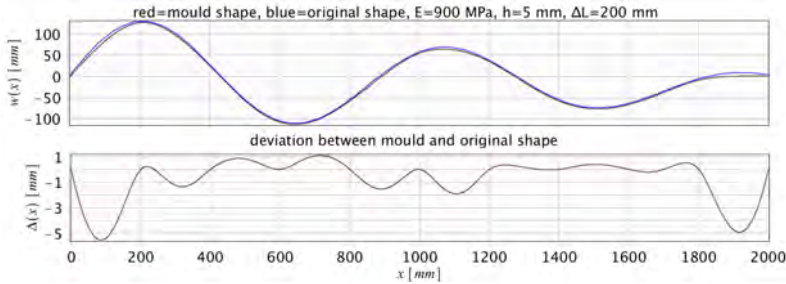


Figure 7.8: 3π sinus function including concrete load and amplitude 300 mm - deviations are increasing to $1.6 \text{ mm} = \Delta L/125$

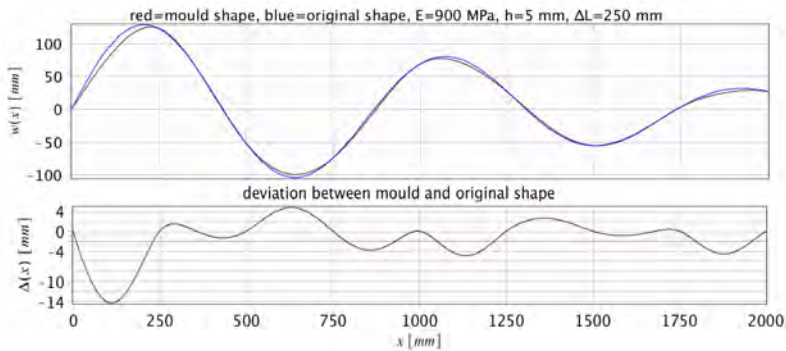
is a trade-off between the low stiffness necessary for small radii and the deflection between the actuators due to the concrete load. This is typical for any flexible mould based on the present principle with actuators and an interpolating strip. It must be said that, in the situation loaded with concrete, the two outer fields generally show a significantly higher deviation than the inner fields. Still, for the second and third field also deviations up to 1 mm are visible.

7.2.7 Complexity of shape versus number of actuators

If a certain shape is more complex, a sufficient number of actuators is necessary to allow control over the mould surface. In Figure 7.9a, the frequency of the sinus-function is increased, whereas the amplitude has been reduced in such a way that the same minimum radius of $R = 150 \text{ mm}$ is reached as in the previous example. Using the same strip material and strip thickness, it can be observed that the absolute value of the deviations, not taking into account the outer two fields, increases to almost $2.0 \text{ mm} = \Delta L/100$.



(a) 11 actuators at 200 mm spacing



(b) 9 actuators at 250 mm spacing

Figure 7.9: Actuator distance has to correspond with complexity of shape

If, while keeping the same shape, for economy reasons the actuator spacing would be increased to 250 mm, Figure 7.9b illustrates that the absolute value of deviation, again not taking into account the outer fields, increases to even $4.9 \text{ mm} = \Delta L/50$ (related now to $\Delta L = 250 \text{ mm}$!). It is concluded that the relation between all parameters in the model results in substantial influence on the accuracy of the mould in case of relatively small changes in the parameters.

7.2.8 Reaction forces

If the reaction forces that follow from the shape examined in Figure 7.9a are looked up in the Maple model, the following values in [N] are found for the 11 actuators from left to right: -61.0, +204.8, +38.3, -66.1, +27.7, +135.4, +71.8, -17.8, +14.5, +117.3 and -4.8 N. Positive here is a reaction force directed upwards and vice versa. From this example it can be seen that even with a quite flexible material such as a 5 mm HDPE strip, reaction forces can be substantial and directed both upwards and downwards. This will impose certain demands on the mechanism that controls the actuators: in many cases the weight of the concrete will not be sufficient to push the flexible mould into its shape. For situations where large downward reaction forces are expected, the actuators must be capable of both pulling and pushing.

7.2.9 Horizontal displacements

An issue not discussed so far are the horizontal displacements that result from the deflection of an originally flat strip in a curved shape. If it is assumed that no axial forces in the strips are introduced by the actuators, but only bending, then the length of the strips will remain constant. In case of large vertical displacements, the tips of the actuators then will have to displace horizontally in order to account for the constant length along the curved strip. The Maple model also calculates the length along the curve. If the length of the half sinus curve in Figure 7.6 on page 107 is taken as example, the length evaluates to 2106 mm which would imply a strain of more than 5% compared to the original 2000 mm in flat situation. In reality this strain does not occur due to the absence of axial forces. For most materials, these axial forces would be extremely high anyhow (in this case $EA\varepsilon = 210\,000 \cdot 200 \cdot 1 \cdot \frac{106}{2000} = 2\,226 \text{ kN!}$), so it is much easier to allow horizontal displacements. In this example, keeping the middle actuator in the centre, the two outer actuators would have to displace horizontally by approximately $106/2 = 54 \text{ mm}$. These effects were also observed in the experiments, and will have important implications for both the design of any flexible mould system and for the measurement system. Two of these effects are 1) that the actuators will need to pivot at least at two points, and 2) that the simple deduction of vertical coordinates has to be corrected due to the slight difference in vertical position of the mould measured over the horizontal axis.

7.2.10 Experimental set-up

The strip model was applied to predict the mould behaviour for deformation tests, producing a number of single-curved concrete elements. This work will be described later in subsection 8.4.3.

7.2.11 Discussion of the strip model

The model can be used to quantify the effects as shown earlier in Figure 7.1 on page 100. The following conclusions were drawn after experimenting with varying parameters in the model:

1. A strip mould can be used to produce single-curved shapes. The shape can be controlled by adjusting the actuator heights. If the bending stiffness of the strip material is chosen accurately, the deflection between actuators can be reduced to a specified minimum;
2. There is a clear connection between the applied mould curvature, the reaction forces, the chosen mould thickness and the chosen mould material; these parameters can not be chosen independently of each other, else, one takes a risk of a) inducing too large or overly small deflections between support points which result in an inaccurate or unnecessarily accurate concrete shape b) yield or creep of the mould material due to bending strains c) inducing large positive and/or negative reaction forces with problems in the support system as result;

3. The self-weight of the concrete is not in all cases sufficient to 'force' the mould into its desired shape. For sharp curves (small radii) relatively large positive or negative support reactions are necessary, that can be realized either by putting additional weight on the mould or by pulling the strips to the supports; this imposes constrictions to the design of the mould apparatus;
4. Horizontal displacements can be in the order of several centimetres. This means that the control point at which the actuator height is set is actually shifting horizontally, which will lead to a different desired height at the shifted position. For an accurate shape description, horizontal displacements should be taken into account; also this imposes constrictions to the design of the mould apparatus;
5. Inaccuracy is largest in the outer left and right fields, since deflections there can only be controlled from one side.

Although very wide strips can be made that will behave according to the model described above, a strip mould can only be used for manufacturing single-curved shapes or, by slightly twisting the mould surface, developable shapes (Pottmann et al., 2010; Van de Straat, 2011). For manufacturing double-curved shapes, however, another mould concept is necessary. The following sections will discuss a plate model, a crossing strip model and the Kine-mould model.

7.3 Plate mould, double-curved

7.3.1 Introduction

As the next step in the development of a mould for double-curved shapes, investigated was up to what extent a simple thin plate can be deformed. In subsection 6.5.2 we already discussed Gauss' remarkable finding that for a material without in-plane extension the Gaussian curvature has to remain constant. For a building material such as steel or timber, though, elongation and shortening due to normal stress will occur, thus allowing *change* of Gaussian curvature.

In the experiments of Schipper and Janssen in 2010, a plate mould was constructed, supported by a matrix of 11×6 actuators, at a spacing of $\Delta L = 200$ mm in both directions. The formwork was based on a plywood (Ned. *triplex*) plate of 2.00×1.00 m² with a thickness of 3.8 mm, which allowed the manufacturing of concrete elements of approximately $1.90 \times 0.90 \times 0.05$ m³ ($L \times W \times h$) (see Figure 7.10a).

7.3.2 Mechanical model

A thin plate with deformations larger than the plate thickness is generally modelled with differential equations that take into account both bending action (B) and stretching action (S). Janssen (2011) worked out a finite-difference model in Excel with a

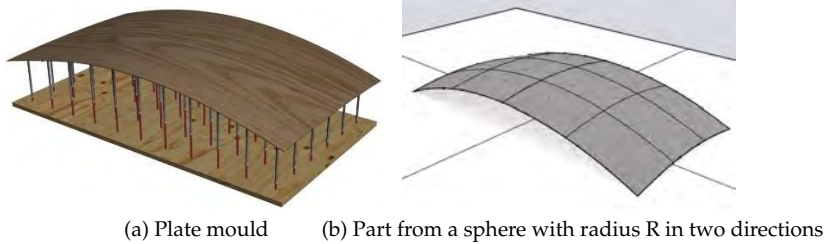


Figure 7.10: (a) plate mould described by Janssen (2011) (b) sphere-shaped element used in Table 7.2

mesh size equal to the grid of actuators to estimate the actuator reaction forces and internal plate stresses resulting from (B) and (S) actions. For further details on this model and the way it was solved, we refer to Janssen (2011).

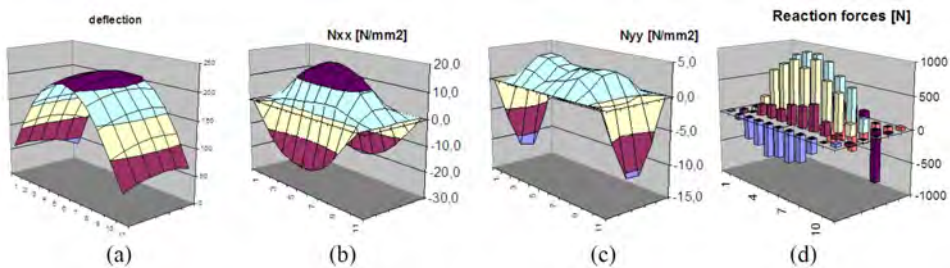


Figure 7.11: A thin plate forced into double curvature (a) - using and Excel finite difference method the in-plane normal stress (b, c) and reaction forces (d) are approximated. Note that the maximum compressive stresses are in the edges of the panel. Furthermore note that the actuator forces along the long edges are negative (the plate is pulled downwards) (Schipper and Janssen, 2011b)

Figure 7.11 shows an example of the in-plane forces that are calculated using the model for a double-curved shape. Using the same model in combination with a parametric geometry in Rhino, the results from Table 7.2 on the next page were obtained. For this purpose the rectangular element was taken from a sphere with a radius halving stepwise from 40 to 2.5 m (see Figure 7.10b). From the table it is concluded that from a radius of 5 m in two directions, the compression stresses (approx. -12 to -19 MPa) are already in the same order of magnitude as the material yield strength. For a radius of 2.5 m the compression stresses are far beyond that yield strength. It is concluded that, for this material, only a limited double-curvature can be reached since otherwise the material will yield.

Table 7.2: Normal stresses in a plate mould increase linearly with increase of Gaussian Curvature K: relation Radius - Gaussian curvature - deflection - extreme normal stresses for a thin timber plate of $2.00 \cdot 1.00 \text{ m}^2$, 11×6 actuators, spaced $\Delta L = 200 \text{ mm}$ in two directions, $E = 8000 \text{ Mpa}$, $h = 4 \text{ mm}$, poisson constant $\nu = 0.23$

sphere radius R [m]	Gaussian curvature K [m ⁻²]	deflection in centre [mm]	extreme n_{xx} [MPa]	extreme n_{yy} [MPa]
40	0.000625	16	-0.3	-0.2
20	0.0025	31	-1.2	-0.7
10	0.0100	62	-4.7	-3.0
5	0.0400	126	-18.9	-12.0
2.5	0.1600	262	-79.1	-50.6

7.3.3 Local buckling

Another phenomenon however occurs even earlier than yielding: due to the high compressive stresses in the outer perimeter of the mould surface, *buckling* effects occur between the actuators, which will lead into a corrugated edge. This behaviour was also observed in the experiments (deformation test 6, see page 152) and is clearly visible in Figure 7.12. Increasing the thickness of the plate to increase the buckling stiffness will help to some extent: the stresses will remain the same since the strains remain the same (forced displacement). The reaction forces in the actuators however will increase proportionally. If the Young's modulus is increased (e.g. using steel instead of timber) strains will also increase proportionally. Although reducing the actuator distance will reduce buckling length, this is not considered an economic solution.

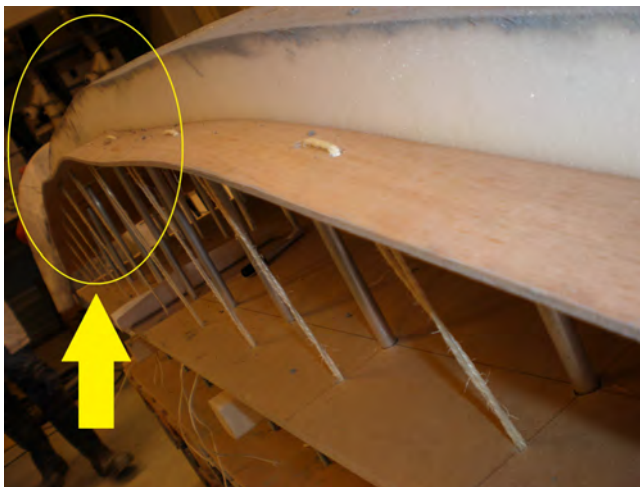


Figure 7.12: Buckling due to internal compression stresses - deformation test 6

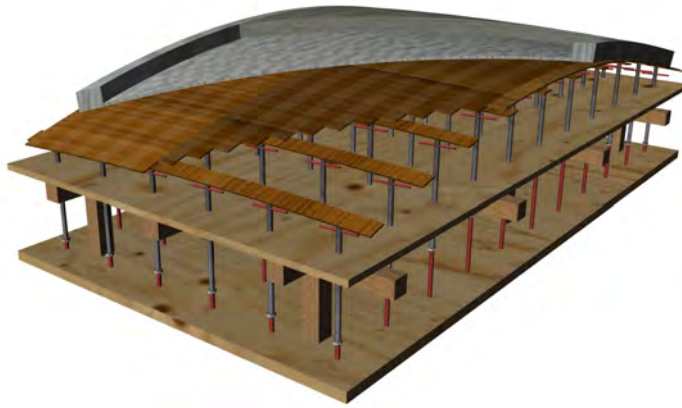


Figure 7.13: Strip-mould (Janssen, 2011; Schipper and Janssen, 2011a)

7.3.4 Discussion of plate model

It is concluded that a plate mould can only be applied for a very limited Gaussian curvature due to fast increasing normal stresses, actuator reaction forces and disturbing buckling effects in the plate edge as soon as Gaussian curvature increases. It is considered not a viable solution for the type of geometries that was found in Chapter 5.

7.4 Crossing-strips mould, double-curved

7.4.1 Introduction

The plate model from the previous section was found not to be a viable solution for strongly double-curved shapes, as a result of local buckling of the mould edge due to high compressive strains and stresses. To prevent this from happening, a way was sought to release the stresses and introduce more freedom in the surface to deform. This was done by dividing the surface in parallel strips at a small distance of each other, supported by a second layer of perpendicular strips (see Figure 7.13).

On top of these strips a flexible rubber mould surface was placed that covers the small openings between the strips without making them visible in the concrete product. This appeared to offer the necessary freedom for forced displacement into stronger curved shapes.

7.4.2 Mechanical model

To determine the forces in the actuators and estimate the necessary thickness of the strips, the linear strip model as described in section 7.2 was extended in two directions: by stacking two layers of strips, the support reactions of the top layer are

applied as loads to the lower layer. A strip mould was used for both the exploratory tests and the extensive tests.

For the exploratory tests that will be described in Chapter 8, a set-up was chosen of 11×6 actuators at a spacing of $\Delta L = 200$ mm. Plywood strips were applied with a thickness of $h = 3.8$ mm and a width of $b = 50$ mm. Janssen (2011) gives a complete description of this process; the model that describes the mechanical behaviour was implemented in an Excel worksheet. This worksheet takes the forced displacements in all actuators (as measured from the architectural CAD-model of the element) as input, and offers the resulting reaction forces and relative deflection of the mould surface between the actuators between as output. Concrete elements of approximately $1.90 \times 0.90 \times 0.05 \text{ m}^3$ ($L \times W \times h$) could be produced with this strip mould.

For the extensive tests that will be described in Chapter 9 on page 167, a set-up of four identical strip moulds was built with similar strips, but with only 9×7 actuators at a spacing of $\Delta L = 140$ mm (see Figure E.1 on page 290 and Figure 9.10 on page 193). Each of the four set-ups could be used to produce an element of $0.80 \times 0.40 \times 0.05 \text{ m}^3$ ($L \times W \times h$).

Both for the exploratory tests and the extensive tests satisfying results were obtained. A clear double-curved geometry was obtained with radii of 3.06 m and 2.50 m, respectively. The strip mould offered sufficient degrees of freedom to apply this curvature.

7.4.3 Limitations of the strip mould

With respect to the accuracy of the model, some remarks can be made:

- The mechanical model only takes into account bending of the strips. Torsion is not modelled; neither is the effect of shearing - necessary for the change in Gaussian curvature (see subsection 6.5.3) - taken into account in the strip model;
- If the concrete weight itself is not sufficient to press the flexible grid of strips into its double-curved shape, additional negative (pointing down) reaction forces are necessary; in practice, these negative reaction forces are difficult to apply; additional weights were used in some cases, having the disadvantage that these disturb the casting process and cannot always be positioned exactly in the right place;
- Due to the sliding and tilting of the strips in the practical set-up, additional inaccuracy is introduced.

Figure 7.14 on the following page demonstrates some of these effects. For the tests on concrete technology as described in Chapter 8 and 9, these limitations were not considered important. In case of the production of architectural elements with high aesthetic quality, though, improvements are necessary. In the work of Eigenraam (2013), important steps were made to improve accuracy, leading to an improved prototype of the strip mould, under the working title Kine-Mould.



Figure 7.14: Some inaccuracy occurs if strong double-curvature is applied: (a) additional weights are necessary (b) strips not in one plane; small deviations in actuator tips

7.4.4 Kine-Mould: an improved crossing-strips mould

In 2014, two grants were obtained to work on an industrial-scale prototype as proof-of-concept: one from Dutch Technology Foundation STW (Schipper et al., 2014) and one from 3TU Built Environment. Among the features of the Kine-Mould are:

- introduction of counter-weights on each actuator that allow for downward support reactions;
- connection of the strips to each other and to the actuators;
- use of the shear-principle to deform from flat to double-curved;
- improved actuator mechanism to allow for horizontal displacements;
- improved flexibility of the strips.

Recently, a patent has been filed for these ideas (Eigenraam and Schipper, 2015). In the Kine-Mould project, also steel mesh as an alternative for strips was investigated (Tissink, 2015). Further discussion of the Kine-Mould, however, is outside the scope of this thesis.

7.5 Work-flow

In subsection 6.4.2 the envisioned work-flow in the factory was already sketched. Before the manufacturing starts, the shape of the elements needs to be analysed in order to make the proper choices for mould size, actuator spacing, edge positioning, strip thickness and other relevant parameters. The calculation models presented here can facilitate in these choices. Figure 7.15 on the next page shows the work-flow

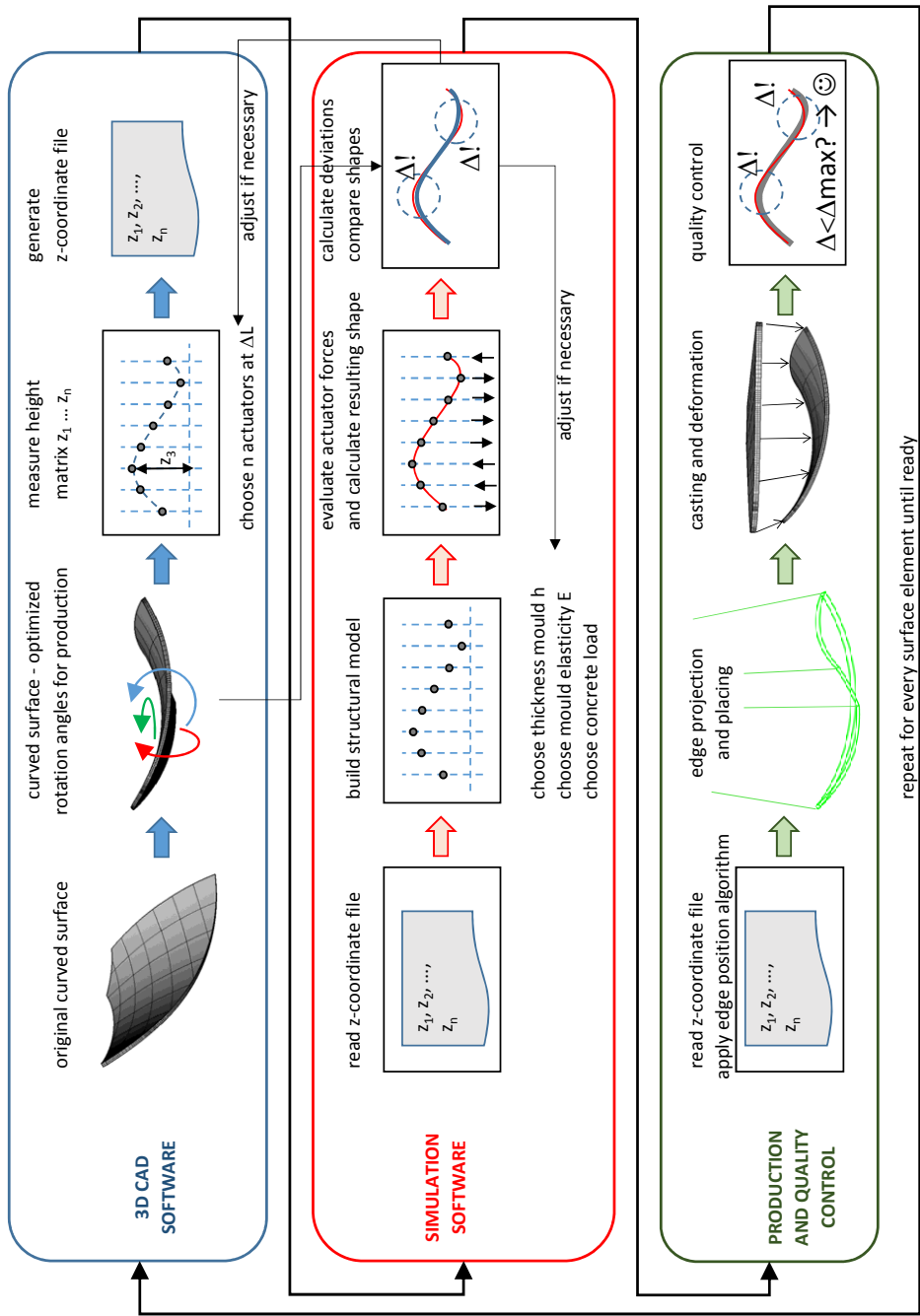


Figure 7.15: Work-flow

that includes the use of the models. For various shapes and curvature combinations, it is likely that adjustments to the flexible mould are necessary to allow the accurate manufacturing of these shapes.

7.6 Discussion

Although the models as presented in this chapter have some limitations, they will provide sufficient accuracy for the tests in the next part of this thesis on concrete technology. The strip model has demonstrated to be valuable to find the relation between concrete load, strip thickness and actuator spacing. It was found that deviations between the intended and the obtained shape are inevitable, but, under the condition of properly chosen parameters, can be reduced to an acceptable level. The plate mould was found to be unreliable due to large internal stresses, leading to buckling effects in the edge of the plate. Production of double-curved shapes with a plate mould therefore is limited to large radii only. For smaller radii, a crossing-strip mould was found to offer the necessary degrees of freedom. The mechanical model of the crossing-strip mould is based on the linear strip model, and does not take into account all mechanical effects. Still, it was found to be useful and sufficiently accurate for the purpose of this thesis.

Part IV

Concrete Technology

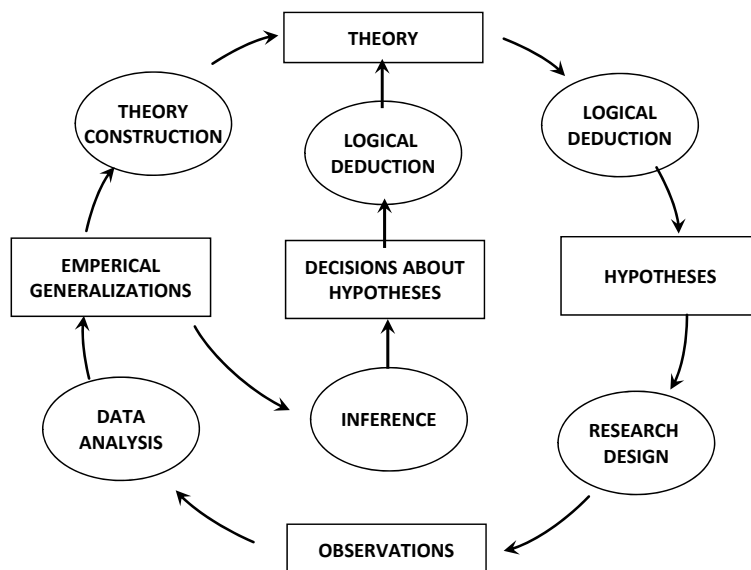


Figure 7.16: Wallace 'Wheel of science'

This part of the thesis will report on the specific characteristics of deforming concrete after casting, a process typical for the flexible mould method. The chapters 8 and 9 in this part follow an empirical research approach: based on existing and known theory, for example concrete rheology and solid mechanics, hypotheses are posed regarding the flexible mould method. These hypotheses are then made operational in tests that can provide useful observations and experimental data. In a next step, from the analysis of observations and experimental data, the validity of the hypotheses can be proved or rejected, from which point generalisations may be drawn to extend the known theory. This circle, from existing theory towards extended theory based on experimental results, is also known as the '*wheel of science*', described by Wallace (1971), see Figure 7.16. Two rounds in this wheel of science are reported here:

1. Chapter 8 describes the first tests with the flexible mould in 2010 and 2011, carried out by the author together with Janssen (2011). These first viability tests concentrated on investigating whether the flexible mould method was applicable at all in the first place, and whether and how the process could be controlled. The experiments were of an exploratory character, and were meant to gain insight into the parameters that are influencing the process. During this round 1 of , evidence was gathered for the validation of some first suppositions¹, among which were the usability of an open mould system, the possibility to successfully deform concrete after casting, and the possibility to deform thin steel reinforcement along with the concrete. From round 1, several

¹in the present research the term *supposition* was considered more appropriate than *hypothesis*

conclusions could be drawn and an initial theory could be developed to model the flexible mould process. Although in these experiments also attention was paid to the design of the mould system itself, the present part IV will only focus on those aspects that are related to concrete technology.

2. Chapter 9 describes round 2, a parameter variation study conducted mainly in 2012 and 2013. The viability tests in round 1 had given a better understanding of which parameters had influence. After the consultation of additional existing theory on these parameters, a number of more refined suppositions could be formulated and consequently tested in round 2, such as hypotheses regarding the strain capacity of fresh concrete during deformation, the application of textiles as flexible reinforcement and the use of super-plasticizers to control the timing of the hardening and deformation process. In round 2 a parameter variation programme was carried out, after which analysis of the data resulted in further empirical evidence for an improved version of the model found in round 1.

Chapter 8

First flexible mould viability tests

8.1 Introduction

8.1.1 Description of the flexible mould process

In a simplified way, the flexible mould method can be illustrated with Figure 8.1. The flexible mould consist of a formwork made of rubber or another flexible material, that is filled with concrete and deformed in a later stage. Stepwise, the procedure of casting a curved concrete element is carried out as follows: by adjusting the height positions of vertical threads, a specific single- or double-curved shape can be pre-installed (step 1). The flexible mould is then filled with concrete (step 2), while the mould is still in horizontal position. During a period of structural build-up, the initial strength of the concrete increases (step 3); the waiting time of 30-60 minutes

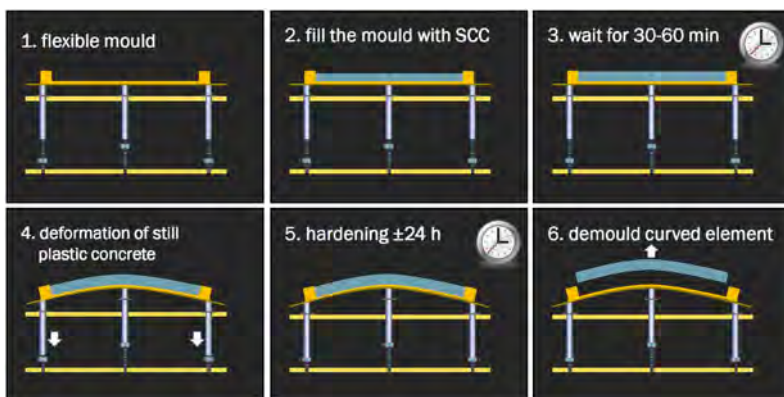


Figure 8.1: The flexible mould principle

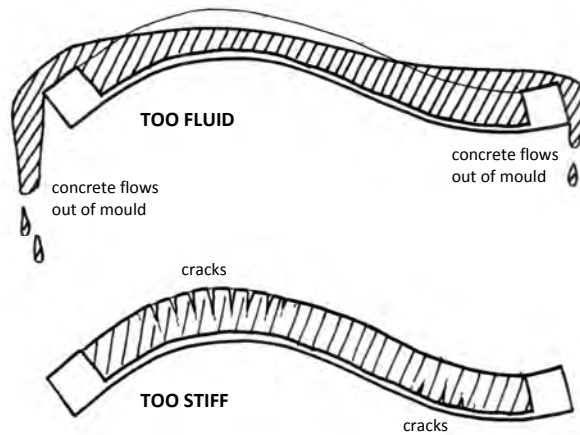


Figure 8.2: Lower and upper boundary: ranging from too fluid to too stiff

is still indicative at this point. Then the mould is carefully deformed into the final shape (step 4), based on the heights that were pre-installed during step 1. Concrete hardens in the deformed mould (step 5) and finally the curved element is demoulded (step 6). After this, the mould can be reused from step 1 to cast another panel with the same or a different curvature.

An alternative use of the flexible mould is the application of concrete *after* deforming the mould into its desired shape. This is possible by using sprayed concrete (this method is already applied presently on CNC-milled moulds) or by using zero-slump concrete that has a high shear yield strength directly after mixing. However, in the present research the method as described above is chosen as central concept.

8.1.2 Imposed deformation in relation to phase transition

The manufacturing process with the flexible mould method may, from a structural mechanics point of view, be seen as analogue to an *imposed deformation*, although at this point it is not clear to what extent this analogy is valid. Looking more closely at Figure 8.1, and imagining this in a three-dimensional situation (with curvature in two directions), two effects are expected as a result of this imposed deformation:

1. Parts of, or, in some cases, the full element will be tilted, compared to the initial horizontal position; for a too fluid concrete, this will be a problem, since it flows out of the mould (see Figure 8.2 top image).
2. Due to the imposed curvature, the concrete element will be stretched, bent and distorted, leading to positive or negative strains and torsional deformation, as already discussed in subsection 6.5.3. If the concrete is too stiff, these imposed strains might cause cracks (see Figure 8.2 bottom image).

The transition from the fluid to the solid phase, therefore, seems most relevant, since the speed and character of that transition will most probably influence the steps in the flexible mould process.

In various earlier research projects at TU Delft (see subsection 4.3), the idea of deforming concrete after casting has already been explored, mostly only theoretically but in few cases also experimentally. Although these researches obviously also aimed at application of the method at industrial scale, a thorough research with respect to aspects related to concrete technology was never carried out, at least not to the knowledge of the author of the present thesis. For industrial application of the method it would be important to fully understand the process and have control over the relevant parameters. Starting from the simple idea as illustrated in Figure 8.1, existing theory was reviewed first to find out whether models could be found that can help to describe the flexible mould process.

8.2 Theory

8.2.1 Modelling the fluid phase: Bingham model

Many fluids can be described using the Newtonian model, which is the most simple model used for fluids. A Newtonian fluid shows a linear relation between internal deviatoric¹ stresses and flow. The Newtonian model implies that flow will directly start at the smallest possible deviatoric stress. Fresh concrete, however, is considered a *non-Newtonian fluid*, which is a category of fluids for which the apparent viscosity depends on the speed at which it is deformed (Zienkiewicz et al., 2005, p6). More specifically, directly after mixing, fresh concrete is often modelled as a *Bingham fluid*, a subset of non-Newtonian fluids (Bingham, 1922; Ferraris and De Larrard, 1998; Wallevik, 2005; Roussel et al., 2005; Kovler and Roussel, 2011). Bingham was an American scientist (1878-1945) that did pioneering work in the field of measuring and describing the behaviour of viscous materials. Concrete rheology, the field of science that studies the behaviour of fluid concrete, makes extensive use of the findings of Bingham. A Bingham fluid has characteristics which clearly distinguish it from Newtonian fluids. The most conspicuous characteristic is the ability of Bingham fluids to *sustain deviatoric stresses without flowing*: before a Bingham fluid will start to flow, a certain minimal shear stress needs to be exceeded, defined as the *yield strength* of the fluid. Other viscous fluids that have a similar ability to resist a certain threshold value of shear stress without flowing are, for example, toothpaste, mayonnaise and various mud-like soils.

Figure 8.3 on the following page shows the relation between shear rate and shear stress for various classes of fluids. The slope between each of the lines and curves and the horizontal axis is the plastic viscosity, so the steeper the line, the thicker (more viscous) the fluid is. Curve 3, line 4 and curve 5 all three represent fluids that will start to flow at the smallest amount of shear stress; these curves cross the

¹The definition of isotropic and deviatoric stresses is worked out in Appendix H on page 337

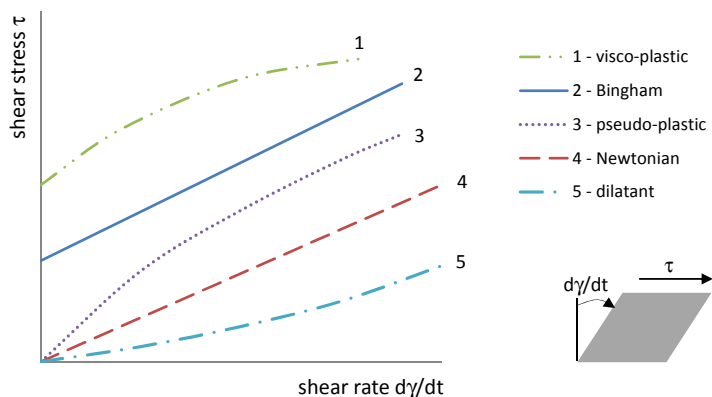


Figure 8.3: Shear rate - stress relation for different classes of fluids - visible is that a Bingham fluid (line 2) will not start flowing (shear rate > 0) at a shear stress below a certain minimum value on the vertical axis, contrary to a Newtonian fluid (line 4)

origin of the graph. Curve 1 and line 2, however, are fluids that start flowing only after a certain yield strength is overcome; their curves cross the vertical axis at a certain yield strength. The rheological behaviour of a Bingham fluid (line 2) can be described by a two-parameter linear model using the *Bingham equation*:

$$\tau = \tau_0 + \mu \dot{\gamma} \quad (8.1)$$

where:	τ	shear stress	Pa
	τ_0	shear yield strength in rest (minimal shear stress necessary to start movement of concrete)	Pa
	μ	plastic viscosity (resistance of concrete to a given shear strain rate)	Pa · sec
	$\dot{\gamma}$	shear strain rate ($= \partial\gamma/\partial t$)	rad/sec

In complex concrete flow situations, such as pumping through narrow pipes, more advanced non-linear rheological models sometimes are applied, such as the 'Herschel-Bulkley' or 'power-law' models (Wallevik and Wallevik, 2011). Use of the linear Bingham model, though, has the advantage that it is a relatively simple model, for which the flow behaviour can be described by only two material parameters: τ_0 and μ . These parameters furthermore can be estimated or determined using empirical tests such as the slump test (to determine τ_0) or by direct measurement using e.g. a rotational viscometer (to determine both τ_0 and μ). Both test methods also have the advantage of being available in the Stevin lab for experimental work in the present thesis, and furthermore are validated and widely accepted. Many numerical values can be found in literature, allowing comparison with the test results of the present research.

In the last two decades much progress has been made in understanding and controlling the rheological behaviour of concrete mixtures. The widespread application of self-compacting concretes (SCC's) nowadays is one of the most important results of this progress. Many publications on SCC's use the Bingham model.

To give an indication of the order of magnitude of the numerical values of the properties, SCC's have a rather low yield strength (typically 5 to 50 Pa) and as a result are easily flowing or even have self-levelling behaviour. Conventional Vibrated Concretes (CVC's) have a much higher yield strength (typically 300 to 750 Pa), do not flow easily, and need compaction through vibration, where vibration overcomes the yield strength through local acceleration. The plastic viscosity of SCC's is typically in the range of 15 to 120 Pa · s (yield strengths and viscosity taken from Wallevik and Wallevik, 2011). A further illustration of several SCC-classes is given in Figure 8.4.

Based on the wide acceptance and the practical advantages mentioned above, the *Bingham model* was chosen to describe the fluid phase in the present research.

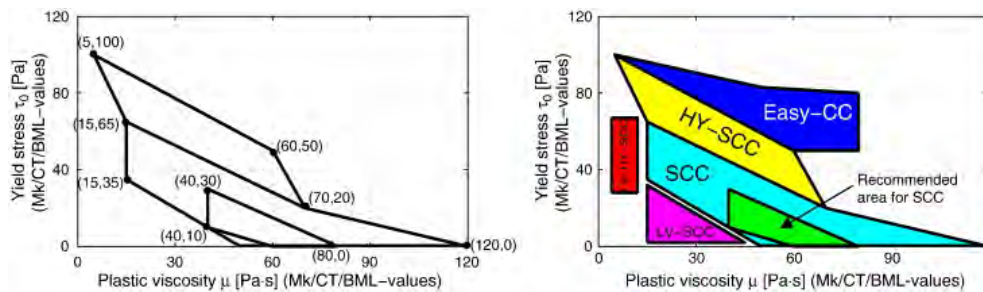


Figure 8.4: Rheograph indicating SCC yield strength and viscosity; LV=low-viscous; HY=high-yield (taken from Wallevik and Wallevik, 2011)

8.2.2 Strength development in the first hour

Introduction

Now that a description of Bingham fluids has been chosen that presumably can be used for the modelling of the fluid phase, it is also necessary to gain understanding of what happens inside the concrete during the hardening in the first hour(s). From literature, it appears that two processes in the fresh concrete take place after casting, that will be described in more detail on the following pages:

1. thixotropic stabilisation (also known as flocculation): as soon as the mixture is in rest, a structural build-up of fine particles starts. This build-up leads to an increase of yield strength τ_0 , known as thixotropic behaviour. This structure can be reduced again by application of shear, e.g. by vibration or remixing, or possibly also by the mould deformation itself. Wallevik (2005, pp 5-12) writes:

“a thixotropic liquid is a sample with an internal structure. During shear the structure is broken down and at rest the structure is rebuilt.

The breakdown as well as rebuilding of the structure takes time and is dependent on the material properties”.

2. hardening: hydration starts to form chemical CSH-products² in the cement paste matrix, that after some time start to bridge the open space between aggregate particles. Initially, these bridges can be easily broken, but gradually the fresh state mixture will become “green” concrete with growing strength.

Thixotropic stabilisation

Thixotropy is a specific type of rheological behaviour. Concrete is considered thixotropic “if it seems to flocculate rather quickly at rest and becomes apparently more and more fluid while flowing during typically several tens of seconds” (Roussel, 2006b). It is this effect that may be used as advantage in the flexible mould process, as the yield strength of the mixture is increasing when left in rest after casting (step 3 in Figure 8.1 on page 123). Due to this effect, it may build up sufficient yield strength not to flow out of the mould under slope arising during deformation. Furthermore, it may be still possible to deform the fresh concrete, if it is still plastic enough to strain without cracking.

As a literature study of Van Breugel (1997) indicates, during the time of that publication it was generally known that in the first hour after mixing the fresh state concrete is still in the so-called dormant stage³. During this stage the cement paste matrix has not yet formed strong bonds between the aggregate particles, and the behaviour of the fresh state mixture is mainly determined by attraction and repulsion forces between particles, in some literature described as “*network of colloidal interactions*” or “*flocculation*”. Roussel (2006b) initially also considered it reasonable that there exists a period for a “*couple of thousands seconds*” in which irreversible effects of hydration are not yet dominating, a period in which colloidal or thixotropic behaviour is dominant.

In Roussel (2006b) a classification for SCC’s was proposed into three categories of thixotropic behaviour (see Table 8.1). This classification might prove useful to come to a controlled increase in shear yield strength in the present research, and help to determine the correct waiting period suggested in Figure 8.1.

For example, a fresh SCC mixture tested in Roussel (2006b) started off at a yield strength of $\tau_0 = 45$ Pa and showed an increase in apparent shear yield strength (flocculation rate) of 0.26 Pa/s, which after 900 s (= 15 min) resulted in a yield strength

²The term CSH (calcium-silicate-hydrate) is based on cement chemistry notation (C=CaO, S=SiO₂, H=H₂O)

³“On contact with water cement grains immediately start to react. This early reaction period, which lasts for only a few minutes, is termed the pre-induction period” ... “The figures show that after a few minutes a stable concentration is reached which remains so for a period of at least 180 minutes. The rapid early reactions in the first few minutes are followed by a period of low reactivity. This period is known as the induction period or dormant stage. The length of this period depends on the fineness of the cement, the temperature and the chemical composition of the cement (including the gypsum content and admixtures). The dormant stage will generally not exceed 5 hours. From the figures” ... “it can be concluded that during this period the chemical composition of the aqueous phase will remain more or less constant.” (Van Breugel, 1997)

Table 8.1: Classification of SCC's according to their flocculation rate (Roussel, 2006b)

flocculation rate A_{thix} [Pa/s]	SCC type
less than 0.1	non-thixotropic SCC
between 0.1 and 0.5	thixotropic SCC
higher than 0.5	highly thixotropic SCC

of around 280 Pa. After mixing for 3 to 4 min, this full strength development could be made undone, showing the reversibility of the thixotropic process. If, for our application, the same medium-thixotropic mixture would be tested after a resting period of 30, 45 or 60 min, one could expect shear yield strengths of 513, 747 or 981 Pa, respectively, as a result of this thixotropic stabilization. This extrapolation was not performed in Roussel (2006b), since only the first 15 minutes were researched. One might, however, expect the trend of increasing yield strengths to be also valid beyond 15 minutes. This will need to be investigated.

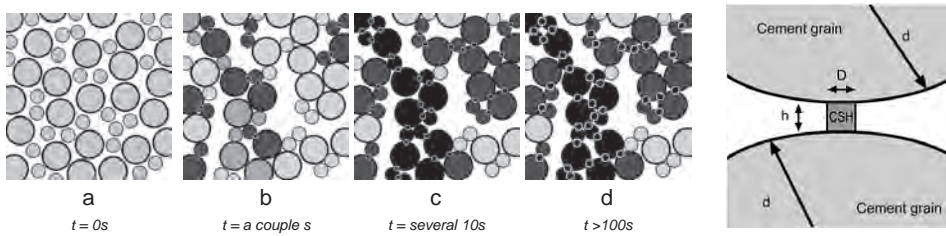


Figure 8.5: Development of CSH-bridges between cement particles during the dormant period (Roussel et al., 2012)

Hardening

Contrary to the above mentioned “network of colloidal interactions” causing thixotropic behaviour, in a recent publication on the thixotropic behaviour of cement pastes (Roussel et al., 2012), it was shown that early hydration (CSH-nucleation starting *directly after* mixing, see Figure 8.5) certainly *is* responsible for a far larger part of the thixotropic behaviour than colloidal effects. These CSH-bridges can still be broken again through powerful mixing and will rebuild as long as sufficient reactive material is available, which explains the thixotropic behaviour that is observed at macro scale. According to Roussel, the strains necessary for breaking the initial CSH-bridges are in the order of magnitude between 1000 and 50 000 $\mu\epsilon$, which is in the same bandwidth as the strains expected as result of the mould deformation process, as we will see later (see Table 9.1 on page 169). The notion of rebuilding strength after mixing, or, in our case, deformation, feeds the thought that deformation after casting does not necessarily result in damage, since the material is still fully reactive. Also this needs further investigation.

8.2.3 Concrete under slope

As could also be seen in Figure 8.1 on page 123, curving a formwork leads to a slope of this formwork with the horizontal plane, which, for a very fluid concrete, will make the concrete flow to the lower part of the mould due to gravity. The self-compacting, self-levelling mixtures that are often used for architectural concrete are actually designed to show exactly this type of easy flowing behaviour. This initial high fluidity will not be beneficial if a limited waiting period before deformation is desired. What growth in yield strength is actually necessary to allow this deformation without concrete flowing out of the mould?

This necessary shear yield strength, denoted here as $\tau_{0,crit}$, may possibly be estimated using equation (8.2), proposed by De Larrard (1999). The equation, stemming from soil mechanics (see Figure 8.6) was used by De Larrard to determine the critical shear yield strength for a stable layer of concrete cast under a slope, an application often found in civil engineering projects during the casting of ramps etc.

$$\tau_{0,crit} = \rho \cdot g \cdot h \cdot \sin(\theta) \quad (8.2)$$

where:	$\tau_{0,crit}$	critical shear yield strength of concrete under slope	Pa
	ρ	density of the concrete	kg/m ³
	g	acceleration of gravity	kg · m/sec ²
	h	height of concrete	m
	θ	slope angle	rad

Reducing the mould to a slope without edges might be somewhat of an oversimplification of the stress situation in the concrete, since the edge of the mould also give some support to the fresh mixture (see Figure 8.6, right image). For larger elements however, the edge of the mould is not always nearby, and with varying curvature, the edge may for some parts of the element also be on the upper end of the slope, not giving any support at all. In this research therefore equation (8.2) will be used,

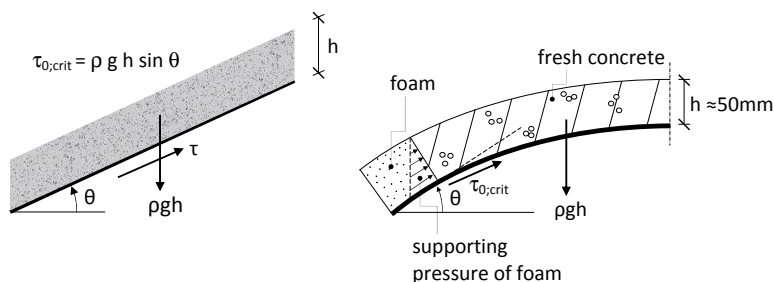


Figure 8.6: left: Critical shear yield strength $\tau_{0,crit}$ of concrete under a slope (after De Larrard, 1999); right: Translation to the case of a mould with fresh concrete (RS / P. Raghunath)

as it is considered on the safe side with respect to overflowing of the mould: it does not rely on any horizontal support, but just on the internal shear strength of the fresh concrete.

Note that in formula (8.2) the critical yield strength $\tau_{0;crit}$ is the only rheological parameter. The plastic viscosity μ_p is not reflected in the formula, which is due to the fact that this parameter only plays a role in the dynamic situation during casting and not in the static stress distribution in rest after casting. To allow deformation, the initial yield stress in rest $\tau = \tau_0$ should first increase to $\tau_{0;crit}$ (Figure 8.7).

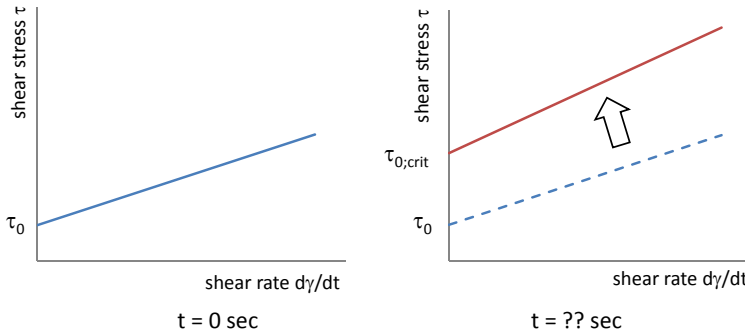


Figure 8.7: Increase in yield strength τ_0 over time until $\tau_{0;crit}$ is reached

8.2.4 Relation between slump and shear yield strength

In order to determine the development of yield strength at several moments during the process, a testing method is needed. A relatively simple way to determine the workability of concrete is the slump test (NEN-EN-12350-2, 2009), although it does not directly give numerical data on the yield strength. The values resulting from the slump tests, however, were empirically linked⁴ to the yield strength by Ferraris and De Larrard (1998), using a BTRHEOM viscometer to measure the yield strength for the same mixtures tested with the slump cone:

$$\tau_0 = \frac{\rho}{347} \cdot (300 - S) + 212 \quad (8.3)$$

where:	τ_0	yield stress	Pa
	ρ	density of the concrete	kg/m ³
	S	slump value, measured with Abram's cone	mm

⁴In chapter 8 (experiments in 2010-2011) this relation was used; in chapter 9 more recent work of (Mueller et al., 2014) will be studied and applied.

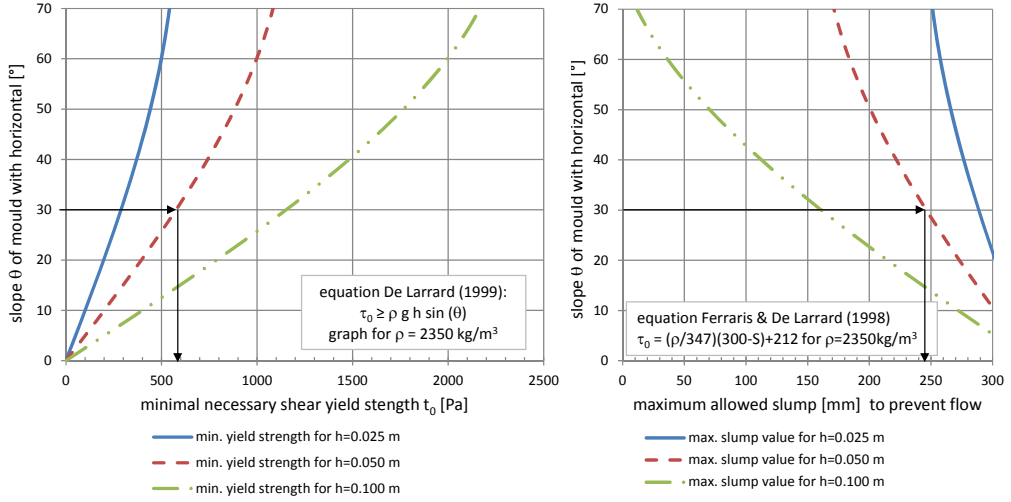


Figure 8.8: Minimal yield stress τ_0 and maximal slump value S necessary for casting under slope θ for concrete layers with thickness h (for $\rho = 2350 \text{ kg/m}^3$), according to Equations 8.2 (left graph) and 8.4 (right graph). Example shown with arrows: if a concrete layer of thickness $h = 0.05 \text{ m}$ (the red dashed line) is cast under a slope of 30° , from the left graph it can be found that a critical shear strength $\tau_{0;\text{crit}}$ of just below 600 Pa is necessary for a stable slope. According to the right graph, this corresponds to a maximum slump value of around $S = 250 \text{ mm}$.

Combining Equations 8.2 and 8.3 yields the maximum slump S for casting under a slope θ :

$$S \leq \frac{73564 + 300\rho - 347 \cdot \rho \cdot g \cdot h \cdot \sin(\theta)}{\rho} \quad (8.4)$$

For several values of the concrete element thickness, the necessary yield strength τ_0 and the maximum slump value S measured with Abrams cone can now be plotted against the slope of the mould θ (see Figure 8.8). For moderate slope angles ($< 30^\circ$) an almost linear relation between slope angle and necessary yield strength is obtained. For the thinnest layer of concrete ($h = 0.025 \text{ m}$) a critical shear yield strength of around 300 Pa is needed for a stable slope of 30° , whereas for a thick layer of concrete ($h = 0.100 \text{ m}$) a critical shear yield strength of around 1150 Pa is needed for the same slope. The corresponding slump values for both examples are $S = 290 \text{ mm}$ and $S = 160 \text{ mm}$, respectively. Although the first slump value is outside the range that was researched by Ferraris and De Larrard (1998) to establish the empirical relation between slump and yield strength, it can be interpreted as a still very plastic concrete. From this it can be concluded that for thin layers under a gentle slope, only a limited shear yield strength is necessary. In chapter 9 further work will be done on this aspect.



Figure 8.9: The natural deflection of steel bars - clearly visible here - is a function of diameter, self weight and support positions (Maasbrug Roermond, image Peter Wijnands Photography)

8.2.5 Bending of reinforcement

In traditional formwork systems a curved shape of the steel reinforcement can be achieved by pre-bending the bars. This task is often performed off-site with automated bending equipment, but for small diameters (up to $\varnothing 16$) it can be done manually, although this is a laborious and heavy job (Lauppe, 2012, p19–20). After bending, these pre-curved bars are placed in or on the formwork.

For large radii one may even rely on the natural flexibility of the bars (see Figure 8.9). For large shell structures with limited curvature, the natural flexibility is often sufficient to follow the shape of the formwork. However, the natural flexibility diminishes rapidly with increasing diameter: the bending stiffness is a function of \varnothing^4 . For small elements with strong curvature (small radius) bars usually need to be forced into shape by plastic deformation.

In the present research, the deformation of the formwork after casting inevitably confronts us with the question which reinforcement can be used, since generally, one cannot expect that steel bars will automatically deform together with the formwork. Before looking at alternatives such as short fibres or textiles, a brief investigation is done to find out up to which curvature and for which diameter traditional steel reinforcement can still be used for the flexible mould method.

It is to be expected that the steel bar will resist forced displacement as a result of its own bending stiffness, but that the fresh concrete around the steel bar, up to an unknown extent, is able to provide counter-forces that will guide the bar in the imposed shape. Figure 8.10 on the following page illustrates this: if the formwork, containing fresh concrete that has stiffened for a certain period and steel rebar, is

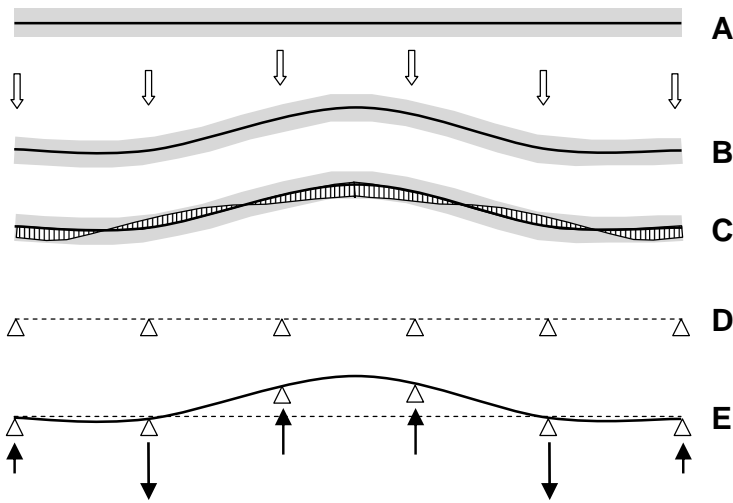


Figure 8.10: Contact forces between fresh concrete and reinforcement bar after forced deformation of the formwork from position A to position B. Image C illustrates an possible distributed contact stress pattern, image D and E illustrate a discrete interpretation of the same.

deformed from the shape in image A to that in B, a steel bar with some bending stiffness will resist the deformation in a manner similar to the distributed contact stress pattern shown in image C. Factors that may influence this stress pattern are expected to be at least the following:

1. the diameter and stiffness of the steel bar;
2. the self-weight of the steel bar;
3. the resistance of the concrete related to its strength development and the diameter of the steel bar.

Using a similar Maple model as discussed in section 7.2, Janssen approached this elastic problem that has various unknowns with a discrete approximation, as shown in image D and E of Figure 8.10: for a 2 meter long mould, 6 support points were imagined, each able to give a reaction force as a result of the displacement. Janssen used a simple beam model to at least get an idea of the order of magnitude of the reaction forces in the six support points, as a function of varying bar diameter $\varnothing 2 - \varnothing 10$ and curvature varying from $R = 1.50$ to $R = 10.0$ m in both upward and downward direction. It was assumed that the concrete was put in a concrete layer of $h = 0.05$ m with a cover of $c = 10$ mm from the lower surface. The weight of the remaining 40 mm of concrete was contributed to the steel bar over an effective width, depending on the diameter of the bar. It was concluded that, by approximation, a steel bar $\varnothing 3$ mm would follow a curvature of $R = 1.5$ m. For further details about the

method, see Janssen (2011, Chapter 7). Other reinforcement options, such as short fibres, flexible steel strands, carbon-, glass- or aramide-strands or -textiles will be discussed later.

8.2.6 Discussion

The literature review of existing theory has resulted in a number of findings relevant for the present research:

1. The Bingham model is often used to describe the behaviour of SCC in the fluid phase; Bingham fluids have the property that a minimum shear stress has to be overcome to make the concrete start flowing;
2. The theory and indicative figures of a.o. Roussel give both an explanation and numerical values for the early strength development as a result of thixotropic behaviour;
3. De Larrard's theory shows that concrete can be cast under a slope and gives a formula that can possibly be used for the situation of our flexible mould;
4. A relation between slump test and yield stress, given by Ferraris and De Larrard, quantifies the development in yield strength over time;
5. It is possible to let steel reinforcement bars follow a limited curvature, depending on the diameter of the bar.

Based on this existing theory, in the following section, the next step in the *wheel of science* is made in the next section: the postulation of a number of first suppositions.

8.3 Suppositions

The mould and the concrete in the mould are stimulated by the deforming supporting system to deform together into a specific and predefined curved shape. Normally this is not the procedure to make complex concrete shapes: for such shapes generally a completely closed formwork is used that is filled from above with a fluid concrete, as was earlier seen in section 2.2.

Based on the notion of De Larrard, that stability of concrete under a slope is possible as long as the yield strength of the concrete is sufficiently high, one might expect that for geometries of which the maximum slope is not too steep, an open mould might be applicable. De Larrard's slope model can then be used to predict the yield strength that is necessary for that specific mould geometry, based on the extreme slope of the formwork.

The necessary yield strength may be the result of an initially stiff concrete, but could also be reached by choosing a SCC mixture with thixotropic properties, that

develops yield strength after casting through the growth of CSH-bridges. The publications of Roussel offer an indication for the speed of this yield strength development.

The thixotropic bonds are still relatively weak in the first stages, as shown by Roussel et al. Based on what is said about the strains necessary to break the initially developed CSH-bridges, it is expected that deformation is still possible, and that this will not lead to a concrete that becomes fully fluid again, as long as the deformation is done slowly and without vibration. After that, still sufficient reactive material is available to result in a fully hardened concrete element. The following suppositions are now formulated:

supposition 1.1 Use of an open mould is possible, as long as the yield strength is sufficiently high to result in a stable slope;

supposition 1.2 De Larrard's slope model can be used for the flexible mould method, by deriving the appropriate yield strength from the extreme values of the slope of the deformed formwork;

supposition 1.3 During the hardening process deformation is possible without flow or cracking as long as the right moment is chosen;

supposition 1.4 Steel reinforcement with sufficiently small diameters can be bent and deformed together with concrete.

To allow testing of these suppositions, a number of experiments was designed.

8.4 Operationalisation

8.4.1 Mini-deformation and mini-slump tests

Firstly, to test whether the use of an open mould is possible (supposition 1.1), a mini-deformation test was designed, to cast and subsequently deform small concrete elements of $400 \times 100 \times 50 \text{ mm}^3$ ($L \times W \times H$). The formwork was made out of flexible material: a Bayer Vivak plate (PET-G-polyester) with a thickness of 1 mm, on which four soft polyether foam edges were glued ($50 \times 50 \text{ mm}^2$ in cross-section, quality SG25 = specific weight 25 kg/m^3). Five formworks were prepared (see Figure 8.11, left), to allow deformation at different moments in time and in different curvatures. The application of curvature was possible by lifting the middle of the mould.

The mini-deformation tests were designed to allow qualitative observations of what happens during deformation: will the concrete stay in the mould, or will it flow over the edges? What waiting time is necessary? What is the influence of the curvature? The test was, as a result of the limited number of viability tests, not suitable to obtain statistically underpinned quantitative information, but it may give a first idea of numerical values useful for further research.

Secondly, since only few slump cones with sizes according to NEN-EN 12350-2 were available, several mini-slump rings were made from PVC-pipe (inner diameter

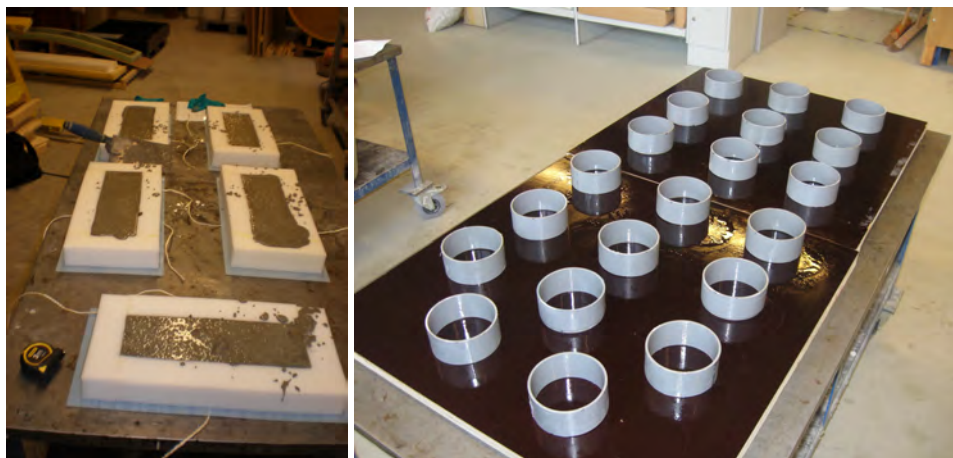


Figure 8.11: Left: mini-moulds for deformation test; right: simple mini-slump tests using multiple PVC-rings (RS / Janssen, 2011)

x height: $\varnothing 112 \times 50 \text{ mm}^2$), to fill them with fresh concrete and lift them at regular intervals of time, to judge in a qualitative manner the development of stiffness of the mixture (see Figure 8.11, right). The observations of the mini-deformation tests are reported in subsection 8.5.1. The mini-slump-tests were used at several moments during the viability study.

8.4.2 Concrete mixtures

Two mixtures were used for the experiments of the viability study (see Table 8.2 on the next page). Both mixtures are self-compacting mortars rather than concretes: mixture m_1 has a maximum aggregate size of 0.25 mm, mixture m_2 of 4 mm. Two different super-plasticizers were used for the mixtures. Mixture m_1 was earlier used by Huyghe and Schoofs (2009) in their experiments (see section 4.4). In the present research, a different plasticizer was applied, and the PVA-fibres were left out to increase workability. Mixture m_1 contained a significantly higher dosage of plasticizers (fly-ash and fine quartz sand were added as mineral additives) than mixture m_2 , which causes a retardation of the stiffness development. Based on the initial testing with mixture m_1 several adjustments were made for the second mixture. Due to the larger maximum aggregate size mixture m_2 is less homogeneous; the shortened processing time and consequently better controllability of the production process outweighed this disadvantage (Grünewald et al., 2012).

8.4.3 Single-curved deformation tests

To test the deformability for a larger scale element, also a test set-up was designed to curve a strip of concrete with a height $h = 0.05 \text{ m}$, a width $w = 0.20 \text{ m}$ and a length

Table 8.2: Applied concrete mixtures in the viability study

ingredients [kg/m ³]	mixture m_1 (very fine)	mixture m_2 (medium-course)
Cement CEM I 52,5 R	526.0	597
Fly-ash	663.0	164
Quartz sand	351.0	-
Superplasticizer Chryso	41.0	-
Fluid Premia 196 con 25% SPL	(=2.66% of total powder content)	-
Superplasticizer BASF Glenium 51 con 35%	-	4.22 (0.55% of total powder content)
Water	299.7	239.6
sand 0.125-0.25 mm	108.0	188.4
sand 0.25-0.5 mm	-	251.2
sand 0.5-1.0 mm	-	376.8
gravel 1-2 mm	-	314.0
gravel 2-4 mm	-	125.6
gravel 4-8 mm	-	-
specific density:	1 989	2 261
<i>other parameters:</i>		
water/cement ratio	0.63	0.41
water/powder ratio	0.21	0.32
cube compressive strength	51.0 MPa (7 days)	69.3 MPa (7 days)
(average of 3 cubes 100x100x100 mm)	78.0 MPa (28 days)	82.3 MPa (28 days)

$L = 2.00$ m. Like the moulds for the mini-deformation tests, also these moulds are flexible: the base plate consisted of plywood ($h = 3.8$ mm) or steel ($h = 1$ mm), the mould edges of polyether foam SG40 or cold foam SG55 with the same cross section as described for the mini-deformation tests. The bending behaviour for the different materials was modelled using the strip model described earlier in section 7.2.

The principle (see top image in Figure 8.12 on the following page) of the single-curved deformation tests was to pre-define a curved shape by preparing various resting points for the flexible mould with varying height. This was done by fixing vertical plates of different heights on a base plate. Initially, the flexible mould was levelled in a horizontal position by a supporting grid and a crane, as shown in the top-left image. In this position, the concrete was cast and finished.

After a chosen waiting period, during which the stiffness development of the concrete could be monitored using the earlier mentioned slump tests, the supporting grid was lowered onto the resting points, thus carefully applying a curvature to the flexible formwork and the concrete. In this curved position, as seen in the top-right image, the concrete then would harden further. The lower three graphs in Figure 8.12 show the shapes that were tested, with a maximum radius varying from $R_{max} = 5.0$ m to $R_{max} = 1.5$ m and a maximum mould slope varying from $\theta_{max} = 5.4^\circ$ to $\theta_{max} = 24.6^\circ$. The observations during the single-curved viability experiments are reported in subsection 8.5.2.

8.4.4 Double-curved deformation tests

A different mould system was designed to test deformability of large scale elements and curvature in two directions. Although in subsection 4.3 more advanced systems for computerized height adjustment were already discussed, for the present research a simpler mechanism was used, which is manually controllable by adjusting the height of nuts on a threaded bar (see Figure 8.13, left). The mould is supported initially by a horizontally levelled plate to allow casting of the concrete. After the chosen waiting period, this plate was lowered, until the mould was supported point-wise by the grid of tubes that each slide over the thread bar and rest on the pre-installed height on a nut and ring.

For the double-curved deformation tests, this principle was scaled up to a mould capable of holding a concrete element of $1.90 \times 0.90 \times 0.05$ m³ ($L \times w \times h$, see Figure 8.13, right two images). The formwork was made out of flexible material: initially this was a plywood plate of 2.00×1.00 m² with a thickness of 3.8 mm, on which four soft polyether foam edges were glued (50×50 mm² in cross-section, quality SG25). In some of the tests, a more advanced support system with thin strips was used, but this is not relevant for now and will be discussed elsewhere.

The shapes for the double-curved elements were derived from the virtual building shape described earlier in subsection 6.2.1. Figure 8.14 on page 142 shows this shape and its dimensions, as well a curvature analysis carried out in Rhinoceros 3D. One might think of a free-form roof structure, which is divided in precast elements, for example as shown in the line pattern. The two areas from where the elements

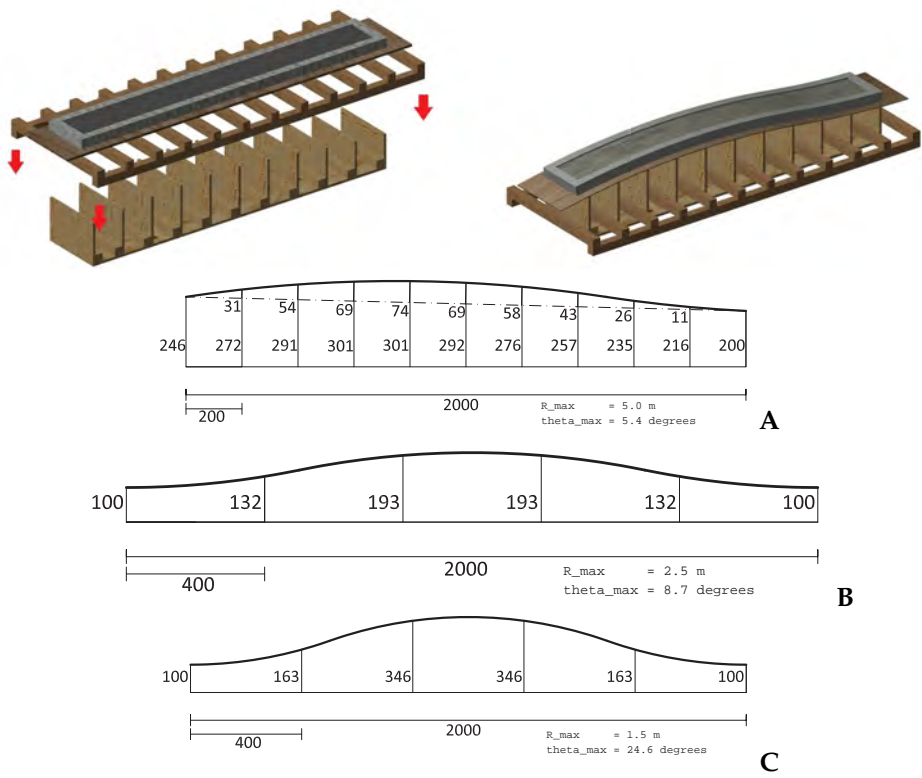


Figure 8.12: top image: test set-up and principle of single-curved deformation tests; lower images: three shapes with increasing maximum curvature and maximum slope (adapted from Janssen, 2011)

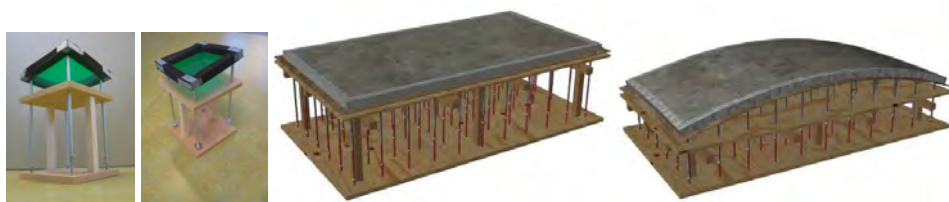


Figure 8.13: left two images: first idea for a simplified height adjustment system
- right two images: worked out set-up for double-curved deformation tests (Janssen, 2011)

were picked to work out in the experiments are circled. The element shape itself is shown in Figure 8.15 on the following page.

From Figure 8.15 it can be seen that both selected elements are clearly double-curved, element D with a positive Gaussian curvature, element A with a negative Gaussian curvature. The difference in height between the highest and lowest point of the upper surface of element D is 186 mm. The maximum local slope with the horizontal plane is around 19.8° . The difference in height between the highest and lowest point of the upper surface of the element A is 210 mm. The maximum local slope with the horizontal plane here is around 27.7° . Although the virtual building shape is only a surface with thickness 0, for both elements a height $h = 0.05$ m (thickness of the curved plate perpendicular to the surface) was chosen. The heights were translated to pin-heights for the mould set-up as shown in Figure 8.13 by combining the 3D-surface with a 200×200 mm square grid of pins, and measuring the height at the crossing points of pins and surface, see Appendix C for more details on this procedure. The results of the viability experiments with the double-curved elements are reported in subsection 8.5.3.

8.5 Observations

8.5.1 Mini-deformation and mini-slump tests

The mini-slump tests with mixture m_1 showed that this mixture remained very fluid for a long period, with the following indicative slump flow : $SF = 200$ mm at $t = 2.5$ hours; $SF = 210$ mm at $t = 4$ hours; $SF = 190$ mm at $t = 5.5$ hours and $SF = 210$ mm at $t = 6.5$ hours (see Figure 8.16 on page 143). It was observed that the chosen method with PVC rings and sealing was not working optimally, since in some cases the concrete stuck to the inner surface of the slump ring and thus was lifted together with the ring. The above slump spread values therefore can not be seen as more than a rough indication that the slump remains rather constant over time. It was also observed that the viscosity of the mixture was rather high: it took 20 to 30 seconds before the mixture would come to rest after the slump tests.

Mixture m_2 demonstrated a much quicker stiffening: directly after mixing, using

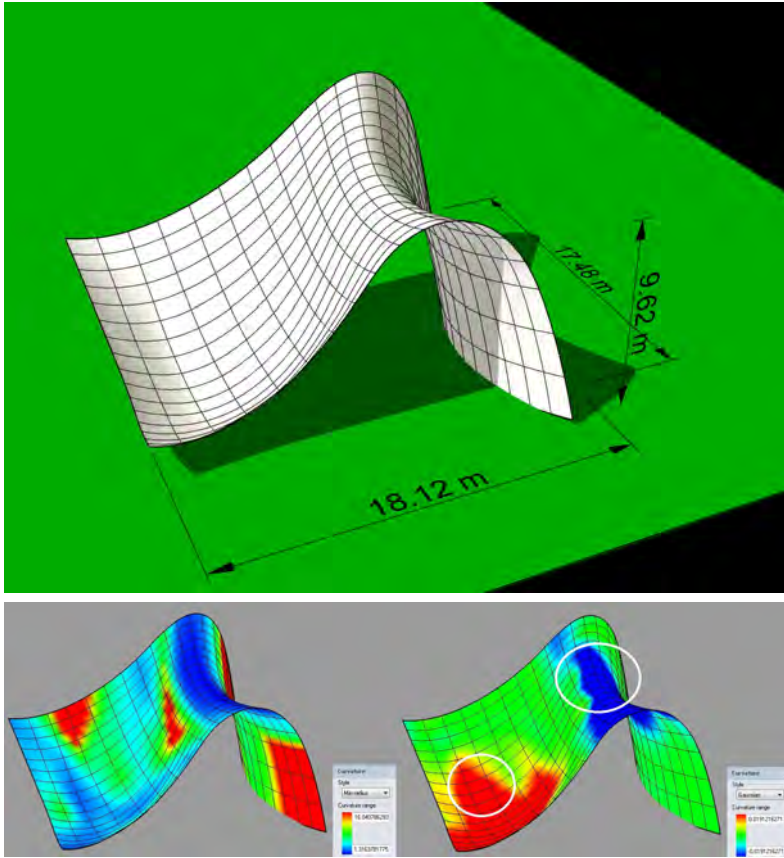


Figure 8.14: Top: virtual building shape, provided by Evolute; bottom left: curvature analysis, minimum radius; the radii of this double-curved surface vary between $R = 1.31$ m and $R = 16.04$ m.; bottom right: Gaussian curvature analysis ($K = \kappa_1 \cdot \kappa_2$), which varies from $K = -0.0191 \text{ m}^{-2}$ to $K = +0.0191 \text{ m}^{-2}$

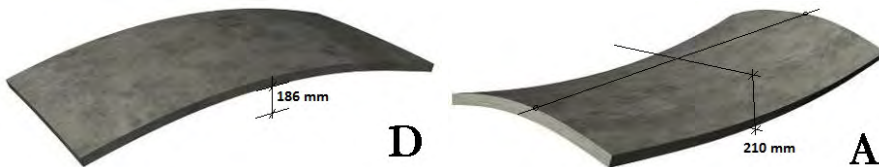


Figure 8.15: In Figure 8.14 the two areas were circled from which the elements are picked for the experiments; the left element D is taken from the red area and has a positive Gaussian curvature, the right element A is taken from the blue area and has a negative Gaussian curvature, indicating a saddle-like shape; the element sizes are approximately $2 \times 1 \times 0.05 \text{ m}^3$. More details can be found in Appendix C (adapted from Janssen, 2011)



Figure 8.16: Mini-slump tests with PVC-rings for mixture m_1 at $t = 1:30$ h:min (left) ; mixture m_2 at $t = 0:45$ h:min (right)

the Abrams cone, the slump flow spread was determined at $SF = 870$ mm, indicating that the mixture was self-compacting and self-levelling ($\tau_0 \approx 24$ Pa according to equation 9.2 on page 173). Already at $t = 0:45$ h:min, the slump value using the PVC-rings had reduced to $S = 0$, leaving the concrete in the shape of the PVC ring after lifting (see Figure 8.16, right). It was, therefore, decided to use mixture m_2 for the remaining tests in the viability study.

The mini-deformation tests gave some useful results: it was observed that in case of deformation at $t = 0:30$ h:min, indeed the concrete would partially, but not fully flow down the slope, as can be seen in the left image in Figure 8.17. The intended element height was $h = 50$ mm. A slope of around 14° was realized by lifting the middle part of the mould for a positive curvature or the ends of the mould for a negative curvature. For stability of the fresh concrete at this slope, according to equation 8.4 on page 132 a shear yield strength of $\tau_0 \approx 300$ Pa is necessary. The element height in the middle however had reduced to 40 (middle) to 45 mm (edges) and at the ends the height had increased to 52 (edges) to 55 mm. This made clear that the concrete was still too fluid at the moment of deformation, so apparently $\tau_0 < 300$ Pa. Unfortunately the mini-slump rings could not be used to obtain a numerical value for the shear yield strength due to the absence of a real conical shape, making the concrete stick to the rings. The larger difference in height at the centreline of the element compared to the difference in height along the long edges also indicated that friction between concrete and the long edges of the mould offered some extra support to the concrete body, so the scale of the test might not be suitable for showing the effects that would occur in a full scale concrete element.

After a longer waiting period, however, plastic deformation of the concrete at $t=0:45$ h:min resulted in a more smooth and more even height of the element. This can be observed in the right image in Figure 8.17. Even here, some height differences of around 5 mm were observed.

8.5.2 Single-curved deformation tests

Test 1

In test 1 geometry A of Figure 8.12 on page 140 was applied to the concrete. The experiment is illustrated in Figure 8.19, page 147. The experiment consisted of a concrete element with size $2.00 \times 0.20 \times 0.05 \text{ m}^3$ that was deformed over a maximum difference between the support heights of $\Delta z = 201 \text{ mm}$, a minimum radius of $R = 5.00 \text{ m}$, resulting in a maximum slope of the mould with the horizontal of $\theta = 5.4^\circ$. The element was reinforced with a double mesh of galvanized steel $\varnothing 3 - 150$, both meshes positioned with a concrete cover of $c = 10 \text{ mm}$ from the bottom surface. As a result of this, 4 thin steel bars were put in the length direction of the element. This reinforcement was also connected to four stirrups, that were later used to lift the element from the mould by crane (image 1 and 2 in Figure 8.19).

Concrete mixture m_2 was prepared, which was not fully self-compacting and self-levelling due to a quick rise in stiffness after mixing (image 3 and 4 of Figure 8.19). Slump rings were filled and tested at several time intervals (image 4-7 of Figure 8.19). Also small prisms were cast and slightly tilted to observe the behaviour of the concrete under a slope (image 8). Finally, at $t = 0:45 \text{ h:min}$, the slump tests indicated that the mixture had stiffened enough to deform the mould at $t = 0:50 \text{ h:min}$ after casting (image 9).

During deformation, the mould successfully followed the predefined geometry, while no cracks were visible during or after deformation. The concrete did not flow down within the mould. After deformation, the concrete was covered with cellophane foil to limit evaporation. The next day, the element was demoulded and inspected. No cracks were visible, the steel rebar came nowhere at the surface of the concrete. The element height had remained constant over the length, indicating that the concrete had indeed not been redistributed over the mould length.

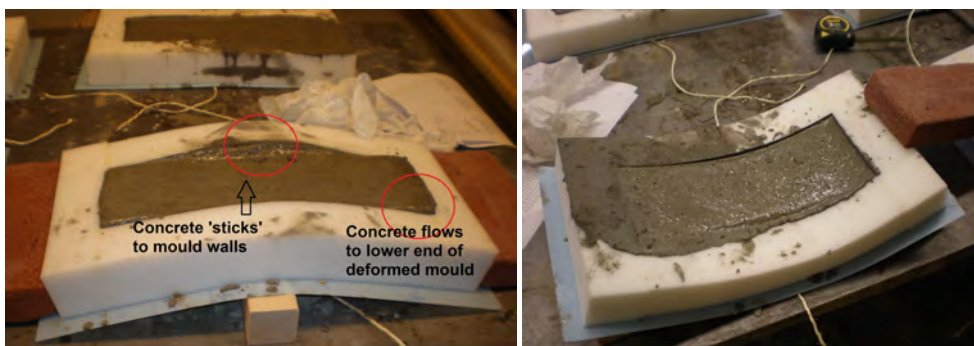


Figure 8.17: Observations during mini-deformation tests

Test 2

In test 2 the same geometry A was applied as in test 1, but using a different mould and edge materials, which for now is not relevant. The same procedure was applied as in test 1, and with similar result. The experiment is illustrated in Figure 8.20 on page 148.

Test 3

In test 3 geometry B of Figure 8.12 on page 140 was applied to the concrete. This experiment again consisted of a concrete element with size $2.00 \times 0.20 \times 0.05 \text{ m}^3$ that was this time deformed over a maximum difference between the support heights of $\Delta z = 93 \text{ mm}$, but with a smaller minimum radius of $R = 2.50 \text{ m}$, resulting in a maximum slope of the mould with the horizontal of $\theta = 8.7^\circ$. In Figure 8.21 on page 149 the deformation process is illustrated by stills from a video sequence (image 4-6).

Despite of the stronger curvature and increased slope, the deformation, again at $t = 0:50 \text{ h:min}$ after casting went successful and resulted in a concrete elements without visible cracks and the correct shape. No steel was visible in the concrete surface, indicating that the rebar had deformed together with the concrete. Wrinkles were visible on the edges of the element as a result of the plastic foil that was used to cure the concrete (image 10).

Test 4

In test 4 geometry C of Figure 8.12 on page 140 was applied to the concrete with again a stronger curvature and steeper slope. The experiment again consisted of a concrete element with size $2.00 \times 0.20 \times 0.05 \text{ m}^3$, but was deformed this time over a maximum difference between the support heights of $\Delta z = 246 \text{ mm}$, a minimum radius of $R = 1.50 \text{ m}$, resulting in a maximum slope of the mould with the horizontal of $\theta = 24.6^\circ$. Images are visible in Figure 8.22 on page 150. This time the deformation at $t = 0:50 \text{ h:min}$ after casting led to a large crack, appearing in the top surface of the concrete in the middle of the element (image 8 and 9).

Test 5

In test 5 the same geometry C as in test 4 was applied once more, but the element was deformed earlier, namely at $t = 0:30 \text{ h:min}$ after casting. Contrary to test 4, now no cracks appeared, neither directly after deformation, nor after demoulding. Since this element was deformed much earlier than in the previous 4 experiments, it was checked if flow of fluid concrete had occurred from the higher to the lower parts of the mould. This was done by measuring the element thickness over the full length of the 2.00 m , at intervals of 0.10 m (see Figure 8.18 on the following page). It was concluded that the concrete had slightly flowed to the lower parts of the mould

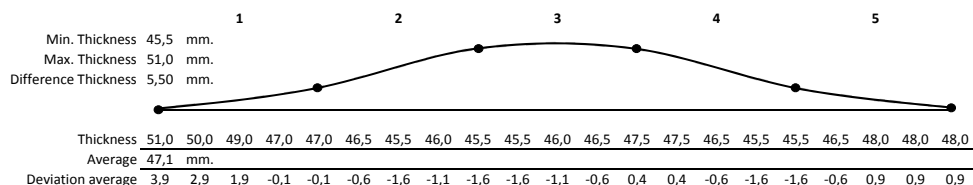


Figure 8.18: Measurement of element thicknesses over the element of experiment 5 at intervals of 10 cm; visible is a slight increase in element thickness in the lower parts compared to the middle part of the element: left and right the thicknesses are 51 mm and 48 mm, respectively, while around the middle, the element thickness has a minimum value of 45.5 mm (adapted from Janssen, 2011).

after the deformation, and therefore, the concrete was too fluid at the moment of deformation, given the slope and curvature of this geometry.

8.5.3 Double-curved deformation tests

Test 6

In test 6 geometry D of Figure 8.15 on page 142 was applied to the concrete. The experiment is illustrated in Figure 8.24 on page 152. The experiment consisted of a concrete element with size $1.95 \times 1.00 \times 0.05 \text{ m}^3$ that was deformed over a maximum difference between the support heights of $\Delta z = 186 \text{ mm}$, a minimum radius of $R = 3.06 \text{ m}$, resulting in a maximum slope of the mould with the horizontal of $\theta = 19.8^\circ$. The element was reinforced with a single mesh of galvanized steel $\varnothing 3 - 100$, positioned with a concrete cover of $c = 10 \text{ mm}$ from the bottom surface. This reinforcement was also connected to four stirrups, that were later used to lift the element from the mould by crane (Figure 8.24, image 1 and 10).

Concrete mixture m_2 was prepared, which was self-compacting and self-levelling, allowing an easy casting procedure (Figure 8.24, image 2 and 3). No slump tests were carried out during test 6. Directly after casting, the casting side was finished manually to obtain a smooth surface. At $t = 0:45 \text{ h:min}$, the mixture had gained sufficient yield strength for deformation, and the element was deformed (Figure 8.24, image 6-9). The deformation went smooth, no cracks appeared during this process, the concrete stayed in place and did not run down the slope. After deformation, the element was covered with plastic to protect it against evaporation (Figure 8.24, image 11). The next day, the element was demoulded. Apart from inaccuracies due to local buckling of the formwork plate, which was discussed earlier in section 7.3, the global shape of the demoulded element was correct. The hardened concrete did not show visible cracks.



Figure 8.19: Deformation test 1, single-curved element $2.00 \times 0.20 \times 0.05 \text{ m}^3$, $\Delta z = 201 \text{ mm}$, $R_{\min} = 5.00 \text{ m}$, slope $\theta_{\max} = 5.4^\circ$; deformation at $t = 0:50 \text{ h:min}$ after casting

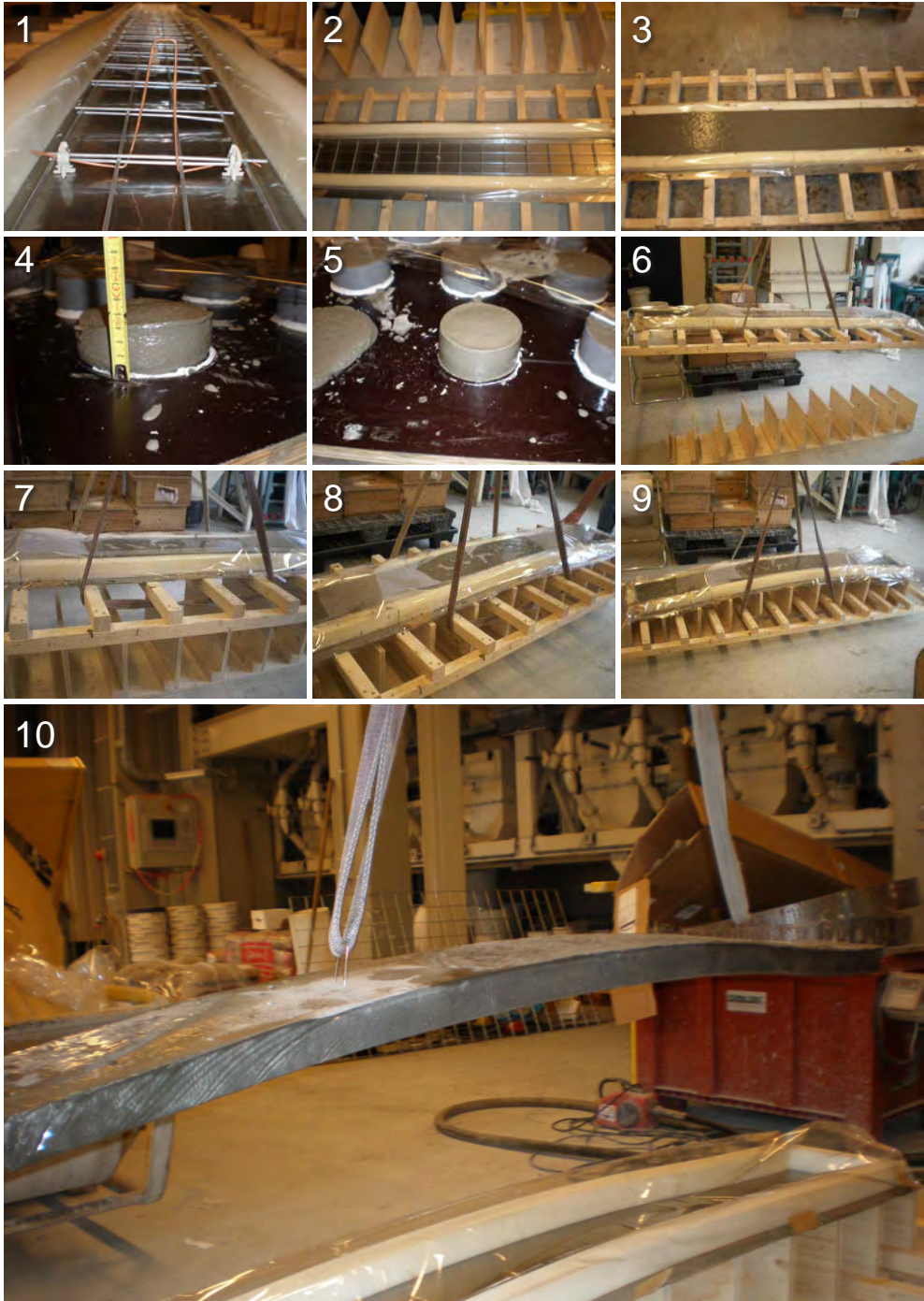


Figure 8.20: Deformation test 2, single-curved element $2.00 \times 0.20 \times 0.05 \text{ m}^3$, $\Delta z = 201 \text{ mm}$, $R_{\min} = 5.00 \text{ m}$, slope $\theta_{\max} = 5.4^\circ$; deformation at $t = 0:50 \text{ h:min}$ after casting

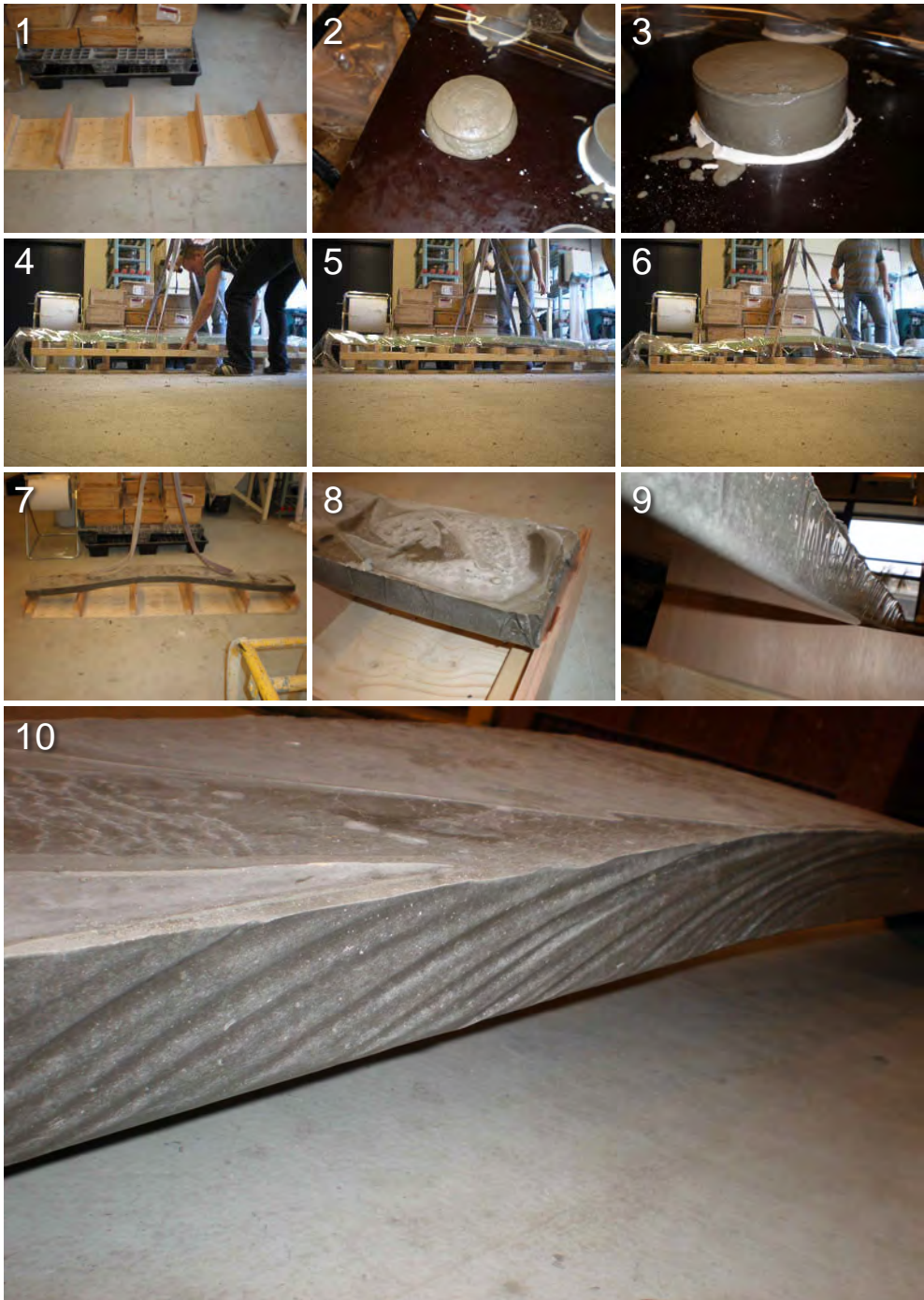


Figure 8.21: Deformation test 3, single-curved element $2.00 \times 0.20 \times 0.05 \text{ m}^3$, $\Delta z = 93 \text{ mm}$, $R_{min} = 2.50 \text{ m}$, slope $\theta_{max} = 8.7^\circ$; deformation at $t = 0:50 \text{ h:min}$ after casting - the wrinkles are the result of using foil to protect the mould.

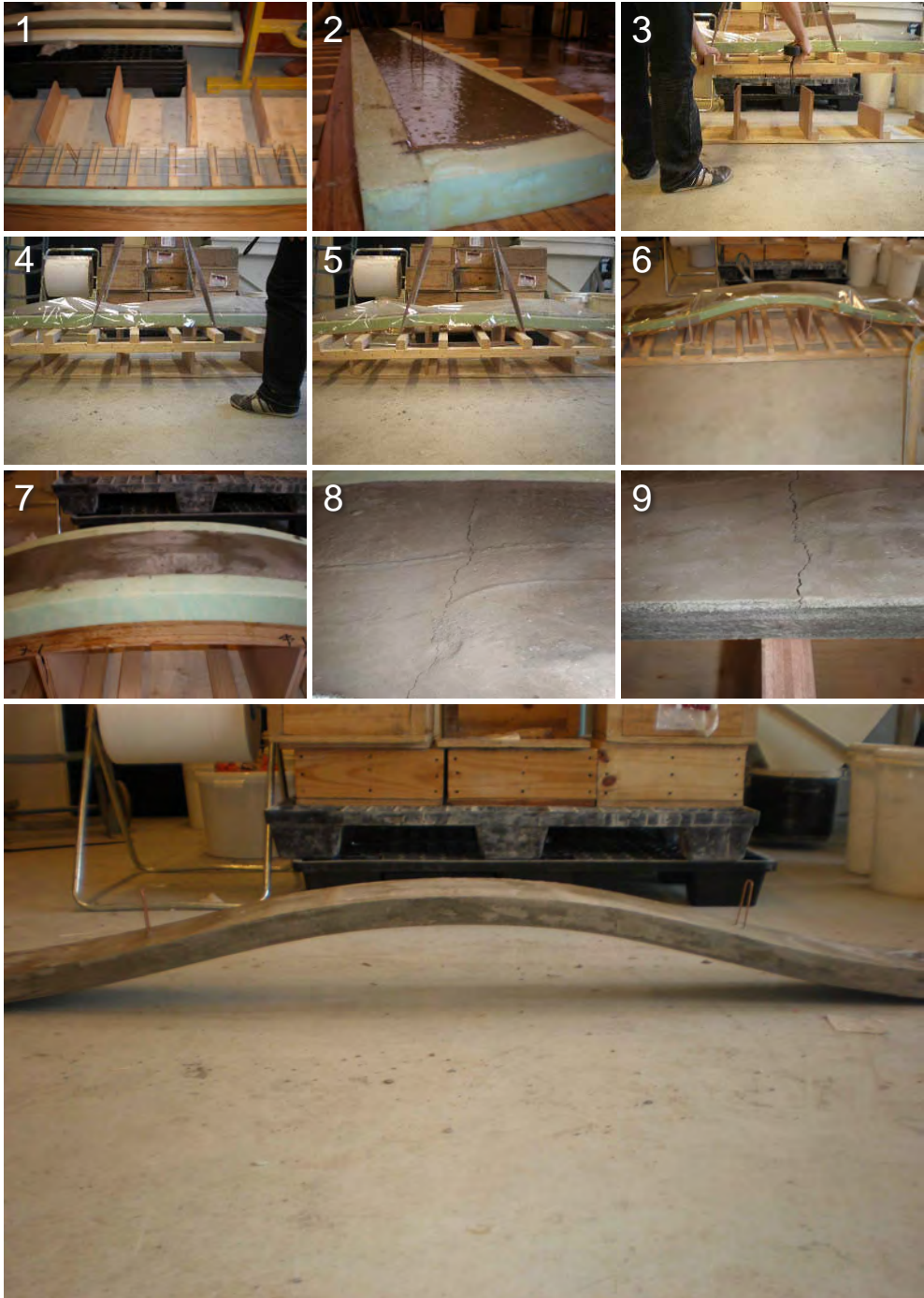


Figure 8.22: Deformation test 4, single-curved element $2.00 \times 0.20 \times 0.05 \text{ m}^3$, $\Delta z = 246 \text{ mm}$, $R_{\min} = 1.50 \text{ m}$, slope $\theta_{\max} = 24.6^\circ$; a crack is visible in the middle (image 8 and 9); deformation at $t = 0:50 \text{ h:min}$ after casting



Figure 8.23: Deformation test 5, single-curved element $2.00 \times 0.20 \times 0.05 \text{ m}^3$, $\Delta z = 246 \text{ mm}$, $R_{\min} = 1.50 \text{ m}$, slope $\theta_{\max} = 24.6^\circ$; deformation at $t = 0:30 \text{ h:min}$ after casting

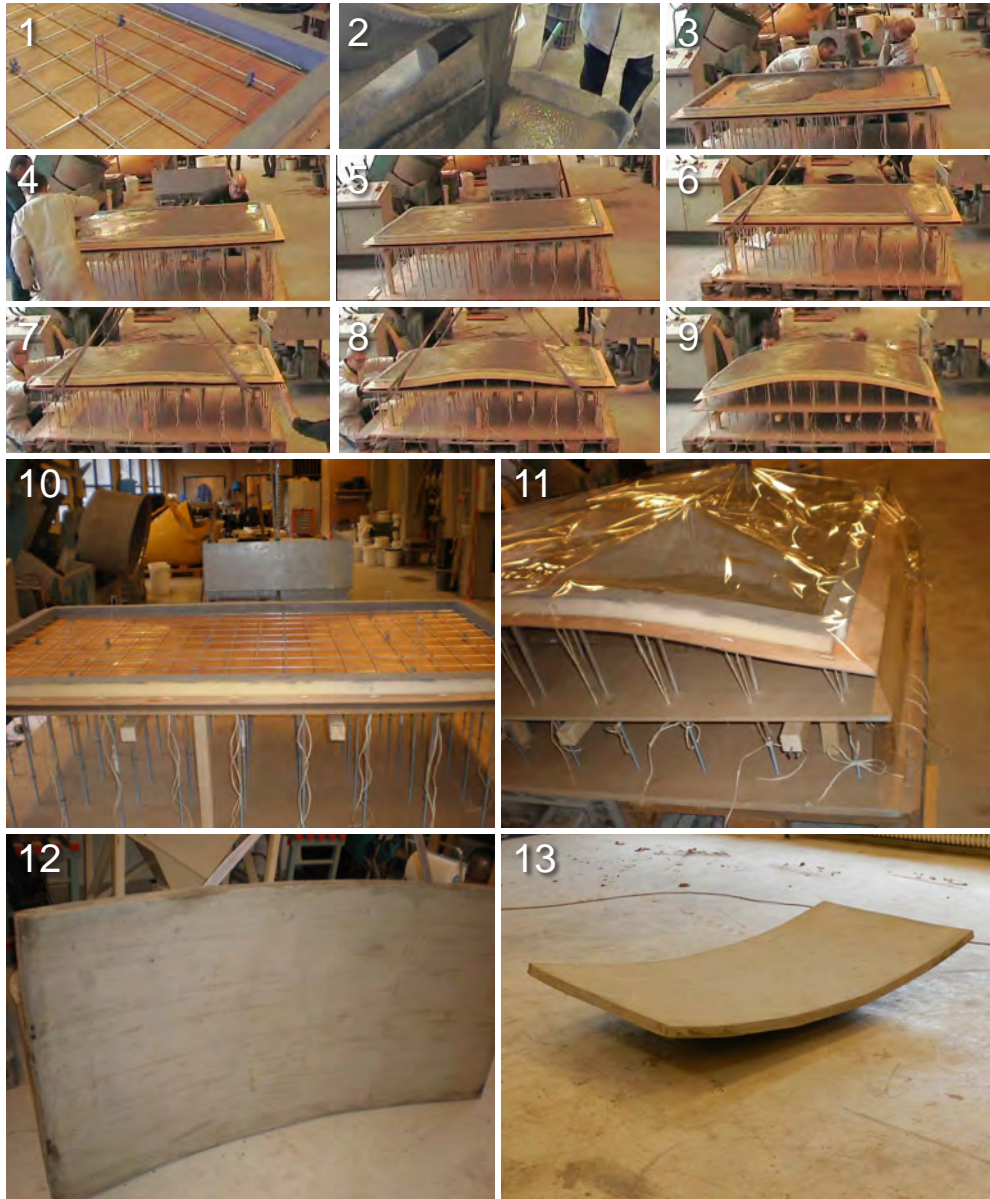


Figure 8.24: Deformation test 6, double-curved element $1.95 \times 1.00 \times 0.05 \text{ m}^3$, $\Delta z = 186 \text{ mm}$, $R_{\min} = 3.06 \text{ m}$, slope $\theta_{\max} = 19.8^\circ$; deformation at $t = 0:45 \text{ h:min}$ after casting

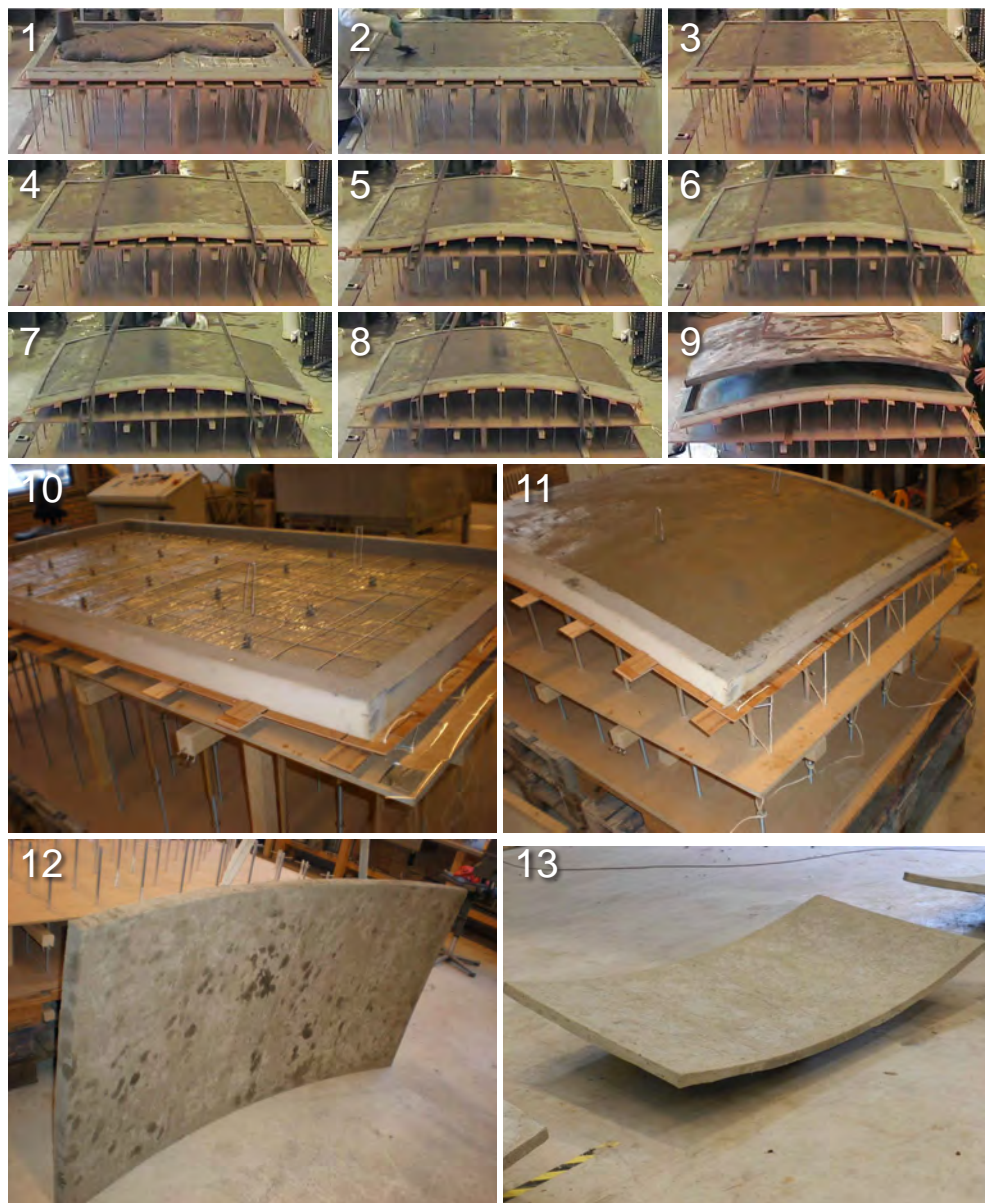


Figure 8.25: Deformation test 7, double-curved element $1.95 \times 0.90 \times 0.05 \text{ m}^3$, $\Delta z = 186 \text{ mm}$, $R_{\min} = 3.06 \text{ m}$, slope $\theta_{\max} = 19.8^\circ$; deformation at $t = 0:45 \text{ h:min}$ after casting

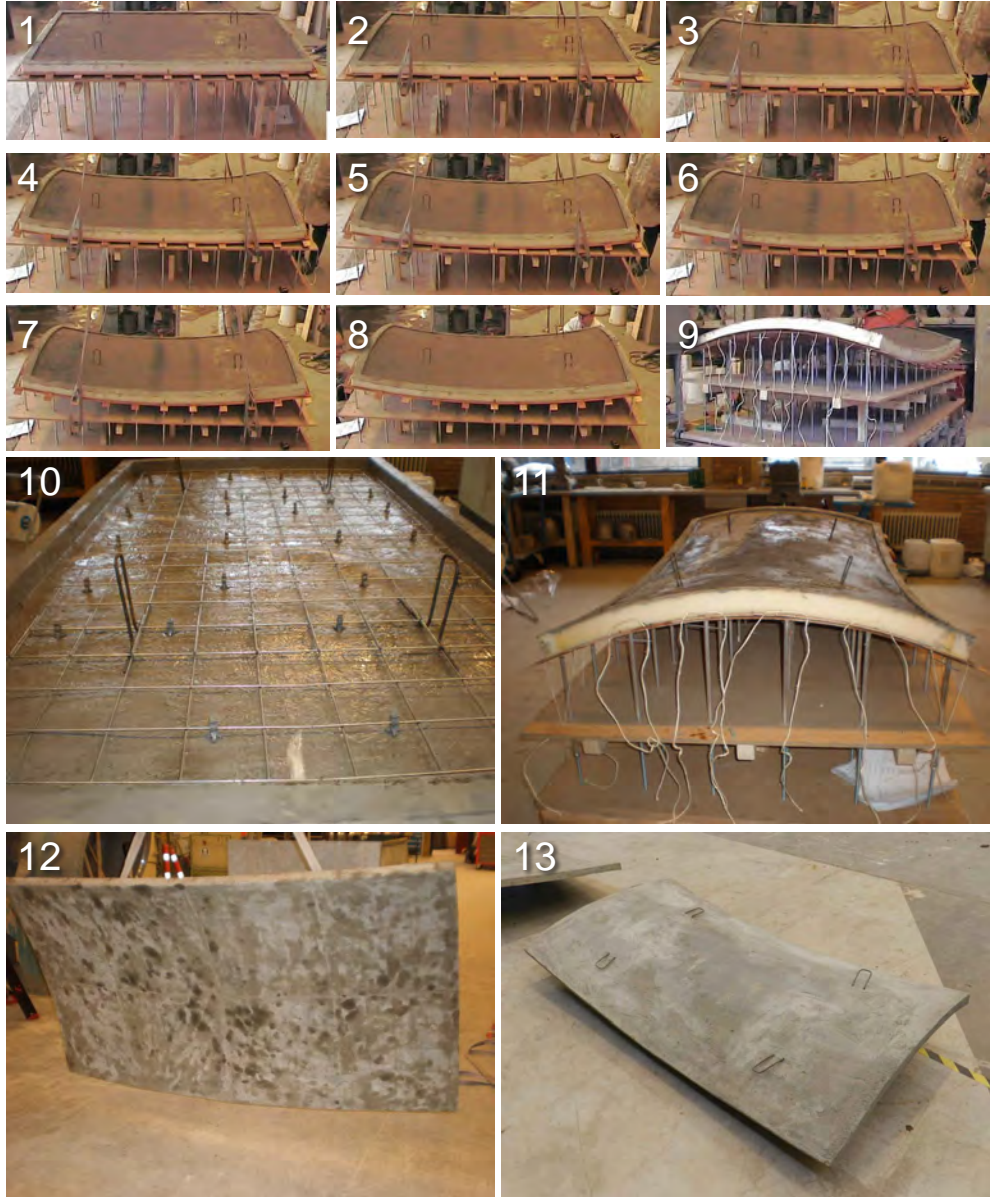


Figure 8.26: Deformation test 8, double-curved element $2.00 \times 1.00 \times 0.05 \text{ m}^3$, $\Delta z = 210 \text{ mm}$, $R_{\min} = 1.73 \text{ m}$, slope $\theta_{\max} = 27.7^\circ$; deformation at $t = 0:45 \text{ h:min}$ after casting

Test 7

In test 7, the same geometry and reinforcement were used as in the previous test. This time, an improved formwork subsystem with strips was used, which was discussed earlier in section 7.4, to prevent the local buckling problem observed in test 6. The experiment is visible in Figure 8.25. Again concrete mixture m_2 was used, but this time the mixture was not self-compacting and self-levelling due to an unintended consequence of a slight variation in mixing procedure: the superplasticizer was added to the mixture before the largest part of water was added, which reduced the effectiveness of the superplasticizer. This led to a quick rise in stiffness after mixing (image 1). As a result of this, the casting went less easy, and mechanical compaction with a vibration needle and manual finishing was necessary to obtain a well-filled mould. Again at $t = 0:45$ h:min, the element was deformed (image 3-8 in Figure 8.24). The deformation went similar to test 6, but resulted in a smoother shape due to the change in formwork subsystem. The demoulded element did not show any visible cracks, but showed quite a rough mould surface as a result of the modified mould material (foam manually smeared with silicones). Also colour differences were visible directly after demoulding, which however disappeared in the days after demoulding.

Test 8

In test 8 geometry A of Figure 8.15 on page 142 and Appendix B was applied to the concrete. The experiment is illustrated in Figure 8.26. The experiment consisted of a concrete element with size $2.00 \times 1.00 \times 0.05 \text{ m}^3$ that was deformed over a maximum difference between the support heights of $\Delta z = 210 \text{ mm}$, a minimum radius of $R = 1.73 \text{ m}$, resulting in a maximum slope of the mould with the horizontal of $\theta = 27.7^\circ$. The element was again reinforced with a single mesh of galvanized steel $\varnothing 3 - 100$, positioned with a concrete cover of $c = 10 \text{ mm}$ from the bottom surface. This reinforcement was also connected to four stirrups, that were later used to lift the element from the mould by crane.

Concrete mixture m_2 was prepared, which showed similar behaviour as in test 7, making mechanical compaction necessary⁵. The casting side was finished to obtain a smooth surface (image 1). At $t = 0:45$ h:min, the mixture was estimated to have gained sufficient yield strength for deformation, and the element was deformed (image 2-8). The deformation went smooth, no cracks appeared during this process, the concrete stayed in place and did not run down the slope. The next day, the element was demoulded. Apart from inaccuracies due to local buckling of the formwork plate, which will be discussed elsewhere, the global shape of the demoulded element was correct. The hardened concrete did not show visible cracks, the reinforcement did not touch the concrete surface as far as visible from the outside of the element. In the next subsection the position of the reinforcement will be discussed in more detail.

⁵At this point we were not yet aware of the importance of the order of addition of water and plasticizer

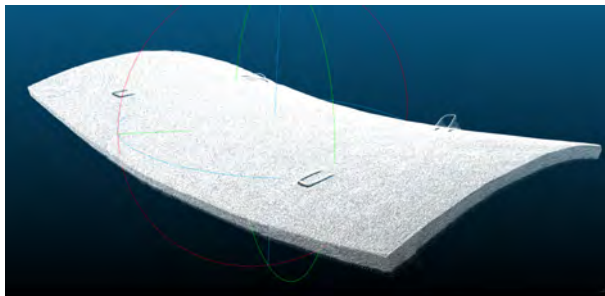


Figure 8.27: Laser scan of the saddle-shaped element cast during deformation test 8

8.5.4 Geometry research

To evaluate the geometrical accuracy of the flexible mould method various laser scans were made, using the Faro Laser Scanner Photon 120/20 (Eigenraam, 2013). Two elements were analysed from the viability study deformation tests 7 and 8 from page 153 and 154, respectively. The intended shapes D and A of these tests were earlier discussed in detail in subsection 8.4.4. For this analysis, the shape of the top surface was analysed, and the edges were not considered yet. Figure 8.27 shows a scan of the element with shape A from test 8.

For the comparison, CloudCompare was applied, which is software that is able to make a best fit between two point clouds. The software does so by applying an advanced least-squares method. The following steps were taken:

1. The architectural surface was exported from the CAD software Rhino to a triangle mesh file that could be read by CloudCompare;
2. The point cloud obtained with the Faro laser scanner was trimmed (irrelevant parts were cut away) until only the surface of the concrete element remained. Surroundings, such as the room in which the scan was taken, were removed from the point cloud;
3. This trimmed point cloud then was also imported in CloudCompare;
4. A best fit was calculated (defined as 3 translations and 3 rotations of the architectural shape from Rhino relative to the scanned point cloud from the laser-scan), and finally
5. The distances between the architectural surface and the measured concrete element were calculated and set out in a histogram and colour graphs.

Figure 8.28 on page 158 shows the outcomes of the comparison of the two elements. For element shape D from test 7 the largest differences were -6 mm and +9 mm. The histogram indicates that panel surface overall is mostly within a few mm of the intended shape. For element shape A from test 8 larger inaccuracies are measured:

Table 8.3: Measured element thickness and concrete cover in x and y direction on reinforcement for test 6, 7 and 8

		test 6	test 7	test 8
thickness [mm]	min	42.0	38.0	37.0
	average	47.1	46.0	44.4
	max	54.0	52.0	49.0
cover x-direction [mm]	min	10	5	4
	average	11.2	8.1	9.7
	max	12	10	18
cover y-direction [mm]	min	13	6	7
	average	16.0	12.0	11.5
	max	24	19	15

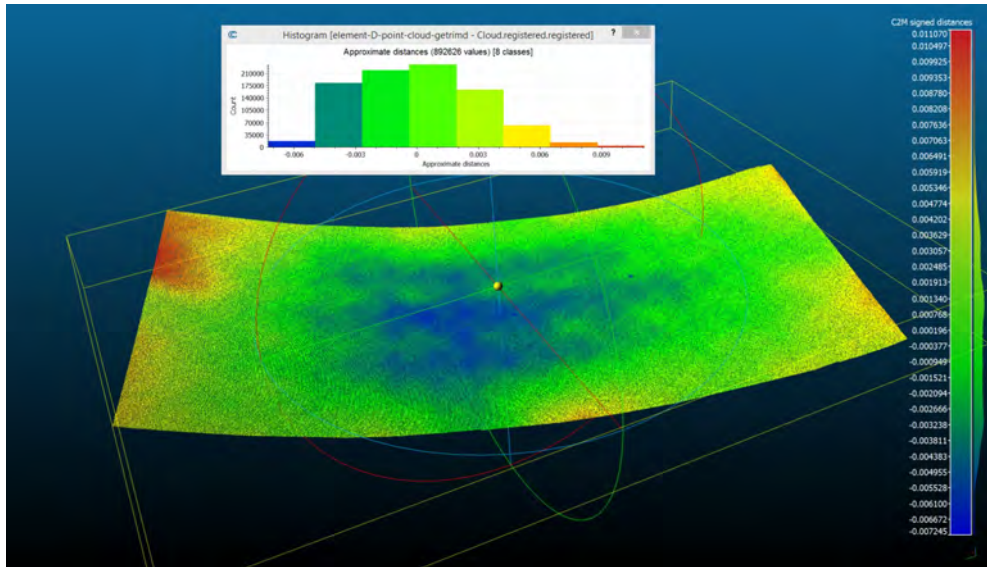
between -44 mm and +39 mm, especially at the corners; the histogram indicates, though, that most of the panel is within the range -10 to +10 mm. In this analysis the position of the edges was not taken into consideration yet, since no accurate geometrical model was available. It is expected that these edges would also have shown rather large differences, though.

8.5.5 Position of reinforcement after deformation

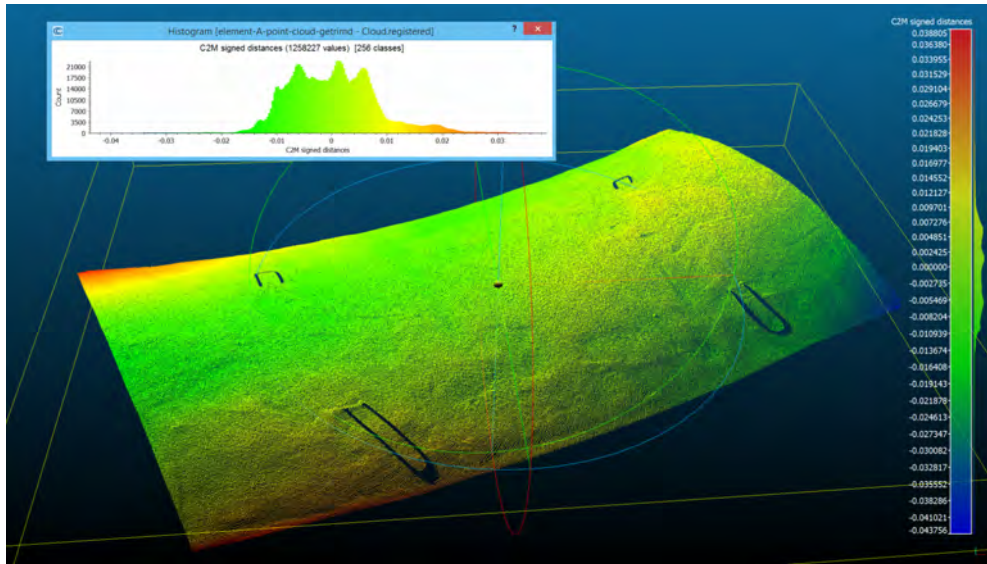
In the deformation tests described above, thin galvanized steel reinforcement bars were applied with a diameter of only 3 mm. As a result of the flexibility this thin rebar was able to follow the imposed deformation without displacement relative to the upper and lower concrete surface. Both the developed yield strength of the fresh concrete and the self weight of concrete and rebar helped in guiding the rebar into its deformed shape. Janssen (2011) calculated for diameters between 3 and 10 mm the necessary forces for curving the rebar into radii between 1.5 and 10 m, showing that, as expected, the smaller the radius of curvature, the thinner the rebar needs to be, to follow the deformation without large forces becoming necessary to keep the rebar in place.

The concrete panels produced during test 6, 7 and 8 were cut into eight segments each to investigate the position of the reinforcement ($\varnothing = 3$ mm at c.t.c. distance 100 mm in both directions). In the second part of Appendix C from page 277, the measurements of the element thickness and the concrete cover on the reinforcement of these panels are shown.

The summarized results are presented in Table 8.3. Figure 8.29 on page 159 shows one segment. It is concluded that the intended element thickness of 50 mm was not reached, and that all panels are slightly thinner (44 to 47 mm average thickness). The concrete cover in the longitudinal (x-) direction of the elements is in the range of 8.1 to 11.2 mm. Although the intended 10 mm cover was not reached at many positions, the reinforcement has clearly followed the overall curvature of the elements without problems, especially if we take into account the large vertical displacements during



(a) element shape D from test 7 - largest differences -6 mm and +9 mm, histograms indicates that panel surface overall is mostly within a few mm of the intended shape



(b) element shape A from test 8 - here larger inaccuracies are measured: between -44 mm and +39 mm, especially at the corners; histogram indicates most of the panel is within range -10 to +10 mm

Figure 8.28: Calculated distance between the architectural element and the laser-scanned concrete element - only the top surface is compared now, so edge position remains to be studied

deformation (186 mm for test 6 and 7, 210 mm for test 8). In this perspective the measured bandwidth of the cover on the reinforcement in x-direction is relatively small, although the minimal covers are not acceptable from a durability point of view, even not for galvanized steel (Gowripalan and Mohamed, 1998). Values lower than 10 mm can also be partially explained by the fact that the distance-holder at many points was slightly pressed into the soft mould surface. The concrete cover in perpendicular (y-) direction shows a larger bandwidth. Still, the reinforcement has roughly followed the shape of the panel. Although, in the cut samples, no voids were observed between hardened concrete and reinforcement bars, it cannot be ruled out that the deformation of the plastic concrete and the embedded reinforcement may locally have led to a loss or reduction of bond between steel and concrete.

Other materials are available for reinforcing the concrete, such as short steel fibres, short carbon or aramide fibres or strands of steel, carbon or aramide. These possibilities for reinforcement will be discussed later in this thesis.

8.6 Data analysis

8.6.1 Mini-slump tests

The mini-slump indicated that mixture m_1 remained too fluid during the first 6.5 hours of the test, so that the use of this mixture would practically lead to a process of mixing and casting in the morning and deformation in the afternoon or evening. At this point in the research it was still a question whether with a lower dosage or different type of plasticizers also mixture m_1 could be used in a more controlled manner. Mixture m_2 resulted in a stiff mixture within the first hour after mixing and casting of the fresh concrete. For both laboratory and concrete factory the use of mixture m_2 was considered beneficial compared to mixture m_1 . The 28-day compressive strength of mixtures m_1 (78.0 MPa) and m_2 (82.3 MPa) were almost the same. Considering the quite different workability of the batches prepared for test 6 (self-compacting) on the one hand and test 7 and 8 (both needed vibration) on the other hand, while using the



Figure 8.29: Cross-section of the element from test 8 after cutting: the reinforcement has followed the curvature within reasonable accuracy

same recipe, it can be concluded that the process of preparing the concrete was not fully controlled, and was critical to unknown factors.

8.6.2 Mini-deformation tests

From the mini-deformation tests it was concluded that the scale of the mould has influence on the imposed deformation: in a small mould relatively much of the concrete volume sticks to the edges of the mould. Due to this, shear forces will be working between concrete and edge in a situation that the mould is under a slope. In a small mould, the concrete will be kept in position by friction forces along the mould edges, more than in a large mould.

It was further observed that concrete in cases of a too fluid mixture did not flow completely out of the mould, but would only redistribute itself partially within the mould, leaving some parts thinner, and other parts thicker than intended and thus reducing the slope of the top surface of the concrete. Based on these observations, the flow criterion proposed by De Larrard in equation 8.2 on page 130 should perhaps not to be seen a sharp borderline between flowing and not flowing, but as the point at which such plastic redistribution is expected. The extent to which this redistribution takes place could then e.g. be dependent on the difference between the calculated yield strength for a stable slope and the real yield strength at that moment. De Larrard in his article uses a safety factor of 1.5 to prevent flow of fresh concrete from a slab cast under slope, but does not give information on the accurateness of the equation based on empirical data. In none of the mini-deformation tests, cracks occurred after deformation or hardening, so apparently the concrete was not too stiff to deform.

8.6.3 Deformation tests

In Table 8.4 the data from the deformation tests are presented, from both single- and double-curved elements. For each test the results are expressed in the last columns, using two simple criteria:

1. were cracks visible after deformation and hardening?
2. did the concrete flow from one part of the mould to another, as a result of still being too fluid at the moment of deformation?

If both questions are answered with 'no', a test is considered successful. It can be seen that only test 4 and 5 were unsuccessful, due to cracking and flowing, respectively.

Is is noted here that the observation method with visible cracks is relatively rough: hair cracks smaller than around 0.05 mm are hardly visible with the eye. Furthermore it is noted that the height of the elements has been measured only for the case in test 5 where a clear height difference due to flow was observed. Despite these notes, the deformation test results were considered reliable to give qualitative information that can be used for underpinning of the suppositions.

Table 8.4: Viability study - deformation test results

test	curvature	Δz [m]	R_{min} [m]	θ_{max} [°]	$\tau_{0;crit}$ [Pa] *)	t_{deform} h:min	cracks visible? concrete flow? success?
1	single	0.201	5.00	5.4	104	0:50	no-no-yes
2	single	0.201	5.00	5.4	104	0:50	no-no-yes
3	single	0.093	2.50	8.7	168	0:50	no-no-yes
4	single	0.246	1.50	24.6	462	0:50	yes-no-no
5	single	0.246	1.50	24.6	462	0:50	no-yes-no
6	double	0.186	3.06	19.8	376	0:45	no-no-yes
7	double	0.186	3.06	19.8	376	0:45	no-no-yes
8	double	0.210	1.73	27.7	516	0:45	no-no-yes

*) *calculated* value based on equation 8.2 on page 130, $h = 0.05$ m and $\rho = 2\,261$ kg/m³

8.7 Empirical generalisations and testing of suppositions

Although generalisations are not fully statistically underpinned due to limited number of tests and exploratory character of the study, evidence for multiple suppositions is found (see for the exact text of the suppositions section 8.3):

regarding supposition 1.1 Use of an open mould is possible; in only 1 out of 8 deformation test a clear redistribution of concrete after deforming the mould occurred. Thickness of the elements could be controlled easily by filling the mould with a self-levelling or very workable concrete mixture when the mould still was in horizontally levelled position. This thickness would not change significantly after deformation. The supposition also stated that the development of a sufficiently high yield strength can be used as a boundary condition before allowing deformation. Whether the shear yield strength is an accurate and sufficient boundary condition to decide if deformation is possible at a certain moment in time, could not be determined with full certainty, but all test results point in this direction and give no contradicting results. **Supposition 1.1** can be considered **tested and true**.

regarding supposition 1.2 De Larrard's slope model gives an indication on the yield strength that is necessary to allow tilting the mould to a certain slope. Although it could not be tested quantitatively, since the yield strength was not measured during the viability study, qualitatively evidence was found that De Larrard's slope model is useful to define the shear yield strength value above which flow of concrete in the deformed mould will no longer occur. **Supposition 1.2** can be considered tested and was found **qualitatively true**. Numerical and quantitative underpinning needs to be done, though.

regarding supposition 1.3 During the early hardening process deformation is possible without flow or cracking if the right moment to deform the mould is chosen. **Supposition 1.3** was tested and found **true at a macroscopic level**: in 7 of the 8 deformation tests at least no visible cracks occurred; further microscopic research is necessary to test whether deformation does not lead to damage at a micro-scale either and fully test the supposition.

regarding supposition 1.4 Reinforcement can be bent and deformed together with concrete within reasonable accuracy; this was tested and found **true**. The position of the reinforcement relative to the mould surface, though, was found to show a bandwidth that would need further reduction in case of industrial application.

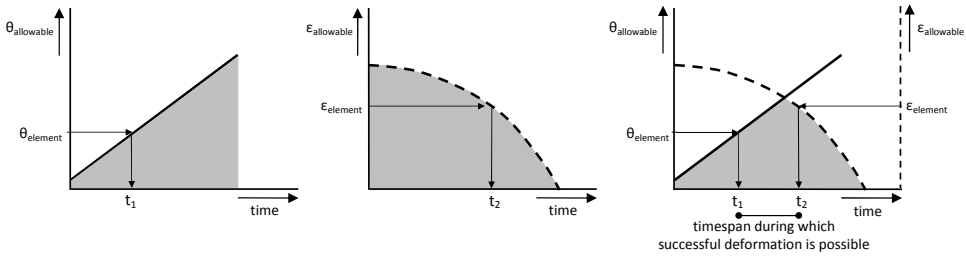


Figure 8.30: *left graph*: slope $\theta_{allowable}$ of the mould is assumed to increase linearly as a function of time due to linear development of the shear yield strength τ_0 in time; if an element after deformation has slope $\theta_{element}$, from the graph t_1 can be read - *middle graph*: the deformability $\epsilon_{allowable}$ is assumed to decrease over time, here plotted as a (assumed) dashed curve; if an element during deformation undergoes a strain $\epsilon_{element}$, from the graph t_2 can be read - *right graph*: both graphs combined in one figure making it possible to read the timespan during which successful deformation is possible (RS, improved version of Janssen, 2011)

8.8 Theory development

Based on the findings in the viability study above, it is possible to construct a model that can help to understand and control the concrete technology aspects of the flexible mould process. As discussed already in subsection 8.1.2, due to deformation of the moulds, the concrete is exposed to two effects:

1. parts of the mould are tilted under varying slope θ with the horizontal plane, and
2. as a result of both the imposed curvature κ and the stretching of the mould, the concrete needs to follow the resulting imposed strains.

For effect 1. it was demonstrated that equation 8.2 on page 130, proposed by De Larrard, is useful, at least qualitatively, and perhaps also quantitatively. Assuming that its quantitative validity for the flexible mould process can be proved in a later stage, it is proposed to use this equation until a better model has been found or until it is proved to be false. For effect 2., the stretching of the concrete, no theory has been found yet, other than the one proposed earlier in Figure 4.6 on page 49 by the author. The developed strain ε in the deformed concrete in that figure was assumed to be proportional to the thickness of the concrete element and to the reciprocal of the radius of curvature ($\kappa = 1/R = d\varepsilon/dz$) over which the element is deformed, similar to a bending problem in a linear elastic material. Any model should at least address the two aspects mentioned here.

An important operational question that needs to be answered to control the process is: *at what moment in time should, for a given concrete mixture and a given geometry, the deformation take place in order to result in a good concrete element?* The proposed model, for this reason, is time-based. The time of deformation t_{deform} is defined as the timespan between casting and the start of deformation of the mould. Two other moments in time are important for the model:

t_1 is defined here as the *lower boundary time* that needs to pass after mixing and placing (after which the concrete is left in rest) to allow stabilisation, resulting in a sufficiently high shear yield strength $\tau_{0,crit}$ to put the mould under a slope θ without the concrete flowing down in the mould.

t_2 is defined here as the *upper boundary time* until which the concrete can still undergo, without (unacceptable) cracking at a macro- or micro-scale, the strain ε following from the deformed and curved geometry of the element.

If a thixotropic concrete mixture is used, an increase in shear yield strength in time can be assumed to take place in the first period after mixing and for a mixture that remains in rest prior to deformation. Roussel et al. (2012) found that in the first 15 minutes this increase is linear (see also subsection 8.2.2). We assume now that this increase in shear yield strength may also be considered linear for a longer period than the first 15 minutes. In the left graph in Figure 8.30 on the preceding page this linear increase in yield strength, translated to an allowable slope $\theta_{allowable}$ using De Larrard's equation is plotted. Not much is known about the function that describes the development of the deformability of the fresh concrete in time, only that is likely to decrease more or less simultaneously with the increase of the early strength. In the middle graph in Figure 8.30 this decrease in deformability, translated to an allowable strain $\varepsilon_{allowable}$ is plotted as a curve of which the exact shape is unknown yet. In the right graph, the two moments t_1 and t_2 are plotted in a combined graph, defining the timespan during which successful deformation is possible.

Until now, only in one test (test 4) the upper boundary t_2 seems to have been exceeded, since a crack appeared during deformation of that test. By applying the same geometry in test 5, but then with an $t = 0:20$ h:min earlier moment of deformation, no visible cracks appeared.

It is interesting to observe that the lower boundary t_1 is depending on the slope θ , whereas the upper boundary t_2 is depending on strain, which on its turn is following from the radius R . A consequence of this observation is that, for the theoretical case of a mould that is given a steep slope θ , but which is hardly curved, so with a large radius R , both t_1 and t_2 will move to the right in the graph, whereas the opposite situation, with a very shallow slope θ but a small radius R , both boundaries will go to left in the graph⁶.

Another interesting consequence is that, for the theoretical case where a steep slope and a strong curvature are combined in the same panel geometry, t_1 and t_2 will approach each other, leading to a more critical timing: in the right graph in Figure 8.30 this is expressed by the tapering shape of the hatched area that becomes more narrow in the top. It is even imaginable, that certain geometries combine a set of θ and R that will lead to an impossible situation, namely $t_2 < t_1$, in other words: the slope is so steep, that at the time a sufficient yield strength is obtained to withstand this slope, the concrete cannot be deformed any more without cracking. For elements with such geometry, the flexible mould method may not be an appropriate production method. An example of an element that might have this problem is shown in Figure 5.8 on page 71.

A model as presented here can be used to combine the geometry of any deformed element and the characteristics of the concrete mixture that is applied to determine the timespan that is delimited by the lower and upper boundaries t_1 and t_2 . At this moment however, not much information is available on the deformability, so this needs to be studied further.

8.9 Concluding remarks

Exploratory experiments were carried out to obtain a first idea of the viability of the flexible mould method. From the experiments, it can be concluded that it is definitely possible to deform concrete after casting, using an open mould system, thus producing single- or double-curved concrete elements. Casting or spraying after deformation of the flexible mould is an alternative method, which, however, was not further investigated in the present research. Elements with a thickness of 50 mm were cast and subsequently deformed. Curvature radii as small as $R = 1.5$ m were realized. Deformation leads to a slope in the formwork; to withstand the gravitational forces, the fresh concrete needs to have a minimal shear yield strength. If a thixotropic SCC is used, the yield strength will increase quickly after casting, allowing deformation within the first hour after casting; the use of self-compacting concrete is preferable above conventional mixtures also for other reasons. Using SCC enables easy filling of the mould; furthermore vibration is not desirable on a fragile set-up as the one used for this method.

In the tests, thin steel reinforcement was used, which deformed along with the

⁶The last situation is more difficult to imagine, though, since it is geometrically impossible to create a strong curvature without a resulting slope somewhere in the mould.

concrete. In 6 out of 8 tests that were carried out in the present research, the obtained curved elements did not show visible cracks or other deficiencies. In one test, a crack appeared, in another test with similar geometry, but deformed earlier, the concrete was somewhat too fluid and redistribution of concrete over the mould length occurred. The four suppositions that had been framed before the experiments, were tested and confirmed, although not all in a fully quantitative manner. Further experiments are needed to provide for additional data. A model was proposed to express the process in two functions: the development of the allowable slope of the mould over time and the development of the allowable strain of the element over time.

From this first round in the 'wheel of science' the following aspects remain that need further testing:

- The slope equation of De Larrard was only applied in a qualitative manner. By measuring the yield strengths and comparing these values to the yield strengths resulting from De Larrard's equation applied to the slope of the deformed formwork, it can be checked whether this equation can be used to define the minimal necessary yield strength from the slope in the flexible mould method;
- It needs to be confirmed that deformation is possible without damage of the micro-structure (in round 1 only the 'visible crack'-criterion was used; round 2 should aim for improved crack analysis and if possible microscopic research); self-healing mechanisms may cure possible micro-cracks, since after deformation the CSH-reactions are proceeding; sufficient reactive cement is available (deducted from what is known of self-healing mechanisms and crack size); it would be interesting to test whether this indeed occurs;
- The function that describes the deformability needs further investigation by determining the development of allowable strain over time;
- It is not clear how the deformation and the resulting strains are related to one another;
- A further investigation of the rheological behaviour is needed, to see whether the yield strength development and moment of deformation can be controlled by, for example, the amount of plasticizer;
- The steel reinforcement after deformation remained within the panel, and followed the deformation quite accurately at most positions. Locally, though, reduced or increased concrete cover was measured. The deformation might have led to a loss of bond between reinforcement and concrete. Further research is needed to check this.

The work carried out during the viability study was presented at various conferences (Schipper and Janssen, fib symposium Prague, 2011, Schipper and Janssen, IABSE/IASS London, 2011 and Grünewald et al., ICFF Bath, 2012), and parts of

it were published earlier in two concrete related magazines Schipper and Janssen (2011c, Concrete Plant International) and Schipper (2011).

Chapter 9

Parameter variation study

9.1 Introduction

In the previous chapter, three suppositions have been confirmed and one more partially confirmed. In addition, a first attempt was done, based on the test results, to define a model with lower and upper boundary times t_1 and t_2 that is adequate to describe the process of deformation *after* casting. This order is typical for the flexible mould method; no models - yet - existed for it. In the present chapter, this model will be developed further by carrying out a number of experiments designed to obtain data on the timing of the production process. Before going through this round 2 in the 'wheel of science', at first additional literature will be reviewed on various aspects relevant for the further research. The following topics will be addressed:

- transition from fluid to solid: which models are available for describing the behaviour of the concrete in the first hours? (section 9.2, first subsections)
- rheology: how can the relevant parameters be measured? (section 9.2, last subsections)
- yield criterions: when does fresh concrete crack under shear or tensile deformation? (section 9.3)
- reinforcement (section 9.4)

After a discussion of the findings from this literature in section 9.5, a number of suppositions will be postulated in section 9.6. In the sections 9.7 to 9.11 tests will be designed, carried out and results analysed. Outcomes of two additional studies by master-students on textile reinforcement and crack forming will also be briefly presented in these sections, in order to be able to check the validity of all suppositions in section 9.12. The chapter is concluded with the presentation of a theory for the flexible mould method, covering the concrete technology aspects in section 9.13. Some concluding remarks in section 9.14 will summarize the results of this chapter.

9.2 Rheology

9.2.1 Comparison between Newtonian fluids, solids and fresh concrete

The fluidity of concrete facilitates its transportation to a mould and its casting into the finally desired shape. That part of the process is, for many applications, covered with sufficient accuracy by the Bingham fluid model, according to many publications on concrete rheology (as discussed earlier in subsection 8.2.1 on page 125). Concrete rheology uses concepts from fluid dynamics, where e.g. *viscosity*, *shear rate* and *shear strength* are important parameters. The use of fluid dynamics concepts for fresh concrete is a logical consequence of the fact that for many practical applications, special interest is laid in mixing, transport and casting phenomena. During the subsequent process of stabilisation and hardening, though, the fluid gradually transforms into a solid. The speed at which this transformation process develops is known to be controlled by many factors: cement dosage and type, temperature, aggregate types and sieve distribution, additives such as plasticizers or retarders (Van Breugel, 1997). This raises at least two questions:

1. Is, during this hardening process, the Bingham model still valid, and, if yes, until when?
2. At what point should then a solid model be applied instead of the Bingham model?

In order to arrive at a clear distinction between fluids and solids, Appendix H gives a brief formal review of the mathematics and mechanics used for a phenomenological description of both phases. For the main text of this thesis, a more intuitive approach is chosen, as described below. To illustrate a number of differences and resemblances between fluids and solids, Table 9.1 on the facing page shows the comparison between Newtonian fluids, solids and fresh concrete, and the mechanics approach that is used for modelling their behaviour. It becomes clear from Table 9.1 that fresh concrete, especially during the first hour after mixing, has characteristics of both fluids and solids, which leaves the questions stated above unanswered. It is for this reason that we need to go back to the point where fluid and solid mechanics come together.

9.2.2 Differences between solids and fluids according to Bingham

Although the term 'Bingham' in most concrete-related literature is linked to the term 'fluid', it was found (Bingham, 1922; Oldroyd, 1947; Papanastasiou, 1987) that a solid material that can support a finite stress elastically without flow, and that flows with constant (or plastic) mobility when the stresses are sufficiently great, in some literature is called a Bingham *solid*. Bingham himself (Bingham, 1922, p215) described the subtle difference between fluids and solids as follows:

Table 9.1: Characteristics of Newtonian fluids, solids and hardening concrete compared

Newtonian fluid	solid	concrete from fresh to early binding
is always a <i>continuum</i> ; no cracks can exist	can be locally interrupted by cracks or other <i>discontinuities</i>	initially no cracks can occur, but after some hardening, cracks are certainly possible (think of e.g. plastic shrinkage)
strains and stresses can be split in an isotropic and deviatoric part	strains and stresses can be split in an isotropic and deviatoric part	strains and stresses can be split in an isotropic and deviatoric part
unable to sustain deviatoric stresses when at rest; deformation <i>velocity</i> is an essential independent variable	can sustain deviatoric stresses when at rest; <i>deformation</i> is an essential independent variable	SCC will flow easily, CVC however needs vibration; after some hardening, motion is no longer tolerated and only stress-strain relations are used
constitutive equations give relation between <i>strain rates</i> and internal stresses	constitutive equations give relation between <i>strains</i> and internal stresses	constitutive equations in literature mostly are restricted to <i>either</i> the fluid phase <i>or</i> the solid phase
<i>molecular cohesion is low</i> , tensile stresses are negligible for general behaviour	<i>molecular cohesion is high</i> , tensile stresses (as well as other stresses) are important for behaviour	molecular cohesion and tensile strength grow with time as a result of the progress of CSH-binding from zero to (substantially) non-zero
elastic behaviour is only found for isotropic strains; displacements as a result of deviatoric strains are generally of a higher order of magnitude and have a plastic (non-reversible) nature	elastic behaviour for isotropic and deviatoric strains; plastic behaviour is found for deviatoric strains; elastic and plastic deformation are of the same order of magnitude	information about elastic or plastic behaviour from literature mostly is restricted to either the fluid phase or the solid phase
volumetric and dynamic (shear) <i>viscosity</i> are major material characteristics	<i>elasticity</i> and <i>plastic yield behaviour</i> are major material characteristics	both categories are of interest
<i>isotropic</i> material behaviour is common, anisotropy is rare	<i>both</i> isotropic material and anisotropic material behaviour <i>are common</i>	in fluid phase, anisotropy is non-desirable (segregation) and is prevented, in the hardened phase, anisotropy is possible, e.g. as a result of the local presence of reinforcement

“Only by the behaviour of materials under shearing stresses are we enabled to distinguish between a fluid and a solid. If a body is continuously deformed by a very small shearing stress, it is a liquid; whereas if the deformation stops increasing after a time, the substance is a solid. This distinction is theoretically sharp like the distinction between a liquid and a gas at the critical temperature, but just as a liquid may be made to pass into a gas insensibly, so a solid may grade insensibly into a liquid. Glass and pitch are familiar examples of very viscous liquids. Paint, clay slip, and thin mud in a similar manner must be classed as soft solids. According to the experiments” ... “the concentration in which the fluidity becomes zero under a very small shearing force serves to demarcate the two states of matter. This simple distinction is not always sharply drawn nor is its significance thoroughly appreciated; and for this reason much labour has been ill-spent in the attempt to measure the viscosity of solids, on the assumption that solids are only very viscous liquids and therefore that plasticity and the fluidity of solids are synonymous terms.”

He classified plastic materials showing a certain yield strength as *soft solids* rather than as liquids. The examples of such materials mentioned above (clay slip and thin mud) could easily be extended to *fresh concrete*. A soft solid, according to Bingham, has the following behaviour:

“In a plastic solid, a certain portion of the shearing force F is used up in overcoming the internal friction of the material. If the stress is just equal to the friction or yield value, the material may be said to be at its elastic limit. If the stress is greater than the friction f , the excess, $F - f$, will be used up in producing plastic flow according to the formula

$$dv = \mu(F - f) dr \quad (9.1)$$

where μ is a constant which we will call the coefficient of mobility in analogy to the fluidity of liquids and gases¹. If we were to plot the volume of flow against the shearing stress we would again obtain a straight line for a given material but it would not pass through the origin, ABC in Figure 9.1”.

It is easy to recognize in equation (9.1) the Bingham equation as found nowadays in most rheology related publications. From Bingham’s point of view, the behaviour of both the fluid and the solid phase for this specific category of materials can actually be modelled with the same equation. This is an important conclusion, which ‘smoothens’ the difference between fluids and solids in the present research.

¹If the formula is presented as $F = f + \frac{1}{\mu} \frac{dv}{dr}$, it is easier to recognize the resemblance with the already discussed Bingham equation (8.1): $\tau = \tau_0 + \mu\dot{\gamma}$. In Bingham’s original equation (9.1) as stated above, dv/dr is the variation in volume flow v as function of distance r . Since the volume flow at each point in the flow is linearly proportional to the velocity, v can also be read as velocity, leading to the unit $(\text{m/s})/\text{m} = \text{s}^{-1}$, which is the same as for shear

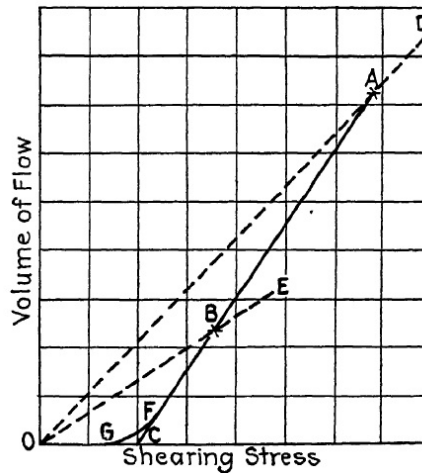


Figure 9.1: Image taken from Bingham (1922), p217. He concluded that connecting two points of his measurements (A and B) with the origin O would result in two different lines (OD and OE) for the viscosity. Bingham concluded that a part of the deformation was elastic and not plastic, namely the part resulting from friction below the yield value. Compare with Figure 8.3 on page 126, but with mirrored x- and y-axis.

9.2.3 Measuring rheological parameters

In section 8.2 the importance of rheological behaviour for the flexible mould method was already discussed. For the parameter variation study in the present chapter a more thorough study is done. According to Tattersall and Banfill (1983), the parameters used to quantify the rheological behaviour of fresh concrete can be divided into three categories:

1. qualitative parameters (e.g. “workable”, “compactable”, “stable”)
2. quantitative empirical parameters (e.g. “slump”, “flow-time T50”)
3. quantitative fundamental parameters (e.g. “viscosity”, “yield value”).

Quantitative empirical parameters (category 2) are often measured to calculate the fundamental values (category 3), which can be used in turn for physical or structural calculations. In the viability study described earlier, only few standardized slump tests were carried out, so mostly *qualitative* information (category 1) was obtained about the behaviour of the mixtures used. To obtain more control over the process it is necessary to measure also *quantitative* parameters (either category 2 or 3). In the Bingham model, the shear yield strength τ_0 and the plastic viscosity μ are the

rate $\dot{\gamma} = \frac{d\gamma}{dt}$ in equation (8.1). Note that in equation (9.1) for μ the reciprocal value of the definition of μ that is used nowadays was applied by Bingham.

two quantitative fundamental material properties that are used to describe the rheological behaviour of the fluid. The numerical values of these parameters and their development during the first hour will provide important information regarding the probability for successful deformation of the mould and concrete.

Various test methods are available for measuring the rheological properties, as described in Luping and Gibbs (2004); Grünwald and Walraven (2005). From these test methods available, the following were applied during the extended tests:

1. slump (suitable for CVC's, measured with the standardized Abrams cone and Haegermann mini-cone)
2. slump flow and flow-time T50 (suitable for SCC's, measured with same cones)
3. direct measurement of yield value and viscosity (suitable for a wide range of mixtures, measured with viscometer)

In the following subsections, these measuring methods are discussed in more detail.

9.2.4 Determination of yield strength with slump (flow) tests

Introduction

First we will now look into the most simple quantitative empirical testing method, using slump cones. In Chapter 8 we already used Equation (8.3) of Ferraris and De Larrard (1998), see page 131. In several more recent articles, the relation between slump flow and yield strength is further investigated:

Roussel and Coussot (2005) compared on one hand experimental results obtained with slump cones and viscometers, and on the other hand numerical simulations and analytical models. The goal was to express a validated relation between slump (flow) and yield strength, both for the standard ASTM Abrams cone and for the smaller paste cone, also known as Haegermann cone (see Table 9.2). Roussel and Coussot (2005) found that good agreement can be found between the values measured with both cones, analytical formulas and numerical simulations, but that some care must be taken with the choice of the relation for different ranges of fluidity.

Table 9.2: Cone properties (after Roussel, 2006a)

cone	ASTM Abrams cone	past cone *)
H_0 [mm]	300	50
r_{min} [mm]	50	35
R_{max} [mm]	100	50
V [m ³] **)	5.498 e-3	0.287 e-3

*) Haegermann cone, used in this research without flow table

$$**) V = \frac{1}{3} \cdot \pi \cdot H_0 \cdot (R_{max}^2 + R_{max}r_{min} + r_{min}^2)$$

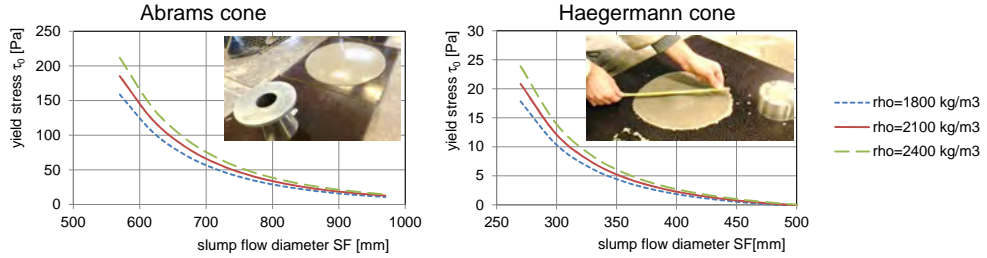


Figure 9.2: Yield stress empirically determined from slump flow diameter for two types of cones and three specific fresh concrete densities; values are reliable only for mixtures with aggregate size smaller than 20% of slump flow circle layer thickness (RS according to equation (9.2) of Roussel and Coussot, 2005).

Measuring very fluid concrete or cement paste

For very fluid *cement pastes* with low yield strength, the first term on the right hand side of the equation of Roussel and Coussot (2005)

$$\tau_0 = \frac{225 \cdot \rho \cdot g \cdot V^2}{128 \cdot \pi \cdot R^5} - \lambda \frac{R^2}{V} \quad (9.2)$$

where:	ρ	specific mass of concrete mixture	kg/m ³
	g	acceleration of gravity	N/kg
	V	volume of cone (see table 9.2)	m ³
	R	spread radius (<i>half</i> of slump flow circle diameter <i>SF</i>)	m
	λ	constant correction coefficient for surface tension and contact angle between concrete and plate ($\lambda = 0.005$ was used by Roussel et al. in set-up with Teflon plate and cement paste)	N/m

proved to give excellent agreement with both numerical simulations and experimental results if the dimensionless yield stress $\tau'_c < 0.03$ using Abrams cone and $\tau'_c < 0.02$ using the Haegermann cone. The dimensionless yield stress for τ'_c can be translated to a real yield stress τ_0 if the specific weight of the concrete ρ and the height of the cone H_0 are filled in:

$$\tau_0 = \rho \cdot g \cdot H_0 \cdot \tau'_c. \quad (9.3)$$

For the Abrams cone this limits the validity of equation (9.2) to values calculated from slump flows above $SF > 0.569$ m and for the small paste (Haegermann) cone above $SF > 0.271$ m. Although validated only for cement pastes, the equations may

also be valid for SCC as long as the maximum aggregate size is limited to around $1/5$ of the height of the slump flow circle. This, however, will generally not be the case in the present research for mixture m_3 (see Table 9.7 on page 192), as this has a maximum aggregate of 8 mm and the layer of concrete after the slump flow test will mostly be thinner than $5 \cdot 8 = 40$ mm. For mixture m_4 though, with a maximum aggregate size of 1 mm, the above equations may be considered valid. For mixture m_3 the equations will still be used, but as an approximation. Figure 9.2 shows the results of Equation 9.2 graphically for both types of cones.

Measuring concrete with limited slump and higher yield value

The *slump flow* value is only useful directly after mixing, and also only for mixtures with high fluidity. For higher yield values, the *slump* value is determined. In the viability study, the empirical relation between slump and yield strength was used according to equation 8.3 on page 131 of Ferraris and De Larrard (1998). In Roussel and Coussot (2005), for mixtures with a higher yield value, the traditional slump tests with both the Abrams and the Haegermann cone were also compared to numerical simulations. It was not possible to find an equation accurately fitting the tests results for the range of limited slump and higher yield values, but the best approximation was found by the authors using the equation

$$\tau_0 = \frac{\rho \cdot g \cdot (H_0 - S)}{\sqrt{3}}, \quad (9.4)$$

which for the Abrams cone yields

$$\tau_0 = \frac{\rho}{0.176} \cdot (0.300 - S) \Leftrightarrow S = 0.300 - 0.176 \cdot \frac{\tau_0}{\rho}. \quad (9.5)$$

(with S in m). Roussel and Coussot (2005, p715) say that this approximation generally overestimates the yield stress for a given slump value. In a more recent article, Roussel (2006a) therefore, proposed the following, slightly corrected, equation for the Abrams cone:

$$\tau_0 = \frac{\rho}{0.176} \cdot (0.255 - S) \Leftrightarrow S = 0.255 - 0.176 \cdot \frac{\tau_0}{\rho} \quad (9.6)$$

According to Roussel, this approximation is valid for slump values in the range $0.050 < S < 0.250$ m. In this article a reference is made to a research by Ferraris and Brower (2003) that compared various viscometers. Comparing the BML Viscometer and the BTRHEOM Viscometer, Ferraris and Brower found the following relation:

$$\tau_{0,BML} = 0.5 \cdot \tau_{0,BTRHEOM} - 122 \quad (9.7)$$

indicating that the absolute values found by the two types of viscometers differ significantly. Apart from this difference in absolute value, a good correspondence is found between the results for both viscometers.

J.E. Wallevik (2006) in another research, also discussing the relation between slump value and yield stress, reported alternative relations. Using the same BML viscometer as used in the present research, the author discusses the various relations between slump and yield stress found in literature. After comparing his test results with those relations, he suggests that a correction for the fraction of cement paste (matrix fraction V_m) in proportion to the total concrete volume should be taken into account, representing the distance between the suspended particles in the mixture. For tests on various mixtures with and matrix volume fractions ranging from $V_m = 321 \text{ l/m}^3$ to $V_m = 3451 \text{ l/m}^3$ he found the following linear regression lines:

$$S = 264.8 - 0.375 \cdot \tau_0 \quad (9.8)$$

$$S = 239.8 - 0.186 \cdot \tau_0 \quad (9.9)$$

The influence of the matrix fraction, according to Wallevik's equations, is large. Since in our research mixtures m_3 and m_4 have even larger matrix fractions of 400 and 520 ltr/m^3 , respectively (see Table 9.7 on page 192), Wallevik's proposed correction for the matrix volume could be used here:

$$S = 300 - 0.416 \cdot \frac{(\tau_0 + 394)}{\rho_{SG}} + \alpha(\tau_0 - \tau_0^{ref})(V_m - V_m^{ref}) \quad (9.10)$$

For the matrix fractions in the present research, however, this would extrapolate to values that make no sense, also because they are far outside the domain of V_m investigated by Wallevik. In his article, Wallevik suggests to re-establish a new but possibly similar relation for other mixtures. Mueller et al. (2014) recently investigated and compared various relations found in literature to yield stresses measured with a ConTec BML 5 co-axial viscometer and the slump (flow) tests using Abrams cone. Based on all sources, Mueller et al. propose two correlation expressions (here expressed as slump-yield stress relation):

$$S = 279.6 - 0.443 \cdot \tau_0 \text{ (equation M2 for fluid mixtures)} \quad (9.11)$$

$$S = 279.5 - 0.291 \cdot \tau_0 \text{ (equation M3 for broad range of mixtures).} \quad (9.12)$$

If the last equation is rewritten including a correction for variable specific weight ρ , the following equation is found, that will also be applied in the calculation of yield stress from the slump tests:

$$\tau_0 = -0.0015 S \cdot \rho + 0.4386 \rho - 70.5263 \text{ (equation M3 rewritten)} \quad (9.13)$$

In Figure 9.3 on the following page the above relations are plotted in the same graph. Indeed, the values for the yield stress found with the BML are generally (far) lower than those found with the BTRHEOM from the same slump values.

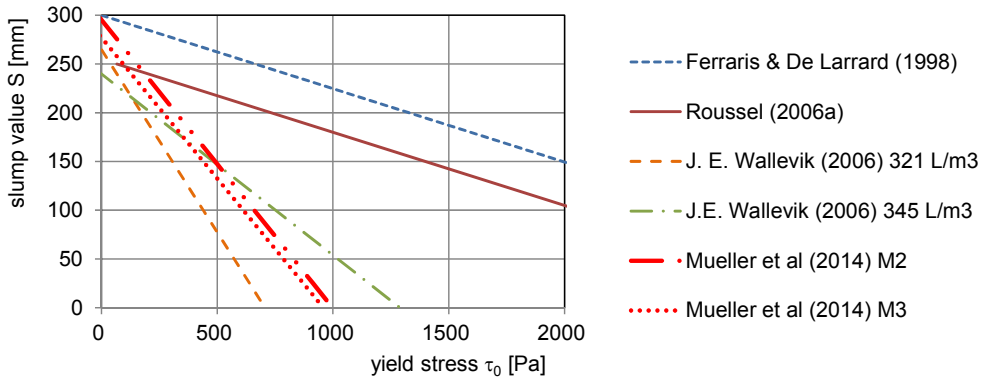


Figure 9.3: Various correlations between slump and yield stress found in literature

Conclusion on slump-yield stress relation

It is concluded that for very fluid concrete mixtures with low yield stress, the slump flow determined with either Abrams or Haegermann cone can be used to determine the yield stress with sufficient accuracy for the purpose of the present research. Based on the measured slump flow diameter, equation 9.2 on page 173 gives a sufficiently reliable indication of the yield stress, since the measured value is only used in the present research to confirm the self-levelling properties. More variation, though, was found in literature between various relations for stiffer concrete mixtures. As it is not possible at this point to determine which expression is most reliable for the mixtures used in the present research, a 'minimum-maximum' approach is chosen: after measuring the slump-value, the minima and maxima from the functions plotted in Figure 9.3 are both evaluated, to obtain an indication for the range in which the real yield stress will be situated.

Wallevik and Mueller both used the same BML Viscometer for fundamental yield strength determination (see next subsection), whereas both Ferraris & De Larrard and Roussel, on the other hand, used a BTRHEOM viscometer. In the present research the BML Viscometer will be used as well, so that the correlations found by Wallevik and Mueller may be more in line with the values found in the present research.

Using multiple slump cones filled with the same mixture, the development of the yield strength during the first hour can be followed, by lifting the slump cones at various moments. In Appendix F the results of all slump tests carried out during the parameter variation study and the calculated yield stresses according to the equations presented above can be found.

9.2.5 Direct measuring with a viscometer

For direct determination of the quantitative fundamental parameters, it was investigated whether the BML Viscometer of ConTec (see Figure 9.4) could be used. The BML Viscometer is a coaxial cylinder viscometer, that shears a cylindrical volume of fresh concrete in a precisely controlled manner. The measuring method was used in addition to the slump (flow) measurements described above. The principles, set-up and calibration are described in Appendix G on page 333.

9.3 Yield criterions from theory of plasticity

9.3.1 Introduction

The techniques described above to measure the yield strength of a given mixture all come from the field of rheology. How does this relate to other yield criterions found in literature on solid mechanics and plasticity? As said, the formal description and deduction of the various available yield criterions require a rather specialistic mathematical notation. Earlier, an intuitive approach was chosen in the present research. In Appendix H the various yield criterions are summarized briefly. From that overview it appears that the Tresca and Bingham yield criterions are in fact identical, and can be used both for fluids and solids, which is a facilitating observation for further work on the transition between both phases. As a logical consequence of our proposed manufacturing method, in which the still plastic concrete is deformed, we are especially interested in the strain capacity of such concrete.

9.3.2 Strain capacity $\varepsilon_{allowable}$

In subsection 6.10 on page 89 an indication was given for the order of magnitude of the strains that can be expected as a result of the deformation of the mould. Now let us look at the strain capacity of fresh and hardening concrete. In Section 8.8 the strain value below which no cracking or other damage occurred was called $\varepsilon_{allowable}$. What value can be found in literature for this strain capacity?

Hammer (2007) investigated deformations, strain capacity and cracking in plastic and early hardening phases of concrete, HSC and SCC in particular. Apart from

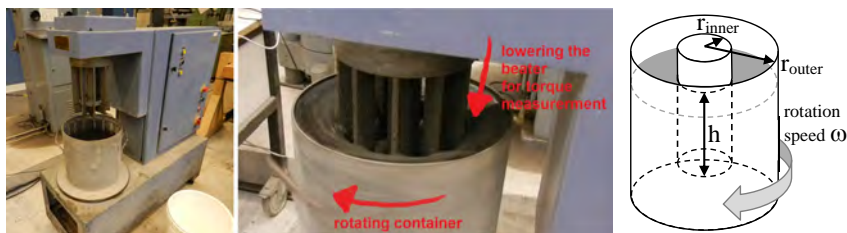


Figure 9.4: BML Viscometer

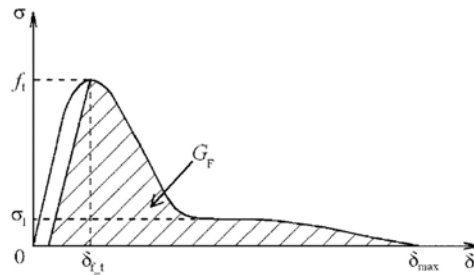


Figure 9.5: Stress-displacement curve of a tensile test on early-age concrete: first an almost linear and elastic part is visible, then after the peak f_t a softening part followed by a horizontal plateau at stress level σ_1 which goes to zero stress at δ_{max} ; note that this graph is measured with a 70 mm gauge, so the graph shows the summed displacements over this 70 mm (taken from Dao et al., 2009)

'internal' causes of cracking, such as shrinkage, he also mentions *externally imposed deformation, such as unwanted movement of the formwork or flow of a slope* as possible driving force. Hammer included in his research the very early stage, directly after adding water to the mixture, as, according to Hammer, cracks can also be initiated in this first hour, e.g. due to evaporation of water. As a result of high powder content, low water to binder ratio and small pores, HSC and SCC mixtures are extra susceptible to evaporation in this early stage. Hammer states that in, what he calls 'the plastic phase' (before initial setting time), the strain capacity may even mainly depend on the evaporation rate: if evaporation is reduced until below bleeding rate, the strain capacity can be considered 'almost infinite', as the concrete then keeps acting as a fluid. In conditions where evaporation was prevented, Hammer found strain capacities above $10\text{‰} = 10\,000\ \mu\epsilon$. However, as soon as evaporation exceeded bleeding rate, internal capillary stress would 'lock' the particles into position, reducing strain capacity - in Hammer's experiments - to an order of magnitude of $100\ \mu\epsilon$. Indeed, as will be shown later in the present research, *curing* of the concrete *with plastic foil* directly after placing appeared to have a *very positive effect on crack prevention*. In his tests, Hammer applied a deformation rate of $20\ \mu\epsilon/\text{sec} = 0.120\text{‰}/\text{min}$ and used a self compacting concrete with a slump flow in the range 600 - 650 mm. The tests on very early age concrete were performed during the first two hours after placing.

Experimental work on the determination of the tensile strength and strain in the first hours after mixing was also done by Dao et al. (2009). They performed tests on three mixtures, starting 1.5 hours or more after mixing. Tensile strength, Young's modulus and also data on the plasticity such as plastic strains and fracture energy were measured (see e.g. Figure 9.5). The concretes mixtures prepared were no-slump (class S1) and half-plastic (class S2) mixtures according to NEN-EN-206-1 (2001) and thus were clearly not SCC's as in Hammer's work and² in the present

²The relatively low slump values compared to SCC's are the result of a high initial shear yield strength.

Table 9.3: Tensile test results on early-age concrete. Mixture a-b(c) means a characteristic 28-day compressive strength of (a) MPa and a targeted slump of (b) mm, test number (c); f_t , ϵ_{f_t} and E are the values measured at the peak in Figure 9.5 (Dao et al., 2009)

*) note the difference between *shear* strength (as discussed in the thixotropy articles above) and *tensile* strength, as for a uni-axial tensile test $\tau_{max} = f_t/2$

mixture	f_c [MPa]	Age [h : mm]	f_t [Pa] *)	ϵ_{f_t} [‰]	E [MPa]
32-25(1)	39.8	1:35	100.	2.070	-
32-25(2)	39.0	2:30	5 500.	0.871	20.4
32-25(3)	36.7	1:50	600.	4.796	-
32-25(4)	45.9	2:30	3 500.	1.472	14.0
32-80(1)	34.6	3:25	7 500.	1.320	30.0
32-80(2)	40.7	3:40	20 900.	1.003	52.0
32-80(3)	41.2	3:00	3 000.	1.821	10.0
32-80(4)	40.8	3:05	3 100.	2.316	7.0
45-80(1)	52.4	2:30	800.	5.537	2.2
45-80(2)	50.0	2:00	600.	6.722	1.0
45-80(3)	46.2	2:10	1 400.	3.736	3.0

research: the mixtures had a limited slump value of only 25 or 80 mm directly after mixing, whereas the mixtures in the present research are in the range very workable to self-levelling. In Dao's research, a constant strain rate of $0.05/70 = 0.714 \text{ ‰/min}$ was applied. The measurements for each mixture at the earliest point in time, coming from the paper of Dao et al., are shown in Table 9.3.

In the research of Dao et al., no measurements were done earlier than 1:35 h:min and most tests even started later than this. No data was thus obtained on the strain capacity in the first hour after mixing. Although extrapolation of the data that was measured is not possible due to the large scatter, the graphs and measurements indicate some trends that are illustrated with the thick lines in Figure 9.6:

1. the authors state that *"the strain at peak tensile stress decreases rapidly with increasing age from thousands of micro-strains, possibly reaching its minimum on the order of tens of micro-strains between 4 and 15 hours, and then increasing slightly to approximately 100 to 150 micro-strains in mature concrete"*;
2. Young's modulus increases rapidly with time, starting off from a value close to zero.

For example, applying an often used relation to estimate the yield strength from the slump value, a slump value $S = 25$ correlates with $\tau_0 = \frac{\rho}{0.347} \cdot (0.300 - S) + 212 = \frac{2360}{0.347} \cdot (0.300 - 0.025) + 212 = 2082 \text{ Pa}$ and a slump value $S = 80$ with a value of $\tau_0 = \frac{2360}{0.347} \cdot (0.300 - 0.080) + 212 = 1708 \text{ Pa}$. The tensile strengths directly after mixing then would be $f_t = 0.5 \cdot \tau_0 \approx 850$ to 1040 Pa directly after mixing.

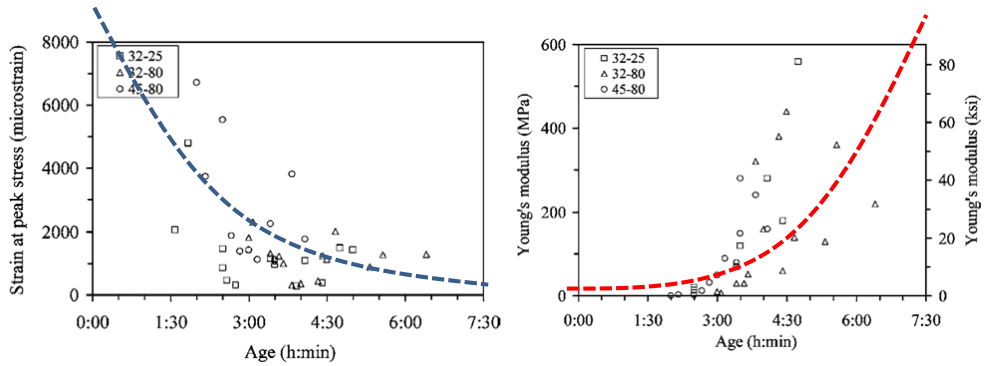


Figure 9.6: Two graphs taken from Dao et al. (2009), showing the development of strain at peak stress (left) and Young's modulus (right) - the thick trend-lines are from the author of this thesis

From the research it becomes clear that, after the peak stress is reached, a relatively long softening area is measured (Figure 9.5). This plastic behaviour is favourable for the flexible mould deformation method. The order of magnitude of strains in the present research ranges from -75% (shortening) to $+25\%$ (elongation). This $+25\% = 25\,000\ \mu\epsilon$ of elongation is significantly higher than the $8\,000\ \mu\epsilon$ shown in the graph left axis of Figure 9.6. Taking into consideration, though, that in the present research *self-compacting* mixtures are applied, which after mixing have a much lower yield strength than the mixtures used by Dao et al., sufficient strain capacity is expected to be available. This expectation is also based on the findings during the viability study, where similar radii were imposed, none of the cases except one leading to visible cracks. Further evidence for larger strain capacities was found during the experiments by Sergiu Troian, that will be discussed in subsection 9.10, where even elongation-strains of around $100\,000\ \mu\epsilon$ were applied in the first hour after mixing without visible cracking.

If at $t = 0$ the freshly mixed concrete would have a Young's modulus approaching $E = 0$ and if the maximum tensile stress according to the Bingham yield criterion is around $f_t = 0.5 \cdot \tau_0$, the maximum allowable strain $\epsilon_{allowable} = 0.5 \cdot \tau_0 / E_{t=0}$ would theoretically approach infinity. This trend is also - to some extent - expressed in the blue curve in the left graph in Figure 9.6. As E will never completely reach zero, as a Bingham fluid, even directly after mixing, shows a small but distinct elastic part, the infinite value in reality will be a high allowable strain value.

Conclusion on imposed strains

Based on all above, it is concluded that 1) a small part of the imposed strains will lead to elastic deformation (roughly the part before the peak in Figure 9.5), 2) if the imposed strains are larger than this, then that surplus part of the strain will lead to plastic deformations, and finally 3) that sufficient elongation capacity can be present

if the mixture is properly designed and if the deformation of the mould is carried out sufficiently early and evaporation is prevented.

At this point it is not clear whether the speed of deformation has influence on the strain capacity. Furthermore it is concluded that the available research on the strain capacity is insufficient to propose an accurate function predicting the upper boundary time t_2 (see p163). It is expected that such a prediction function can be only made for a specific mixture by experimentally determining the limits of deformation before cracking occurs.

As in a good process $t_1 < t_{deform} < t_2$, it would neither be favourable if the speed of the production would not be hindered by a long waiting period for initial hardening, nor if the time of deformation would be very soon after casting or within a very limited bandwidth. Time of deformation t_{deform} can, therefore, be considered a *targeted* value, fixed on a number of minutes that suits best in the production process. It is expected to be controllable to a great extent by modifying the dosage of super-plasticizers or retarders in the fresh mixture. In the experiments, various deformation moments and various dosages of plasticizers will have to be tried out. This makes the rheological behaviour of the mixture an important characteristic, as was also concluded from the tests during the viability study. In the next subsection various methods will be discussed to measure this behaviour.

9.4 Reinforcement

In the viability study thin steel reinforcement was applied successfully. The used diameter $\varnothing 3$ mm ($A_s = 7.07 \text{ mm}^2$ per bar) was small though, and the percentage of reinforcement was well below the minimum percentage that prevents brittle failure. In the viability tests 1 to 5, two wire meshes of $\varnothing 3$ -150 directly on top of each other were applied, effectively leading to $\varnothing 3$ -75, which equals $\rho = 0.20\%$. According to NEN-EN-1992-1-1 (2005), the minimum reinforcement is approximately:

$$A_{s;min} \geq \frac{0.26 \cdot f_{ctm} b_t d}{f_{yk}}. \quad (9.14)$$

For the high concrete grades applied in this research, the average tensile strengths were in the range of $f_{ctm} \approx 7 - 12 \text{ MPa}$. For $f_{yk} = 500 \text{ MPa}$ this yields a minimum reinforcement percentage in the range of at least $0.36 - 0.62\%$. In case of elements with $h = 50 \text{ mm}$ and $d \approx 40 \text{ mm}$ this results in $A_{s;min} = 146 - 250 \text{ mm}^2/\text{m}$, leading to a required dense bar spacing $\varnothing 3$ -45 and $\varnothing 3$ -25, respectively. It was not tested if this amount of reinforcement would bend without problems during the deformation process. For tests 6 to 8, the reinforcement followed the deformation within reasonable accuracy, although at some points the concrete cover became different than intended.

For applications in which the required moment capacity would be larger than M_{cr} or for load cases that lead to more centric tensile loads, such as temperature shortening or shrinkage, even larger amounts of reinforcement would be required,

leading to a proportionally denser spacing, or to the need for larger diameters that are more difficult to bend. Increase of the element thickness beyond 50 mm would not be the first option, as this could lead to conflicts with the deformation process: a thicker element leads to larger strains during imposed deformations. Furthermore $A_{s,min}$ would increase proportionally with increasing d . An alternative solution for such applications could be the application of reinforcement materials that are easier to bend and have a higher tensile strength f_{yk} , such as glass fibre textiles or other fibrous materials, either as strands, bundles or in short mixed fibres. Some of these materials, as a thinner concrete cover of the reinforcement is necessary, might be suitable for application in thin elements, as the ones manufactured in this research. In section 9.9 some additional work will be presented on glassfibre textile reinforcement in combination with the flexible mould method.

9.5 Discussion of section 9.1 to 9.4

In the previous sections a review of additional literature and some theoretical exercises have been carried out. This has resulted in a number of conclusions relevant for the further work:

1. In Bingham's view, *fluids* and *solids* are dealt with in the same way. Hardening concrete can be seen as a Bingham solid; the yield criterion for such a solid is identical to the Tresca yield criterion that is used in theory of plasticity.
2. Further empirical material was found on the relation between slump (flow) and shear yield strength; this can be used in the further research to calculate the yield strength from slump tests; for very fluid concrete this empirical relation is more accurate than for stiffer mixtures, where a significant spread between the various equations was found.
3. Tests with a viscometer need to be carried out to obtain calibrated data as well as data on thixotropic behaviour and viscosity.
4. The strains resulting from imposed deformation can be split in a contribution from out-of-plane bending (B) and one from in-plane strains (S) resulting from elongation, compression or shear; these strain components, when added, are expected to be in the range of tens of ‰ (tens of thousands of micro-strains), depending on curvature radius and element height; based on publications of Hammer (2007) and Dao et al. (2009), that both report on the tensile properties of early-age concrete, in combination with the findings during the viability study, it is expected that an SCC in the first hour after casting will have sufficient strain capacity to take the imposed deformation without cracking. A boundary condition is that evaporation is prevented by proper curing measures directly after placing.
5. Application of traditional steel reinforcement bars is limited in terms of diameter. The use of thin bars results in a dense bar spacing, already when only

the minimum reinforcement percentage is to be met. Higher reinforcement percentages will result in even higher density that may impair the proper filling of the mould. Steel may, therefore, not be the most suitable material to reinforce concrete, given the fact that always sufficient concrete cover is required. Alternatively, mixed fibres or strands of flexible fibrous materials such as glass fibre, carbon or aramide may offer a practical solution that meets the requirements for strength, deformability and durability.

Based on this additional theory, a number of new suppositions will be postulated in the next section.

9.6 Suppositions

Based on the theoretical considerations in the previous section, the following suppositions therefore are now postulated:

supposition 2.1 De Larrard's slope model in combination with Roussel's model for thixotropic strength development is accurate and sufficient for determining the lower boundary t_1 of the deformation time in the flexible mould process (Figure 8.30 on page 162). In supposition 1.2 (section 8.3) this was also partially addressed and already proven true qualitatively - quantitative data, however, is still necessary.

supposition 2.2 The upper boundary t_2 (Figure 8.30 on page 162) of the deformation time is determined from the point where the decrease in time of the plastic strain capacity $\varepsilon_{allowable}$ meets the strain necessary for the imposed deformation.

supposition 2.3 A safe and workable assumption for the strain distribution due to deformation is according to Euler-Bernoulli ("flat cross-sections remain flat after bending"), implying $\partial\varepsilon/\partial z = \text{constant}$ over the section height.

supposition 2.4 A safe and workable assumption for the friction between the concrete and the silicone mould surface is that no slip occurs between both materials during and after deforming the mould and concrete.

supposition 2.5 Modifying the concrete mix design can effectively control the lower and upper boundary times t_1 and t_2 mentioned above.

supposition 2.6 Textile reinforcement (TRC) and mixed fibre reinforcement (FRC) can be used to effectively reinforce the concrete elements and will follow the deformation accurately.

supposition 2.7 Cracks that are caused as a result of the imposed deformation can (partially) be cured due to self-healing effects in the yet relatively fresh concrete mixture.

To allow testing of these suppositions, a number of experiments were designed.

9.7 Operationalisation

9.7.1 Research variables

Introduction

In order to test the suppositions from the previous section, appropriate tests need to be designed. First the research variables and their possible mutual dependency were first examined more closely. According to the research design technique described by Creswell (2009), variables under consideration in a research can be distinguished in, among others, *independent and dependent* variables, which roughly are similar to *causes and effects*. Practically this distinction leads to a clearer definition of laboratory tests: by modifying only one variable at a time, the effect of changing this single variable can be observed from the test results, hopefully leading to evidence for certain relations and regularities between variables. A third category are *intervening* variables, that are positioned between the independent and dependent variables. From the viability study in the previous chapter and the theoretical study above it has already become clear that (at least) the following aspects and variables are of interest:

variable 1: curvature

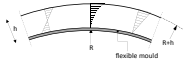




Curvature in this research was considered an *independent variable* (=input value, chosen by researcher), as it is based on considerations outside of the influence of the concrete manufacturer and defined mainly by the architectural geometry. In the parameter variation study both double-curved and single-curved geometry were applied. In the tests of the viability study, radii between 1.5 and 5 meter were chosen. Also in the extended tests, a number of different values for the curvature were selected, see Table 9.4 on the next page. The first two rows in the table represent single-curved elements, the rows 3 to 5 represent double-curved elements. The radius in both x and y direction were kept constant over the length. The radius of the element was defined here as the radius of the surface of the mould³.

variable 2: strain and stress due to deformation

Both strain and stress were considered *intervening variables*, since they cannot be directly measured in an easy way inside a fluid or hardening concrete, but are clearly important for the success of the deformation process. In the current thesis research no attempts were undertaken to actually measure the stresses during deformation. The strains are solely calculated from the imposed deformation. The stress was considered an unknown function of ϵ (imposed total strain) and E (Young's modulus) at

³A small simplification is made here: if the height of the concrete element is e.g. 0.05 m, the centre of the element will have a radius slightly smaller or larger than the radius of the mould surface, namely $\pm 0.5\%$ (0.025 on ± 5.0 m) to $\pm 1.6\%$ (0.025 on ± 1.5 m), depending on whether a positive or negative curvature is applied to the element. For the purpose of the tests, this difference is considered negligible.

Table 9.4: Different constant mould surface curvatures chosen for the extended tests.

set-up	R_x [m]	R_y [m]	κ_x [m ⁻¹]	κ_y [m ⁻¹]	Gaussian	shape
R_1	+ 1.5	∞	+ 0.667	0	0	 single curved positive
R_2	-/- 1.5	∞	-/- 0.667	0	0	 single curved negative
R_3	+ 2.5	+ 2.5	+ 0.400	+ 0.400	+ 0.160	 sphere positive
R_4	+ 2.5	-/- 2.5	+ 0.400	-/- 0.400	-/- 0.160	 saddle
R_5	-/- 2.5	-/- 2.5	-/- 0.400	-/- 0.400	+ 0.160	 sphere negative

the time of deformation, and possibly of more variables, such as relaxation or plastic flow.

variable 3: element height

Two different element thicknesses were used (see Table 9.5, left). The element height was considered an *independent variable*, as it is basically chosen by the architect or structural engineer, and is not following from the manufacturing process.

Table 9.5: Left: different element thicknesses for the extended tests. In the present work, only h_1 and h_2 could be tested. Right: three different moments of deformation targeted for the extended tests.

element thickness h [m]		time of deformation t_{deform} [h:min]	
h_1	0.025	$t_{deform;1}$	0:30
h_2	0.050	$t_{deform;2}$	0:45
h_3	0.100	$t_{deform;3}$	1:00

variable 4: time of deformation

The deformation time⁴ t_{deform} was considered an *independent variable*, as it is a target value to which the process is tailored. The goal was to work towards a t_{deform} between 30 and 60 minutes after mixing, preferably not much shorter (preparation time) or much longer (production speed, start of hydration) and also not too critical, as a larger bandwidth between t_1 and t_2 enables a more flexible production process. Based on the viability test, the target moments in Table 9.5 (right) were chosen. The points obtained by these tests also helped to obtain a rough applicability area for each combination of curvature and mixture.

variable 5: scale

With small (low volume) elements, scale effects will occur: friction between the edge of the mould and the fresh concrete volume may lead to disturbing hindering of deformation, scaling the height will lead to scaling of the strain. Tests with large elements (large volume), however, require larger equipment for mixing, higher costs of ingredients, higher mixing effort and test elements that are more heavy to handle, but may have the advantage of being closer to 1:1 scale, thus reducing unwanted scale effects.

The scale in this research was an *independent variable* (may have influence on the outcomes, but is not a prime output variable of interest). Chosen was for not scaling the height (thickness) of the elements, leading to $h = 0.025$ m or $h = 0.050$ m. The length and width of the elements, though, were scaled in comparison to the sizes that can be expected in practical applications: $L \times W = 0.80 \times 0.40$ m², which is relatively small compared to cladding panels applied in projects. The volume of each test element was exactly 16 litre, resulting in a weight of about 40 kg for the 0.050 m high elements and half of these values for the 0.025 m high elements. The 1:5 scale for the horizontal dimensions (not the thickness) was estimated to reduce the edge effect reported in the tests of the viability study.

variable 6: geometry

Apart from scale, the geometry of the test elements may also influence the outcomes. With geometry, all further dimensional parameters other than the curvature are meant here, such as 1) the shape of the elements in the plane of the mould, see Figure 5.8 on page 71: using polygonal elements or elements with non-parallel edges or even curved edges will result in a more complex manufacturing process 2) the thickness of the panels, e.g. using parallel upper and lower element surfaces (equal thickness) will require a different casting procedure from using test elements with strengthening ribs (Figure 9.7). In the present experiments ribs were not used. The geometry was considered an *independent variable*. For the tests, simple rectangular

⁴The term *deformation time* can be read as *moment of deformation*. The latter term was not used here to prevent confusion with the term *bending moment*

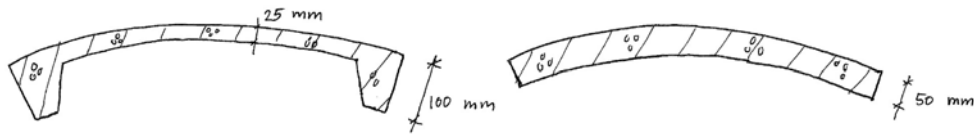


Figure 9.7: Panels with and without strengthening ribs

panels of prismatic thickness were chosen. This implies that the outcomes of the research are not necessarily valid for more complex geometries.

variable 7: definition of successful deformation

Successful deformation was defined by a number of measurable performance characteristics, such as absence of visible and non-visible (micro-) cracks, equal height of the test element, smooth surfaces of the hardened element (e.g. no bleeding, no patterns of formwork visible), accuracy of geometry, homogeneous distribution of aggregates over the element and the absence of influence of deformation on compressive and bending tensile strength. The judgement of the elements was first done with the naked eye and later using more advanced methods, such as microscopic polarizing and fluorescent analysis of thin sections (section 9.10). For the check of the overall geometry, laser scanning was applied. Other tests, such as measuring the permeability (indicating porosity) were not performed in the present research, but might offer additional information. The same goes for determination of possible variation of Young's modulus (ΔE) and/or specific weight ($\Delta \rho$) over the element height (indicating a possible 'stretching' effect of the concrete as a result of the deformation). Successful deformation was considered a *dependent variable*, since it is the effect of choices and procedures discussed above.

variable 8: deformation speed

Apart from the *time* of deformation, even the deformation *speed* (duration) going from the flat to the curved shape may be of influence on whether an element is successfully deformed or not. The strain capacity tests of Dao et al. (2009) were carried out at a strain rate of 0.714 %/min and the tests of Hammer (2007) at 0.120 %/min. Generally, in the viability study of Janssen and Schipper, the deformation took place much faster, at a rate between approximately 5 and 50 %/min. A time between half a minute and 5 minutes was generally used to lower the crane that was carrying the element from the horizontal and lifted casting position to the pre-installed pin-bed heights with curvature, manually guide the deformation and fix the mould into its final position using clamps. A higher strain rate increases the chance of cracking, according to Hammer. The deformation speed is considered an *independent variable*, since it can be chosen and controlled externally. Due to the relatively slow movement, it is expected that inertia effects do not influence the tests. In the research,

further, a deformation speed will be aimed at within the boundaries and with similar method as mentioned above.

variable 9: concrete mixture

To choose the right concrete mixture, the necessary specifications were determined by looking at the desired behaviour in different stages:

variable 9 concrete mixture - stage 1: mixing Preferably, the concrete recipe should allow easy mixing of ingredients into a homogeneous mixture with the standard available equipment in precast concrete industry. Small variations should not have too much influence. Often this is referred to as a *robust* mixture. In the used laboratory the equipment consisted a.o. of an Eirich R09/T 150 litre forced pan mixer for large concrete elements and Hobart 5 litre bakery mixers for small test elements. The forced pan mixer is considered standard industrial equipment used for high quality architectural concrete, SCC and UHPC mixtures (Kuch et al., 2010). The Hobart mixer is more convenient for laboratory use in situations where smaller amounts of fresh concrete are prepared. Desirable characteristics for the mixing stage are: ease of mixing procedure, resulting in homogeneous and stable mixture. The mixing procedure was documented for each test.

variable 9 concrete mixture - stage 2: casting stage Desirable qualitative parameters for the casting stage that followed from the viability study are: workability for sufficient time to fill multiple moulds or test cubes from the same batch; sufficient filling capacity to fill the mould without need for compaction, correct filling around possible reinforcement bars and along edges of the mould; self-compacting and self-levelling properties to result in smooth and even top surface, or, if not self-levelling, than ease of finishing; no segregation, equal distribution of aggregates over whole element. Ideally, the mixtures used will have all above mentioned characteristics. In order to determine whether this is the case, quantitative empirical (slump tests) and fundamental (viscometer) parameters were measured to allow future reference.

variable 9 concrete mixture - stage 3: fresh state stabilisation stage The strength development in the first hour was already discussed in subsection 8.2.2. From that discussion it was concluded that the use of a *thixotropic* mixture would be beneficial to quickly reach sufficient strength to prevent the concrete from flowing down the slope while maintaining strain capacity without cracking. Given a specific mould set-up, the determination of a minimum shear yield value $\tau_{0,crit}$ is now first needed in order to deform without the risk of mixture flowing out due to the slope. Let us determine this slope for a simple geometry: if a rectangular mould with length L and element height h is curved from the horizontal plane into a circular shape with radius R , the following relation for $\tau_{0,crit}$ can be derived from equation (8.2) and the goniometric relation between

Table 9.6: Critical yield strength $\tau_{0,crit}$ necessary for casting under slope θ , depending on mould radius R , element length L and element height h - based on $\rho = 2400 \text{ kg/m}^3$ (see Fig. 9.8 below for explanation of the used variables)

Slope θ and critical yield strength $\tau_{0,crit}$		$R = 1.5 \text{ m}$		$R = 2.5 \text{ m}$		$R = 5.0 \text{ m}$	
horizontal length L [m]	element height h [m]	θ [°]	$\tau_{0,crit}$ [Pa]	θ [°]	$\tau_{0,crit}$ [Pa]	θ [°]	$\tau_{0,crit}$ [Pa]
0.80	0.025	15.5	157	9.2	94	4.6	47
0.80	0.050	15.5	314	9.2	188	4.6	94
0.80	0.100	15.5	628	9.2	377	4.6	188
2.00	0.025	41.8	392	23.6	235	11.5	118
2.00	0.050	41.8	785	23.6	471	11.5	235
2.00	0.100	41.8	1570	23.6	942	11.5	471

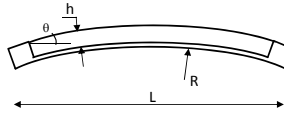


Figure 9.8: Critical yield stress for circular mould geometry

circle radius, chord length and the angle between chord and circle tangent:
 $\tau_{0,crit} = \rho \cdot g \cdot h \cdot \frac{L}{2R}$.

variable 9 concrete mixture - stage 4: mould deformation stage For the chosen values of L , h and for various radii R the critical yield strengths $\tau_{0,crit}$ were calculated, using the equation above. These values are presented in Table 9.6. From this table it was concluded that the necessary critical yield strength for small elements ($L = 0.80 \text{ m}$) is between roughly 50 and 600 Pa, whereas for larger (real scale, $L = 2.00 \text{ m}$) elements, the necessary critical yield strength lays within 100 and 1 600 Pa. If all mixtures are to be deformed in a time interval $t_{deform} = 30 - 60 \text{ min} (= 1800 - 3600 \text{ sec})$, then Figure 9.9 on the following page can be used to find an indication of the developed yield strength. Things that can be observed from Figure 9.9 are:

- three values for initial yield strength directly after mixing are visible: 10 Pa, 75 Pa and 150 Pa (representing concretes with variable workability, in the range from SCC to almost CVC)
- long, thick and/or small-radius elements need a higher yield strength than short, thin and/or large-radius elements (see difference between the two arrows pointing at y-axis)
- SCC mixtures with a very low initial yield strength of 10 Pa require at least some thixotropic behaviour in order to reach a yield strength sufficiently

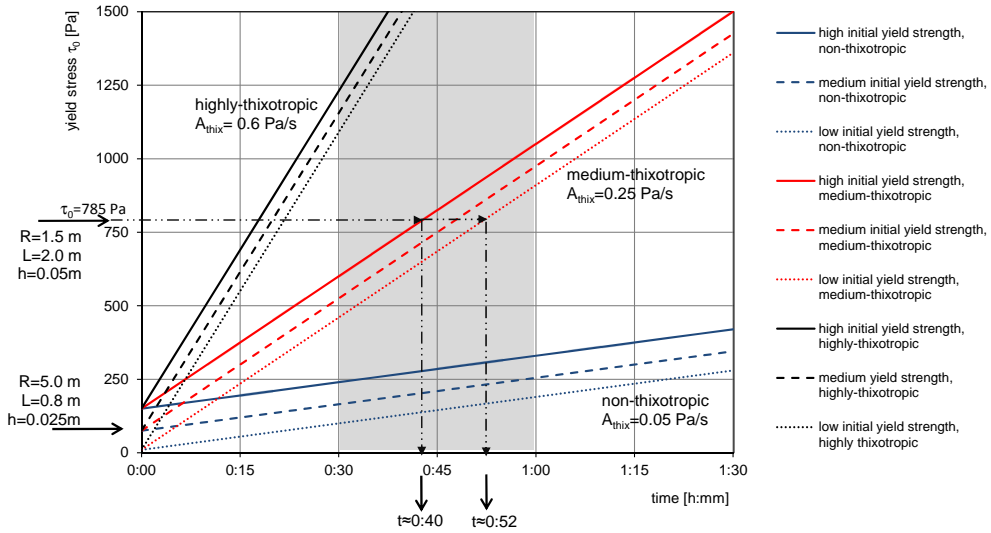


Figure 9.9: Development of yield values mixtures with different initial yield strength and no, medium and high thixotropy. Example: a circular-shaped element with a radius $R = 1.5$ m, a length $L = 2.00$ m and a height $h = 0.05$ m will need a minimal yield strength of around 785 Pa (according to Table 9.6) in order not to flow out of the mould. From the graph above it can be read that, for a medium-thixotropic mixture, this yield strength will be reached after a resting period of approximately 40 to 52 minutes after casting, depending on the initial yield strength directly after mixing

high for deformation anywhere between 30 and 60 minutes (grey box)

- low-thixotropic mixtures show smaller difference in yield strength between 30 and 60 minutes, which makes time of deformation less critical than for medium- or highly-thixotropic mixtures. It is known that mixtures holding fine powders, such as fly ash, quartz sand and/or limestone flour, will show thixotropic behaviour. From this we can conclude that these fractions should be present in the chosen mixture. The degree of thixotropy, expressed by parameter A_{thix} introduced by Roussel (2006b), should be preferably chosen in the range $A_{thix} = 0.1 - 0.3$ Pa/s (called a 'thixotropic mixture' in Roussel's classification).

The higher values for the yield strength in Figure 9.9 and Table 9.6 already come in the same range as the early strengths of hardening concrete mixtures, indicating that the needed strain capacity might become conflicting with the strength necessary for keeping the fresh mixture in the mould. The tests will later demonstrate that this conflict occurs only if the strain capacity is reduced as a result of evaporation of water due to a lack of curing measures. The considerations around yield strength development make it clear that during further

tests, measuring the development of the yield strength in time will provide important information regarding the chance of success for the deformation process.

variable 9 concrete mixture - stage 5: hardened state stage After hardening, aspects that are of importance follow from the field of application of the elements. For example, façade panels will need a strength different from that of load-carrying structural members. A number of typical performance characteristics for the hardened concrete are shared by many fields of application (although the numerical values might differ per application): e.g. strength, stiffness, weight, durability. Then there are also differences as a result of the application: colour, surface texture, porosity, need for reinforcement, etcetera. It was expected that the spread of compressive strengths resulting from the different mixtures would sufficiently demonstrate the potential of the flexible mould casting method.

The following parameters were measured and analysed: 1) cube compressive strength after 1 day and after 28 days (all mixtures) 2) flexural tensile strength (all mixtures) 3) presence of (micro-) cracks. It would be interesting to examine the desired properties for the complete life-cycle of the element, in order to be sure that the governing situation will be well known. If, for example, shrinkage during hardening would lead to larger cracks than the deformation process, it would not make sense to only focus on the deformation process. Or, if certain reinforcement is necessary for transport or structural loads, it must be possible to include this reinforcement in the deformation process, else the successfully deformed elements will be of no practical use. These life-cycle characteristics will, however, be discussed later on.

variable 9 concrete mixture - conclusion: Two concrete mixtures were tested (see Table 9.7 on the next page). The mixtures are a course-grained (≤ 8 mm) and a fine-grained (≤ 1 mm) concrete. Both mixtures can be self-compacting and self-levelling, depending on the dosage of plasticizer added and whether segregation occurs at high dosages. The initial yield strengths directly after mixing were initially unknown. Both mixtures were expected to be thixotropic, although the value of A_{thix} was unknown at forehand. The amount of plasticizers was varied to obtain a proper workability, while measuring the rheological parameters.

variable 10: presence and type of reinforcement

It was decided to define a separate series of tests with textile reinforcement, which will be discussed in section 9.9. In the first series of extended tests, however, no reinforcement was applied.

Table 9.7: Applied concrete mixtures

ingredients [kg/m ³]	mixture m_3 (coarse)	mixture m_4 (fine)
cement CEM I 52,5 R	400	570
fly-ash	160	100
Omya Betoflow D	-	100
superplasticizer Chryso Fluid	variable *)	variable *)
Premia 196 con 25% SPL		
water	172	225
sand 0.125-0.25 mm	48.3	232.8
sand 0.25-0.5 mm	128.8	413.8
sand 0.5-1.0 mm	208.7	646.5
gravel 1-2 mm	290.3	-
gravel 2-4 mm	372.6	-
gravel 4-8 mm	564.3	-
specific density:	2 345	2 288
other parameters:		
water/cement ratio	0.43	0.40
water/powder ratio **)	0.31	0.29
matrix volume V_m [litre/m ³])**)	400	520

*) amount of plasticizers was varied during tests between 0,6 and 1,1%

of total powder content, see subs. 9.8.2

**) parts below 0.125 mm plus water are defined here as matrix (acc. to Wallevik, 2006, p1215);

V_m was calculated based on $\rho = 2\,670\text{ kg/m}^3$ for all particles $> 0.125\text{ mm}$

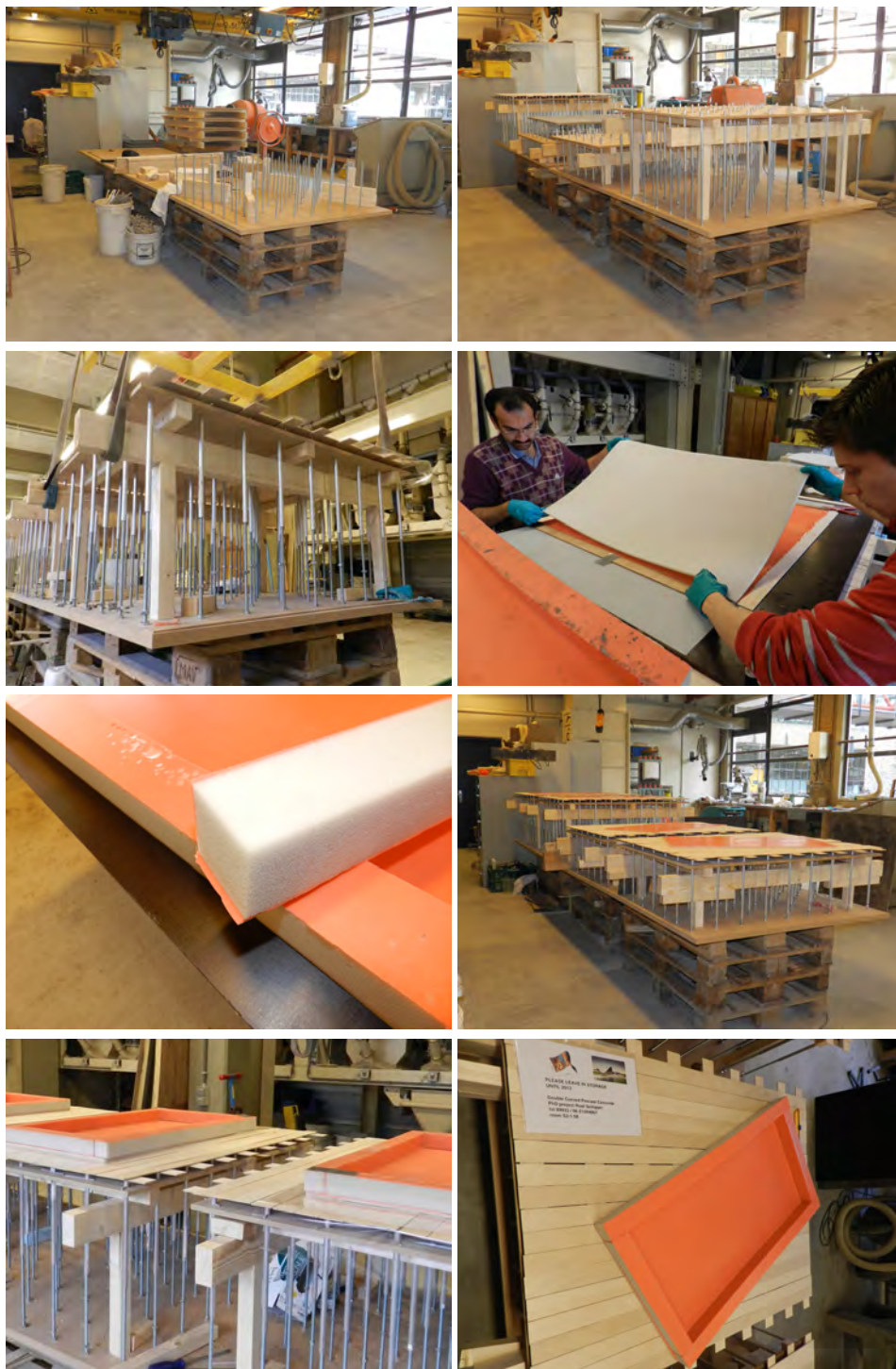


Figure 9.10: Preparation of frame for shape adjustment and of silicone moulds

9.7.2 Test set-up for unreinforced elements

In Appendix D on page 287, figure D.1 the dependencies between all the variables mentioned above are depicted. The population of the test elements was filled by making choices for each (set of) independent variables, as shown in Table 9.8.

Table 9.8: Number of necessary tests

independent variable	number of choices	
	series	overall
curvature (see Table 9.4 on page 185)	R_1 to R_5	5
element height (see Table 9.5 on page 185)	h_1 and h_2	2
concrete mixture (see Table 9.7 on page 192)	m_3 and m_4	2
time of deformation (see Table 9.5 on page 185)	t_1 to t_3	3
geometry	1	1
scale	1	1

The total number of tests comprises 5 curvatures \times 2 element thicknesses \times 2 mixtures \times 3 deformation times = 60 tests. In most tests, 4 elements were cast from one single batch of concrete. To allow for quick and simultaneous variation of parameters, a set of four identical moulds was prepared. Some of the preparation work and images of the moulds can be seen in Figure 9.10 on the previous page. An elevation is visible in Figure E.1 in Appendix E. The height of each separate mould and frame could be adjusted independently, in the same manner as shown earlier in a simplified way in Figure 8.1 on page 123. Results of the experiments with this set-up are reported in subsection 9.8.2.

9.8 Observations

9.8.1 Measuring rheological properties with BML viscometer

To measure the fundamental parameters for yield strength and plastic viscosity of concrete mixture m_3 , the ConTec BML Viscometer was used (see Figure 9.11). The set-up, calibration and measurement procedure are described in Appendix G.



Figure 9.11: ConTec BML Viscometer

In the following, measurement results of mixture m_3 are discussed that show the evolution of the yield strength over time (see Figure 9.12). The container for the test with the BML-Viscometer was filled directly after mixing. After filling the container, several up- and down-curves were completed, increasing and decreasing the rotation speed between $N = 0.03$ rps and $N = 0.39$ rps in seven steps of 5 sec each (see the dashed blue line in the top graph in Figure 9.12). A maximum torsional moment (resistance) up to $T = 9.5$ Nm in the first 1300 sec was recorded. From these measurements, a yield strength $\tau_0 = 0 - 10$ Pa, and a plastic viscosity of about $\mu \approx 40$ Pa · s were obtained shortly after mixing. A slump flow measurement at the same moment gave $SF = 720$ mm, which according to Equation (9.2) represents a yield stress $\tau_0 = 2$ Pa. A flow-time $T_{50} = 5.7$ s was measured. This flow time indicates a relatively high viscosity of the mixture. Figure 9.12 also shows that repeated up-down curves after $t = 2000$ s yielded a slightly higher resistance (up to $T = 11$ Nm), which is equal to a yield strength of $\tau_0 = 23$ Pa, caused mainly by thixotropy, as we will see below.

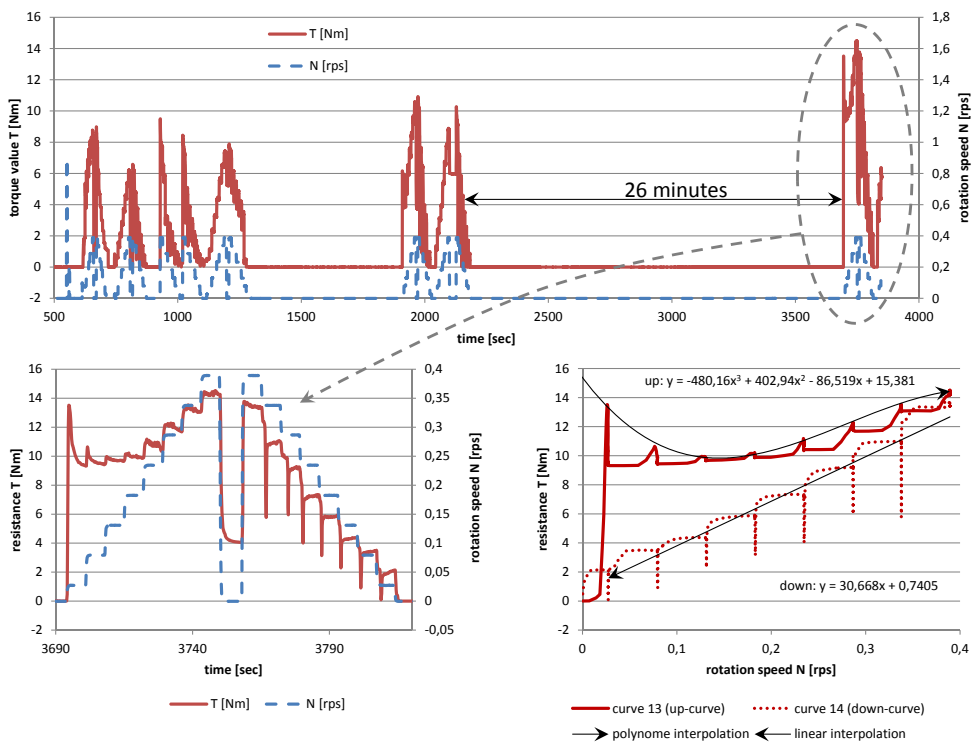


Figure 9.12: Test of mixture m_3 with BML viscometer indicating thixotropic behaviour; top graph: results of the first 4000 sec (67 min) of the test; lower graph: measurement in the period 3690-3820 sec after a resting period of 26 minutes, clearly showing increase in yield value as a result of the resting period.

After a rest period of 26 minutes, the repeated test showed a distinct rise of resistance to almost $T = 14 \text{ Nm}$, which however was decreasing again rapidly due to the shear and movement of the mixture (Figure 9.12: left-lower diagram). In line with expectations, the rotation of the container during the measurement resulted in a breakdown of the structure that was build-up before, behaviour that is typical for a thixotropic mixture. Only at higher shear rates the resistance of $T = 14 \text{ Nm}$ is exceeded again. If the up-curve in the $G - H$ diagram would have been interpolated linearly, it would not be clear which values represented the actual yield strength, since the rheological characteristics apparently changed due to the measurement itself. A third-order polynomial curve was used to approximate the yield strength at a shear rate of $N = 0 \text{ rps}$; the interpolated curve crosses the y-axis at $T = 15.38 \text{ Nm}$, which equals a yield strength of about $\tau_0 = 600 \text{ Pa}$. This value is in the range of yield strengths discussed in Table 9.6 on page 189.

To compare the BML-values with the slump test: the slump (with Abrams cone) at this moment was $S = 30 \text{ mm}$. Using the function for model M3 of Mueller et al. (2014) plotted in Figure 9.3 on page 176 this slump value would represent a yield stress $\tau_0 = 855 \text{ Pa}$, which is in the proximity of the interpolated BML-value of 600 Pa . If a similar interpolation is made for the curve after about $t \geq 2000 \text{ s}$, the yield value is $\tau_0 = 260 \text{ Pa}$. (Abrams cone slump: $S = 190 \text{ mm}$, $\tau_0 = 301 \text{ Pa}$, again using M3 from Figure 9.3 on page 176).

The initial up- and down-curves directly after mixing are, of course, not influencing the mix in the Abrams cone slump test, and the results, therefore, cannot be compared directly. The mixture tested with the BML should have been kept completely at rest until the time that the slump cone was lifted, which was not the case. This explains, to some extent, that the values determined with the BML are slightly lower than that using the slump-yield stress formulas shown in Figure 9.3 on page 176. The apparent increase of yield strength in 26 minutes gives an $A_{thix} \approx (600 - 260) / (26 \times 60) = 0.22 \text{ Pa/s}$, which would classify this mixture as medium-thixotropic according to Roussel (2006b). The development of yield stress due to thixotropy will also be measured using slump tests at various moments during the deformation test. This will be discussed in subsection 9.8.3.

From the BML Viscometer tests the following conclusions are drawn:

1. Mixture m_3 has self-compacting and self-levelling characteristics directly after mixing (yield strength between $\tau_0 = 0 \text{ Pa}$ and 10 Pa ; plastic viscosity about $\mu \approx 40 \text{ Pa} \cdot \text{s}$).
2. After a little less than half an hour of resting, the yield strength of mixture m_3 has increased to at least $\tau_0 = 600 \text{ Pa}$. Roussel's thixotropy rate apparently is $A_{thix} \approx 0.22 \text{ Pa/s}$ (classified as medium-thixotropic).
3. The observation of the mixtures during the slump tests gives a good indication with respect to the development of the yield strength if model M3 from Figure 9.3 on page 176 is used.

Mixture m_3 is suitable for use in the flexible mould method with respect to its thixotropic development of yield strength in the first hour after casting. Whether deformation is possible without cracking has to be determined by deformation tests, which will be described now. For mixture m_4 no BML measurement was carried out, but based on the increased fine particle content as compared to mixture m_3 even more thixotropic behaviour is expected to be present.

9.8.2 Deformation tests - plain concrete - summarized report

The tests were grouped in batches, each batch generally comprising four elements cast from the same batch of freshly mixed concrete, but with different time of deformation or shape into which the element was deformed or a variation in curvature. For most batches a flat element and three curved elements were cast, to allow comparison. Appendix E on page 289 gives an overview of the general procedure followed with casting, deformation, hardening and demoulding of the elements and shows the test set-up. Table 9.9 gives an overview the most important test results. Batch 1 to 18 are in plain concrete - the batches 19 and 22 refer to the tests with textile-reinforced concrete that will be discussed later. In subsection 9.8.3 a detailed report is offered for the interested reader.

9.8.3 Deformation tests - plain concrete - detailed report

In the present subsection, each batch will be described in detail, highlighting interesting aspects and showing relevant images of findings during the experiments. Appendix F on page 295 offers all registered data per test.

Batch 1 (mixture m_3 - 0.63% plasticizer)

Mixture m_3 was prepared with 0.63 % of plasticizers (% related to the weight of the total powder content). Apart from some test cubes, no elements were cast, but the development of the slump-value in the first hour was tested. The slump flow directly after mixing was $S_{flow} = 750$ mm (flow-time $T_{50} = 2.0$ sec), indicating that the mixture was self-compacting and self-levelling. Three slump cones (Abrams) were filled with the fresh mixture without tamping. At $t = 0:15$, $t = 0:30$ and $t = 0:45$ h:min (all times measured from the moment of addition of water during the regular mixing procedure), slump values were measured of $S = 225$ mm, $S = 168$ mm and $S = 123$ mm respectively, indicating a clear rise of yield strength during the first hour after mixing, which can also be seen from Figure 9.13 on page 200. Similar graphs can be found in Appendix F for all batches where slump tests were done. The cube compressive strength was 82.3 MPa after 28 days.

Batch 2 (mixture m_3 - 0.80% plasticizer)

Batch 2 was prepared with the intention of making a trial casting for one single-curved concrete element, numbered 2.1. The same recipe m_3 as in batch 1 was used,

Table 9.9: Overview of deformation tests

element	height [m]	mix- ture	plast [%]	sc/ dc	R_{min} [m]	t_{deform} [h:min]	slope θ	$T_{0,crit}$ [Pa]	$T_{0,real}$ [Pa]	ϵ_R [%]	flow?	cracks?	success?
												mould finish	
3.1	0.050	m3	0.77	sc	-1.5	0:45	15.5	307	202	-33.3	yes	no	yes
4.1	0.050	m3	0.64	sc	1.5	0:30	15.5	307	202	33.3	no	no	limited
4.2	0.050	m3	0.64	sc	1.5	0:45	15.5	307	678	33.3	no	no	no
4.3	0.050	m3	0.64	sc	1.5	1:01	15.5	307	930	34.5	no	no	no
5.1	0.050	m3	0.77	sc	1.5	0:40	15.5	307		33.3	no	yes	no
5.2	0.050	m3	0.77	sc	1.5	0:50	15.5	307	960	33.3	no	yes	no
5.3	0.050	m3	0.77	sc	1.5	1:00	15.5	307	960	33.3	no	no	no
6.1	0.050	m3	1.10	sc	1.5	1:15	15.5	307	149	33.3	yes	no	yes
6.2	0.050	m3	1.10	sc	1.5	0:59	15.5	307	255	33.3	yes	no	yes
6.3	0.050	m3	1.10	sc	1.5	0:45	15.5	307	149	33.3	yes	no	yes
10.1	0.050	m3	0.75	sc	1.5	0:20	15.5	307	184	34.5	no	no	yes
10.2	0.050	m3	0.75	sc	1.5	0:34	15.5	307	254	34.5	no	no	yes
10.3	0.050	m3	0.75	sc	1.5	0:51	15.5	307	394	33.3	no	no	yes
11.1	0.050	m3	0.65	sc	1.5	0:50	15.5	307	307	33.3	no	no	yes
11.2	0.050	m3	0.65	sc	1.5	1:00	15.5	307		33.3	no	no	yes
11.3	0.050	m3	0.65	sc	1.5	1:16	15.5	307		33.3	no	no	yes
12.1	0.025	m3	0.65	sc	1.5	0:36	15.5	154	194	16.7	no	no	yes
12.2	0.025	m3	0.65	sc	1.5	0:48	15.5	154	394	16.7	no	no	yes
12.3	0.025	m3	0.65	sc	1.5	1:00	15.5	154	340	16.7	no	no	yes
13.2	0.025	m3	0.65	sc	-1.5	1:02	15.5	154	449	-16.7	no	no	yes
13.3	0.025	m3	0.65	sc	-1.5	0:47	15.5	154	303	-16.7	no	no	yes
13.4	0.025	m3	0.65	sc	-1.5	0:34	15.5	154	121	-16.7	no	no	yes

(table continued on next page)

Table 9.9 (continued) Overview of deformation tests

ele- ment	height [m]	mix- ture	plast [%]	sc/ dc	R_{min} [m]	t_{deform} [h:min]	slope θ	τ_{0crit} [Pa]	τ_{0real} [Pa]	ϵ_R [%]	flow?	cracks?	success?
14.2	0.050	m ₃	0.70	sc	-1.5	1:07	15.5	307	836	-33.3	no	no	yes
14.3	0.050	m ₃	0.70	sc	-1.5	0:48	15.5	307	325	-33.3	no	no	yes
14.4	0.050	m ₃	0.70	sc	-1.5	0:35	15.5	307	132	-33.3	no	no	yes
15.2	0.050	m ₃	0.70	dc	-2.5	0:35	9.2	184	291	-20.0	no	no	yes
15.3	0.050	m ₃	0.70	sc	-1.5	0:50	15.5	307	396	-33.3	no	no	yes
15.4	0.050	m ₃	0.70	sc	-1.5	1:07	15.5	307	890	-33.3	no	no	yes
16.2	0.050	m ₃	0.70	dc	-2.5	0:48	9.2	184	361	-20.0	no	no	yes
16.3	0.050	m ₃	0.70	dc	-2.5	1:03	9.2	184	819	-20.0	no	no	yes
16.4	0.050	m ₃	0.70	dc	-2.5	1:17	9.2	184		-20.0	no	no	yes
17.2	0.025	m ₃	0.70	dc	-2.5	1:02	9.2	92	686	-10.0	no	no	yes
17.3	0.025	m ₃	0.70	dc	-2.5	0:49	9.2	92	358	-10.0	no	no	yes
17.4	0.025	m ₃	0.70	dc	-2.5	0:32	9.2	92	212	-10.0	no	no	yes
18.2	0.050	m ₄	0.59	sc	-1.5	0:59	45.0	794	763	-33.3	no	no	yes
18.3	0.025	m ₄	0.59	dc	-2.5	0:45	9.2	90	4	-10.0	no	no	yes
18.4	0.025	m ₄	0.59	dc	-2.5	0:42	9.2	90	3	-10.0	no	no	yes
19.4	0.025	m ₄	0.65	sc	1.5	0:30	15.5	150	600	16.7	no	no	yes
19.3	0.025	m ₄	0.65	sc	-1.5	1:00	15.5	150	800	-16.7	no	no	yes
22.2	0.025	m ₄	0.64	dc	2.5	0:45	9.2	90	700	10.0	no	no	yes
22.1	0.025	m ₄	0.64	dc	-2.5	0:55	9.2	90	725	-10.0	no	no	yes

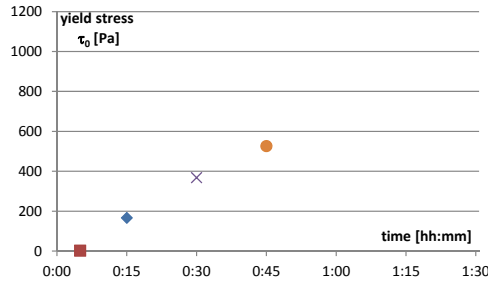


Figure 9.13: Development of yield stress in time, calculated from slump (flow) tests - batch 1

with the exception that 0.80 % instead of 0.63 % plasticizers was used, in order to increase the workability. No other tests were carried out with this mixture other than casting the element itself. It was a very fluid mixture, self-compacting and self-levelling. At $t = t_{\text{deform}} = t_2 = 0:45 \text{ h:min}$ the mould was deformed into a single-curved radius $R_1 = +1.5 \text{ m}$. The intended height of the element was $h_2 = 0.05 \text{ m}$. However, it was found out that the fluidity was still too high. (see Figure 9.14a). Signs of segregation were visible. Flow resulted in a varying thickness of the element from the ends to the centre. The element itself, though, turned out to be very smooth on the mould surface (see Figure 9.14b). Few air bubbles were observed on the edges of the element⁵.

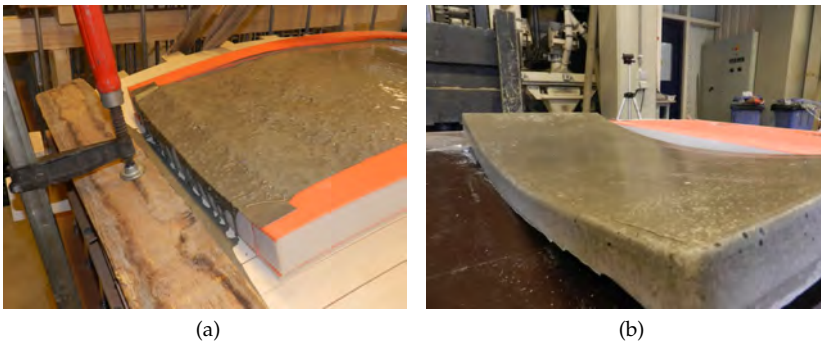


Figure 9.14: Batch 2 - element 2.1 (a) during casting - mould is overflowing, due to fluidity and slight segregation of concrete, still too high at 45 minutes after mixing (b) after demoulding - smooth surface, but unequal thickness

⁵More images of batch 2 can be found on the project website: [casting and deformation](#) and [demoulding](#).

Batch 3 (mixture m_3 - 0.70% plasticizer)

For batch 3, again mixture m_3 was prepared, now with 0.77% of plasticizers, to reduce flow and segregation. It still resulted in a fluid mixture, easy to place, self-compacting but not really self-levelling: some manual finishing of the surface was necessary after casting. Like in batch 2, again at $t = t_{\text{deform}} = t_2 = 0:45$ h:min the mould was deformed into a single-curved radius, this time in the opposite curvature, namely $R_2 = -1.5$ m. The height of the element again was $h_2 = 0.05$ m. The slump flow directly after mixing was only $S_{\text{flow}} = 575$ mm (flow-time $T_{50} = 2.0$ sec), which was less than expected based on the only slight reduction of plasticizer compared to the previous test. At $t = 0:30$, $t = 0:45$ and $t = 1:08$ h:min, slump values were measured of $S = 210$ mm, $S = 215$ mm and $S = 200$ mm respectively, which is interpreted as a lack of stiffening in the first hour. Yet, the deformation went successful, since no concrete flowed out of the mould. The element itself turned out to be smooth on the mould surface (see Figure 9.15b and c). This time, the element thickness was constant and accurate over the whole panel⁶. This panel had a negative curvature, meaning that the finishing surface was not stretched but compressed by the deformation. No cracks were visible in the finishing surface or mould surface. The cube compressive strength was 70.8 MPa after 28 days.

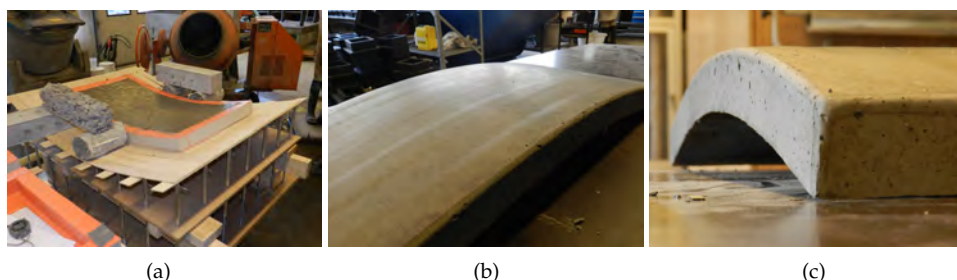


Figure 9.15: Batch 3 - element 3.1 during casting and after demoulding. (a) mould ballasted with extra weights; (b) and (c) smooth surface, smooth curvature, equal element thickness, some bubbles

Batch 4 (mixture m_3 - 0.64% plasticizer)

Batch 4 was the first batch with an entire series of four elements (with one element flat) that were cast at once. Still using mixture m_3 , the proportion of the plasticizer was further reduced to 0.64% (related to total powder content) with the intention of getting the right fluidity with a maximum economy. But surprisingly it turned out that the mixture was very unworkable. It was far from self-compacting, hard to place in the moulds and manual compaction was required. The thickness of the element again was $h_2 = 0.05$ m. The mixture turned out to be so stiff that at $t = 0:00$, $t = 0:30$

⁶More images of batch 3 can be found on the project website: [casting and deformation](#) and [demoulding](#).

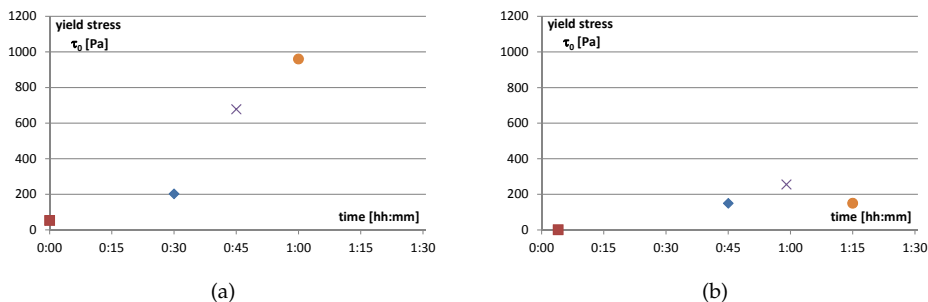


Figure 9.16: Development of yield stress in time, calculated from slump (flow) tests (a) batch 4 (b) batch 6 - drop-out at 1:15 due to collapsed concrete cone during slump test

and $t = 0:45$ h:min, slump values were measured of $S = 215$ mm, $S = 80$ mm and $S = 0$ mm respectively. This development of slump values in time shows a quick rise of yield strength, as can also be seen in the plot of the calculated yield strengths in the left graph in Figure 9.16.

At at $t = 0:30$, $t = 0:45$ and $t = 1:00$ h:min, the deformation took place into a single-curved radius $R_1 = +1.5$ m of element 4.1, 4.2 and 4.3 respectively. Element 4.4 remained undeformed. Surface cracks were visible in the upper finishing surface of the elements immediately after deformation, increasing in number with the time passed between mixing and deformation (see Figure 9.38 on page 225).

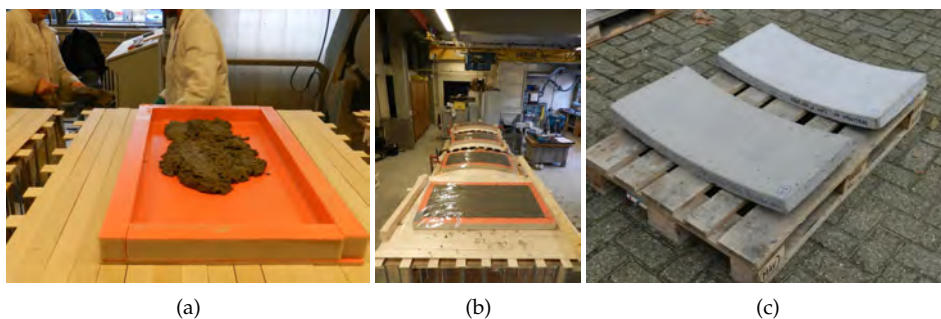


Figure 9.17: Batch 4 - element 4.1 to 4.4 during casting and after deformation and demoulding. (a) workability not good (b) four elements, 1 flat, 3 curved. (c) many bubbles in surface, badly compacted; overall shape quite OK

The elements (see Figure 9.17) had many air enclosures with a diameter between 1 and 10 mm on the mould surface and on the edges. The finishing was far from satisfactory. It was also difficult to release the moulds from the elements without

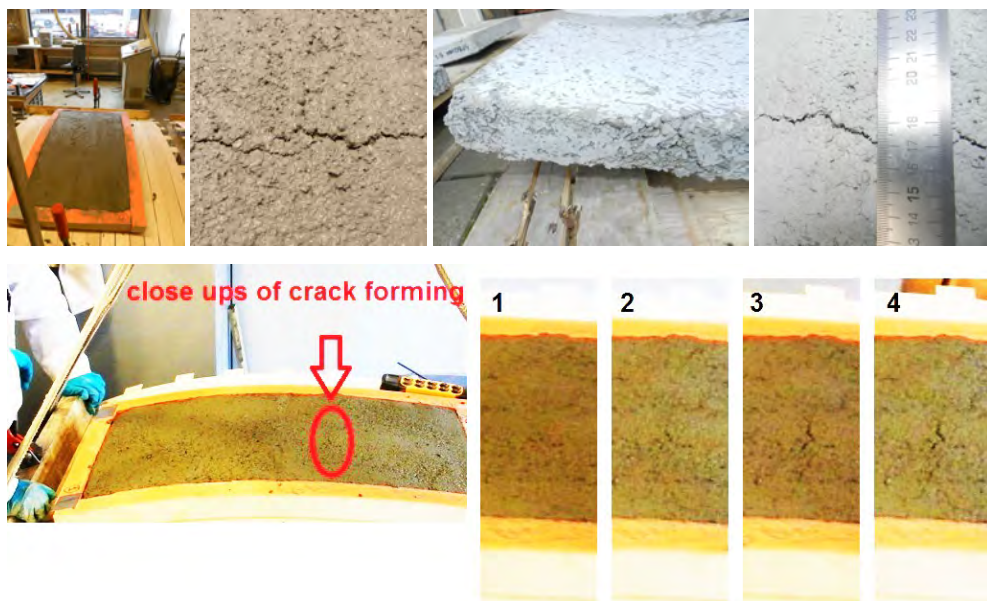


Figure 9.18: Batch 5 - elements during casting and after demoulding: as a result of very limited workability the compaction was insufficient, the filling ability was not good and cracks occurred in the finishing surface during deformation. The video-sequence (step 1-4) in the lower image shows that the cracks clearly are the result of the deformation

damaging the moulds.⁷ The cube compressive strength was 61.8 MPa after 7 days; the cube tested at 28 days for measuring the compressive strength was not deemed reliable.

Batch 5 (mixture m_3 - 0.77% plasticizer)

Batch 5 showed a more or less similar result, even though the amount of plasticizer was increased again back to 0.77%, while still using mixture m_3 . It appeared, that the *mixing order* was prone for improvement during batch 4 to 9: the plasticizer was added early, together with the first 50% of the water. This lead to unpredictable behaviour of the plasticizers, possibly as a result of quick adsorption of that admixture by the cement. In later tests, where first 50% of water was added, and plasticizer only in the second 50% of water, this phenomenon did not occur.

Effectively, the workability of the mixture was very limited. As a result, the filling ability of the mixture was insufficient, leading to large empty spaces in the mould (see Figure 9.18). Element thickness $h_2 = 0.05$ m was chosen. During deformation

⁷More images of batch 4 can be found on the project website: [casting and deformation](#) and [demoulding](#).

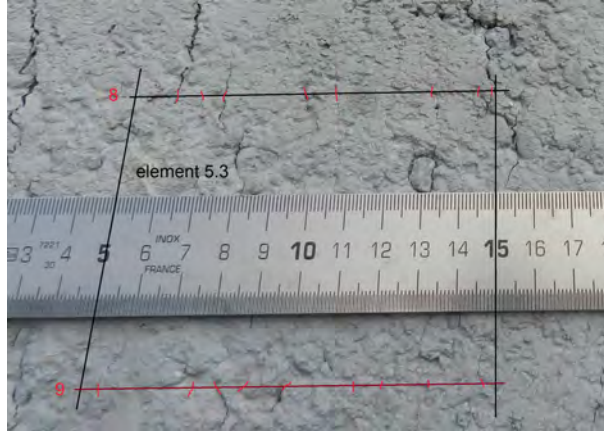


Figure 9.19: Detail of casting surface of element 5.3 - impression of the size and distance of cracks in the finishing surface; the smallest cracks still visible with the eye or after zooming in on the digital image (crack width estimated at 0.05 to 0.2 mm) are on an average distance of around 11 mm; three medium-sized cracks are visible in the top of the picture (crack width 1 to 2 mm).

into a single-curved radius $R_1 = +1.5$ m at $t = 0:40$, $t = 0:50$ and $t = 1:00$ h:min, elements 5.1, 5.2 and 5.3 all developed cracks, mostly in the main strain direction resulting from the curvature, but some also under 30 degrees with this main direction. The larger cracks had a length of 150 to 200 mm. These cracks developed in the upper surface, a few had a width of around 3 to 4 mm and a estimated depth of 5 mm from the top surface. Also some medium-sized cracks with a crack width of 1 to 2 mm developed at regular distances of 50 to 70 mm, and smaller cracks with width < 1 mm were visible at centre-to-centre distances of around 11 mm (See Figure 9.19).

The lower image in Figure 9.18 clearly shows that the cracks were indeed a result of the deformation process. The flat panel 5.4 (not deformed) did not crack. At $t = 0:48$ and $t = 1:00$ h:min, slump values were measured of $S = 0$ mm both. Earlier slump values were not measured due to the casting difficulties mentioned above, but the mixture then was still somewhat more plastic.⁸

Batch 6 (mixture m_3 - 1.10% plasticizer)

In batch 6, again the same radius $R_1 = +1.5$ m and same element thickness $h_2 = 0.05$ m were used. Still experimenting with various amounts of plasticizer due to the non-altered mixing order, this mixture m_3 with 1.1% plasticizer (related to total powder content) segregated easily. The mixture had a slump flow of $S_{flow} \gg 900$ mm directly after mixing, and at $t = 0:45$, $t = 0:59$ and $t = 1:15$ h:min, slump values

⁸More images of batch 5 can be found on the project website: [casting and deformation](#) and [demoulding](#).



Figure 9.20: Batch 6 - segregation problems lead to bleeding of cement water and unequal element thickness - furthermore cracks appeared in the finishing surface of element 6.1 and 6.2. Cores were drilled and sliced to observe the cracks in more detail

were measured of $S = 230$ mm, $S = 200$ mm and again $S = 230$ mm, respectively. This development of slump values in time shows a limited rise of yield strength, as can also be seen in the plot of the calculated yield strengths in Figure 9.16 on page 202.

To counteract segregation, the mixture was remixed for around 10 seconds before filling each of the moulds, starting with mould 6.1 and ending with 6.4. As a result of the remixing, the fresh concrete remained self-compacting and in the beginning also self-levelling, but despite the remixing slight segregation stayed visible (bleeding of cement water of top surface, larger grains seemed to sag in the mixture), especially in the two first moulds 6.1 and 6.2 that were filled. During the filling of the third and fourth mould, it became clear that the workability reduced at fast pace, even though the slump tests indicated something different⁹.

Therefore it was decided to start with the deformation (again into a single-curved radius $R_1 = +1.5$ m) of mould 6.3 at $t = 0:45$, then 6.2 at $t = 0:59$ and finally 6.1 at $t = 1:15$ h:min. This resulted in a time for stabilisation of 15, 40 and 63 min, for mould 6.3, 6.2 and 6.1 respectively. Element 6.3 did not show cracks as a result of deformation. Some cement water was flowing over the edge of the mould, though. Element 6.1 and 6.2 both developed cracks as a result of the deformation, possibly for mould 6.2 also as a result of some shocking during the deformation due to a stuck deformation mechanism. The cracks in element 6.1 were smaller than in element 6.2.

⁹The difference between slump tests (indicating low yield strength) and experienced workability (indicating high yield strength) may possibly be explained by the fact that a non-representative part of the segregating volume for the slump cone samples may have been taken, resulting in a mixture in the moulds different from that in the slump cones.

After demoulding, the elements appeared to have a good finish on the mould side and edges (see Figure 9.20). Few air bubbles and blobs were seen. The finishing surface of mainly element 6.2 and less also of 6.1 had many cracks, and also the thickness of element 6.2 varied as a result of segregation and flow. To assess the crack depth and width, cores were drilled from all four elements of this batch, and these cores were sliced into sections for closer observation¹⁰. More on this will be reported below.

Batch 7, 8 and 9 (mixture m_3 - 1.00% plasticizer)

For batch 7, the amount of plasticizer was slightly reduced to 1.0% in order to obtain less bleeding and segregation. The slump flow now, however, did not come above 500 mm, indicating that the mixture was neither self-compacting nor self-levelling. The results of batch 7 were assessed as not useful and thus not reported here. As there was no consistency in the mixtures obtained in the previous tests, it was decided to do just a test on the proportions of the mixture itself in a small volume.

For batch 8, the contents for a small volume of concrete (7 litre) were weighed. The dosage of plasticizer was kept at 1.0%. The mixture now proved to be very fluid, self-compacting and self-levelling. The immediate slump flow was also satisfactory. However, the slump flow after 45 min was quite high ($SF = 700$ mm) and the concrete appeared to segregate then. Since this mixture was better than the batches of 4 to 7 and easier to handle, it was decided to repeat the same test. Batch 9 appeared to behave similarly to batch 8. The slump flow, measured directly after mixing, was satisfactory. The slump flow after 45 minutes was quite high but less than batch 8. Thus it was decided to use the same proportion for the next test for 100 litre for casting the elements. No elements were cast, apart from some prisms for strength testing. The cube compressive strength ($40 \times 40 \times 40$ mm³) was around 91 MPa after 28 days.

Batch 10 (mixture m_3 - 0.75% plasticizer - improved mixing order from here on)

From this test on, the mixing order was modified. It appeared important to add the plasticizer *after* the cement absorbs water to work effectively. Also the mixer now was slightly wetted before pouring the ingredients, and also the slump cones and slump base plate were oiled. Only 0.75% of plasticizer, related to total powder content, was added and the mixture was prepared with the changed mixing procedure. The mixture seemed fluid, self-compacting and self-levelling. However, it was segregating a bit and stabilizer was added to reduce the segregation. The mixture was very workable, but not entirely self-levelling. It was easy to place and a little bit of manual compaction was necessary. The element thickness was $h_2 = 0.05$ m. The mixture had a slump flow of $SF = 650$ mm directly after mixing, and at $t = 0:20$, $t = 0:31$ and $t = 0:54$ h:min, slump values were measured of $S = 220$ mm, $S = 200$ mm

¹⁰More images of batch 6 can be found on the project website: [inspection of demoulded elements and drilled cores](#)

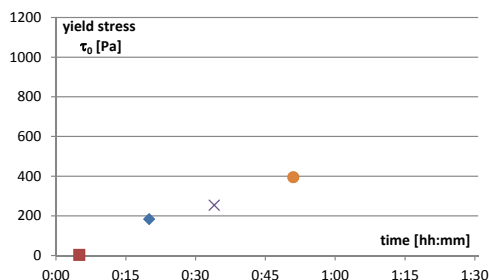


Figure 9.21: Batch 10 - development of yield stress in time, calculated from the slump (flow) tests

and $S = 160$ mm respectively. This development of slump values in time shows a moderate rise of yield strength, as can also be seen in the plot of the calculated yield strengths in Figure 9.21.

The deformation of element 10.1, 10.2 and 10.3 at $t = 0:20$, $t = 0:34$ and $t = 0:51$ h:min, respectively, went smooth. Again the same radius $R_1 = +1.5$ m was used. However, small surface cracks were visible immediately after deformation (see Figure 9.22). These cracks were most visible in element 10.2 and 10.3, hardly visible in panel 10.1 and not visible in element 10.4 (the flat panel). The cracks were distributed at intervals of roughly 5 mm to 10 mm for element 10.2 and had a slightly finer distribution for element 10.3 (crack intervals of around 5 mm). The crack widths were not measured, but, as could be observed in the high resolution images, were more in the order of magnitude of one or two tenths of millimetres than of whole millimetres, and clearly of much smaller width than the cracks observed earlier in batches 4, 5 and 6.

The elements had a good finish on the mould side, except for some air bubbles

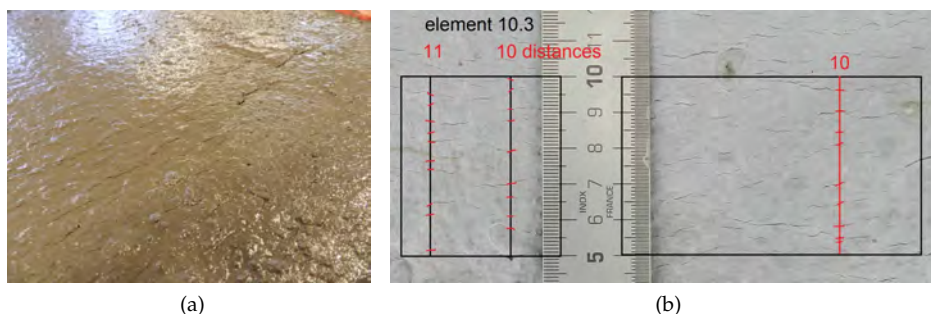


Figure 9.22: Batch 10 - improved mixing order led to better workability; still small cracks, very much alike the type of cracks usually observed after plastic shrinkage developed in finishing surface of the mould (a) immediately after deformation (b) after hardening

and blobs of concrete sticking out due to the deterioration of the moulds (see Figure 9.22b). The finishing surface had small cracks perpendicular to the direction of deformation, as observed immediately after deformation and described above. The cube compressive strength was around 71 MPa after 28 days¹¹.

Batch 11 (mixture m_3 - 0.65% plasticizer)



Figure 9.23: Batch 11 - repeated test compared to batch 10 with similar results: cracks in the finishing surface

For batch 11, still using mixture m_3 , the percentage of plasticizer was reduced to 0.65%, to avoid the segregation observed during the previous mixture. The mixture was workable, self-compacting, non-segregating but not entirely self-levelling. It was easy to place and a little bit of manual compaction was necessary. So, it was quite consistent with the previous mix. The mixture had a slump flow of $SF = 640$ mm and a flow-time $T_{50} = 11$ sec directly after mixing, and even at $t = 0:10$ and $t = 0:15$ slump flows of $SF = 570$ mm and $SF = 610$ mm respectively were measured. At $t = 0:45$ h:min, a slump value was measured of $S = 185$ mm. Not enough concrete was made to fill all slump cones and cubes. All moulds were filled to an element thickness $h_2 = 0.05$ m. The deformation of element 11.1, 11.2 and 11.3 at $t = 0:50$, $t = 1:00$ and $t = 1:16$ h:min, respectively, was for all elements executed roughly half an hour later than for batch 10, but went smooth, nonetheless. Again the same radius $R_1 = +1.5$ m was used. Surface cracks were visible immediately after deformation (see Figure 9.23a and c). Element 11.1 showed a cracking pattern much similar to that of element 10.3, both were deformed around $t = 0:50$ h:min. Element 11.2 and 11.3 showed a slightly finer crack distance, between 3 and 5 mm, but for element 11.3 the crack width seemed less evenly distributed over all cracks: some cracks were clearly wider than others (see Figure 9.24a). Element 11.3 was deformed quite late at $t = 1:16$ h:min.

The elements had a good finish, except for some air bubbles and blobs of concrete sticking out due to the deterioration of the moulds¹².

¹¹More images of batch 10 can be found on the project website: [casting and deformation](#) and [inspection](#).

¹²More images of batch 11 can be found on the project website: [casting and deformation](#) and [inspection](#).

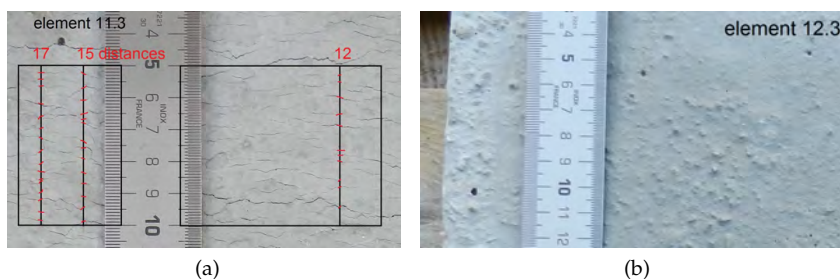


Figure 9.24: (a) element 11.3 - visible cracks in the finishing surface
(b) element 12.3 - no visible cracks.

Batch 12 (mixture m_3 - 0.65% plasticizer)

Batch 12 was the first batch in which an element thickness $h_1 = 0.025$ m was tested, still using mixture m_3 . Again the same radius $R_1 = +1.5$ m was applied. The workability was consistent with the previous batch. The moulds were placed in reverse order, as the actuators were adjusted for deformation of moulds 2, 3 and 4. Mould 1 remained flat.

The mixture had a slump flow of $SF = 650$ mm directly after mixing, with a flow time $T_{50} = 10$ sec; at $t = 0:31$, $t = 0:45$ and $t = 0:59$ h:min, slump values were measured of $S = 220$ mm, $S = 165$ mm and $S = 180$ mm respectively. The third slump cone collapsed while releasing the cone. Placement was easy. It was, however, difficult to get a uniform element thickness $h_1 = 0.025$ m within the moulds with an edge height of $h_2 = 0.05$ m. The moulds were covered with foil immediately after placing.

The deformation at $t = 0:36$, $t = 0:48$ and $t = 1:00$ h:min went smoothly. This time, no visible cracks were noticed immediately after deformation¹³. Additional weights had to be placed on the moulds to get a uniform curvature. After demoulding, the elements had a smooth finish except for the effects of the deteriorated mould. Contrary to the specimens of batch 10 and 11, no cracks were visible (see Figure 9.24b)¹⁴.

The elements were also combined in a set-up to get an impression of the accuracy and continuity of the curvature (see Figure 9.25). It appeared that the curvature was quite accurate, but that the shape of the edges was not fitting due to deformation of the edge of the mould before hardening.

Batch 13 (mixture m_3 - 0.65% plasticizer)

For batch 13, the same mixture m_3 was used, similar to batch 11 and 12, with identical amount of plasticizer 0.65% (related to total powder content). Element thickness

¹³It could be due to the effect of the foil, or because the strain caused by deformation for a thickness of 25 mm panel is half of that for 50 mm panel.

¹⁴More images of batch 12 can be found on the project website: [casting and deformation](#) and [inspection](#).



Figure 9.25: Batch 12 - fitting of the cast elements in a curved shape: curvature is quite continuous, edge shape does not fit very well, due to deformation of the mould edge

$h_1 = 0.025$ m was tested again, but now the opposite single-curved shape with radius $R_1 = -1.5$ m was applied. The workability of the fresh concrete was similar to the previous test, though the slump flow was slightly less than the previous ones. The mixture had a slump flow $SF = 610$ mm directly after mixing, and at $t = 0:30$, $t = 0:45$ and $t = 0:58$ h:min, slump values were measured of $S = 240$ mm, $S = 190$ mm and $S = 150$ mm respectively¹⁵. The placing of concrete in the moulds was in reverse order as during the previous batch. The moulds were covered with foil immediately after placing. The deformation at $t = 0:34$, $t = 0:47$ and $t = 1:02$ h:min went smooth. No cracks were seen after deformation. Additional weights had to be placed on the moulds to get uniform curvature. The elements had a smooth finish except for the effects of the deteriorated mould. No cracks were visible¹⁶, nor on the mould surface of the elements, nor on the finishing surface. The cube compressive strength ($150 \times 150 \times 150$ mm³) was around 84 MPa after 28 days.

Batch 14 (mixture m_3 - 0.70% plasticizer)

Batch 14 had the purpose of casting elements with a thickness $h_2 = 0.05$ m and again the single-curved shape with radius $R_1 = -1.5$ m. The proportion of the plasticizer was increased to 0.70%. The fluidity slightly increased, resulting in a slump flow of $SF = 700 - 800$ mm, with a flow time $T_{50} = 4$ sec; at $t = 0:31$, $t = 0:46$ and $t = 1:01$ h:min, slump values were measured of $S = 235$ mm, $S = 180$ mm and $S = 35$ mm respectively. The placing was in reverse order as the last one. The moulds were

¹⁵The third slump cone 'collapsed' while releasing the cone (see an example of this phenomenon in the top left image of Figure 9.29 on page 214): due to some randomness of where the first yielding of the fresh concrete takes place, the slump value with Abrams cone can give different results, even with identical concrete. According to the code, such a slump test is formally considered invalid. For the slump flow, this issue is not relevant. For our purposes, though, the slump tests is considered the most practical and common way of measuring the workability and will be used. The small Haegermann cone does not show this issue, since the proportion between height en diameter is different. For this reason, the Haegermann cone was also used in a number of tests.

¹⁶Images of batch 13 can be found on the project website: [casting and deformation](#) and [inspection](#).



Figure 9.26: Batch 15 - double-curved panel 15.2 with thickness of 50 mm and radius of ± 2.5 m in two directions

covered with foil immediately after placing. No cracks were seen after deformation. The elements had a smooth finish except for the effects of the deteriorated mould. No cracks were visible¹⁷. The cube compressive strength ($150 \times 150 \times 150 \text{ mm}^3$) was around 71 MPa after 7 days. A 28-day cube was only tested on a mini-cube ($40 \times 40 \times 40 \text{ mm}^3$) and was around 84 MPa.

Batch 15 (mixture m_3 - 0.70% plasticizer)

Batch 15 had the purpose of casting one element with a thickness $h_2 = 0.05 \text{ m}$ and a double-curved shape with radius $R_1 = R_2 = -2.5 \text{ m}$ was applied (sphere-shape, see Figure 9.26). The proportion of the plasticizer was again 0.70%. The fluidity, therefore, remained quite constant compared to batch 14, resulting in a slump flow of $SF = 715 \text{ mm}$. At $t = 0:29$, $t = 0:43$ and $t = 1:03 \text{ h:min}$, slump values were measured of $S = 190 \text{ mm}$, $S = 160 \text{ mm}$ and $S = 20 \text{ mm}$ respectively. The concrete was covered with foil immediately after placing. No cracks were seen after deformation. The elements had a smooth finish except for the effects of the deteriorated mould. It was, therefore, decided to fabricate new moulds for the later tests. No cracks were visible. The cube compressive strength ($150 \times 150 \times 150 \text{ mm}^3$) was around 40 MPa after 1 day. A 7- or 28-day cube were not tested¹⁸.

Batch 16 (mixture m_3 - 0.70% plasticizer)

Batch 16 was used to cast the first series of double-curved elements with new moulds. The new moulds consisted of 3 moulds of silicone finish surface and 1 of polyurethane finish surface. The polyurethane moulds were used for the flat elements. Like in batch 15, thickness $h_2 = 0.05 \text{ m}$ and a double-curved shape with radius $R_1 = R_2 = -2.5 \text{ m}$ was applied, but now three elements were cast and deformed at various moments in time.

¹⁷Images of batch 14 can be found on the project website: [casting and deformation](#) and [inspection](#).

¹⁸More images of batch 15 can be found on the project website: [casting and deformation](#) and [inspection](#).



Figure 9.27: Batch 16 - visual inspection of elements; element thickness is 50 mm, radius in two directions is - 2.5 m; the elements are shiny since new silicone moulds were used (PR)

The mixture was prepared with the same proportions as for the previous batches 14 and 15 and directly after mixing had consistent workability, though it stiffened faster. The mixture had a slump flow $SF = 730$ mm directly after mixing, with a flow time $T_{50} = 5$ sec; at $t = 0:45$, $t = 1:01$ and $t = 1:15$ h:min, slump values were measured of $S = 170$ mm, $S = 40$ mm (cone collapsed) and $S = 190$ mm, respectively.

The polyurethane mould was oiled to facilitate easy release; the moulds were placed in reverse order. The side pieces of the polyurethane mould started bulging out during the placing of the concrete, because the silicone sealant did not stick to polyurethane. Additional weights were placed along the edges to prevent it from bulging out. The deformation was also done in reverse order (starting at mould 4, ending with mould 2) at $t = 0:48$, $t = 1:03$ and $t = 1:17$ h:min. Mould 3 and 4 did not deform smoothly due to some issues with the actuators. The other deformations went smooth. However, the mould still didn't touch the actuators of second and third rows at most places.

The elements have a good shiny reflective finish. The polyurethane mould, though, gave a less glossy finish. The reflection of the lathes was visible again over the surface, like with the first test with the first set of moulds. The elements have few air bubbles. No cracks were visible. The edges of the elements are straighter than the ones cast with the old moulds¹⁹. The cube compressive strength ($150 \times 150 \times 150$ mm³) was around 85 MPa after 28 days.

Batch 17 (mixture m_3 - 0.70% plasticizer)

For batch 17 the same curvature was used as in batch 16, but the element thickness was reduced to $h_1 = 0.025$ m again. The mixture was prepared with same proportions as for the previous batches 14 to 16 and had consistent workability. The mixture had a slump flow $SF = 685$ mm directly after mixing, with a flow time $T_{50} = 5$ sec; at $t = 0:30$, $t = 0:46$ and $t = 0:59$ h:min, slump values were measured of $S = 215$ mm,

¹⁹More images of batch 16 can be found on the project website: [casting](#), [deformation](#) and [inspection](#).

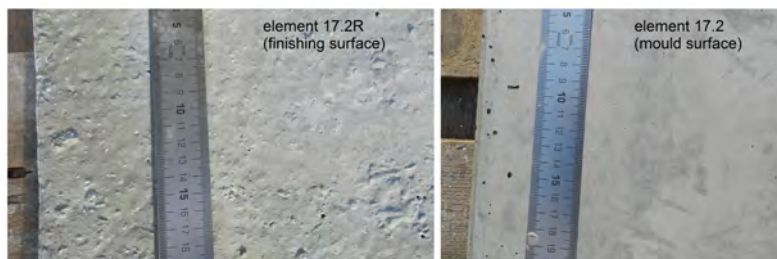


Figure 9.28: Analysis of one element of batch 17: no cracks are visible

$S = 175$ mm and $S = 85$ mm respectively. The deformation was done at $t = 0:32$, $t = 0:49$ and $t = 1:02$ h:min.

All the moulds were oiled this time. The moulds were filled in reverse order (starting with mould 4, ending with 2). The deformation was also done in this order. All deformations went smoothly this time. However, the mould still didn't touch the actuators of second and third rows at most places.

The elements again had a somewhat shiny reflective finish, but less than the previous batch. The polyurethane mould element had an even less glossy finish. The reflection of the lathes was visible over the surface. The elements had few air bubbles. No cracks were visible (see Figure 9.28). The edges of the elements were straighter than the ones cast with the old moulds²⁰. The mini-cube compressive strength ($40 \times 40 \times 40$ mm³) was around 93 MPa after 28 days.

Batch 18 (new mixture m_4 - 0.59% plasticizer)

Batch 18 was the first batch in which a mixture containing only fine aggregates, mixture m_4 , was used. For this batch various element thicknesses and curvatures were applied. The largest aggregate size was 1 mm, and Omya Betoflow D calcium carbonate was used as fine filler, still together with fly-ash. The amount of plasticizer that was used in this mixture was 0.59%. The mixture had a slump flow $SF = 865$ mm directly after mixing, with a flow time $T_{50} = 3$ sec. The mini-slump²¹ flow was $S_{mini-flow} = 280$ mm; With Abram's cone again at $t = 0:24$ a slump flow of $SF = 650$ mm and at $t = 0:42$ a slump flow of $SF = 620$ mm were found. It was concluded that the mixture was relatively fluid compared to earlier mixtures, and also for a longer time. It was interesting to see that parallel to slump test 2 and 3, the mini-slump test did not result in a flow-spread situation, but in an upstanding cone with a slump value of around $S_{mini} = 5$ mm in test 2 and $S_{mini} = 0$ mm in test 3. Furthermore it was observed that slight tapping of the mini-cones would result in a flow circle again, after regained fluidity of the mixture due to the vibration induced by slight tapping.

²⁰Images of batch 17 can be found on the project website: [casting](#), [deformation](#) and [inspection](#).

²¹Haegermann-cone, used without stroking table, upper diameter 70 mm, lower diameter 100 mm, height 60 mm, (Roussel et al., 2005)



Figure 9.29: Difference between Abrams cone (top-left) and Haegermann cone (top-right) with slump tests at same moment and with same mixture.

Effect of vibration on the mixture (other images): fluidity will be regained easily after slight tapping of the cone



Figure 9.30: Batch 18 - Tilted mould for element 18.2 over around 30° with the horizontal, so that a lower part of the circle-shape is described. This allowed testing of casting under a slope of around 45° at the edge of the mould (normally only 15° with $R_1 = -1.5$ m, see Table 9.6 on page 189). As can be seen in the right image, the element was cast successfully

The deformation of the moulds was done at $t = 0:42$, $t = 0:45$ and $t = 0:59$ h:min²². Two elements with a thickness of $h_2 = 0.05$ m were deformed into a double-curved shape with radius $R_1 = R_2 = -2.5$ m. The third element with the same thickness was deformed into a single-curved shape with a radius of $R_1 = -1.5$ m., but the whole circle-shape mould was tilted over around 30° with the horizontal, so that a slope of 45° was created at the edge of the mould (see Figure 9.30).

After demoulding, the elements were inspected. The surface of the elements was smooth, locally small air bubbles could be observed. No cracks were visible. The deformation under a slope of 45° appeared to have gone well.

²²Images of batch 18 can be found on the project website: [casting and deformation](#) and [inspection](#).

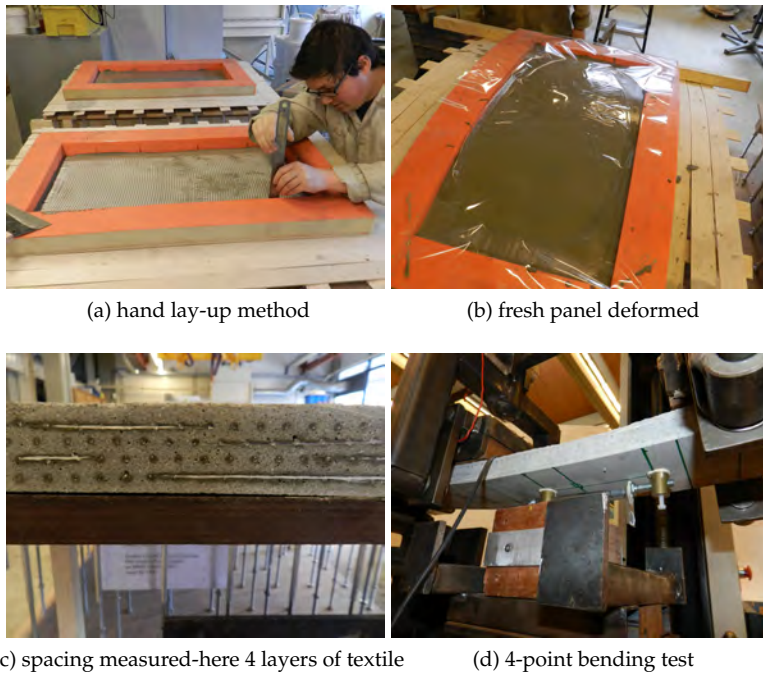


Figure 9.31: Tests with textile reinforcement

9.9 Additional tests: textile reinforcement

In the viability study traditional steel reinforcement was applied with small diameters and additional protection against corrosion through galvanising. In section 9.4 it was already shown that the use of small diameter traditional steel reinforcement in elements for high concrete grades will lead to a relatively small rebar spacing, even for amounts of reinforcement just around the minimal allowed percentage. Furthermore the concrete cover will always be very limited as a result of the total element thickness of only a few centimetres.

A research group at RWTH Aachen has experimented with thin shell structures reinforced with glass fibre *textiles*, resulting in TRC: Textile Reinforced Concrete. In various publications (Hegger et al., 2008a,b; Scholzen et al., 2012), the possibilities and mechanical properties of TRC are outlined. Some of these results were applied in the present research to investigate the possibility to reinforce double-curved concrete elements with textiles. In this section the result of the reinforcement with glassfibre textiles will be summarized briefly. The work was extensively reported by Kok (2013), Schipper et al. (2013) and Kok et al. (2014). Some images of the tests are shown in Figure 9.31 and more on the [website](#).

Although only experiments were done with glassfibre textiles, the outcomes are also relevant for other textiles made of carbon fibre or Aramide/Kevlar. Batch 19 to

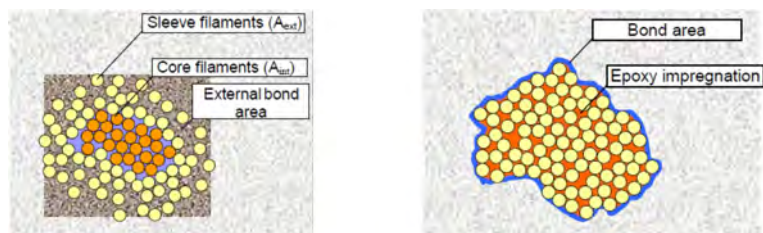


Figure 9.32: Impregnation of glassfibre yarns with epoxy (Brameshuber, 2006)

22 were used to investigate the behaviour of textiles during the deformation process and the effect on the strength. A brief summary of the experiments and outcomes:

- Textiles deformed well together with the still plastic concrete when the flexible mould method was applied. By cutting a number of deformed panels the position of the textile after hardening could be measured, showing that the textiles had followed the curvature of the elements and that the concrete layers between the textile effectively acted as spacers.
- Textiles add significantly to both flexural and tensile strength of the concrete. The presence of textiles lead to a ductile material behaviour.
- The position of the yarns in the cross section had slightly changed as a result of both the production method (hand lay-up method) and the deformation, influencing the flexural strength accordingly. The tensile strength of the TRC remained uninfluenced.
- Numerical simulation in Ansys resulted in good correspondence with the experimental results: this opens the opportunity to determine maximum stresses and strains during the life cycle of each element, thus allowing for a proper detailing, textile placement and anchoring.
- In terms of cost efficiency, the method using textiles with manual labour is considered a little laborious to use and expensive per 'unit of strength'.

Some of the known issues with durability of glassfibre (Jong and Reijgersberg, 1988; Stupré-report studie groep 30, 1988; Gerritse, 1990; Vamberský, 1991) can be successfully addressed by impregnation of the fibre yarns with epoxy (Figure 9.32) and proper attention to detailing and connection. In the present research, though, non-impregnated yarns were applied.

9.10 Additional tests: microscopy

So far, the judgement of the elements after deformation has been done only with the naked eye and high resolution photography. To investigate and quantify whether the deformation influences the concrete on a microscopic level, Troian (2014) carried out

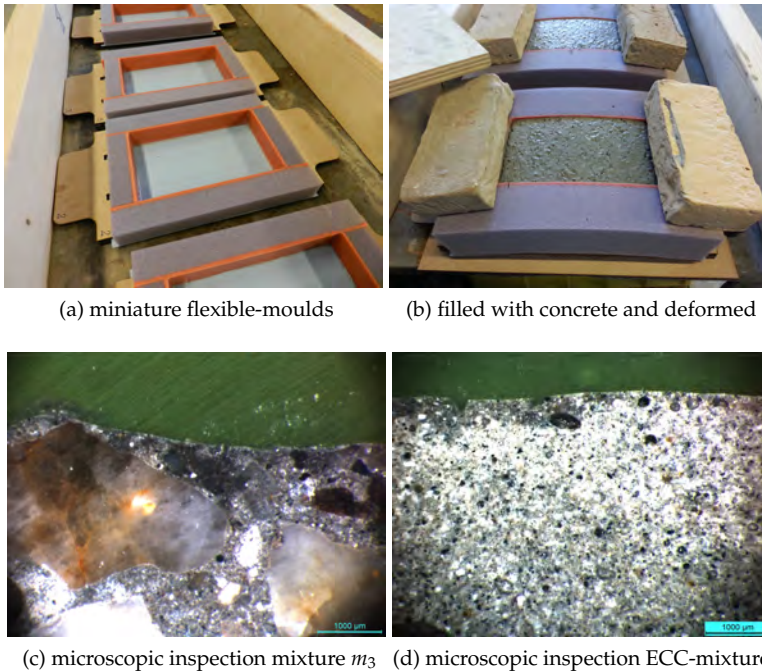


Figure 9.33: Petrographic research (Troian, 2014)

several tests. Concrete elements were cast and deformed using the flexible mould method. Using microscopic analysis, the consequences of the deformation were quantified for several element thicknesses, curvature radii and times of deformation. Crack size, frequency and pattern were measured. Furthermore, the effects of modifying water/cement ratio, addition of mixed wood fibres and addition of PVA fibres were examined. The specimens were prepared using a miniature flexible mould (Figure 9.33), an improved version of the ones used in the deformation viability tests. The following conclusions were drawn:

- Radii between 0.25 m and 1.00 m were investigated, which was significantly smaller than any of the radii in the batches 1-18. Despite this strong curvature, cracks size and frequency in many cases were limited. For mixture m_3 , the frequency of cracks clearly decreased with increasing the radius (less curvature); panels deformed with a radius of 1.0 m will generally have cracks smaller than 0.1 mm in width, none of them deeper than 1 mm.
- Deformation time has an important impact on crack width: with mixture m_3 , deformation after 90 minutes should be avoided. Deformation after 45 minutes led to cracks of only 0.01 mm depth, whereas deformation after 90 minutes resulted in cracks deeper than 0.1 mm.
- Element thicknesses of 25 and 50 mm were investigated. The size and depth of the cracks found was larger with the thicker panel.
- Water/cement ratio's for mixture m_3 were varied between 0.38 and 0.50. A lower water/cement ratio clearly lead to higher crack frequency and larger crack width and depth.
- With respect to durability, the data from the petrographic research can be used to estimate the impact of the flexible mould method for various applications, such as architectural concrete exposed to the outside climate, or interior cladding of buildings. No further research was carried out, though, to provide quantitative data for this, since it would largely depend on the project conditions, loads and applied type of reinforcement.
- A strain-hardening cementitious composite and a wood fibre reinforced concrete both performed better than mixture m_3 . So, this track definitely deserves further attention if the flexible mould method is to be used in real projects.
- No cracks were observed in the surface of the specimens facing the mould.

The overall conclusion from the microscopic research was that the flexible mould method can certainly be applied without the risk of large and frequent cracks.

9.11 Data analysis

9.11.1 Introduction

In the following subsections, the results from the experiments are analysed. The parameter variations are discussed, and it is investigated whether confirmation can be found for the earlier stated suppositions. First Figure 9.34 on the facing page represents numerical data from the tests: in Figure 9.34a the moment of deformation after casting is plotted against the yield strength calculated from the measured slump tests. In 9.34b the curvature and the thickness of each element are translated into the calculated strain of the finishing (top) surface of the mould.

Elements with in total 4 different radii - partially single-curved, partially double-curved - have been successfully deformed for both element thickness h_1 and h_2 , and in most combinations of thickness and curvature also for both concrete mixtures m_3 and m_4 . Successfully is defined here as: no flow of concrete within or out of the mould, smooth mould-side surface and no visible cracks; further exploration of accurate shape and possible microscopic cracks will be addressed later.

From Figure 9.34a it can be observed that with both concrete mixtures successful deformation could be carried out, and also at all chosen times $t_{deform;1} = 0:30$, $t_{deform;2} = 0:45$ and $t_{deform;3} = 1:00$ h:min. In some cases deformation was even successful (slightly) before or after this range. Apparently the moment of deformation after casting, within a certain range, is not a very critical variable with the given mixtures.

9.11.2 Development of yield stress to find t_1

Development of yield stress

Figure 9.34a shows a rather broad scatter of yield strength development over time. The dosage of plasticizers and the moment of adding it to the mixture appeared to be quite sensitive aspects in the yield strength development. Large differences were found with similar recipes but with variation of these two variables. Therefore, we will first focus at the yield stresses, calculated from the slump test results for the batches 14 to 17, that were all done with the same mixture, the same amount of plasticizers (0.70%) and the same mixing order, resulting in a rather consistent behaviour. Figure 9.35 shows the calculated yield stresses for these four batches in the first hour.

The yield stress values were calculated according to Equation 9.5 on page 174 of Roussel and Coussot (2005) for the *slump flow* test (directly after mixing) and Equation 9.12 on page 175 of Mueller et al. (2014) for the *slump* tests (after some time of stiffening). The data points show an increasing yield stress development in the first hour, starting as a self-compacting concrete ($\tau_0 = 1.6 - 2.7$ Pa at $t = 0:05$ h:min) and developing into a rather stiff mixture ($\tau_0 = 686 - 890$ Pa around $t = 1:00$ h:min). It can be concluded that this mixture shows a clear change of workability in the first hour from self-compacting to practically non-workable. According to

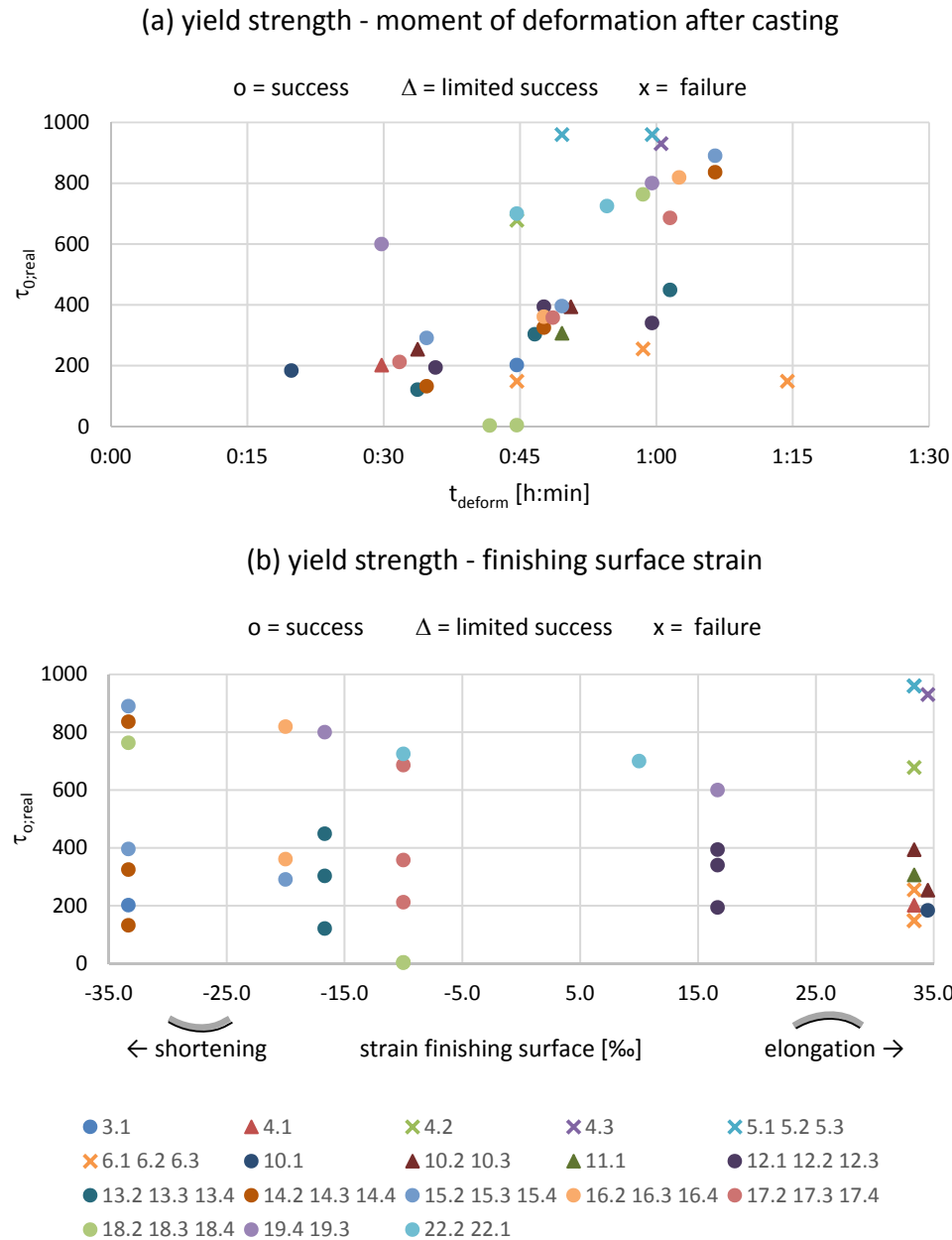


Figure 9.34: Diagrams representing all test results; plotted against vertical axis is calculated shear yield strength, against (a) horizontal axis time of deformation and (b) calculated strain in finishing surface . At some points overlapping dots have been shifted slightly for sake of clarity.

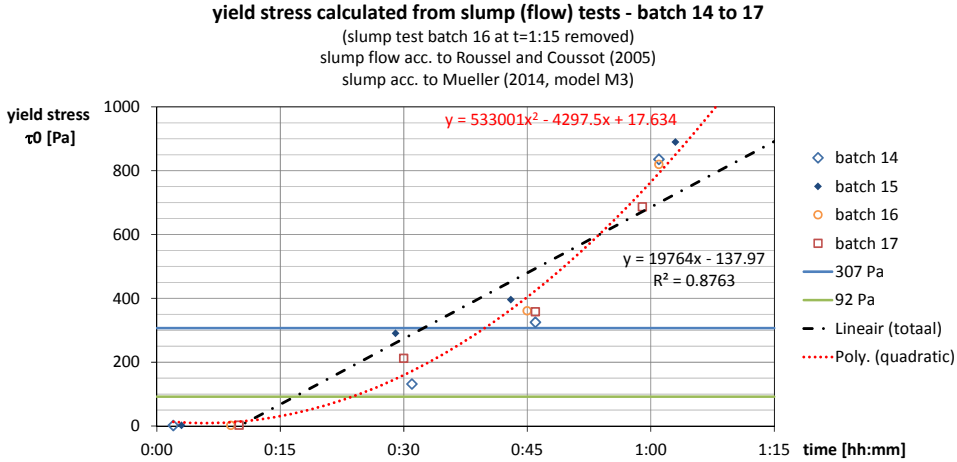


Figure 9.35: Yield stresses calculated from the slump tests for batch 14 to 17 according to equation M3 of Mueller (2014), using mixture m_3 . A quadratic trend line is drawn.

the classification of Roussel, mixture m_3 was earlier classified as a *medium-thixotropic* mixture with $A_{thixo} = 0.22$ Pa/sec based on BML viscometer measurements. The research of Roussel (2006b), as discussed earlier on page 127, showed a linear development of the yield stress in the first 15 minutes. If the data points in Figure 9.35 are interpolated linearly, the thixotropic strength increase is $A_{thixo} = 19764/3600 \cdot 24 = 0.23$ Pa/sec, which shows good resemblance with the value found using the BML viscometer, taken into account, however, a starting point that is not $t = 0$, but around $t = 0:10$ h:min. Taking into account that after adding water to the mixture at $t = 0$ the mixing and placing of the concrete generally takes at least ten minutes, this correction of the origin of the linear interpolation may even be explained from this process. From Figure 9.35 it furthermore becomes clear that if the strength development is interpolated using a quadratic trend curve a better fit is obtained than using a linear trend.

Finding the correct lower boundary t_1

The elements in the batches 14 to 17 all had an element length $L = 0.80$ m, a height $h_2 = 0.05$ m or smaller and a radius of $R_1 = 1.5$ m or larger. According to Table 9.6 on page 189, for this geometry the critical yield strength, necessary for the concrete in order to stay in the mould, was in the range $94 \text{ Pa} \leq \tau_{0,crit} \leq 314 \text{ Pa}$. It is interesting to see now from the test results what time the mixtures needed to reach this yield strength. From 9.35 it is concluded that the necessary yield strength in the range $94 \text{ Pa} \leq \tau_{0,crit} \leq 314 \text{ Pa}$ is reached around roughly the first 30 to 45 minutes after mixing. All tests in the batches 14 to 17 - except for one - were done with a measured

yield strength that was higher than the calculated $\tau_{0,crit}$, and in none of the cases flow occurred. Even in the one case where the measured yield strength was lower than the calculated $\tau_{0,crit}$ (element 14.4) no flow occurred.

In all tests where *flow* occurred (test 3.1, 6.1, 6.2 and 6.3), the measured yield strength was *lower* than the calculated necessary $\tau_{0,crit}$. This confirms supposition 2.1 that t_1 calculated according to De Larrard's slope model in combination with Roussel's thixotropic strength development can be used with sufficient accuracy to calculate the right moment of deformation after casting.

9.11.3 Development of strain capacity - finding t_2

Strain distribution over the height

The bending process brings along a forced deformation. As already stated earlier, a linear strain distribution over the height of the element was assumed. Observation of the mould surface showed that in this plane no in-plane extension occurred, at least not with the single-curved tests. As the mould surface itself did not extend during deformation, the strain distribution as shown in the right image in Figure 9.36 was taken as starting point for the calculated strains. Evidence supporting this

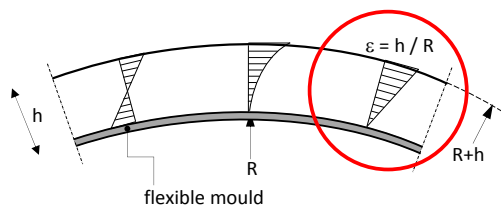


Figure 9.36: No strain near to mould surface with negative curvature - the right distribution is the most probable one.

assumption of a linear strain diagram is (a.o.) the following: element 11.3 with a thickness $h_2 = 0.050$ m was deformed with a positive radius of $R_1 = +1.5$ m. In the concrete that had faced the mould surface during casting, deformation and hardening, no cracks were visible, see Figure 9.37a. The total strain calculated according to assumption $\epsilon = h_2/R_1 = 0.033 = 33$ mm/m. For an element with a length of $L = 0.8$ m the summed crack widths then should be in the order of magnitude of $w_{tot} \approx 0.8 \cdot 33 = 26$ mm. In element 11.3 the measured crack distance was between 3 and 4 mm, resulting in a total number of cracks between $800/4 = 200$ and $800/3 = 267$. The individual average crack widths then, according to the calculated strain, should be in the order of $26/267 < w < 26/200 \Leftrightarrow 0.10 \text{ mm} < w < 0.13 \text{ mm}$. This calculated crack pattern shows good correspondence to the pattern shown in Figure 9.37c. As similar observations were made for other tests, the assumption about the strain distribution is considered to be sufficiently accurate for the purpose of this research. For a negative curvature, the same strain distribution will be used, but then leading to a shortening strain (Dutch: *stuik*).

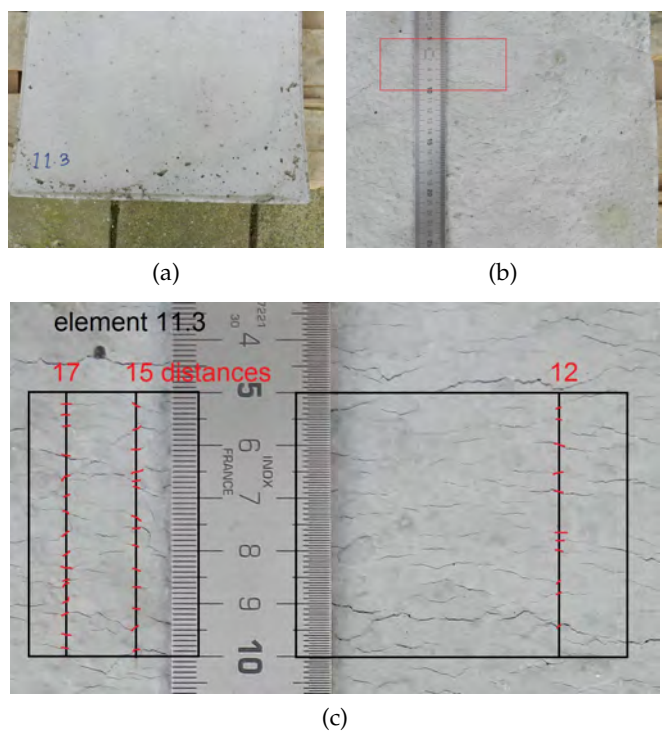


Figure 9.37: Element 11.3 front (a), rear (b) and detail of crack pattern in rear (c)



Figure 9.38: Surface cracks in finishing surface of elements 4.1, 4.2 and 4.3 (from left to right, image scale circa 16 x 12 cm)

Relation between time and strain capacity

Due to the combination of various radii and element thicknesses, the calculated surface strain resulting from the deformation is in the range between -33 and +33‰ (shortening=negative, elongation=positive), assuming a linear strain diagram according to the right image in Figure 9.36. From the lower image in Figure 9.34 it can be observed that only problems occurred during the largest elongation strains, but that even here multiple successful tests were carried out.

Successfully placed and deformed was, for example, element 3.1 of batch 3. No cracks were visible in the finishing surface, possibly also as a result of the fact that this element had a negative curvature, making that the finishing surface was under compression during the deformation. On the mould surface, however, also no cracks were visible, which could mean two things: the strain capacity of the concrete was sufficient to stretch without cracking, or locally no strain was present.

In batch 4, the elements 4.1, 4.2 and 4.3, all with a thickness $h_2 = 50$ mm, were deformed at $t = 0:30$, $t = 0:45$ and $t = 1:00$ h:min, respectively. At the moment of deformation the calculated yield strength was $\tau_0 = 202$ Pa for the first deformed element, up to, for the last deformed element, $\tau_0 = 678$ Pa (see Figure 9.3 on page 176). Cracks developed shortly after deformation, especially in the element deformed as last at $t = 1:00$ h:min. Since these elements had a positive curvature, meaning elongation in the finishing surface of the element, it is concluded that the strain capacity was not sufficient for the calculated strain $\epsilon = h/R = 50/1.5 = 33$ mm/m, which was necessary for the deformation into a radius of 1.5 m (see the red circled strain distribution in Figure 9.36).

In batch 5, the slump values that were measured at $t = 0:45$ and $t = 1:00$ h:min were both zero, which, according to calculation, is similar to a yield strength of at least $\tau_0 \geq 960$ Pa. That the deformation lead to cracks is not surprising, as the strain capacity in batch 4 was also not sufficient, and the mixture of batch 5 was less workable, so probably had a higher yield strength at an earlier moment. Batch 5 clearly demonstrates the relation between crack forming and deformation from the video stills (9.18). If the number of cracks over the full element length of $L = 800$ mm are added up after multiplying each with the estimated individual crack width, the order of magnitude of the developed strain seems to be in the same order as the

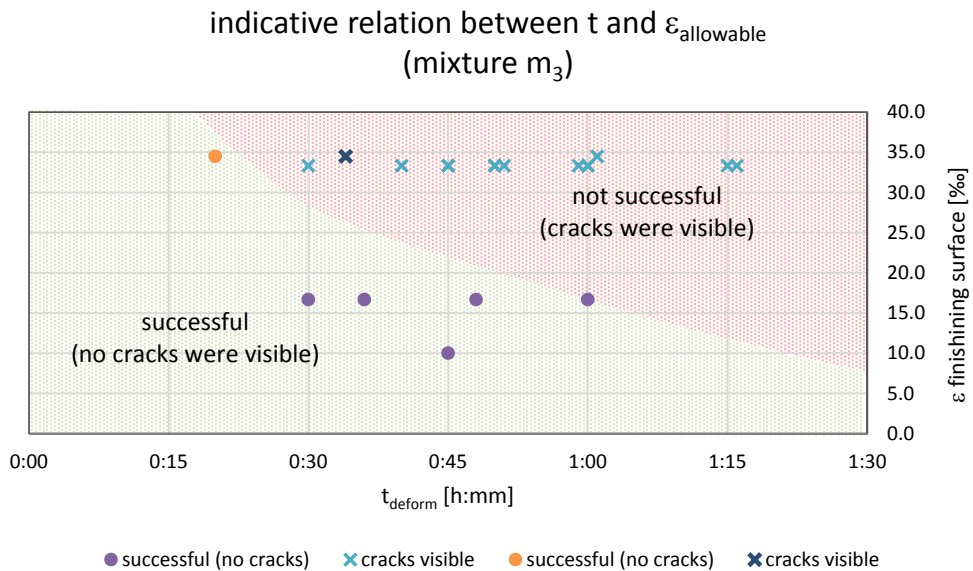


Figure 9.39: Indicative relation between t and $\epsilon_{allowable}$ for mixture m_3 : the lower left area contains all successful tests, the top right area all tests in which cracks were observed

above mentioned 33 mm/m.

In batch 10, a good workable mixture was obtained, and much lower yield strengths were measured than with batch 5. Although the same element geometry was applied ($h_2 = 50$ mm, $R_1 = +1.5$ m, finishing surface strain $\epsilon = +33$ ‰) as in batch 5, batch 10 resulted in much smaller crack widths. Element 10.1, that was deformed very early at $t = 0:20$ h:min, at that moment having a calculated yield strength of $\tau_0 = 187$ Pa, hardly showed any visible cracks in the finishing surface. Apparently a surface strain of $\epsilon = +33$ ‰ for mixture m_3 was possible without visible cracking.

If all tests using mixture m_3 with a positive strain in the finishing surface (elongation) are plotted against the time that the deformation was done, Figure 9.39 is obtained. Although the number of data points is limited, a rough demarcation can be made, separating successful and non-successful tests. This demarcation is comparable to the type of line that was already sought in the proposed model from the previous chapter, Figure 8.30 to find the upper boundary time t_2 for a specific mixture.

Two other observations were made: 1) compressive strains (shortening) in no single case have lead to problems and 2) in no single case cracks were observed in the surface of the concrete *directed towards* the mould.

In the tests of Troian (2014) strains between 25 and 200 ‰ were imposed upon the test specimens by varying radii between 0.25 and 1.00 m with element thick-

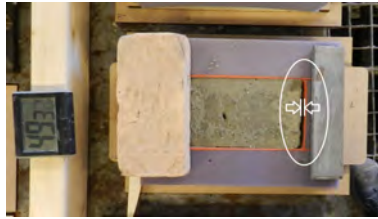


Figure 9.40: Imposed deformation of small specimens - in this case the top surface has elastically shortened, leaving a gap of 2 to 5 mm between mould and specimen

nesses of 0.025 and 0.050 m. Since also mixture m_3 was used, the results might offer information additional to Figure 9.39. Two issues hinder this:

1. different measuring methods were used: visual judgement and microscopic judgement, leading to a different resolution of observations
2. the length of the specimens in both tests were significantly different - for the relatively short (15 cm) specimens used in the microscopic research an imposed deformation is more difficult to obtain than in the longer specimens of the parameter variation study (80 cm). Figure 9.40 shows that this can sometimes lead to side effects.

Based on the available data it was unfortunately not possible to derive a function that can be used to calculate t_2 . The expected trend, however, confirmed that for a mixture with the desired thixotropic strength development the allowable strain reduces (quickly) with time within the first hour.

9.11.4 Effect of concrete mixture on t_1 and t_2

Looking over both viability tests and parameter variation study, a wide variation of fluidities of concrete have been tested. For instance mixture m_1 in Figure 8.16 on page 143 even after 6.5 hours still was too fluid to deform. Similar results were found by recent tests carried out by a concrete manufacturer applying the flexible mould method, see Figure 9.41 on the following page. On the other hand, also many examples were found of mixtures that were hard to place and started with an already initially too high yield strength: these elements often showed (wide) cracks as a result of the deformation. For mixtures m_3 and m_4 good results were obtained, although for mixture m_4 an insufficient amount of tests was done to retrieve t_1 and t_2 .

For each specific mixture, tests will have to be carried out in advance to determine strength development and strain capacity. For the determination of t_1 a combination of viscometer tests and repeated slump (flow) tests after several stabilisation intervals are needed. Strain capacity can only be found by deforming the concrete and



Figure 9.41: Very fluid mixture flows over mould edge after deformation

imposing a specified strain at several moments in time. Simple deformation tests may be sufficient for this, as was seen in section 9.10.

9.12 Empirical generalisations and suppositions testing

Below, the suppositions from section 9.6 will be repeated, and, consequently, discussed in the light of the data analysis.

regarding supposition 2.1 - *De Larrard's slope model in combination with Roussel's model for thixotropic strength development is accurate and sufficient for determining the lower boundary t_1 of the deformation time in the flexible mould process*

Using slump (flow) tests and/or viscometer tests, the thixotropic increase of yield strength over time A_{thix} for a specific mixture can be determined. From the maximum slope angle of the mould, following from the architectural geometry and the position of the element in the mould, the necessary yield strength $\tau_{0,crit}$ can be calculated using De Larrard's slope model, and from $\tau_{0,crit}$ and A_{thix} the lower boundary t_1 can be determined: $t_1 = \tau_{0,crit} / A_{thix}$ (assuming a self-levelling mixture with very limited yield strength at $t = 0$). It was observed, though, that the thixotropic strength development is not necessarily linear (see Figure 9.35) and that yield strength measurements show quite some scatter. Despite these observations, it did not significantly influence the value of the approach in the tests. **Supposition 2.1** is, therefore, considered **tested and true**.

regarding supposition 2.2 - *The upper boundary t_2 of the deformation time is determined from the point where the decrease in time of the plastic strain capacity $\epsilon_{allowable}$ meets the strain necessary for the imposed deformation.*

Within this research it appeared not possible to determine an exact function for upper boundary t_2 , the moment that the decrease of the strain capacity $\epsilon_{allowable}$ in time meets the strain necessary for the imposed deformation. Figure 9.39 gives an indicative boundary, though, showing that for limited strains ($\epsilon \leq 16.7\%$) mixture m_3 showed good results up to $t_2 = 1:00$ h:min and for larger strains ($\epsilon = 33\%$) mixture m_3 showed one successful test at $t_2 = 0:20$ h:min.

The microscopic research showed that even for larger strains deformation is possible without unacceptable cracks, but then it depends very much on what is considered acceptable crack size and frequency for the application at hand. **Supposition 2.2** is, therefore, **considered not proven**. It was not falsified either, though, since the general trend that in time the strain capacity reduces was underlined in all tests.

regarding supposition 2.3 - *A safe and workable assumption for the strain distribution due to deformation is according to Euler-Bernoulli, implying $\partial\epsilon/\partial z = \text{constant}$ over the section height.*

The strain distribution due to the forced deformation was not measured. Both the parameter variation study and the microscopic research demonstrated, though, that there was a clear relation between radius, element thickness and cracking risk. For the practical determination of the risk of cracking, it appeared to be a safe and workable assumption to use the strain distribution according to Euler-Bernoulli with zero strain in the mould surface. **Supposition 2.3** is considered **tested and true**.

regarding supposition 2.4 - *A safe and workable assumption for the friction between the concrete and the silicone mould surface is that no slip occurs between both materials during and after deforming the mould and concrete.*

This supposition assumed a no-slip situation between mould and concrete. The forced deformation for the elements in most of the parameter variation study can be considered as 'developing' the mould surface over a pre-formed pin-bed, especially the single-curved tests. As the strips of the mould did not extend during this process, the silicone intermediate layer did not extend in-plane either. In none of the single-curved tests the concrete therefore, was forced to extend in this plane, so a mechanism that would result in slip simply was absent. For double-curved tests, it was found that in-plane shear deformation of the mould surface is necessary to go from flat to double-curved. Due to the limited size of the test set-up (elements 80x40 cm) in the parameter variation study, this shear deformation was not significant. **Supposition 2.4** therefore, is considered **tested and true for single-curved elements**, but **not-tested** and therefore, **undetermined** for the **double-curved elements**.

regarding supposition 2.5 - *Modifying the concrete mix design can effectively control the lower and upper boundary times t_1 and t_2 mentioned above.*

Modifying the concrete mix design, and more specifically the dosage of superplasticizer, is an effective way to influence t_1 and t_2 : looking at the range of concrete mixtures applied during viability tests, parameter variation study and microscopic tests, this **supposition 2.5** is considered **true** in a **quantitative sense for t_1** , and only in **qualitative sense for t_2** . Possibly further research on a specific mixture can result in a reliable prediction for t_2 .

regarding supposition 2.6 - *Textile reinforcement (TRC) and mixed fibre reinforcement (FRC) can be used to effectively reinforce the concrete elements and will follow the*

deformation accurately.

From the additional tests it has become clear that textile and fibres can be effectively used to reinforce concrete elements, and that (for the case of textile) this reinforcement will also follow the deformation accurately. **Supposition 2.6** is considered **tested and true**.

regarding supposition 2.7 - *Cracks that are caused as a result of the imposed deformation can (partially) be cured due to self-healing effects in the still relatively fresh concrete mixture.*

The crack sizes measured during the microscopic research in many cases were in the category that self-healing could be viable if sufficient reactive material is available. As the concrete is already deformed at a very early age it is likely that self-healing can occur. However, no systematic research was carried out to investigate this. **Supposition 2.7** therefore, is considered **not proven**.

9.13 Theory development

In addition to the first and viability experiments of Chapter 8, the present Chapter 9 has discussed additional literature review and extensive experiments. From this work, further understanding has followed. The following relevant findings were done:

- The theory of Bingham is also applicable in the stages of early hardening, in the transition from fluid to solid; it was furthermore concluded that the Bingham and Tresca yield criterions are identical, which can be useful if a numerical approach would be chosen; in the present research, this was not done.
- Various equations were found to use slump (flow) tests to determine the yield strength of a mixture. For very fluid concrete Equation 9.2 of Roussel and Coussot (2005) was deemed sufficiently accurate for the research; For stiffer mixtures, Eq. 9.11 and 9.12 of Mueller et al. (2014) were used. An alternative measuring method using the BML viscometer yielded comparable data.
- Thixotropic behaviour can be used to influence the lower boundary for the moment of deformation t_1 . By determining A_{thix} , t_1 can be calculated indicatively.
- Data on strain capacity in the first hour after casting was neither found in literature nor measured. From our own tests, it was found that tensile strains in the range of 5 to 33‰ could be applied without visual cracks. In none of the tests with 16‰ tensile strain cracks were visible. Microscopic research showed that crack size and frequency are indeed limited, in some cases even with larger strains. The upper boundary time t_2 could not be determined as function of the required strain, since insufficient data was available to derive such a function. It was, however, possible for the specific mixture m_3 applied in this research to acquire a number of data points in Figure 9.39: successful deformation was

carried out between 0:20 and 1:00 h:min. It is advisable to carry out new tests for each new mixture to determine t_2 .

- In specimens where the curvature was such that the finishing side was under compression no cracks were visible in any situation, neither on the mould side nor on the finishing side.
- Textiles reinforcement, mixed fibres and thin steel reinforcement were applied with success. Textiles followed the deformation with acceptable accuracy, for the thin steel reinforcement the concrete cover locally showed large discrepancies from the intended value.

9.14 Concluding remarks

Based on the results of the parameter variation study and the conclusions on the suppositions as stated in the previous section, the following stepwise approach is proposed for the manufacturing of double-curved precast concrete elements for a given project, as far as the concrete technology aspects are concerned:

1. **overall-geometry analysis:** analyse the architectural surface with respect to curvature (minimum overall radius). A small radius will lead to larger strains. The strain that is necessary to reach the minimal radius is equal to the element thickness divided by the radius: $\epsilon_{\text{necessary}} = h_{\text{element}} / R_{\text{min;element}}$. In the present research, the maximum strain that has been applied in the parameter variation study without visible cracks was 33‰. This and possibly also larger strains may be acceptable depending on the curing method and on what crack size and frequency is deemed acceptable for the function of the element (see step 3).
2. **element subdivision:** depending on the available flexible mould dimensions the overall architectural surface is again analysed with respect to the feasibility to precast it in smaller segments: visible joint positions between elements should be chosen. This is an architectural choice, but with technical consequences: the larger the elements, the larger the dimensions of the flexible mould need to be, but also the larger the maximum slope of the individual elements possibly is (step 4). Also transport restrictions have to be considered, not only for trucks and packaging, but also for the strength of the elements: larger elements in general need additional reinforcement for transport.
3. **functional and structural analysis:** what will be the function of the elements: which loads need to be taken, what is the desired architectural quality, to what climate will the elements be exposed, what manufacturing accuracy is required, what joint width and detailing is allowed? Does the element thickness chosen in step 1 fit with all these requirements? What type and amount of reinforcement is needed (e.g. textiles, mixed fibres, thin steel reinforcement)?

4. **element position in mould:** investigate the possible placing of the element in the available flexible mould and optimise this placing in terms of slope, maximum difference in actuator height and necessary shear angle for reaching the required double-curvature. This is a computational process. In the present research, a maximum slope angle of 45 degrees and a maximum difference in actuator height of around 0.5 m was applied.
5. **produce project data:** derive the necessary data per element for further steps: maximum slope angle, minimal radius, maximum shear deformation. From the collected data for each element a distribution histogram for the total project can be made, useful for possible optimisation.
6. **first concrete mixture choice:** based on a.o. the architectural appearance, strength, durability, element thickness, chosen reinforcement principle a first concrete mixture will be proposed.
7. **concrete mixture optimisation:** based on the data collected in step 5, the mixture from step 6 may need further optimisation; depending on the maximum slope angle θ_{max} and the element thickness h the thixotropy A_{thix} of the mixture may need to be influenced in such a way that the desired lower boundary for deformation t_1 is reached within an acceptable time span (e.g. around 30 minutes after mixing or after placing). To reach a sufficiently thixotropic mixture, the powder content of the mixture (cement, limestone flour, fly-ash, silica-foam, etc.) generally needs to be high. In the present research, powder contents were between 560 and 770 kg/m³. Determination of A_{thix} can be done with sufficient accuracy using slump flow and slump tests. If a viscometer is available, comparison of yield strengths from slump tests and viscometer can give helpful additional information.
8. **check deformability:** deformation tests with the proposed mixture need to be done to find the upper boundary t_2 . These deformation tests can be done in a simple set-up with relatively small specimens, similar to the mini-deformation tests carried out in the present research. By imposing the required curvature at several moments in time, under good surveillance of rheological parameters, the forming of cracks can be evaluated. The element thickness needs to be equal to the thickness of the real elements.
9. **casting and deformation:** the actual manufacturing process needs to be carried out under continuous surveillance of relevant data: rheological parameters, visual observations, geometry check, etc. Possibly feedback from the manufacturing is used to adjust or fine-tune earlier choices made in one of the steps above.
10. **curing / post-processing:** immediately after the elements have been cast, even before deformation, the curing process will influence the final quality: after casting elements should immediately be covered with foil to prevent evaporation and reduction of strain capacity. Furthermore, the conditions under

which the elements are stored for hardening, at what moment are the elements demoulded, how are they stored until transport to the building site should be carefully defined.

11. **mould cleaning and maintenance:** the moulds will need a good check-up after demoulding, possible wear and irregularities need to be evaluated and possibly fixed to maintain a high standard for the next elements in line.
12. **quality evaluation:** various quality checks are generally carried out before elements are transported: aesthetic judgement, cube/prism tests, 3D geometry scan and comparison, etc.

This stepwise approach will need further detailing depending on each specific project, but can offer a useful outline of the process of manufacturing double-curved concrete elements. Figure 9.42 on the next page presents a flow diagram of the above steps. It is an extension of the diagram shown earlier in Figure 7.15 on page 117 with some of the concrete technology aspects from this chapter and the previous one.

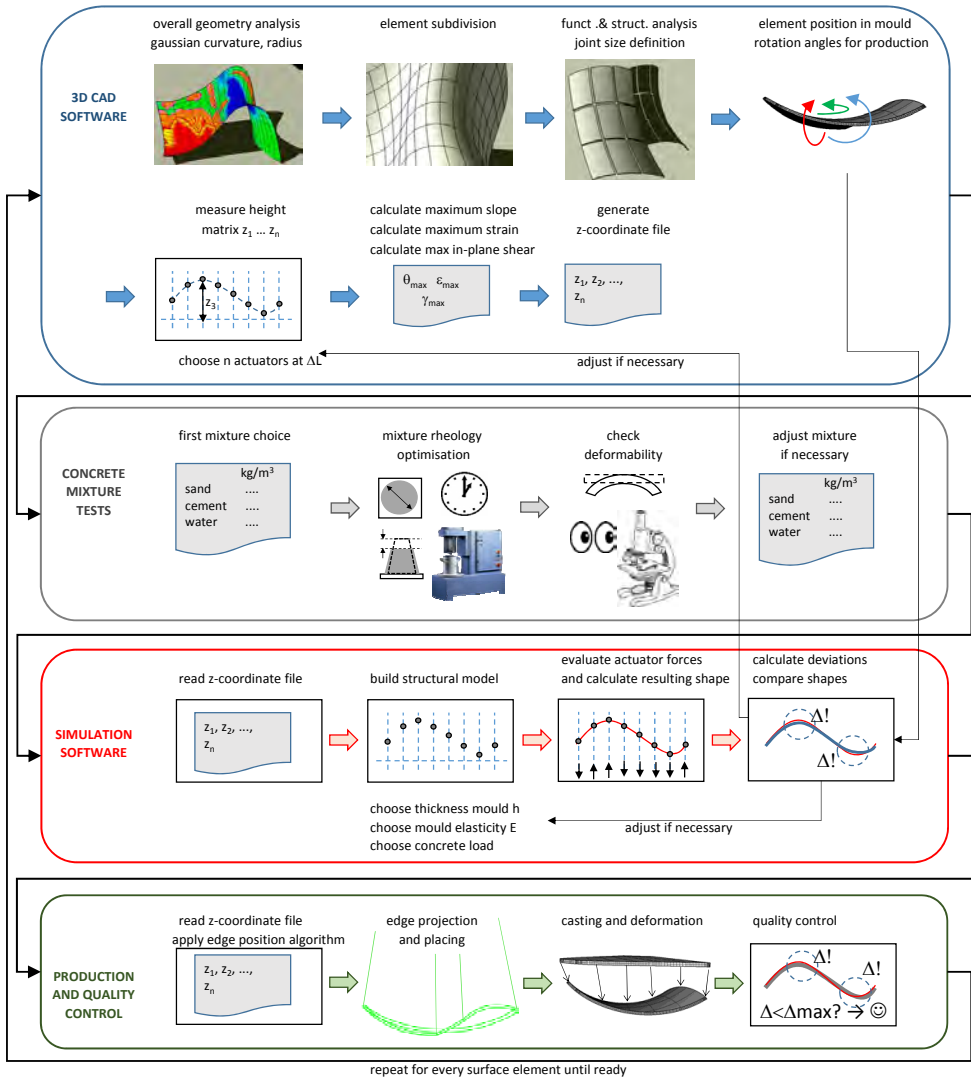


Figure 9.42: Flow-diagram of preparation and manufacturing procedure

Part V

Final remarks

Chapter 10

Conclusions and Recommendations

10.1 Introduction

The objective of this study was to develop and improve the flexible mould method for the manufacture of double-curved precast concrete elements. These elements are applicable for the construction of (building) structures with complex, double-curved geometry. In this thesis, presently available production methods were discussed and compared to the flexible mould principle. The flexible mould principle was tested, further developed and found to be a simplified and effective production process with industrial potential, forming a valuable addition to these available techniques. The research question formulated at the start of the research was:

*How can the flexible mould concept be effectively used
to manufacture double-curved precast concrete elements?*

The research has delivered many practical and theoretical results that contribute to the answer to this question. The results of the research are now presented, grouped in three sections: the *conclusions* (section 10.2) present the findings from literature review, calculations, analysis of buildings and experiments, as well as the conclusions built upon these findings and form the underpinning of a theoretical framework that covers many aspects of the flexible mould method. Since the research is all about a manufacturing method, it was found important to include many *practical recommendations* (section 10.3) that can be directly applied in projects in which the flexible mould method is used. Finally also *recommendations for further research* are formulated (section 10.4) to address unanswered questions or interesting future exploration tracks.

10.2 Conclusions

The research has resulted in the following conclusions:

available techniques for free-form concrete surfaces are expensive or (still) have limitations with regard to surface finish quality or control over the exact shape. Due to lack of repetition of elements in free-form architecture there clearly exists a need for a flexible mould principle that allows repetitive use of the same mould for multiple unique shapes. CNC-milled timber or foam formwork is the technology applied most, presently. In the investigated architectural projects the number of unique elements in some cases was in the order of hundreds to thousands, underlining the need for efficient and cost-effective mould methods.

other industries than the building industry have applied the flexible mould principle, but mainly for rapid prototyping purposes. Examples were found from a.o. automotive, maritime and aerospace industry.

early patents of the flexible mould concept for building construction were already found dating from 1928. In total more than 60 relevant patents were retrieved somehow related to the flexible mould method as discussed in this thesis. Yet, none of these patents offer complete solutions for concrete technology, reinforcement and exact behaviour of the mould surface (also referred to as 'interpolating layer') and edge placement. In the present research, these topics were investigated. In many cases no evidence could be found that the patents have been applied in real projects.

many authors have investigated the flexible mould principle. A flexible mould system is believed to be potentially cost effective, limiting both labour and material costs. In terms of possible level of detail, the flexible mould is positioned between CNC-milled formwork and traditional curved timber or steel formwork.

distinction can be made between *load-bearing elements*, spanning larger distances, sometimes carrying floors of large live loads and (thin) *cladding panels*, carrying mainly self-weight, wind-load, snow, etc. This distinction may be gradual.

precast concrete rather than cast in-situ concrete is seen in literature as appropriate technology for the flexible mould, both for load-bearing and for architectural (cladding) elements. In some cases sprayed concrete is mentioned in relation to the flexible mould. In case of precasting, the assembly during the construction stage requires special attention due to the complex geometry and fitting.

integrated design-to-production or a 'file-to-factory' process is deemed essential, using innovative tools for parametric design, panellization, structural analysis and construction stage. The complex geometry requires special attention for the exact placement of the mould edges; computational techniques may be

needed for this, as well as a numerical quality check of the accuracy after manufacturing, for example using laser scanning. These issues have been addressed in the present research.

two approaches are possible for a feasible production of double-curved surfaces for architectural purposes: *rationalisation* or *mass-customisation*. In recent years, considerable progress has been made in the development of computer algorithms to facilitate the rationalisation process, leading to significant cost reductions. Yet, rationalisation is an optimisation process that can never reduce costs beyond a certain point where the aesthetics of the building are becoming too much compromised.

deformation after casting gives better thickness control and reduces need for compaction, since self-levelling concrete can be applied, even in combination with an open and curved mould. The use of an open mould is possible, as long as the interval for minimum and maximum deformation time $t_1 \rightarrow t_2$ is respected:

lower boundary t_1 is needed to allow the concrete to develop sufficient shear yield strength, to prevent concrete flowing out of the mould. It is determined by *element thickness* and *maximum slope* of the mould. Use of thixotropic mixtures proved helpful for quickly reaching the needed shear yield strength. After initial concrete mixture design, the mixture can be optimised for t_1 by influencing thixotropy parameter A_{thix} . For measurement of shear yield strengths with sufficient accuracy, slump (flow) tests can be used. Viscometer tests can serve as more exact underpinning and calibration.

upper boundary t_2 is limited by the *strain capacity* of the concrete mixture at a given time. The *necessary* strain capacity is determined by the *curvature*, *element thickness* and the *acceptable* crack size/frequency. There is a clear relation between a.o. crack size/frequency, element geometry and moment of deformation. This relation differs per concrete mixture. What crack size/frequency is still acceptable can only be determined if more is known about function, reinforcement and durability parameters of the project. The presence of fibres in the mixture has a positive influence: it reduces crack size/frequency. Curing the concrete with foil directly after casting prevents evaporation and notably increases the strain capacity. For specific curvatures only compressive strains occur, and t_2 is less important.

curved surfaces with zero Gaussian curvature are easier to manufacture with the flexible mould method than curved surfaces with non-zero Gaussian curvature, since the last category not only is deformed out-of-plane, but also in-plane. Separation of out-of-plane bending effects (B) and in-plane stretching effects (S) is necessary. Single-curved or developable elements only show the (B) effect.

the (Bending) effect is responsible for the largest tensile and compressive strains in the concrete during the deformation process and is only dependent on the *radius* of the curvature and the *thickness* of the element;

architectural examples show that a curvature radius between 0.75 m and 45 m was applied in the buildings studied. In many cases curvature in one direction was dominant.

the (Stretching) effect is resulting in *in-plane shear strains* in the present flexible mould design. The value of these strains is only dependent on the *Gaussian curvature*, the *absolute size* of the concrete element and its *position* in the mould.

three types of moulds were applied: single-curved moulds, a double-curved plate mould and a double-curved strip mould. The last one shows the best geometrical accuracy of the two double-curved variants. A plate mould is inherently restricted by its design: basically it is only useful for developable surfaces with zero Gaussian curvature or very limited Gaussian curvature.

the behaviour of the strip mould and its actuators are a complex mechanical engineering topic, that has only been addressed superficially in this thesis. Some relations that were investigated are those between curvature radius, strip thickness, concrete layer thickness and accuracy.

reinforcement can be deformed together with the concrete element. In the present research thin steel and glass fibre textile reinforcement were applied as discrete reinforcement. Both followed the deformation within acceptable accuracy, although the textile performed better than the steel. Mixed fibres can also be applied in combination with the flexible mould method and had a positive effect on the strain capacity for the two mixtures with fibres that were investigated.

10.3 Practical recommendations

The research has demonstrated that the flexible mould method is a viable method for the production of double-curved concrete elements. Some recommendations for manufacturers or other stakeholders who consider the use of this method for a specific project:

- The flexible mould method has been successfully tested for single- and double-curved precast concrete elements with a radius down to 1.50 m and an element thickness up to 50 mm. Elements were reinforced with very thin galvanized steel rebar, mixed fibres or glass fibre textile. Until this moment, the maximum element size was approximately $2 \times 1 \text{ m}^2$, but larger elements are expected to be feasible.
- For elements with required high aesthetic surface quality, the method needs further development; in many tests, the overall geometry was good, but the texture of the concrete surface was not up to satisfaction compared to use of a CNC-milled formwork; currently progress is already made on this aspect

in two projects sponsored by the Dutch Technology Foundation STW and by 3TU.Bouw.

- Application of the method requires knowledge of rheological behaviour and mixture design; the mixtures that may be successfully used in traditional pre-cast elements may need optimisation with respect to flow, yield strength development and strain capacity. For this purpose, at least slump (flow) tests need to be done at various moments, and for initial mix design also the use of a viscometer will be very helpful. This last instrument unfortunately is not standard equipment in most concrete plants.
- For determining of the limits of deformation with respect to crack size/ frequency, a laboratory is needed once the concrete mixture has been developed to judge deformation test results. For future projects using the same mixture, these laboratory tests might be superfluous.
- An integrated design-to-production process is an absolute must: due to the complex geometry and the impact of this geometry on all aspects of the manufacturing, all parties involved should cooperate to make the use of this method possible (to some extent this is true for all complex geometry projects). Computational skills are needed to determine design parameters and control the manufacturing process. This is a skill normally not found among traditional concrete manufacturers, but indispensable for this method. This also opens opportunities: manufacturers that are capable of offering an integrated solution will profit from this advantage in a growing niche market.
- An impression of a possible production line was sketched in Figure 6.7. An essential element in this line is the split between high-tech and medium-tech parts: the flexible mould should be kept as simple and robust as possible, relying on a clear kinetic mechanism. Installation of the actuator heights could be done by one central robotised system, such as the Pinbed Wizzard of Karel Vollers c.s., whereas a larger number of flexible moulds can move around in the factory that have at this central station been pre-configured with the correct heights. If for each flexible mould a fully automated system is pursued, the method will become quickly economically infeasible. This is, however, not necessary.
- Although economical viability was not investigated in the present study, this issue is an inevitable condition for further development of the method. A rough indication for the construction costs (materials and labour) of the most recent prototype (Schipper et al., 2015) with a mould surface size of $1.2 \times 1.2 \text{ m}^2$ is approximately € 5000 (so € 3500 per m^2 mould surface). On top of that, the labour and material costs for the element itself are estimated on approximately € 500 per m^2 concrete element. The time that was necessary for development is not included in this sum. The mould is fully reusable, except for the silicone rubber surface and edges, which at present show an unacceptable deterioration

after a number of casting and demoulding cycles. More durable materials are needed for this. The costs of this rubber surface and edges are estimated at approximately 10% of the mentioned amount. An indication for the current state-of-art alternative, CNC-milling, is € 250 to € 1000 per m^2 mould surface, a wide range, dependent on required materials and finishing. These milled moulds often are single-use, though. Based on these indicative figures, it is expected that for specific categories of projects the flexible mould method is certainly economically viable.

10.4 Recommendations for further research

During the research, many interesting side-tracks had to be skipped in order to be able to answer the main research question in due time. Future research on the following aspects is recommended:

- How can the flexible mould method be made fully sustainable, both in the material choice for the mechanism and for the elements that are produced? An integrated research would be needed to investigate the environmental impact of the method. The profile of clients interested in free-form architecture may also be interested in reducing their environmental footprint and contributing to a better world not only in the aesthetic value of the building, but also in the applied technology and materials.
- The concrete mixtures used in the present research all had a relatively high Portland cement dosage. In terms of carbon footprint, much optimisation is possible. A direction for this could be the approach of particle-packing optimisation or the application of alkali-activated binders. The flexible mould method is also likely to be applicable for other materials, such as natural resins.
- Although, in the cut samples, no voids were observed between hardened concrete and reinforcement, it cannot be ruled out that the deformation of the plastic concrete and the embedded reinforcement may locally have lead to a loss or reduction of bond between reinforcement and concrete. This may especially be the case for steel mesh and textile reinforcement, and probably less for mixed fibres. In cases where steel or textile reinforcement are applied in the flexible mould method, it is recommended to further investigate whether this negative effect indeed occurs.
- An integrated computational tool for element subdivision and optimal position in the mould with respect to slope angle and shear deformation could result in a more streamlined production process. Manual computation per element is considered too much time-consuming. In addition, further research on automated calculation of the accurate projection of the edge position is necessary.
- Long-term effects of the production method such as creep, shrinkage, durability and aesthetic long-term performance have not been investigated. For

the type of high-end projects addressed by this method, such investigation is certainly necessary to avoid future damage (and claims!) due to unforeseen effects.

- The structural connection of the cladding or permanent formwork elements with anchors to a load-bearing structure needs further investigation. For cladding elements, these anchors will be typically positioned at the rear side of the panel, not visible for architectural reasons. For this type of connections, examples can already be found from projects in GFRC (see e.g. Feirabend et al., 2014). For permanent formwork, Two types of connections are necessary: a permanent one, to connect the cast-in-place concrete to the precast element (see e.g. Kim et al., 2010), and a temporary one, to support the permanent formwork in the building stage, when the cast-in-place concrete is still fluid. Further research is needed to investigate these connections.
- If double-curved elements are to be used as thin precast shell segments, and thus as part of the load-bearing structure, further development is necessary first. The joint between the elements then is no longer an open joint (as in the present work) but becomes a structural connection that needs to transfer normal and shear forces and bending moments. For example, buckling effects in thin shells are strongly influenced by the stiffness of the structural edge connection. Moreover, the structural behaviour of the element themselves also becomes even more critical than in an application as cladding or permanent formwork. For load-bearing elements, compliance with various codes for load-bearing elements is required, more than for non-load-bearing elements. This asks for further testing and experimental underpinning. Tests that are required are (among others):
 - proof-loading of elements after curving
 - designing, constructing and testing of various edge connections
 - investigation of long-term material behaviour

It is the expectation that, with the help of industrial partners, application of the flexible mould method in a project is possible with the current knowledge, and will help to create sufficient confidence in the potential of the method. Some of the recommendations mentioned above can be embedded in the project, the necessary research funded from the expected financial benefits following from the reduced mould costs.

Bibliography

- Aigner, F. (2014). Eine Betonkuppel zum Aufblasen - Freiformflächen aus Beton. 15
- Allen, D. H. (2013). *Introduction to the Mechanics of Deformable Solids - Bars and Beams*. Springer New York. 337
- Balz, M. (2011). Working with Heinz Isler. *IASS Journal*, 52-3(169):155–160. 19
- Béchet, E., Duboeuf, F., and Virlez, G. (2013). Université de Liège - course computer aided design in mechanical engineering. 78
- Beesley, P., Noufaily, F., Magus, M., Tyrrell, J., and Williamson, S. (2004). *Digital Fabricators - Michael Stacey, curator with Philip Beesley and Vincent Hui, University of Waterloo*. University of Waterloo School of Architecture Press. 18
- Behloul, M. and Quidant, S. (2008). Patent WO 2008/056065 A2: Moulding device and method for making the same / Dispositif de moulage et procede de fabrication. 32, 33
- Behloul, M. and Quidant, S. (2011). Patent US 7,901,615 B2: Moulding device and production process. 32, 33
- Bekiroglu, S. K. (2010). Assembling Freeform Buildings in Precast Concrete - Heydar Aliyev Cultural Center. In Vambersky, J. and Schipper, H., editors, *Precast2010 - Het nieuwe bouwen in prefab beton - Assembling freeform buildings in precast concrete*. Delft University of Technology. 70
- Beléndez, T., Neipp, C., and Beléndez, A. (2002). Large and small deflections of a cantilever beam. *European Journal of Physics*, 23(3):371. 103
- Bergsma, O. (1995). *Three Dimensional Simulation of Fabric Draping*. PhD thesis, Delft University of Technology. 92
- Bingham, E. (1922). *Fluidity and Plasticity*. McGraw Hill Book Co Inc. 125, 168, 171
- Blaauwendraad, J. (1984). *Niet-lineaire numerieke constructiemechanica*. Technische Universiteit Delft, Faculteit der Civiele Techniek. 338, 339, 341
- Blaauwendraad, J. (2004). *CT5141 Theory of Elasticity - Direct Methods*. TU Delft. 340

- Boers, S. (2006). *Optimum forming strategies with a 3D reconfigurable die*. PhD thesis, Technische Universiteit Eindhoven. 42
- Boothby, T. and Rosson, B. (1998). Preservation of historic thin-shell concrete structures. *Journal of Architectural Engineering*, 4(1):4–11. 60
- Bösiger, H. (2011). The building of Isler shells. *IASS Journal*, 52-3(169):161–169. 11, 12, 19
- Brameshuber, W. (2006). Textile Reinforced Concrete - State-of-the-Art Report of RILEM TC 201-TRC. Technical Report rep036, RILEM. 217
- Brooks, H. and Aitchison, D. (2010). A review of state-of-the-art large-sized foam cutting rapid prototyping and manufacturing technologies. *Rapid Prototyping Journal*, 16(5):318–327. 14
- Bull, J. (2011). Inside Crossrails first station. <http://www.londonreconnections.com/2011/inside-crossrails-first-station/>. 13, 71
- Calladine, C. R. (1983). *Theory of shell structures*. Cambridge University Press. 86, 88, 91
- Ceccato, C., Hesselgren, P., Pauly, M., Pottmann, H., and Wallner, J. (2010). *Advances in Architectural Geometry 2010*. SpringerWienNewYork. AAG10. 80
- Chhabra, N. and Singh, R. (2011). Rapid casting solutions: a review. *Rapid Prototyping Journal*, 17(5):328–350. 17
- Chilton, J. (2000). *The Engineer's Contribution to Contemporary Architecture - Heinz Isler*. Riba Publications Thomas Telford. 61
- Clark, N. S. (2012). An engineers aspect - Eduardo Torroja. 60
- Cohen, G. (1958). Frank Lloyd Wright's Guggenheim museum - He adds new dimensions to the use of poured concrete in building construction. *Concrete Construction*. 60
- Consiglieri, L. and Consiglieri, V. (2010). Morphocontinuity in the work of Eero Saarinen. *Nexus Network Journal*, 12(2):239–247. 60
- Creswell, J. W. (2009). *Research Design: Qualitative, Quantitative, and Mixed Methods Approaches*. SAGE Publications, Inc., 3rd edition. 184
- Dao, V., Dux, P., and Morris, P. (2009). Tensile properties of early-age concrete. *ACI Materials Journal*, 106(6):483–492. 178, 179, 180, 182, 187
- De Larrard, F. (1999). Why rheology matters. *Concrete International*, 8:79–81. 130
- Diks, M. (2005). Translucent sandwichsysteem voor dubbel gekromde toepassingen. Master's thesis, Technische Universiteit Delft, Faculteit Bouwkunde. 46

- Dispenza, K. (2011). Zaha Hadid's Heydar Aliyev Cultural Centre: Turning a Vision into Reality. *buildipedia.com*. 69
- Eekhout, Friedrich, Lockefer, Slotboom, Velkamp, and Vollers, editors (2004). *Blob in the Faculty*. Publikatieburo Bouwkunde, Faculty of Architecture, Delft University of Technology. 45
- Eigenraam, P. (2013). Flexible mould for production of double-curved concrete elements. Master's thesis, Delft University of Technology. 47, 91, 115, 156
- Eigenraam, P. and Schipper, H. R. (2015). Patent NL2011770C: Apparatus for forming a curved panel from a flat panel. 116
- Eigensatz, M., Kilian, M., Schiffner, A., Mitra, N., Pottmann, H., and Pauly, H. (2010). Paneling architectural freeform surfaces. *ACM Transactions on Graphics*, 29, Article 45(4). 80, 82
- Eisel, U. (1979). Patent DD137423 (A1): Form. 33
- Escrig, F. and Sánchez, J. (2005). La bóveda de hormigón del Club Táchira en Caracas - The concrete vault of Club Táchira in Caracas. *Informes de la Construcción*, 57(499-500):133-144. 60
- Feirabend, S., Emami, A., and Riedel, E. (2014). Eine einzigartige Fassade aus Glasfaserbeton. *Bautechnik*, 91(3):181-185. 243
- Ferraris, C. and Brower, L. (2003). Comparison of concrete rheometers - first phase test results indicate comparability between different devices. Technical report, NIST. 174
- Ferraris, C., de Larrard, F., and Martys, N. (2001). *Fresh Concrete Rheology: Recent Developments*, pages 215-241. The American Ceramic Society. 264
- Ferraris, C. F. and De Larrard, F. (1998). Modified slump test to measure rheological parameters of fresh concrete. *Cement, Concrete and Aggregates, CCAGDP*, 20(2):241-247. 125, 131, 132, 172, 174
- Garcia, M. (2010). Amanda Levet Architects. *Architectural Design*, 80(1):106-113. 13
- Garlock, M. and Billington, D. (2008). *Félix Candela, Engineer, Builder, Structural Artist*. Princeton University Art Museum. 60
- Gauss, K. F. (1827). *General Investigations of Curved Surfaces of 1827 and 1825*. Project Gutenberg translation 2011. 78, 85
- Gerritse, A. (1990). Thin-walled Fibre Reinforced Concrete Facades - Proposals for design rules for GRC. In Hogeslag, A., Vamberský, J., and Walraven, J., editors, *Prefabrication of Concrete Structures - Proceedings of the International Seminar Delft*, pages 89-102. Delft University Press. 217

- Gowripalan, N. and Mohamed, H. (1998). Chloride-ion induced corrosion of galvanized and ordinary steel reinforcement in high-performance concrete. *Cement and Concrete Research*, 28(8):1119 – 1131. 159
- Greco, C. (1995). The "ferro-cemento" of Pier Luigi Nervi the new material and the first experimental building. In *Spatial structures: heritage, present and future: proceedings of the IASS International symposium 1995: June 5-9, 1995, Milano, Italia*, volume 1, page 309. SGE. 60
- Groeneveld, H. (2008). Deformation control in explosive forming. In Deribas, A. A. and Scheck, Y. B., editors, *Proceedings of the IXth International Symposium on Explosive Production of New Materials: Science, Technology, Business, and Innovations (EPNM-2008)*, Lisse, The Netherlands, 2008. 43
- Grünewald, S. (2004). *Performance-based design of self-compacting fibre reinforced concrete*. PhD thesis, Technische Universiteit Delft. 335
- Grünewald, S., Janssen, B., Schipper, H. R., and Walraven, J. C. (2012). Deliberate deformation of concrete after casting. In *Proceedings of the Second International Conference on Flexible Formwork, ICFF*, pages 132–139. CICM and University of Bath, Dept. of Architecture and Civil Engineering. 137, 165
- Grünewald, S. and Walraven, J. (2005). Self-compacting concrete with viscosity agents in the fresh state. Technical report, TU Delft, Faculty of Civil Engineering and Geosciences, Dept. of Structural and Building Engineering. 172
- Hammer, T. (2007). *Deformations, strain capacity and cracking of concrete in plastic and early hardening phases*. PhD thesis, Norwegian University of Science and Technology, Trondheim. 177, 182, 187
- Hartog, E. D. (2008). Prefabrication of concrete shells. Master's thesis, Delft University of Technology. 47, 48, 68
- Hegger, J., Zell, M., and Horstmann, M. (2008a). Textile reinforced concrete - realization in applications. In Walraven, J. C. and Stoelhorst, D., editors, *Tailor Made Concrete Structures: New Solutions for Our Society: Proceedings of the International FIB Symposium 2008, Amsterdam, The Netherlands, 19-21 May 2008*. Taylor & Francis Group. 216
- Hegger, J., Zell, M., and Horstmann, M. (2008b). Toepassingen van textielgewapend beton. *Cement*, 4:54–55. 216
- Hennik, P. and Houtman, R. (2008). Pneumatic formwork for irregular curved thin shells. In Oñate, E. and Kröplin, B., editors, *Textile Composites and Inflatable Structures II*, volume 8 of *Computational Methods in Applied Sciences*, pages 99–116. Springer Netherlands. 15

- Holzer, C., Garlock, M., and Prevost, J. (2008). Structural Optimization of Félix Candela's Chapel Lomas de Cuernavaca. In *Fifth International Conference on Thin-Walled Structures Brisbane, Australia*. 60
- Hosford, W. F. (2013). *Fundamentals of Engineering Plasticity*. Cambridge University Press. 340, 341
- Huijben, F. (2014). *Vacuomatics: 3D Formwork Systems*. PhD thesis, Eindhoven University of Technology. 15
- Hull, Feygin, Baron, Sanders, Sachs, Lightman, and Wohlers (1995). Rapid prototyping: current technology and future potential. *Rapid Prototyping Journal*, 1(1):11–19. 17
- Huyghe, K. and Schoofs, A. (2009). Precast double curved concrete panels. Master's thesis, Delft University of Technology. 7, 44, 45, 48, 49, 88, 100, 137
- Isler, H. (1994). Concrete shells derived from experimental shapes. *Structural Engineering International*, 4(3):142–147. 3, 61, 62, 67
- Iwamoto, L. (2009). *Digital Fabrications, Architectural and Material Techniques*. Princeton Architectural Press. 20
- Jansen, H. (2004). Prefabricage bij blobconstructies - een civiele kijk op blobarchitectuur. Master's thesis, Technische Universiteit Delft, Faculteit Civiele Techniek. 45, 46
- Janssen, B. (2011). Double curved precast load bearing concrete elements. Master's thesis, Delft University of Technology. 47, 105, 114, 115, 121, 135, 137, 162
- Jaques, L. and Lagrange, T. (2010). Patent WO 2010/130927 A1: Moulding device and production method - Dispositif de moulage et procede de fabrication. 32
- Jong, P. and Reijgersberg, A. (1988). SBR-publicatie 168 - gevelelementen van glasvezelversterkt cement. Technical report, Stichting Bouwresearch, Rotterdam. 217
- Kachanov, L. (1971). *Foundations of the theory of plasticity*. North-Holland Publishing Company - Amsterdam, London. 340
- Khoshnevis, B., Russell, R., Kwon, H., and Bukkapatnam, S. (2001). Crafting large prototypes. *IEEE Robotics and Automation Magazine*, 8(3):33–42. 18
- Kim, G. B., Pilakoutas, K., and Waldron, P. (2010). Development of GFRP-reinforced GFRC for thin permanent formwork applications. *Magazine of Concrete Research*, 62(4):283290. 65, 243
- Kleespies, H. and Crawford, R. (1998). Vacuum forming of compound curved surfaces with a variable geometry mold. *Journal of Manufacturing Systems*, 17(5):325–337. 42

- Kok, M. (2013). Textile reinforced double curved concrete elements - manufacturing free-form architecture with a flexible mould. Master's thesis, Delft University of Technology. 47, 216
- Kok, M., Schipper, H., Grnewald, S., and Nijse, R. (2014). Double-curved textile reinforced concrete panels with tensile strain-hardening characteristics. In Schlangen, E., Sierra Beltran, M., Lukovic, M., and Ye, G., editors, *SHCC3 - 3rd International RILEM Conference on Strain Hardening Cementitious Composites, 3-5 November 2014, Dordrecht, The Netherlands*, number ISBN: 978-2-35158-150-6. RILEM S.A.R.L. Publications. 216
- Kolarevic, B. (2001). Digital fabrication: Manufacturing architecture in the information age. In *Proceedings of Association for Computer Aided Design in Architecture (ACADIA 2001)*. Buffalo, New York, pages 268–277. 13
- Kosche, F. (1999). Patent DE 198 23 610 A 1 - Integriertes rechnergestütztes Entwurfs-Konstruktions- und Fertigungsverfahren unter Verwendung eines Schaltisches für frei geformte Bauteile und erhärtende Materialien - method for producing three dimensional shell sections. 34
- Kovler, K. and Roussel, N. (2011). Properties of fresh and hardened concrete. *Cement and Concrete Research*, 41(7):775 – 792. Special Issue: 13th International Congress on the Chemistry of Cement. 125
- Kristensen, M. K. and Raun, C. (2011). Patent WO2012065614 (A1): A flexible mat for providing a dynamically reconfigurable double-curved moulding surface in a mould. 36, 51
- Kuch, H., Schwabe, J.-H., and Palzer, U. (2010). *Manufacturing of Concrete Products and Precast Elements - Processes and Equipment*. Verlag Bau+Technik GmbH. ISBN 978-3-7640-0519-1. 12, 188
- Kundu, P. K. and Cohen, I. M. (2008). *Fluid Mechanics (4th Edition)*. Elsevier. 340
- Lauppe, J. (2012). Reinforcement toolbox - a parametric reinforcement modelling tool for curved surface structures. Master's thesis, Delft University of Technology. 133
- Leach, N., Carlson, A., Khoshnevis, B., and Thangavelu, M. (2012). Robotic construction by contour crafting: The case of lunar construction. *International Journal of Architectural Computing*, 10(3):423–438. 17
- Liu, Y.-T. (2003). *Diversifying Digital Architecture: 2003 Far Eastern International Digital Architecture Design Award*. Birkhäuser. 62
- Liu, Y.-T. (2007). *Distinguishing Digital Architecture: 6th Far Eastern International Digital Architecture Design Award*. Birkhäuser. 61, 62

- Liu, Y.-T. and Lim, C.-K. (2009). *New Tectonics, Towards a New Theory of Digital Architecture: 7th Feidad Award*. Birkhäuser. 62
- Luping, T. and Gibbs, J. (2004). Testing SCC - Test Methods for Self-Compacting Concrete to be used in WP6. Technical report, Growth Contract Work Package 6 (WP6) report. 172
- Makowsky, Z. S. (1969). Plastics Structures of Renzo Piano. *Systems, Building and Design*, pages 37–54. 22
- Martin-Saint-Léon, J., Birnie, L., Jacques, L., and Corvez, D. (2011). The Louis Vuitton Foundation - a ship in white Ductal. 32, 62
- Menges, A. (2006). Manufacturing diversity. *Architectural Design*, 76(2):70–77. 13
- Michel, M. (2012). Electronic controlled adaptive formwork for freeform concrete walls and shells. In Müller, H. S., Haist, M., and Acosta, F., editors, *Proceedings of the 9th fib International PhD Symposium in Civil Engineering, July 22 to 25*, number ISBN 978-3-86644-858-2. Karlsruhe Institute of Technology (KIT), Germany, KIT Scientific Publishing, Karlsruhe. 52
- Michel, M. and Knaack, U. (2014). Grundlagen zur Entwicklung adaptiver Schalungssysteme für frei geformte Betonschalen und Wände. *Bautechnik*, 91(12):845–853. 52, 53
- Milinkovic and Milinkovic (2010). Prefabricated building structure built with prefabricated ferro-concrete ribbed element sandwich type cast in moulds. 37
- Mitchell, W. and McCullough, M. (1994). *Digital Design Media*. Van Nostrand Reinhold, New York. 50
- Moiralis, G. (2013). Analysis and design of free form precast planks - investigate the possibility of applying the flexible mould method in free form floors. Master's thesis, Delft University of Technology. 66
- Mueller, F. V., Wallevik, O., and Khayat, K. (2014). Linking yield stress of a co-axial cylindric viscometer and parameters of consistency tests using the Abrams cone. In Wallevik, O., Bager, D., Hjartarson, B., and Wallevik, J., editors, *Environmentally Friendly Concrete Eco-Crete - Proceedings of the International Symposium on Eco-Crete, Reykjavik, Iceland 13.-15. August*, pages 217–224. 131, 175, 196, 220, 230
- Mungan, I. and Abel, J., editors (2011). *Fifty Years of Progress for Shell and Spatial Structures: In Celebration of the 50th Anniversary Jubilee of the IASS (1959-2009)*. International Association for Shell and Spatial Structures. 14, 60, 61, 62
- Munro, C. and Walczyk, D. (2007). Reconfigurable pin-type tooling: A survey of prior art and reduction to practice. *Journal of Manufacturing Science and Engineering*, 129(3):551–565. 38, 42

- Nachbauer, W., Hasler, M., and Kluibenschedl, A. (2012). Bauwerk mit mindestens einem gekrmmten Konstruktionselement aus Beton sowie ein Verfahren zur Erstellung eines derartigen Bauwerks. 37
- Nakajima, N. (1969). A newly developed technique to fabricate complicated dies and electrodes with wires. *Bulletin of JSME*, 12(54):1546–1554. 41
- NEN-EN-12350-2 (2009). NEN-EN 12350-2 (en) - Testing fresh concrete - Part 2: Slump-test. 131
- NEN-EN-1992-1-1 (2005). Eurocode 2: Design of concrete structures part 1-1: General rules and rules for buildings. 181
- NEN-EN-206-1 (2001). NEN-EN 206-1 (en) - Concrete - Part 1: Specification, performance, production and conformity. 178
- Oesterle, S., Vansteenkiste, A., and Mirjan, A. (2012). Zero waste free-form formwork. In Orr, J., Evernden, M., Darby, A., and Ibell, T., editors, *Proceedings of the Second International Conference on Flexible Formwork, ICFF*. CICM and University of Bath, Dept. of Architecture and Civil Engineering. 30, 52
- Oldroyd, J. G. (1947). A rational formulation of the equations of plastic flow for a bingham solid. In *Mathematical Proceedings of the Cambridge Philosophical Society*, volume 43, pages 100–105. 168
- Oosterhoff, J., editor (1969). *Kunststoffen in dragende konstrukties - een verzameling tijdschriftartikelen, gebundeld ten behoeve van de leergang "kunststoffen in dragende konstrukties" op 17 en 17 oktober 1969 te Delft*. Stichting Post-Doktoraal Onderwijs in het Bouwen. 22
- Papanastasiou, T. C. (1987). Flows of materials with yield. *Journal of Rheology*, 31(5):385–404. 168
- Piano, R. (1969). Progettazione sperimentale per strutture a guscio - experimental project of shell structures. *Casabella*, 335:38–49. 6, 7, 22, 23, 24
- Pöggeler, H. (1982). Een kiene bekisting voor een moeilijk schaaldak. *Cement*, XXXIV(3):139–145. 12
- Pottmann, H., Asperl, A., Hofer, M., and Kilian, A. (2007). *Architectural Geometry*. Bentley Institue Press–Exton–Pennsylvania–USA. 20, 76, 79, 85
- Pottmann, H., Huang, Q., Deng, B., Schiftner, A., Kilian, M., Guibas, L., and Wallner, J. (2010). Geodesic patterns. *ACM Trans. Graph.*, 29(4):43:1–43:10. 111
- Pronk, A. and Houtman, R. (2005). Making blobs with a textile mould. In Oñate, E. and Kröplin, B., editors, *Textile Composites and Inflatable Structures*, volume 3 of *Computational Methods in Applied Sciences*, pages 305–322. Springer Netherlands. 15

- Pronk, A. and Moncrieff, E. (2009). WAAS - Workshop Advanced Architectural Structures - reader of the workshop, held at TU Eindhoven, march 9 to 13, 2009. 43
- Quack, M. (2000). Double curved facade elements constructed from glasfibre reinforced cement. Master's thesis, Technische Universiteit Delt, Faculteit Bouwkunde, Vakgroep Bouwtechnologie. 45
- Raun, C. and Kirkegaard, P. (2012). Reconfigurable double-curved mould. In Orr, J., Evernden, M., Darby, A., and Ibell, T., editors, *Proceedings of the Second International Conference on Flexible Formwork, ICFF*, pages 292–299. CICM and University of Bath, Dept. of Architecture and Civil Engineering. 51
- Raun, C., Kristensen, M. K., and Kirkegaard, P. H. (2010). Flexible mould for precast concrete elements. In *Proceedings of the International Association for Shells and Spatial Structures (IASS) Symposium 2010, Shanghai*. 36, 51
- Raun, J. and Henriksen, T. (2014). Patent 51403: Verfahren zur Herstellung eines flächenartigen Elements mit von einer ebenen Oberfläche abweichender Oberfläche, Formteil zur Herstellung eines derartigen flächenartigen Elements sowie flächenartiges Element. 36, 54
- Roosbroeck, M. V. (2006). The construction of prefab concrete shells - morphology - segmentation - material - production method. Master's thesis, Delft University of Technology. 46
- Roussel, N. (2006a). Correlation between yield stress and slump: Comparison between numerical simulations and concrete rheometers results. *Materials and Structures*, 39(4):501–509. 172, 174
- Roussel, N. (2006b). A thixotropy model for fresh fluid concretes: Theory, validation and applications. *Cement and Concrete Research*, 36(10):1797–1806. 128, 129, 190, 196, 222
- Roussel, N. and Coussot, P. (2005). 'Fifty-cent rheometer' for yield stress measurements: From slump to spreading flow. *Journal of Rheology*, 49(3):705–718. 172, 173, 174, 220, 230
- Roussel, N., Ovarlez, G., Garrault, S., and Brumaud, C. (2012). The origins of thixotropy of fresh cement pastes. *Cement and Concrete Research*, 42(1):148 – 157. 129, 163
- Roussel, N., Stefani, C., and Leroy, R. (2005). From mini-cone test to Abrams cone test: measurement of cement-based materials yield stress using slump tests. *Cement and Concrete Research*, 35(5):817 – 822. 125, 213
- Ruttico, P. and Lorusso, P. (2013). Bitmap-driven parametric wall for robotic fabrication. In Hesselgren, L., Sharma, S., Wallner, J., Baldassini, N., Bompas, P.,

- and Raynaud, J., editors, *Advances in Architectural Geometry 2012*, pages 205–212. Springer Vienna. 14
- Schafer, B. (2012). Lecture 17: New Building Forms of Maillart & Isler. 60
- Scheurer, F. (2009). *Size Matters: Digital Manufacturing in Architecture*, pages 59–65. Princeton Architectural Press. 82
- Scheurer, F. (2010). Materialising complexity. *Architectural Design*, 80(4):86–93. 13, 66
- Schipper, H. R. (2011). Производство Бетонных Элементов С Двумя Криволинейными Контурами - Применение Передовых Производственных Методов В Создании Свободных Архитектурных Форм (Manufacturing Of Double-curved Concrete Elements - Enabling free-form architecture through advanced manufacturing methods). Бетон И Железобетон (*Concrete and Reinforced Concrete*), 1:48–52. 166
- Schipper, H. R., Eigenraam, P., Grünewald, S., Soru, M., Nap, P., Van Overveld, B., and Vermeulen, J. (2015). Kine-mould: Manufacturing technology for curved architectural elements in concrete. In *Proceedings of the International Society Of Flexible Formwork (ISOFF) Symposium 2015, Amsterdam*. 96, 241
- Schipper, H. R., Eigenraam, P., Nap, P., Overveld, B., and Grünewald, S. (2014). Kine-Mould - Manufacturing architectural elements with complex geometry using a flexible kinematic mould system. Technical report, Proposal for Technology Foundation STW Valorisation Grant phase 1. 116
- Schipper, H. R., Grünewald, S., Kok, M. A. D., Nijse, R., and Raghunath, P. (2013). Frei geformte Betonfertigteile - Verwendung von SVB und Textilbewehrung. *BetonWerk International*, (5):174–180. 216
- Schipper, H. R. and Janssen, B. (2011a). Curving concrete - a method for manufacturing double curved precast concrete panels using a flexible mould. In *2011 IABSE-IASS conference London*. 100, 105, 114, 165
- Schipper, H. R. and Janssen, B. (2011b). Manufacturing double-curved elements in precast concrete using a flexible mould - first experimental results. In Sruma, V., editor, *Proceedings fib Symposium PRAGUE*, volume 1, pages 883–886. ISBN 978-80-87158-29-6. 112, 165
- Schipper, H. R. and Janssen, B. (2011c). Manufacturing double curved precast concrete panels. *Concrete Plant International*, 4:32–38. 166
- Scholzen, Chudoba, and Hegger (2012). Dünnwandiges Schalentragsystem aus textillbewehrtem Beton - Entwurf, Bemessung und baupraktische Umsetzung. *Beton- und Stahlbetonbau*, 107-11:767–776. 216

- Soar, R. and Andreen, D. (2012). The role of additive manufacturing and physiomorphic computational design for digital construction. *Architectural Design*, 82(2):126–135. 17
- Song, A.-p., Wu, W.-w., and Zhang, J. (2010). A reconfigurable stamping die and its stamping process. *Journal of Shanghai Jiaotong University (Science)*, 15(3):313–318. 43
- Spuybroek, L. (2004). *NOX: machining architecture*. Thames and Hudson, London. 7, 34, 50, 51
- Ströbel, D. and Singer, P. (2008). Recent developments in the computational modelling of textile membranes and inflatable structures. In Oñate, E. and Kröplin, B., editors, *Textile Composites and Inflatable Structures II*, volume 8 of *Computational Methods in Applied Sciences*, pages 253–266. Springer Netherlands. 15
- Stupré-report studie groep 30 (1988). Glass fibre reinforced cement (GRC) - Design rules for architectural panels (in Dutch). Technical report, Stupré. 217
- Tattersall, G. and Banfill, P. (1983). *The rheology of fresh concrete*. Pitman Advanced Pub. Program (Boston). ISBN 0273085581. 171
- Ter Maten, R. (2011). Ultra high performance concrete in large span shell structures. Master's thesis, Delft University of Technology, Faculty of Civil Engineering and Geosciences. 47, 68
- Tissink, A. (2013). Dini worstelt niet alleen met techniek. *Cobouw*. 17
- Tissink, A. (2015). Geweven verenstaal oplossing voor flexibele mal. *Cobouw*, February 18 nr. 32:6–7. 116
- Troian, S. (2014). Crack evaluation in double-curved concrete elements. Master's thesis, Delft University of Technology. 217, 218, 226
- Vamberský, J. (1991). GVC gevelelementen. *Cement*, 5:81–85. 217
- Vamberský, J. N. J. A. and Schipper, H. R., editors (2010). *Precast2010 - Het nieuwe bouwen in prefab beton - Assembling freeform buildings in precast concrete*. Delft University of Technology. repository.tudelft.nl/search/ir/?q=precast2010. 20
- Van Acker, A. (1996). Automated production of precast architectural elements. *Structural Engineering International*, 2:113–116. 30
- Van Breugel, K. (1997). *Simulation of Hydration and Formation of Structure in Hardening Cement-Based Materials*. Delft University Press, second edition - revised version of the author's phd-thesis edition. 128, 168
- Van de Straat, R. (2011). Parametric modelling of architectural developables. Master's thesis, TU Delft. 111

- Veenendaal, D., West, M., and Block, P. (2011). History and overview of fabric formwork: using fabrics for concrete casting. *Structural Concrete*, 12(3):164–177. 16
- Vollers, K. and Rietbergen, D. (2007). Adjustable mould for annealing freely curved glass panes. In *Glass Performance Days*, pages 105–107. 44, 48
- Vollers, K. and Rietbergen, D. (2008). Patent WO 2009002158 (A1): A method and apparatus for forming a double-curved panel from a flat panel. 36, 44
- Vollers, K. and Rietbergen, D. (2010). Patent NL 2001738 (C2): Curved panel producing method, involves depositing viscous-liquid material on horizontal plane of mold, hardening viscous-liquid material, providing flexible material in mold, forming edge profile, and cutting profile at regular intervals. 36
- Wallace, W. (1971). *The Logic of Science in Sociology*. Transaction Publishers. 121
- Wallevik, J. E. (2006). Relationship between the bingham parameters and slump. *Cement and Concrete Research*, 36(7):1214 – 1221. 175, 192
- Wallevik, O. H. (2000). *Rheology of Cement Suspensions - manual of BML Viscometer*. The Icelandic Building Research Institute (IBRI). 333
- Wallevik, O. H. (2005). *Rheology of fresh concrete such as SCC - Dr. Wallevik Rheology course*. The Island Building Research Institute. 125, 127, 333
- Wallevik, O. H. and Wallevik, J. E. (2011). Rheology as a tool in concrete science: The use of rheographs and workability boxes. *Cement and Concrete Research*, 41(12):1279 – 1288. Conferences Special: Cement Hydration Kinetics and Modeling, Quebec City, 2009 and CONMOD10, Lausanne, 2010. 126, 127, 334
- Weilandt, A., Grohmann, M., Bollinger, K., and Wagner, M. (2009). Rolex learning center in lausanne: From conceptual design to execution. In Domingo, A. and Lazaro, C., editors, *Proceedings of the International Association for Shell and Spatial Structures (IASS) Symposium 2009, Valencia, Evolution and Trends in Design, Analysis and Construction of Shell and Spatial Structures*. 62, 65
- West, M. (2001). Fabric-formed concrete structures. In *Proceedings First International Conference on Concrete and Development, Tehran, Iran, April*, pages 133–142. 16
- West, M. (2008). Thinking with matter. *Architectural Design*, 78(4):50–55. 19
- West, M. and Araya, R. (2009). Fabric formwork for concrete structures and architecture. In *Int. Conf. Textile Composites and Inflatable Structures, Barcelona, Spain*, pages 5–7. 16
- West, M. and Araya, R. (2012). Recent fabric formwork construction projects: Tilt-up walls, precast columns and slabs. In *Proceedings of the Second International Conference on Flexible Formwork, ICFF*, pages 390–397. CICM and University of Bath, Dept. of Architecture and Civil Engineering. 16

- Witt, A. and Boyer, P. (2013). Euclid: An open, cross-platform, cloud geometry optimizer and library. In *Advances in Architectural Geometry 2012*, pages 295–304. Springer. 82
- Woodington, W. (2014). Shear-deforming textile reinforced concrete for the construction of thin double-curved freeform structures. Master's thesis, Delft University of Technology. 92, 93, 94
- Zienkiewicz, O. C., Taylor, R. L., and Nithiarasu, P. (2005). *The Finite Element Method for Fluid Dynamics*. Elsevier Butterworth-Heinemann. 125

Acknowledgement

Successfully carrying out a PhD thesis research not only requires time and labour, but also support and patience of many, many people. From the beginning in 2008, Prof. Jan Vamberský has been involved as my first promotor. His patience has been truly challenged at moments that my educational tasks pushed the research to the background. But, with his everlasting optimism and sincere encouragement he supported me in keeping the project in motion and finalizing the writing process. He reviewed many draft versions. In the last years, my second promotor, Prof. Klaas van Breugel, took the time to carefully go through the chapters on concrete technology. His conscientious comments have, without any doubt, contributed much to the quality of this thesis. Thank you, both!

Dr. Steffen Grünewald has been involved in many of the laboratory experiments that have been conducted, and his valuable expertise on the design and preparation of concrete mixtures was of great help. I have appreciated working with you! Countless other colleagues have offered help in some way over the years: Dr. Karel Vollers with his knowledge on complex geometry and inspiring pioneering work on the flexible mould, the staff of the Stevin 2 laboratory and Microlab with the experimental work: Ton Blom, Edwin Scharp, Albert Bosman, Fred Schilperoort, Maiko van Leeuwen, Gerrit Nagtegaal and Kees Baardolf: thanks for helping me in the practical execution of the multitude of tests.

Various former master students at a certain moment chose the topic of the flexible mould for their final thesis work: a.o. Bas Janssen, Marijn Kok, Peter Eigenraam, Grigorios Moiralis and Sergiu Troian, now all MSc, have done parts of the work reported in the present PhD thesis: without your contribution, smart and creative thinking and experimental work, the flexible mould project would never have succeeded. Especially with Peter, that is also involved in the follow-up project Kine-Mould, I have spend many hours on figuring out possible improvements. Peter, your practical skills in the workshop are beyond praise.

My friend from India, Prashanth Raghunath, MSc, has been patiently working on the preparation, execution and reporting of numerous experiments as research assistant for the project. We calculated that - at a certain moment - we had weighed, mixed, placed, demoulded and stored several *tons* of concrete, not to speak of all the cleaning work. Furthermore, the conscientious review of my English spelling, carried out by you together with your wife Manasa Prashanth, was very necessary

and is highly appreciated. Apart from being a valuable co-worker, our friendship has even brought me to India in 2014, an amazing journey. Thanks for all your effort!

Matteo Soru, MSc, has also been working as research assistant on an improved design of our flexible mould, and helped us with computational aspects as well as practical work in the lab. *La lasagna era deliziosa, Matteo!*

Fellow researchers Sander Pasterkamp, Karel Terwel, Jeroen Coenders, Anke Rolvink and Dick van Keulen: thanks for the many PhD-meetings we had, in which we not only mutually commented each others PhD research, but in which you all also helped me to proceed in the right direction. Marjo van der Schaaf, thanks for all your administrative work in the background, filling in forms, listening to our complaints, and advising us - rookie scientist - on the sometimes strange ways of the academic world.

As material sponsors, Conovation and ENCI have provided various concrete ingredients to make all experimental work feasible. Dutch Technology Foundation STW and 3TU.Built Environment have granted the follow-up project Kine-Mould, allowing the further development and industrial implementation of the ideas. mbX / Microbeton has offered their cooperation in this implementation, which is currently still ongoing. Thanks all for your trust and support! Finally, some personal words in Dutch:

Judith, mijn lieve vrouw, bedankt voor je geduld, liefde en ondersteuning in de afgelopen jaren! Je hield telkens het gezin draaiend op momenten dat ik weer eens achter de computer zat. Zonder jouw aanmoedigingen was het nooit gelukt. Je bent een schat!

Onze kinderen Hans, Esther, Wim en Bauke: bedankt voor jullie geduld tijdens alle uren dat je het even zonder mij moesten stellen. De uitspraak 'papa werkt aan z'n promotie' gaan we zeker niet missen in huize Schipper..

Graag bedank ik ook m'n ouders Hans en Coby, die me de voorliefde voor de bouw en voor kunst hebben meegegeven. *Bouwkunst* bleek inderdaad een mooi onderwerp voor een promotieonderzoek.

Tenslotte dank ik God voor Zijn liefdevolle leiding en hulp in de afgelopen jaren. Toevallige ontmoetingen bleken vaak niet toevallig, puzzelstukjes vielen vaak op z'n plek zonder mijn inspanning. U bent de grote Architect!

Curriculum

Roel Schipper graduated under prof. Jan Vamberský in 1993 from the Faculty of Civil Engineering of TU Delft, group Building Engineering. After this, he worked for a period as researcher on BIM-related issues for the European project COMBINE (Computer Models for the Building Industry in Europe).

In 1994 he joined Van Dorsser Raadgevende Ingenieurs, a building physics consultancy office, which later merged into Royal Haskoning DHV. He was involved in the modernization of various Dutch museums, among which are the Van Gogh Museum in Amsterdam and the Gemeentemuseum in The Hague. He worked on the design and refurbishment of numerous office and residential buildings, penitentiaries and shopping malls. During this period he was mainly focused on building physical aspects, such as acoustics, daylight studies, energy performance, temperature simulation and wind-tunnel research.

In 1997 he joined Ingenieursbureau Concretio, a structural engineering firm. Leaving the field of building physics, he worked on the full width of structural engineering, designing concrete, timber and steel structures for residential and office buildings, industrial warehousing and hydraulic structures. Between 2002 and 2010 he was involved in the inspection and monitoring of several hundreds of houses built on wooden pile foundations, constructed in the period 1800-1950, as well as the design of foundations refurbishment options in cases of severe deterioration. He was one of the co-founders of KCAF, the Dutch Knowledge Centre for Approach of Foundation problems, and is still involved in the present work of this centre.

In 2008, Roel Schipper started as lecturer-researcher at TU Delft in the section Structural and Building Engineering, responsible for various courses in Structural Design, Façades and Building Physics in both bachelor and master curriculum. In 2010 he completed the University Teaching Qualification programme. Since 2008, the topic of the flexible mould has been a leading thread through his research activities, resulting in the present thesis, a valorisation grant from the Dutch Science Foundation STW and a 3TU.Bouw Lighthouse grant of the three Dutch Universities of Technology (both grants obtained together with co-workers).

Roel Schipper is married and is father of four children.

List of definitions and abbreviations

CNC: Computer Numerically Controlled: many machining and manufacturing processes are automatically executed, until the 80's mainly numerically controlled with analogue equipment, and nowadays mostly controlled digitally by computers. Examples are drilling, milling, cutting, machining and polishing.

die: Three-dimensional surface, usually milled in a metal block, used in many industries as basis-shape for casting, moulding, injecting, pulling or pressing a material in the exact shape of this surface. Often a double die block is used to control the shape of both front and back of the formed material. Due to the relatively high costs of fabrication of an accurate die, it is usually applied for mass-production of identical products.

ECC: Engineered Cementitious Composites - strain hardening composites with a normal strength matrix and a moderate synthetic fibre content of about 2-3 volume%. A typical ECC has a tensile strain capacity of 3%-5%, with multiple cracks spaced less than 3 mm, and a tensile strength still in a relatively normal range: between 4 and 7 MPa. The result is a strain hardening, multicracking and ductile material.

EPS: Expanded Polystyrene, often used in large blocks as base material for the milling or cutting of formwork. After milling the EPS generally needs a treatment with a smooth and strong top coating before being usable as formwork

FRC: Fibre-Reinforced Concrete - a concrete with enhanced ductility and strength through the addition of (mostly) short fibres of glass, carbon, plastic, steel or a choice of many possible other materials

GFRC: Glass-fibre Reinforced Concrete

FRG: Fibre-Reinforced Gypsum - a gypsum with enhanced ductility and strength through the addition of (mostly) short fibres of glass, carbon, plastic, steel or a choice of many possible other materials; mostly used for mockup-reasons due to limited strength in comparison to FRC

GFRG: Glass-fibre Reinforced Gypsum

FRP: Fibre-Reinforced Plastic or Polymer - a plastic such as e.g. polyethylene, polyurethane or epoxy, sometimes transparent, which is strengthened with fibres of, for example, glass, carbon, aramide to enhance strength and other structural behaviour

GRP or GFRP: Glass-fibre Reinforced Plastic or Polymer- FRP using glassfibre as strengthening material

HDPE: High Density Polyethylene - a plastic that can be used as mould material

HPC: High Performance Concrete - a concrete meeting special combinations of performance and uniformity requirements that cannot always be achieved using conventional constituents and normal mixing (Ferraris et al., 2001)

HSC: High Strength Concrete: a concrete with cube compressive strength in the range 50 to 100 MPa.

MDF: Medium-Density Fibre board - a plate material based on compressed wood fibres, used for the framework of the moulds in the tests

mould: a hollow container with a particular shape into which soft or liquid substances are poured, so that when the substance becomes hard it takes the shape of the container (source: Cambridge Advanced Learner's Dictionary & Thesaurus; *US: mold*)

SCC: Self-Compacting Concrete or Self-Consolidating Concrete - A concrete that can be placed without vibration and flows easily in very narrow gaps. Usually a slump flow of more than around 650 mm is the criteria for calling a mixture self-compacting (Ferraris et al., 2001), although strictly speaking a mixture with lower slump flow that doesn't need mechanical compaction could also be called self-compacting. Often used as synonym for 'self-levelling' concrete.

TRC: Textile Reinforced Concrete - a concrete that is strengthened by adding layers of a woven textile, often consisting of yarns of glass fibre. The textile adds both strength and ductility to the concrete.

soffit: the underside of an architectural structure such as an arch, a balcony, or overhanging eaves

UHPC: Ultra-High Performance Concrete, the category of concrete mixtures that, in hardened state, is characterized by very high cube compressive strengths, typically in the range 100 to 150 MPa (the word 'performance' in this abbreviation is often used as synonym for 'strength').

Appendix A

Patents related to the flexible mould

In this appendix the most important patents related to the topic the flexible mould are described, that could be found in the Espacenet database. Espacenet offers access to worldwide inventions and technical developments from 1836 to today. URL's linking to the patents can be found in the bibliography. The patents are sorted on year of the invention.

Inventor	Year	reference	reconfigurable? actuation method/ control or shape	actuator/distance reduction to practice? apparatus method/ curvature	edge solution	radius	element size		single- or double- formed product/ base material
							element thickness	element size	
1 Parry	1928	GB296477	y manual bolting		a s				RC, in-situ
2 Hulsh	1948	GB600543	y manual bolting		a s				RC, in-situ
3 Hawes	1952	GB668371	y manual bolting		a s				RC, in-situ
4 Hawes	1952	GB668379	y manual bolting		a s				RC, in-situ
5 Alweg Forschung	1960	GB847515	y manual bolting	d	a d	> 10 m	box		RC
6 Matthews	1962	GB897994	y inflation pressure	-	a, m d	-	var	a few m?	RC, FRC, resins, insul.mat.
7 Oosterheld	1965	GB1007101	y vacuum pressure		a, p, m s x s	cutting	10-20 mm	contin	FRC
8 Eternit	1967	GB1075406	n draping/pressing of concr		a, p, m s x s	cutting	10-20 mm	contin	FRC
9 Eisel	1979	DD137423	y NC, hydraulic cylinders	a	a, m d	flexible profiled edge	var	a few m?	RC, gypsum
10 Tilly	1979	EP000837	y bending of plate over die	n.a.	a, p, m s	parallel edges	> 1 m	contin	RC, cores of foam
11 Mygind	1983	GB2108187	y manual bolting		a s				RC, in-situ
12 Maier	1985	DK442684	y manual bolting	n.a.	a s	> 5 m	var	contin	RC
13 Frei-Zigerlig	1986	DE3526955	y manual bolting	n.a.	a s, segm	n.a.		a few m?	RC, in-situ
14 Alonen	1986	GB2170752A	y CNC machining of wax	-	m free	milled	var		RC
15 Vidal	1987	EP0238168	y manual bolting	var	a s, segm	profiled plate	10 cm	few m	RC
16 Laloux	1988	FR2612545	y CNC, actuators (hydr/electr)	a -	a free	flexible profiled edge	-	-	RC
17 Dittmann	1989	EP0313048	y CNC machining of wax	-	m free	milled	var	a few m?	RC
18 Ishii Masao	1989	JP56456504	n textile filter, using die	n.a.	m free	die	10-50 cm	1 m	RC
19 Baudet / North Sails	1992	EP0475083	y manual bolting	d	yes a, p, m d	1-25 m	a few mm	a few m	laminated fabric sails
20 Lecherf	1992	FR2672921	y manual bolting	n.a.	a s	> 5 m	var	contin	RC
21 Tanigawa Hiroshi	1992	JP04315658	y layering of plywood, die	n.a.	a s	die		contin	RC, in-situ
22 Krug	1993	CA113049	y manual bolting	d	yes a, p, m d	glass edge preformed	a few mm	1x2.5 m	glass
23 Jones and Brown	1993	GB2265933	y manual bolting	d	a s	-	var	contin	RC
24 Noguchi Kozo	1993	JP05154821	y chain, plates and die	n.a.	a s	0.5-1 m	a few mm	a few m?	dispersed stone in resin
25 Godbhere	1994	GB2268699	y CNC, actuators (hydr/electr)	d	a d	free edges	a few mm	a few m?	fibre reinforced plastics
26 Heinzie Otto	1995	CH685303	y manual bolting	n.a.	a s	> 5 m	var	contin	RC, in-situ
27 Erz	1995	DE19509078	y manual bolting	d	a, m s	none	> 10 cm	contin	RC, in-situ
28 Nakano Masao	1996	JP08258026	y NC, hydraulic cylinders	single	a d	blocks			C
29 Imura Hiroyuki	1996	JP08333840	y free bending of concrete	n.a.	p, m s	closed box	a few cm		FRC, precast
30 Sykes	1996	WO960593	y manual bolting	d	yes a, p, m d	glass edge preformed	a few mm	1x2.5 m	glass

Inventor	Year	reference	reconfigurable? actuation method/ control or shape	actuator distance adjacent, distant?	reduction to practice or apparatus, method			edge solution curvature		radius			element size		single- or double- sided mould formed product base material
					n.a.	m	free	flexible profiled edge	-	0.95 x 1.00 m	25 mm	s	FRC or harden. mat.		
31 Liu Nong	1997	CN1147440	Y	draping of flexible formwork over	d	a, m	free	flexible profiled edge	-	2x3-4x10 m	var	s	RC		
32 Kosche	1998	DE19823610	Y	CNC, hydraulic cylinders	a	a	d	n.a.	?	< 1 m	a few mm	d	metal plates		
33 Hoffman	1998	US5851563	Y	CNC, actuators (hydr/electr)	n.a.	m	s	cutting	0.5-1 m	contin	10-20 mm	s	FRC		
34 Oohi Kunio	2002	JP2002234018	n	draping of concr over die	a	a	d	-	-	sails	foil		reinft plastic		
35 Yamahada	2002	JP2002201526	Y	CNC, actuators (hydr/electr)	-	m	d	-	-	-	-		-		
36 Liron - Zeilmakerij	2006	FR2866858	Y	Inflation pressure	n.a.	p, m	d	dle	0.5 - 2.0	0.9x0.3-3.8x1.0 m	10-50 mm	n.a.	FRC, precast		
37 Kasahara Natsue	2006	JP2006305774	n	draping of concr over die	a	a, p, m	free	flexible profiled edge	-	a few m?	var	s, d	RC, FRC, resins		
38 Gould	2006	WO200604855A1	Y	CNC, hydraulic cylinders	d	a, m	d	-	-	-	glass	s	glass		
39 Rietbergen and Vollers	2007	US2010147030	n	CNC, draping softened glass	d	exp	a, m	d	-	-	-	s	-		
40 Vollers and Rietbergen	2008	NL20001738	Y	CNC, actuators (hydr/electr)	d	exp	a, m	d	flexible profiled edge	-	a few m?	s	fluid-viscous mat		
41 Behloul and Quidant	2008	WO2008056065	Y	CNC actuators (hydr/electr)	d	yes	a, m	d	closed box	-	1 m	d	RC, FRC, gypsum		
42 Guangjun Li	2009	CN101650756	Y	CNC, hydraulic cylinders	a	a	d	parallel edges	< 1m	contin	a few mm	d	aluminum		
43 Enrong Wang	2009	CN201202271	Y	manual bolting	d	a	s, segm	n.a.	-	contin	var	d	RC, in-situ		
44 Jacques and Lagrange	2009	WO2010130927	Y	CNC actuators (hydr/electr)	d	yes	a, m	d	closed box	-	1 m	d	RC, FRC, gypsum		
45 Xinqun Ouyang et al.	2010	CN101845956	Y	man, hydraulic cylinders	d	a	s, circ	n.a.	-	contin	var	d	RC, in-situ		
46 Nachbauer - Application	2010	EP2444560	Y	actuators (hydr/electr)	-	-	p	d	-	a few m?	2-10 cm	-	UHPC, FRC		
47 Milinkovic and Milinkovic	2010	RS20090078	n	n.a.	n.a.	p, m	s, segm	n.a.	-	a few m	var	d	RC, in-situ		
48 Haeger	2010	WO2010107359	Y	describes only application		p, m	ruled surf	grooved profile	5 m	9 m	20-50 cm	s	RC		
49 Kristensen and Raun	2010	WO2012065614	Y	CNC, actuators (hydr/electr)	d	exp	a, m	d	flexible profiled edge	> 1 m	a few cm	s	RC, FRC, gypsum		
50 Mingzhe Li	2011	CN102135224	Y	CNC, worm wheels	a	a	d	n.a.	-	-	a few mm	d	metal plates		
51 Zhongyi Cai	2011	CN102205366	Y	CNC, actuators (hydr/electr)	a	a	d	n.a.	0.5-1 m	< 1 m	a few mm	d	metal plates		
52 Mingzhe Li	2011	CN102248053	Y	CNC, worm wheels	a	a	d	n.a.	-	-	a few mm	d	metal plates		
53 Wang	2011	US2011300254	Y	CNC, actuators (hydr/electr)	a	a	d	-	0.5-1 m	< 1 m	a few mm	d	metal plates		
54 Gang et al.	2012	CN102720139	Y	manual bolting	-	-	a	s	-	contin	var	d	RC		
55 Glorieux	2012	WO2012021946	Y	NC, hydraulic cylinders	d	a, p, m	s	parallel edges	1-25 m	contin	a few mm	s	resins, polyester		
56 Chen Yuening	2013	CN202824318	Y	CNC actuators (hydr/electr)	a	a	d	none	-	-	-		metal plates		
57 Bian Halbo	2013	CN202866274	Y	manual bolting	n.a.	a	s, segm	n.a.	-	contin	var	s	RC, in-situ		
58 Raun	2013	WO2013104369	Y	CNC, actuators (hydr/electr)	d	exp	a	d	n.a.	?	< 1 m	s	thermoforming materials		
59 Jepsen / Henriksen	2014	AT514035	n	describes process of using intermediate mould in plastic	n.a.	exp	m	d	intermediate mould	?	a few mm or cm	d	concrete		

Inventor	Year		Direct or indirect (file) cavity		Precast or in-situ mold surface material and details		Deformation after casting application		Title	
1. Parry	1928				steel, tapered plates		no	hyperbolic cooling towers	Improvements in or relating to shuttering for concrete structures	
2. Hulsh	1948				timber and steel, strips		no	curved surfaces merging into flat surfaces	Improvements in and relating to forms for use as shuttering in constructional work in concrete	
3. Hawes	1952				steel, curved table		no	arches or curved structures	Improvements in or relating to shuttering for use in erecting arched roofs, floors, ceilings and similar arched structures formed in concrete and like material	
4. Hawes	1952				steel, inner/outer ring		no	arches or curved structures	Improvements in or relating to shuttering for use in forming arched roofs and other curved concrete and like structures	
5. Alweg Forschung	1960	d	pr		steel, twisted strips		no	curved beams for mono-rails	Improvements in or relating to the production of prefabricated concrete structural members	
6. Matthews	1962	d	pr		plastic, rubber or fabric sheets		yes	dome-shaped or multi-curved structures	Improvements relating to the moulding of multi-curved structures	
7. Oosterheld	1965				flexible material, corrugated		yes	double corrugated fibre-cement sheet	Device for corrugating sheets of fibrous cement	
8. Eternit	1967	d	pr		steel, corrugated		yes	double corrugated asbestos-cement sheet	A method and apparatus for manufacturing asbestos-cement sheets corrugated in one direction and curved substantially in the direction of the generatrices of the corrugations	
9. Eisel	1979	d, i	pr, i-s		plastic foil		no	precast elements for domes and shells	Form	
10. Tilly	1979	d	pr		steel, extrusion, plate		yes	curved load-bearing elements	Load bearing wall panels and method of manufacture thereof	
11. Mygind	1983	d	i-s		steel, plate		no	hyperbolic cooling towers	Formwork for jump forming curved hollow upright concrete structures:adjustable radially and for inclination	
12. Maier	1985	d	i-s		steel, plate		no	curved concrete walls with var radius	Formwork for curved surfaces, round structures, and like constructions	
13. Frei-Zigerlig	1986	d	i-s		steel and timber plate		no	curved floors and walls	Formwork and process for casting a container from concrete	
14. Alonen	1986	i	pr		wax, milled		no	freeform concrete elements	Method for the manufacture of moulds	
15. Vidal	1987	d	pr		steel, joined with rubber, strips		no	precast arches or vaults, half-elements	Method and apparatus for moulding curved concrete sections.	
16. Laloux	1988	d	pr		flexible material in closed box		no	freeform elements	Reusable formwork modules making it possible to form varied architectural shapes	
17. Dittmann	1989	i	pr		wax, milled		no	freeform concrete elements, also every-day elements of limited repetition	Process for the automatized manufacturing of special products from concrete or from reinforced concrete	
18. Ishii Masao	1989	i, d	pr		filter cloth		no	random shapes	Molding of cement product	
19. Baudet / North Sails	1992	d	pr		reinforced rubber on splines		no	double-curved sails	Sail of one piece three dimensional laminated fabric having uninterrupted load bearing yarns	
20. Lecherf	1992	d	i-s		steel, plate		no	curved concrete walls with var radius	Circular formwork	
21. Tanigawa Hiroshi	1992	d	pr, i-s		double layer of plywood, cylinder		no	curved mould materials with diff radius	Flexible moulding plywood for concrete mold and mold assembling method	
22. Krug	1993				silicone coating on membrane, Dow Corning		yes	automotive windshields	Adjustable press face	
23. Jones and Brown	1993	d	i-s		steel, plate		no	curved walls	Adjustable formwork system	
24. Noguchi Kozo	1993	d	pr		hard rubber strips		yes	artificial marble elements	Production of curved artificial marble	
25. Godbehere	1994	d	p		deformable material		no	aerospace elements	Forming fibre reinforced plastics laminate	
26. Heinze Otto	1995	d	i-s		steel, plate		no	silo's and the like	Shuttering adjustable to different radii of curvature	
27. Erz	1995	d	i-s		steel, strips		no	vaulted roofs	Shuttering for overhead concrete arches	
28. Nakano Masao	1996	d	pr		steel, box		no	blocks with curved surface	Mold frame for concrete block with curved surface	
29. Imura Hiroyuki	1996	d	pr		bending post-hardening, pattern		yes	curved and patterned surfaces	Cement flexible board and manufacture thereof	
30. Sykes	1996				membrane		yes	automotive windshields	Apparatus for and method of bending glass sheets	

Inventor	Year		Direct or indirect (file) cathin- mould surface material and details		Application after casting	Title
	Year	d	pr	rubber membrane, thin		
31 Liu Nong	1997	d	pr	rubber membrane, thin	yes	curved surfaces for shells, cones, twisted surfaces
32 Kosche	1998	d	pr	flexible membrane, supported by grid	yes	freeform concrete elements
33 Hoffman	1998	d	p	hard rubber	no	aerospace elements
34 Oohi Kunio	2002	d	pr	steel, corrugated	yes	curved cement products, lost formwork
35 Yamahada	2002					
36 Lion - Zeilmakerij	2006	d				Pin-connected construction of general purpose forming die
37 Kasahara Natsue	2006	d	pr	n.a., pre-formed by extrusion	yes	Manufacturing method of cement-based cured product and molding machine of cement-based molded product
38 Gould	2006	d	pr	flexible membrane, supported by grid	no	freeform elements
39 Rietbergen and Vollers	2007	-	-	none, rods on ribs	yes	double-curved glass panes
40 Vollers and Rietbergen	2008	d	pr	flexible membrane, supported by grid	yes	freeform elements
41 Behoul and Quidant	2008	d	pr	rubber in closed box	yes	freeform tiles / façade elements
42 Guangjun Li	2009	d		PU membrane 30-50mm Shore 70-90	yes	rapid prototype aircraft wing leading edge
43 Enrong Wang	2009	d	i-s	steel, ribbed panels	no	curved walls or roofs
44 Jacques and Lagrange	2009	d	pr	rubber in closed box	yes	freeform tiles / façade elements
45 Xinqun Ouyang et al.	2010	d	i-s	steel, inner/outer ring	no	tunnel liners, curved walls
46 Nachbauer - Application	2010	d	pr		-	permanent double-curved concrete formwork
47 Milinkovic and Milinkovic	2010	i	pr / i-s	precast ferro-concrete, lost formwork	no	tunnel liners
48 Haeger	2010	d	pr	steel, plate	no	segments of concrete telecom towers
49 Kristensen and Raun	2010	d	pr	flexible membrane, supported by grid	yes	freeform tiles / façade elements
50 Mingzhe Li	2011					Applications not described
51 Zhongyi Cai	2011			rubber, membrane	yes	stretch-forming of thin metal plates
52 Mingzhe Li	2011					Plastic processing
53 Wang	2011			rubber, membrane	yes	stretch-forming of thin metal plates
54 Gang et al.	2012	d	i-s	steel	no	curved walls
55 Glorieux	2012	d	p	corrugated	yes	arched roof-elements for barrel vaults
56 Chen Yuerning	2013	n.a.		rubber, membrane	stretch	façade plates in curved metal
57 Bian Halbo	2013	d	i-s	steel, strips	no	tunnel liners, curved walls
58 Raun	2013	d	p	rubber, membrane	yes	façade elements
59 Jepsen / Henriksen	2014	i	p	made with Adapa device	no	façade elements

Appendix B

Maple model for single strip

**Beam supported at 11 points, $L = 10 \times \Delta L$
after Janssen (2011), improved algorithm by RS**

All values in [N] and [mm]

**General definitions of vertical displacement of a beam due to point load F and
equally spread load q**

restart;

displacement at location x due to q

$$wq := \frac{q \cdot x}{24 \cdot EI} \cdot (L^3 - 2 \cdot L \cdot x^2 + x^3) :$$

displacement at location x due to F

If x is located left of F

$$wfL := \frac{F \cdot b \cdot x}{6 \cdot EI \cdot L} \cdot (2 \cdot L \cdot (L - x) - (b)^2 - (L - x)^2) :$$

If x is located right of F

$$wfR := \frac{F \cdot a \cdot (L - x)}{6 \cdot EI \cdot L} \cdot ((2 \cdot L \cdot b) - b^2 - (L - x)^2) :$$

**Equations of superimposed displacements w_n for $n=2..10$
due to support reactions R_i for $i=2..10$ and q-load**

Equation in support point n

for n from 2 to 10 do

$$x := (n - 1) \cdot \Delta L : L := 10 \cdot \Delta L : wPq[n] := wq :$$

for i from 2 to 10 do

$$a := (i - 1) \cdot \Delta L :$$

$$b := (11 - i) \cdot \Delta L :$$

$$F := R[i] :$$

$$w[i, n] := \begin{cases} wfR & i \leq (n - 1) \\ wfL & i > (n - 1) \end{cases} :$$

end do:

$$eq[n - 1] := w[n] = wPq[n] - \sum_{j=2}^{10} w[j, n] :$$

end do:

Solve reaction forces

$$sol := solve(\{eq[1], eq[2], eq[3], eq[4], eq[5], eq[6], eq[7], eq[8], eq[9]\},$$

$\{R[2], R[3], R[4], R[5], R[6], R[7], R[8], R[9], R[10]\} : assign(\%);$

Reaction forces in 1 and 11 follow from moment equilibrium around 11 and 1

$$R[1] := \frac{\frac{1}{2} \cdot q \cdot (10 \cdot \Delta L)^2 - \sum_{j=2}^{10} (R[j] \cdot (11 - j) \cdot \Delta L)}{10 \cdot \Delta L} :$$

$$R[11] := \frac{\frac{1}{2} \cdot q \cdot (10 \cdot \Delta L)^2 - \sum_{j=2}^{10} (R[j] \cdot (j - 1) \cdot \Delta L)}{10 \cdot \Delta L} :$$

Forced displacements: here the shape of the mould is defined by giving the displacements in each support point. Point 1 and point 11 are assumed to be kept at $w_1=w_{11}=0$.

Assume a circle radius is made with $R=5000$

All values in mm related to the original horizontal level; downwards displacement is positive

$w := [0.0, -36.59, -64.87, -84.97, -97.00, -101.00, -97.00, -84.97, -64.87, -36.59, 0.0] :$

Properties of the mould

$$EI := \frac{1}{12} \cdot b \cdot h^3 \cdot E :$$

$\#E := 210000 : (\text{steel})$

$E := 7000 : (\text{timber})$

Distance between support points (actuators)

$\Delta L := 200 :$

$b := \Delta L : (\text{actuators are set up in a square grid in two directions})$

Weight of the concrete on the mould surface

$\gamma_b := 2400 :$

$d := 50 :$

$\text{evalf}(q = -\gamma_b \cdot b \cdot d \cdot 10^{-8}) ; assign(\%);$

$q = -0.2400$

(3.2.1)

Allowable maximum relative deflection of the mould between two actuators in mm

$wu := -1 :$

Border conditions

In the original tests, the mould was placed loosely on the support points, so no downward reaction forces could be realized; for this reason, the stiffness of the mould was delimited by the border condition that no negative support reactions are allowed

for j **from** 10 **to** 20 **do**

$eq[j] := R[j - 9] \leq 0 :$

end do;

Condition for local deflection of mould between two support points

$$eq[21] := wu < \frac{1}{384} \frac{q \cdot \Delta L^4}{EI} :$$

$$eq[22] := h \geq 0 :$$

Solve range of allowable mould heights

$$\begin{aligned} sol := \text{solve}(\{eq[10], eq[11], eq[12], eq[13], eq[14], eq[15], eq[16], \\ eq[17], eq[18], eq[19], eq[20], eq[21], eq[22]\}, \{h\}); \\ \{h \leq 6.5034, 2.0465 < h\} \end{aligned} \quad (3.4.1)$$

Choice of mould height

Based on the above allowable range of mould heights, the following value is chosen in [mm]

$h := 1 :$

$$wu := \frac{1}{384} \frac{q \cdot \Delta L^4}{EI};$$

$$-8.5714 \quad (3.5.1)$$

$$\text{evalf}\left(I_{zz} = \frac{1}{12} \cdot b \cdot h^3\right);$$

$$I_{zz} = 16.6667 \quad (3.5.2)$$

Support reactions in [N]

for n **from** 1 **to** 11 **do**

$R[n] :$

end do;

	-19.0823
	-54.2330
	-46.3293
	-48.4515
	-47.8709
	-48.0659
	-47.8709
	-48.4515
	-46.3293
	-54.2330
	-19.0823

(3.6.1)

Graph of deflection

```

x := 'x';
for n from 2 to 10 do
  F := R[n] :
  a := (n - 1) · ΔL :
  b := (11 - n) · ΔL :
  uL[n] := wfL :
  uR[n] := wfR :
end do;

i := 'i'; j := 'j'; k := 'k';
u[1] := wq - ∑i=210 uL[i] :

for k from 2 to 9 do
  i := 'i'; j := 'j';
  u[k] := wq - ⎛ ∑i=2k uR[i] ⎞ - ⎛ ∑j=k+110 uL[j] ⎞ :
end do;

i := 'i'; j := 'j';
u[10] := wq - ∑j=210 uR[j] :

x := 'x';
with( plottools ) :
with( plots ) :
for k from 1 to 10 do
  W[k] := plot(u[k], x = (k - 1) · 200 .. k · 200) :

```

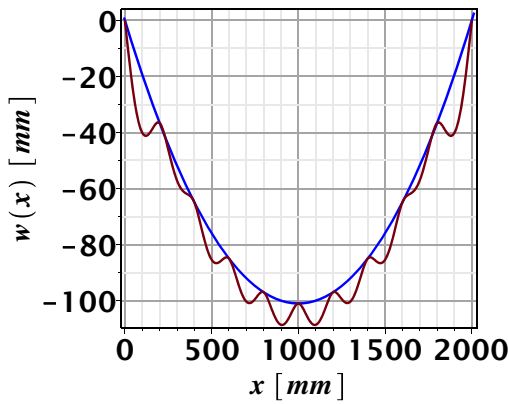
end do:

#1.37..1.775

$c1 := \text{ellipticArc}([1000, 4899], 5000, 5000, 4.51..4.9165, \text{color} = \text{blue}) :$

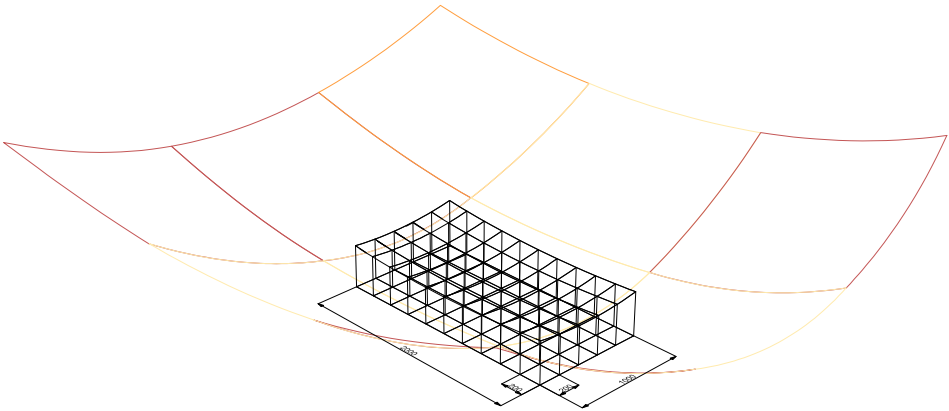
$\text{display}(\{W[1], W[2], W[3], W[4], W[5], W[6], W[7], W[8], W[9], W[10],$
 $c1\}, \text{title} = \text{'Shape of the mould } h = 1.0 \text{ mm'}, \text{font} = [\text{Helvetica}, \text{bold}, 14], \text{labels} = [$
 $'x \text{ [mm]}'', 'w(x) \text{ [mm]}'], \text{labeldirections} = [\text{horizontal}, \text{vertical}], \text{gridlines} = \text{true},$
 $\text{axes} = \text{boxed}, \text{size} = [1000, 300]);$

Shape of the mould h
= 1.0000 mm



Appendix C

Geometry double-curved elements viability research



DOUBLE-CURVED ELEMENT D $\Delta Z = 186 \text{ mm}$ $\theta_{\text{max}} = 19,8 \text{ degr}$

	1	2	3	4	5	6	7	8	9	10	11
A	61	112	156	186	204	208	200	179	145	100	51
B	63	116	161	192	210	216	209	189	155	111	61
C	61	117	163	195	214	220	214	194	162	118	66
D	56	114	161	194	214	221	215	196	165	121	68
E	48	107	155	188	209	217	212	194	164	121	67
F	35	97	145	179	201	209	206	188	159	117	61

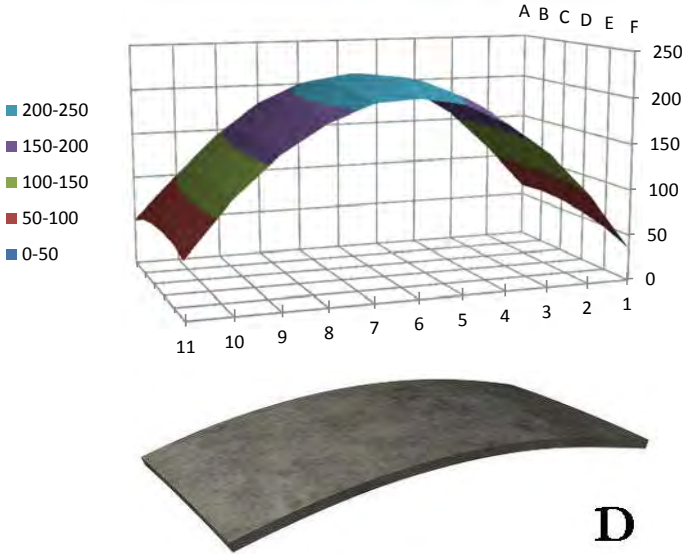
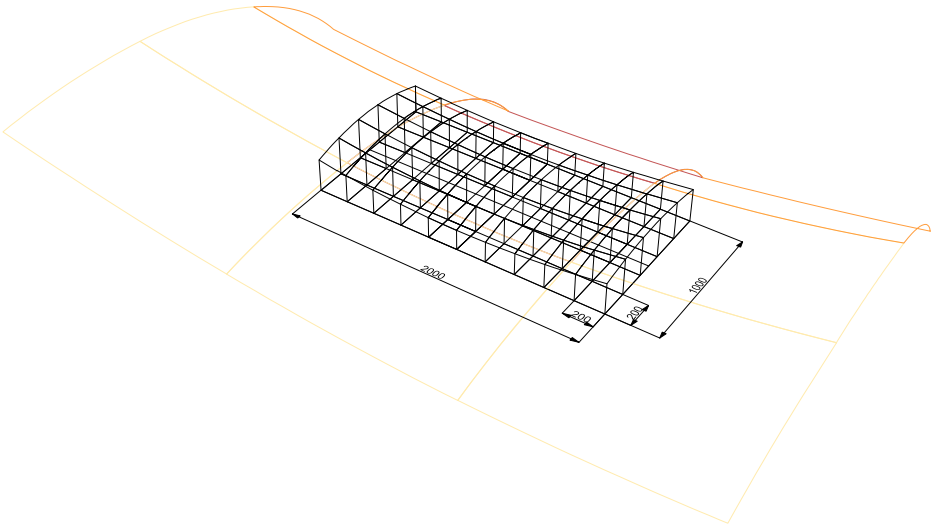


Figure C.1: Double-curved element D for viability experiments - projection of $2.00 \times 1.00 \text{ m}^2$ mould system on roof surface for determination of actuator heights; note: this element was cast upside-down.



DOUBLE-CURVED ELEMENT A $\Delta Z = 210 \text{ mm}$ $\theta_{\text{max}} = 27,7 \text{ degr}$

	1	2	3	4	5	6	7	8	9	10	11
A	95	72	51	39	35	37	46	61	84	113	144
B	173	144	120	103	93	92	96	109	130	156	190
C	217	183	154	133	121	116	119	130	148	175	210
D	225	186	155	131	117	112	113	123	141	168	205
E	197	155	123	99	85	78	81	91	109	138	177
F	135	92	60	35	21	15	19	32	53	86	127

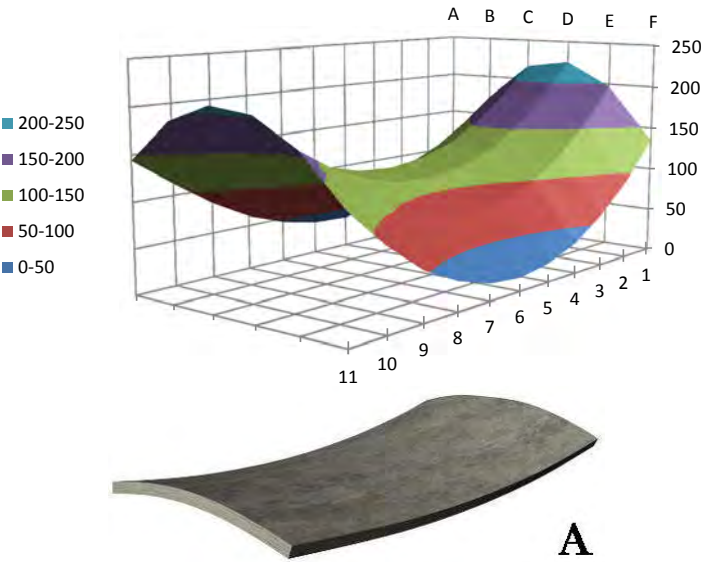


Figure C.2: Double-curved element A for viability experiments - projection of $2.00 \times 1.00 \text{ m}^2$ mould system on roof surface for determination of actuator heights

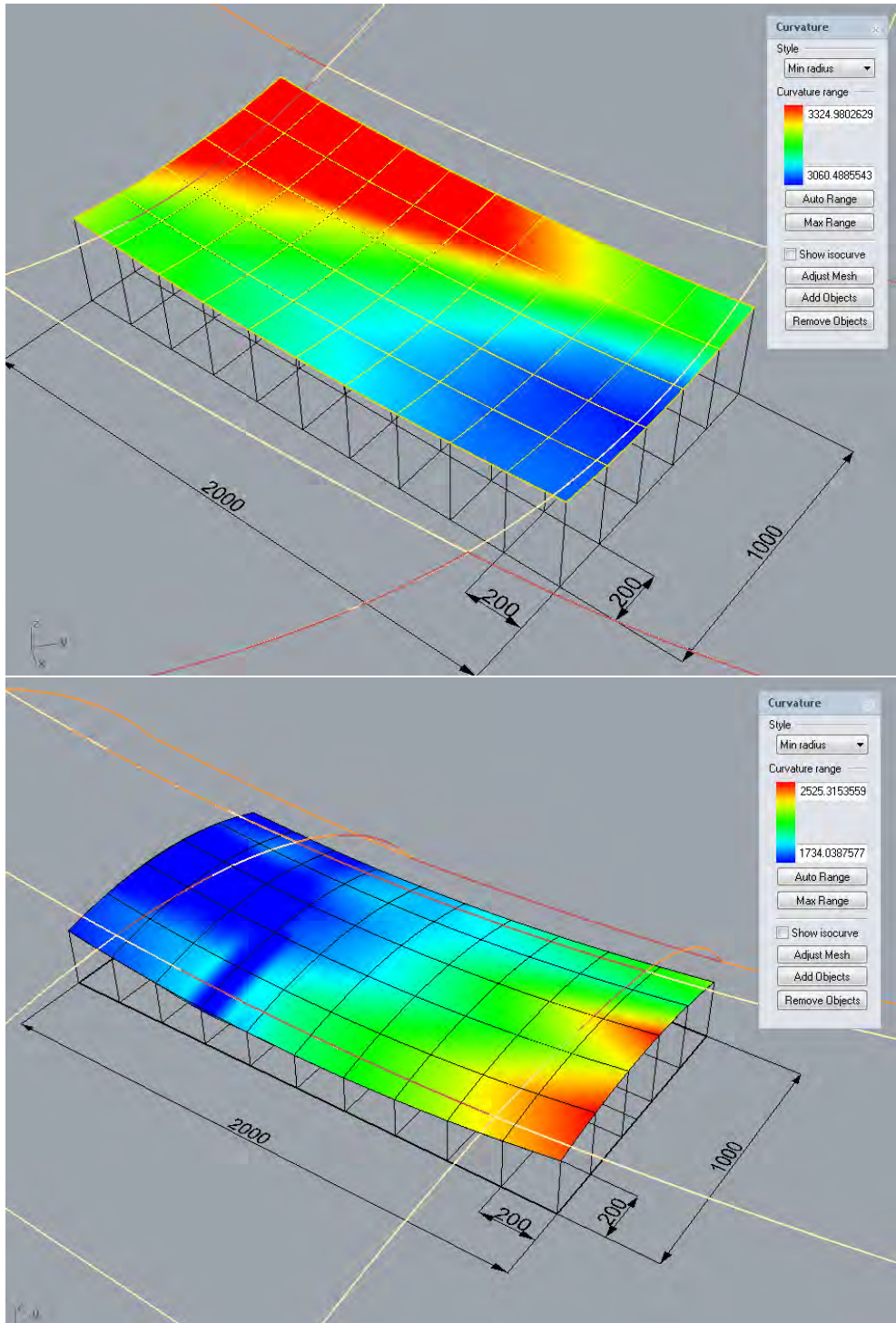


Figure C.3: Curvature analysis of element A and D for double-curved viability experiments - Element D (top) has a minimum radius of $R_{min} = 3.06$ m; element A (bottom) has a minimum radius of $R_{min} = 1.73$ m

Viability tests #6 - measurements element thickness and reinforcement cover
december 2014

cover on reinforcement x-direction (measured from mould surface = bottom of panel)

10	11	10
10	11	11
11	11	12
11	11	11
11	12	12
11	12	12
11	11	12
11	11	12
11	11	12
11	11	12
11	11	11

cover on reinforcement y-direction (measured from mould surface = bottom of panel)

23	17	14	14	14	13	13	14	15	15	16	15	15	15	15	16	16	19	24
$\phi 3-100$																		

applied: galvanized steel mesh # $\phi 3-100$

Viability tests #6 - measurements element thickness and reinforcement cover
december 2014

element thickness											
50	51	50	47	47	45	46	43	43		max	54.0 mm
45		52		50		47		45		average	47.1 mm
43	46	48	52	51	51	50	48	44		min	42.0 mm
44		47		54		46		44			
45	46	45	46	49	47	47	45	42			

Δ from average thickness											
-2.9	-3.9	-2.9	0.05	0.05	2.05	1.05	4.05	4.05		max	5.1 mm
2.05		-4.9		-2.9		0.05		2.05		average	0.0 mm
4.05	1.05	-0.9	-4.9	-3.9	-3.9	-2.9	-0.9	3.05		min	-6.9 mm
3.05		0.05		-6.9		1.05		3.05			
2.05	1.05	2.05	1.05	-1.9	0.05	0.05	2.05	5.05			



Viability tests #7 - measurements element thickness and reinforcement cover

december 2014

element thickness

45	47	50	45	48	45	44	50	44	max	52.0 mm
45		52		48		46		40	average	46.0 mm
46	47	45	52	48	47	47	52	45	min	38.0 mm
44		45		50		49		52		
45	38	42	41	40	42	43	48	44		

 Δ from average thickness

0.97	-1	-4	0.97	-2	0.97	1.97	-4	1.97	max	8.0 mm
0.97		-6		-2		-0		5.97	average	0.0 mm
-0	-1	0.97	-6	-2	-1	-1	-6	0.97	min	-6.0 mm
1.97		0.97		-4		-3		-6		
0.97	7.97	3.97	4.97	5.97	3.97	2.97	-2	1.97		



Viability tests #8 - measurements element thickness and reinforcement cover
december 2014

element thickness											
44	45	46	45	44	45	45	47	44		max	49.0 mm
39		45		45		47		39		average	44.4 mm
40	44	48	49	47	47	45	44	39		min	37.0 mm
37		47		44		45					
43	45	47	45	41	45	45	45	45			

Δ from average thickness											
0.36	-0.6	-1.6	-0.6	0.36	-0.6	-0.6	-2.6	0.36		max	44.4 mm
5.36		-0.6		-0.6		-2.6		5.36		average	1.2 mm
4.36	0.36	-3.6	-4.6	-2.6	-2.6	-0.6	0.36	5.36		min	-4.6 mm
7.36		-2.6		0.36		-0.6		44.4			
1.36	-0.6	-2.6	-0.6	3.36	-0.6	-0.6	-0.6	-0.6			



Appendix D

Research variables parameter variation study

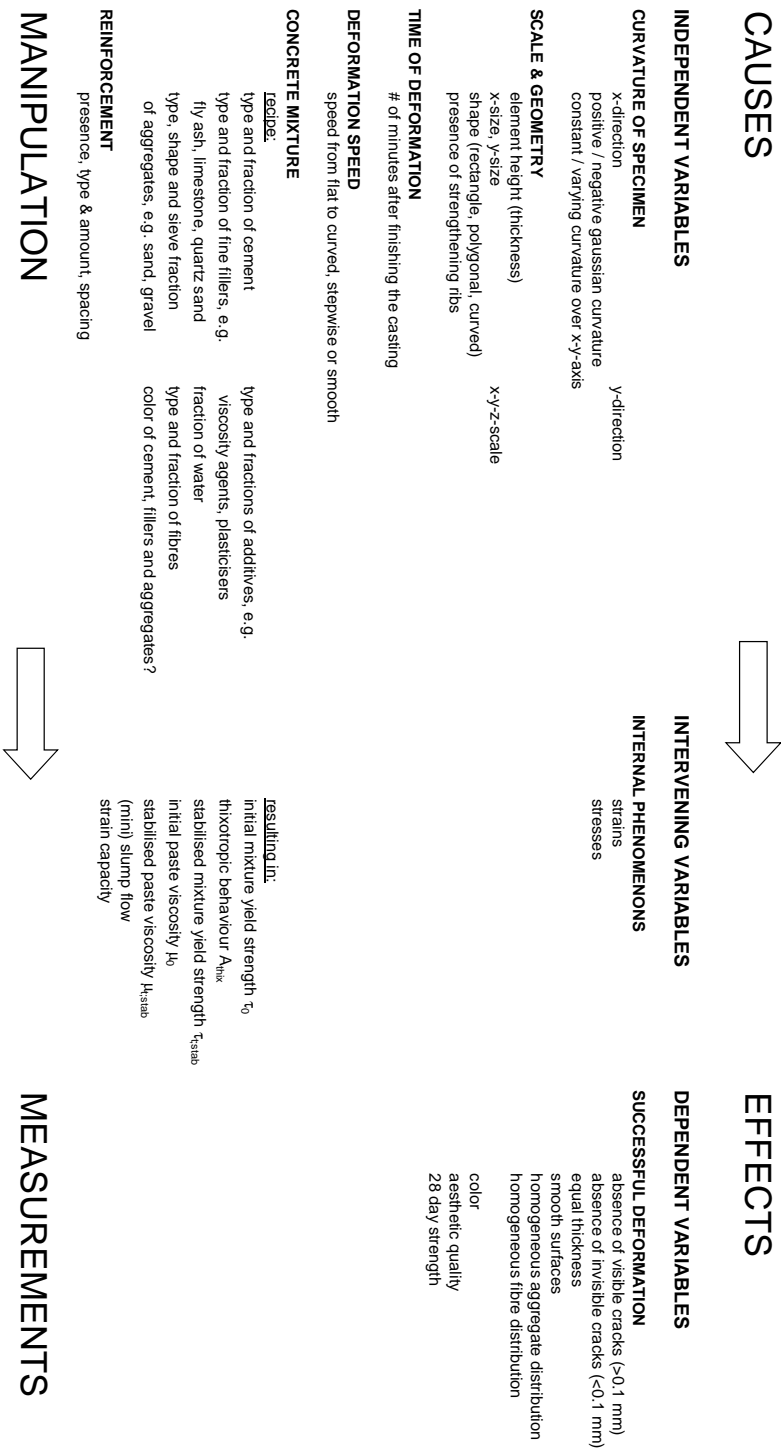


Figure D.1: Overview of variables for laboratory research

Appendix E

General procedure casting, deformation and hardening

The moulds for the parameter variation study were based on similar, slightly modified set-up as the strip-model used in the viability study: a 25 mm thick base plate of MDF, a secondary lifting and levelling platform of 12 mm thick MDF, and a grid of pins at intervals of 140 x 140 mm, made out of threaded galvanized steel rods M10, aluminium tubes 13 x 1 mm and nuts M10 for the height adjustment of the tubes over the threads. On top of this grid of pins a field of crossing plywood lathes was placed of 50 x 3.8 mm (width x thickness). The lathes were loosely fixed to the aluminium tubes by nails, leaving some place for horizontal sliding. The flexibility of the lathes was modelled with the strip model and was investigated numerically. More on this was reported in section 7.4. On top of the lathes, the silicone-and-foam rubber moulds were placed. The foam used for the bottom layer of the mould was a 10 mm polyether foam layer of specific weight 25 kg/m³ (SG25). The edges were made of flexible foam strips of 50 x 50 mm² cross-section, also of polyether SG25. To prevent concrete from being absorbed by the foam, and in order to obtain a smooth surface texture, all foam in direct contact with concrete was covered with a 1 mm layer of two-component silicone rubber with a Shore-A value of 20. This was done by casting a layer of silicone on a smooth surface and after that draping the foam in the silicone. After hardening of the silicone, it would be connected to the foam. In the following figures, the steps are visible that have been taken for the various tests.

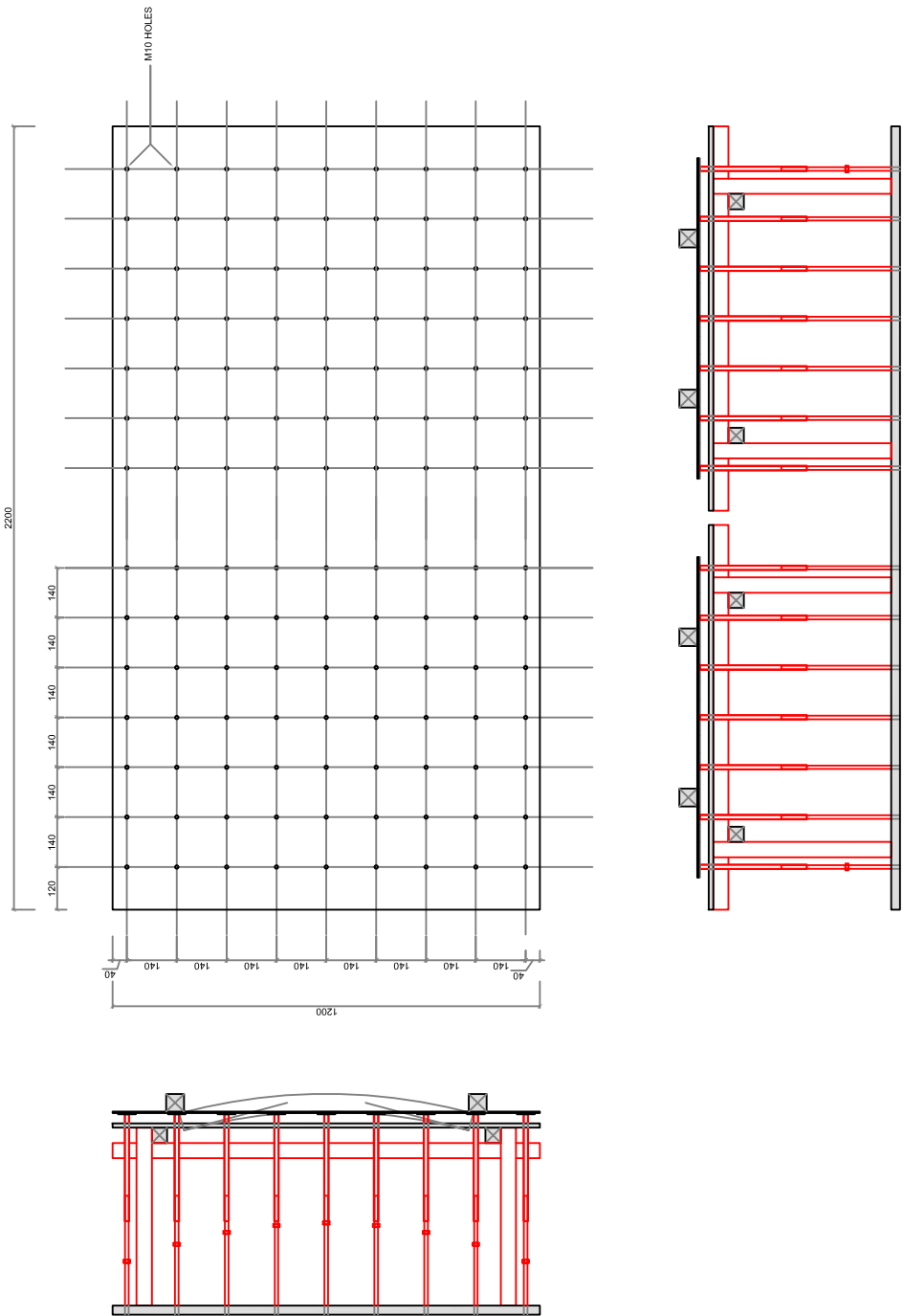


Figure E.1: Elevation and cross-section of the moulds with support system (RS / P. Raghunath)



01 - weighing concrete ingredients



02 - setting up and checking mould shape



03 - mixing



04 - testing slump flow



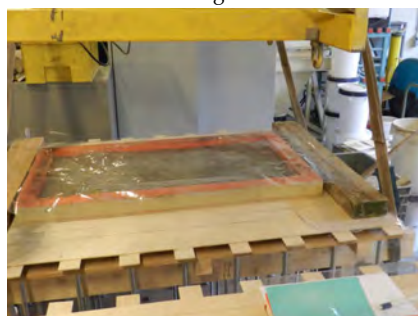
05 - filling moulds



06 - filling moulds



07 - filling and covering cubes and prisms for later testing



08 - covering with foil to prevent evaporation



09 - waiting for and testing initial yield strength development



10 - cleaning equipment



11 - deformation



11 - deformation



12 - deformation



13 - deformation



14 - deformation



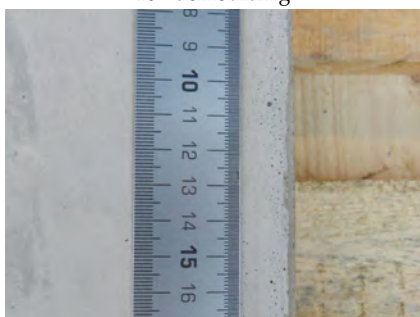
15 - next day: demoulding



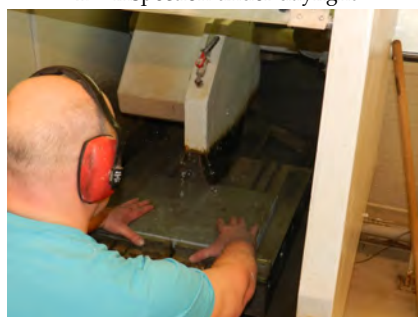
16 - demoulding



17 - inspection under daylight



18 - inspection



19 - sawing specimens for inspection



20 - sawing sections for inspection



21 - inspection of sections

Appendix F

Casting and deformation tests

batch**1**

casting date

September 7, 2012

start mixing

10:30

mixture recipe
(per 1000 ltr)

sand 0.125-0.25 mm

48 kg

sand 0.25-0.5 mm

129 kg

sand 0.5-1.0 mm

209 kg

gravel 1-2 mm

290 kg

gravel 2-4 mm

373 kg

gravel 4-8 mm

564 kg

CEM I 52,5 R**400 kg**

Fly-ash

160 kg

Superplast Chryso Premia 196

3.50 kg (0.63% of pwd)

water**172 kg**

specific mass

2349 kg/m³

wcf

0.430

wpf

0.307

batch volume

50 ltr

strength



time cubes:

cube compr [MPa]

3 day	17 day	28 day
Sep 10	Sep 24	Oct 05
14:00	15:30	15:33

60.8 75.2 82.3

cube split [MPa]

- - -

time prisms:

14:00 - -



prism bending tensile str [MPa]

8.8 - -

mini prism cube compr [MPa]

- - -

mini prism cube compr [MPa]

- - -

temperatures

room

- °C

aggregates

- °C

cement + fly-ash

- °C

water

- °C

fresh concrete directly after mixing

- °C

mixing procedure



aggregates + cement + fly-ash

20 sec

add 50% of water then

40

add 50% of water + plastic then

90

scraping of mixer then

90

*used the Eirich
mixer*

240 sec

workability /
rheologyslump flow [mm] / τ_o [Pa]

750

1.6

at t = 0:05 h:min

slump time T50 [sec]

2.03

at t = 0:05 h:min

Mueller M3

slump #1 [mm] / τ_o [Pa]

225

167

at t = 0:15 h:min

slump #2 [mm] / τ_o [Pa]

168

368

at t = 0:30 h:min

slump #3 [mm] / τ_o [Pa]

123

526

at t = 0:45 h:min

batch 1 (continued)

general remarks about the mixture: first test mixture

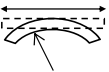
placing -

video of placing -
placing time -

video of deformation -
deformation -



geometry specimen length
specimen width
specimen height
radius Rx
radius Ry



hardening -

demoulding -
inspection date -

description of the batch first test mixture to check mixing, slump values and slump development over time

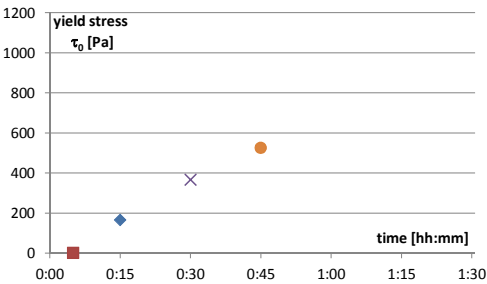


Figure: Development of yield stress in time based on the slump (flow) tests

	mould 1	mould 2	mould 3	mould 4	
	-	-	-	-	mm
	-	-	-	-	mm
	-	-	-	-	mm
	-	-	-	-	mm
	-	-	-	-	mm

batch**2**

casting date

September 24, 2012

start mixing

15:30

mixture recipe
(per 1000 ltr)

sand 0.125-0.25 mm

sand 0.25-0.5 mm

sand 0.5-1.0 mm

gravel 1-2 mm

gravel 2-4 mm

gravel 4-8 mm

CEM I 52,5 R

Fly-ash

Superplast Chryso Premia 196

water

specific mass

wcf

wpf

mixture m₃

48 kg

129 kg

209 kg

290 kg

373 kg

564 kg

400 kg

160 kg

4.48 kg (0.80% of pwd)

172 kg2349 kg/m³

0.430

0.307

batch volume

16.7 ltr

1 day 7 day 28 day

strength



time cubes:

cube compr [MPa]

cube split [MPa]

time prisms:



prism bending tensile str [MPa]

mini prism cube compr [MPa]

mini prism cube compr [MPa]

	1 day	7 day	28 day
time cubes:	-	-	-
cube compr [MPa]	-	-	-
cube split [MPa]	-	-	-
time prisms:	-	-	-
prism bending tensile str [MPa]	-	-	-
mini prism cube compr [MPa]	-	-	-
mini prism cube compr [MPa]	-	-	-

temperatures

room

aggregates

cement + fly-ash

water

fresh concrete directly after mixing

	1 day	7 day	28 day
room	-	°C	
aggregates	-	°C	
cement + fly-ash	-	°C	
water	-	°C	
fresh concrete directly after mixing	-	°C	

mixing procedure



aggregates + cement + fly-ash

add 50% of water then

add 50% of water + plastic then

scraping of mixer then

20 sec

40

90

90

240 sec

*used the Hobart
kitchen mixer*workability /
rheologyslump flow [mm] / τ_o [Pa]

slump time T50 [sec]

- - at t = h:min

-

slump #1 [mm] / τ_o [Pa]slump #2 [mm] / τ_o [Pa]slump #3 [mm] / τ_o [Pa]

- at t = h:min

-

- at t = h:min

-

- at t = h:min

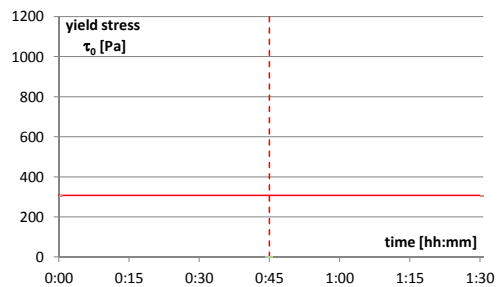
batch**2 (continued)**

general remarks
about the mixture:

very fluid concrete

placing

*concrete is self levelling,
easy to place, no
vibration needed.*



video of placing
placing time

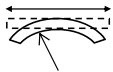
mould 1 filled at	0:14	h:min
mould 2 filled at	-	h:min
mould 3 filled at	-	h:min
mould 4 filled at	-	h:min

video of deformation
deformation



mould 1 deformed at	0:45	h:min	<i>Too fluid, concrete flows out of mould resulting in uneven cast surface</i>
mould 2 deformed at	-	h:min	
mould 3 deformed at	-	h:min	
mould 4 deformed at	-	h:min	

geometry



	mould 1	mould 2	mould 3	mould 4	
specimen length	800	-	-	-	mm
specimen width	400	-	-	-	mm
specimen height	50	-	-	-	mm
radius Rx	1.5	-	-	-	m
radius Ry	∞	-	-	-	m

hardening

-

demoulding

DSCN2189 demould spec 2.1.MOV

inspection date

September 25, 2012

description of the batch

The mixture was prepared with the intention of making a trial casting for 1 single curved concrete element. There were no other tests carried out with this mixture other than casting the element itself. It was a very fluid mixture, self compacting and self-leveling. Formation of air bubbles was noticed after the mould was levelled. It was found out that the fluidity was still too high to be deformed at 45 minutes: the concrete started flowing out from the centre to the edges and the excess cement water and concrete accumulated thus, and flowed out of the moulds onto the timber lathes. The heavier aggregates seemed to settle at their original position, while the finer particles flowed out to the edges from the top surfaces. This resulted in a deformed profile for the casting surface and thus varying thicknesses of the element from the ends to the center.

The element itself turned out to be very smooth on the mould surface. The reflection of the lathes was noticed on the surface. Few air bubbles seen on the edges of the element.

batch**3**

casting date

September 25, 2012

start mixing

15:45

mixture recipe
(per 1000 ltr)

sand 0.125-0.25 mm

48 kg

sand 0.25-0.5 mm

129 kg

sand 0.5-1.0 mm

209 kg

gravel 1-2 mm

290 kg

gravel 2-4 mm

373 kg

gravel 4-8 mm

564 kg

CEM I 52,5 R**400 kg**

Fly-ash

160 kg

Superplast Chryso Premia 196

4.30 kg

(0.77% of pwd)

water**172 kg**

specific mass

2349 kg/m³

wcf

0.430

wpcf

0.307

batch volume

53.5 ltr

strength



time cubes:

cube compr [MPa]

	1 day	7 day	28 day
Sep 26	14:50	13:56	15:55

30.7

61.8

70.8

cube split [MPa]

-

-

-

time prisms:

10:40



prism bending tensile str [MPa]

-

10.5

11.1

mini prism cube compr [MPa]

-

71.3

75.8

mini prism cube compr [MPa]

-

-

77.4

temperatures

room

-

°C

aggregates

-

°C

cement + fly-ash

-

°C

water

-

°C

fresh concrete directly after mixing

-

°C

mixing procedure



aggregates + cement + fly-ash

20 sec

used the Eirich

add 50% of water + plastic then

40

mixer

add 50% of water then

90

scraping of mixer then

90

240 sec

workability /
rheologyslump flow [mm] / τ_o [Pa]

575

6.2

at t = 0:00 h:min

slump time T50 [sec]

2.0

Mueller M3

slump #1 [mm] / τ_o [Pa]

210

220

at t = 0:30 h:min

slump #2 [mm] / τ_o [Pa]

215

202

at t = 0:45 h:min

slump #3 [mm] / τ_o [Pa]

200

255

at t = 1:08 h:min

batch**3 (continued)**

general remarks
about the mixture:

very fluid concrete

placing

*concrete is not really self
levelling, but still easy to
place, no vibration
needed.*

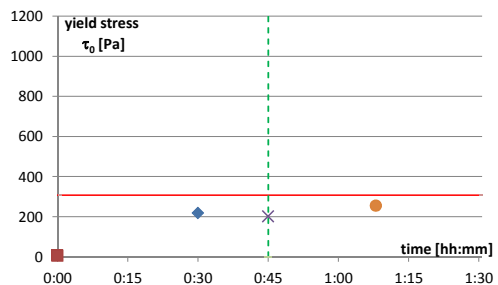


Figure: development of yield stress in time
based on the slump (flow) tests

video of placing
placing time

mould 1 filled at
mould 2 filled at
mould 3 filled at
mould 4 filled at

? h:min
- h:min
- h:min
- h:min

*directly after slump
flow test*

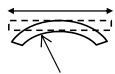
video of deformation
deformation



mould 1 deformed at
mould 2 deformed at
mould 3 deformed at
mould 4 deformed at

0:45 h:min
- h:min
- h:min
- h:min

geometry



specimen length
specimen width
specimen height
radius Rx
radius Ry

mould 1 mould 2 mould 3 mould 4

800	-	-	-	mm
400	-	-	-	mm
50	-	-	-	mm
-1.5	-	-	-	m
∞	-	-	-	m

hardening

-

demoulding

-

inspection date

September 26, 2012

description of the batch

The mixture from batch 2 was repeated for testing the panel with opposite curvature. This time additional volume of concrete was prepared to carry out the slump tests and to fill in the cubes and prisms. The mixture was quite fluid but not self-levelling. The slump flow however was less than the expected value of 750-800mm. The mixture was easy to place and showed less formation of air bubbles on the surface than batch 2. The slump tests, however, showed that concrete wasn't hardening very fast, as the slump values didn't vary much over the 3 intervals. The deformation of the element was a smooth process. No hitches were seen. However, the mould wasn't touching the actuators at all points, especially at the edges. Additional weights had to be added on the mould to ensure the curvature was maintained.

The element was smooth. The reflection of the lathes is again visible on the surface. Air bubbles were noticed on the mould surface and on the sides.

batch

4 (continued)

general remarks
about the mixture:

mixture much too stiff

placing

hard to place

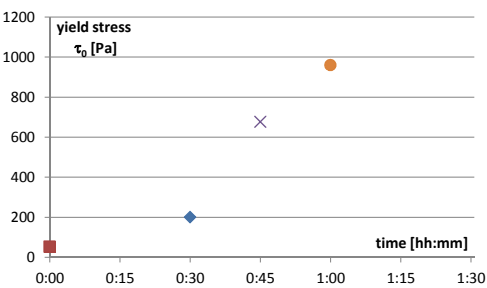


Figure: Development of yield stress in time based on the slump (flow) tests

video of placing
placing time

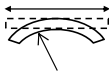
DSCN2388.MOV	
mould 1 filled at	0:10 h:min
mould 2 filled at	0:20 h:min
mould 3 filled at	0:30 h:min
mould 4 filled at	0:40 h:min

video of deformation
deformation



mould 1 deformed at	0:30 h:min
mould 2 deformed at	0:45 h:min
mould 3 deformed at	1:00 h:min
mould 4 deformed at	- h:min

geometry



	mould 1	mould 2	mould 3	mould 4	
specimen length	800	800	800	800	mm
specimen width	400	400	400	400	mm
specimen height	50	50	50	50	mm
radius Rx	1.5	1.5	1.5	∞	m
radius Ry	∞	∞	∞	∞	m

hardening

covered with plastic

demoulding

-

inspection date

October 2, 2012

description of the batch

The first of the batches where an entire series of 4 elements (with one element flat) were cast at once. The proportion of the plasticiser was reduced to 0.64% with the intention of getting the right fluidity with a maximum economy. But it turned out that the mixture was very dry and stiff. It was far from self compacting. It was hard to place the concrete in the moulds. It required manual compaction to get it levelled as much as possible. The mixture turned out to be so stiff that after 1 hour the slump was zero. Surface cracks were visible in the elements immediately after deformation.

The elements had many air bubbles, some of them as big as 1cm wide, on the mould surface and on the edges. The finish was far from satisfactory. It was difficult to release the moulds from the elements as well. The mould had started wearing off slowly, and blobs of concrete jutting out of the surface had penetrated into the foam layer through the silicone layer.

batch**5**

casting date

October 3, 2012

start mixing

10:28

mixture recipe
(per 1000 ltr)

sand 0.125-0.25 mm

48 kg

sand 0.25-0.5 mm

129 kg

sand 0.5-1.0 mm

209 kg

gravel 1-2 mm

290 kg

gravel 2-4 mm

373 kg

gravel 4-8 mm

564 kg

CEM I 52,5 R**399 kg**

Fly-ash

160 kg

Superplast Chryso Premia 196

4.31 kg (0.77% of pwd)

water**172 kg**

specific mass

2349 kg/m³

wcf

0.431

wpcf

0.308

batch volume

100 ltr

strength



time cubes:

	1 day	7 day	28 day
	Oct 04	Oct 10	Oct 31
12:47	13:11	-	
38.79	52.61	-	
-	-	-	
-	-	-	
-	-	-	
-	-	-	
-	-	-	

cube compr [MPa]

cube split [MPa]

time prisms:



prism bending tensile str [MPa]

mini prism cube compr [MPa]

mini prism cube compr [MPa]

temperatures

room

not measured

aggregates

not measured

cement + fly-ash

not measured

water

not measured

fresh concrete directly after mixing

not measured

mixing procedure



aggregates + cement + fly-ash

20 sec

used the Eirich

add 50% of water + plastic then

40

mixer

add 50% of water then

90

scraping of mixer then

90

240 sec

workability /
rheologyslump flow [mm] / τ_o [Pa]

-

at t = 0:00 h:min

slump time T50 [sec]

-

Mueller M3

slump #1 [mm] / τ_o [Pa]

-

at t = n.a. h:min

slump #2 [mm] / τ_o [Pa]

0

960

at t = 0:48 h:min

slump #3 [mm] / τ_o [Pa]

0

960

at t = 1:00 h:min

batch

5 (continued)

general remarks
about the mixture:

mixture much too stiff

placing

hard to place

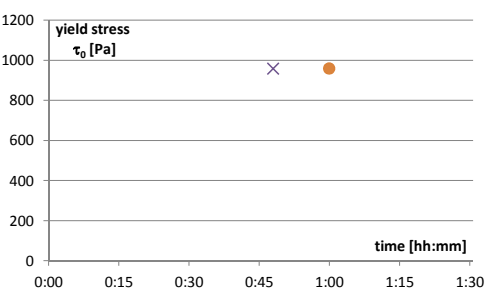


Figure: Development of yield stress in time based on the slump (flow) tests

video of placing
placing time

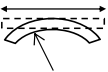
mould 1 filled at	0:15	h:min
mould 2 filled at	0:35	h:min
mould 3 filled at	0:35	h:min
mould 4 filled at	?	h:min

video of deformation
deformation



mould 1 deformed at	0:40	h:min
mould 2 deformed at	0:50	h:min
mould 3 deformed at	1:00	h:min
mould 4 deformed at	-	h:min

geometry



	mould 1	mould 2	mould 3	mould 4	
specimen length	800	800	800	800	mm
specimen width	400	400	400	400	mm
specimen height	50	50	50	50	mm
radius Rx	1.5	1.5	1.5	∞	m
radius Ry	∞	∞	∞	∞	m

hardening

-

demoulding

-

inspection date

October 4, 2012

description of the batch

As the mixture of the batch 5 was far from satisfactory, the proportion of the plasticiser was elevated back 0.77% as in batch 3. However, the mixture didn't show any signs of improvement and it was as dry and stiff as batch 4. Hence the slump flow test were ignored, and the filling of the moulds started directly. The placement was hard as in batch 4. Manual compaction was inevitable. The mixture was so stiff that each of the two slump tests had zero slump. Surface cracks were visible suring and immediately after deformation.

The elements, as expected, had many air bubbles. They turned out to be rougher than batch 4. However, the finish of the curved elements improved slightly from element 5.1 to 5.3. The flat element was extremely rough. The results of this batch were far from satisfactory.

batch**6**

casting date

October 10, 2012

start mixing

10:28

mixture recipe
(per 1000 ltr)

sand 0.125-0.25 mm

48 kg

sand 0.25-0.5 mm

129 kg

sand 0.5-1.0 mm

209 kg

gravel 1-2 mm

290 kg

gravel 2-4 mm

373 kg

gravel 4-8 mm

564 kg

CEM I 52,5 R**399 kg**

Fly-ash

160 kg

Superplast Chryso Premia 196

6.16 kg (1.10% of pwd)

water**172 kg**

specific mass

2350 kg/m³

wcf

0.431

wpcf

0.308

batch volume

100 ltr

strength



time cubes:

cube compr [MPa]

cube split [MPa]

time prisms:



prism bending tensile str [MPa]

mini prism cube compr [MPa]

mini prism cube compr [MPa]

1 day 7 day 28 day

Oct 11 Oct 17 Nov 07

15:00 14:00 16:00

39.0 71.7 71.78

3.1 4.1 -

- - -

- - -

- - -

- - -

temperatures

room

22.4 °C

aggregates

24.7 °C

cement + fly-ash

25.1 °C

water

23.2 °C

fresh concrete directly after mixing

27.8 °C

mixing procedure



aggregates + cement + fly-ash

20 sec

add 50% of water + plastic then

40

add 50% of water then

90

scraping of mixer then

90

240 sec

*used the Eirich
mixer**continued mixing after first slump flow test**60 sec*workability /
rheologyslump flow [mm] / τ_o [Pa]

>> 900 < 0.7

at t = 0:04 h:m in

slump time T50 [sec]

*not measured (too quick)**segregation*

Mueller M3

slump #1 [mm] / τ_o [Pa]

230

149

at t = 0:45 h:m *)

slump #2 [mm] / τ_o [Pa]

200

255

at t = 0:59 h:m *)

slump #3 [mm] / τ_o [Pa]

230

149

at t = 1:15 h:m *)

**) still moving*

batch**6 (continued)**

general remarks
about the mixture:

fluid, segregation

placing

easy to place

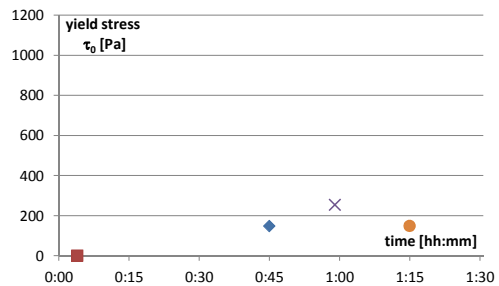


Figure: Development of yield stress in time based on the slump (flow) tests

video of placing
placing time

[DSCN2555.MOV](#)

mould 1 filled at	0:12	h:min	10 sec of remixing before filling next
mould 2 filled at	0:20	h:min	mould
mould 3 filled at	0:27	h:min	
mould 4 filled at	?	h:min	oiled before casting to try this out

video of deformation
deformation

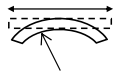
[DSCN2555.MOV](#)

mould 1 deformed at	1:15	h:min	cracks in surface, concrete stays in mould
mould 2 deformed at	0:59	h:min	cracks in the middle, but also cement
			water flowing over edge; mould got stuck during deformation; extra movement of mould
mould 3 deformed at	0:45	h:min	cement water flow over edge
mould 4 deformed at	n.a.	h:min	



geometry

	mould 1	mould 2	mould 3	mould 4	
specimen length	800	800	800	800	mm
specimen width	400	400	400	400	mm
specimen height	50	50	50	50	mm
radius Rx	1.5	1.5	1.5	∞	m
radius Ry	∞	∞	∞	∞	m



hardening

See below

demoulding

See below

inspection date

October 11, 2012

description of the batch

The proportion of the plasticiser was increased to 1.1% to achieve a fluid concrete. The mixture turned out to be self-compacting, self-levelling and very fluid. However, segregation was observed. Segregation was observed during slump flow test as well. So the concrete was remixing for a few seconds before placing in the moulds. The concrete was very fluid and very easy to place in the first 2 moulds, but it started hardening very fast and hence a slightly stiffer concrete was placed in the moulds 3 and 4. Since the fluidity of the concrete was very high, for the first two, it was decided to deform the elements in the reverse order. Nevertheless, the cement water flowed over the mould while deforming. Mould 2 got stuck, so there was extra movement during deformation. Surface cracks were seen immediately in moulds 1 and 2. The mixture was very sticky and it was very hard to clean the tools and the floor.

The elements had a good finish on the mould surface and on the edges. Few air bubbles and blobs were seen. The cast surface had many shrinkage cracks perpendicular to the direction of deformation, and a few air bubbles. The bigger aggregates were distinctly visible on the cast surface at many places.

batch**7**

casting date

October 15, 2012

start mixing

13:30

mixture recipe
(per 1000 ltr)

sand 0.125-0.25 mm

sand 0.25-0.5 mm

sand 0.5-1.0 mm

gravel 1-2 mm

gravel 2-4 mm

gravel 4-8 mm

CEM I 52,5 R

Fly-ash

Superplast Chryso Premia 196

water

specific mass

wcf

wpf

batch volume

mixture m₃

48 kg

129 kg

209 kg

290 kg

373 kg

564 kg

400 kg

160 kg

5.60 kg

(1.00% of pwd)

> **172 kg**2351 kg/m³

> 0.430

> 0.307

*note: wcf not clear, since**amount of water added**was not denoted during**tests*

strength



time cubes:

cube compr [MPa]

cube split [MPa]

time prisms:



prism bending tensile str [MPa]

mini prism cube compr [MPa]

mini prism cube compr [MPa]

1 day 7 day 29 day

Oct 16 Oct 22 Nov 13

13:00 16:30 11:01

34.0 47.1 50.5

4.7 4.0 5.8

12:30 16:30 11:30

6.3 9.6 12.2

33.1 56.9 73.2

31.9 56.2 72.9

*cubes shapes not unifor
hence results not accur*

temperatures

room

aggregates

cement + fly-ash

water

fresh concrete directly after mixing

22.4 °C

21.7 °C

22.7 °C

21.7 °C

- °C

mixing procedure



aggregates + cement + fly-ash

add 50% of water + plastic then

add 50% of water then

scraping of mixer then

20 sec

40

90

90

240 sec

*used the Eirich**mixer**kept 0.5 kg of water**behind before first mixing*workability /
rheologyslump flow [mm] / τ_o [Pa]

450

21.1

at t = 0:05 h:min

slump time T50 [sec]

- (never reached 500 mm)

*added rest of water, remixed for 60 seconds**added more water in order to try to get mixture workable, but without success.*

Mueller M3

*) video DSCN2613

slump #1 [mm] / τ_o [Pa]

160

396

at t = 0:15 h:m *)

slump #2 [mm] / τ_o [Pa]

0

960

at t = 0:47 h:m

slump #3 [mm] / τ_o [Pa]

-

at t = - h:m

batch**7 (continued)**

general remarks
about the mixture:

not workable

placing

*hard to place,
compaction necessary*

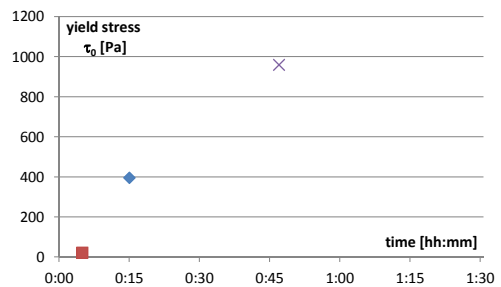


Figure: Development of yield stress in time
based on the slump (flow) tests

video of placing
placing time

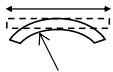
mould 1 filled at	-	h:min
mould 2 filled at	-	h:min
mould 3 filled at	-	h:min
mould 4 filled at	-	h:min

video of deformation
deformation



mould 1 deformed at	-	h:min
mould 2 deformed at	-	h:min
mould 3 deformed at	-	h:min
mould 4 deformed at	-	h:min

geometry



	mould 1	mould 2	mould 3	mould 4	
specimen length	-	-	-	-	mm
specimen width	-	-	-	-	mm
specimen height	-	-	-	-	mm
radius Rx	-	-	-	-	m
radius Ry	-	-	-	-	m

hardening

-

demoulding






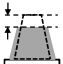
-

inspection date

October 16, 2012

description of the batch

The amount of plasticiser was slightly reduced (to 1%) in order to obtain a mixture of slightly lesser fluidity. But the mixture turned out to be very dry and stiff. The slump flow didn't reach 500 mm. So a slight addition of water was made to the mixture. However it didn't improve the mixture. Even a second instance of additional water didn't make any change to the mixture and slump flow still remained withing 500 mm. The mixture was hardening fast, and hence we proceeded with placing the moulds. It was extremely hard to place and we stopped the casting after 3 moulds, and decided not to deform them, as it would be a waste. Only the cubes and prisms were filled. The elements were thrown away after demoulding.

batch		8				
casting date		October 17, 2012				
start mixing		14:30				
mixture recipe (per 1000 ltr)			mixture m₃			
	sand 0.125-0.25 mm		49 kg			
	sand 0.25-0.5 mm		126 kg			
	sand 0.5-1.0 mm		214 kg			
	gravel 1-2 mm		290 kg			
	gravel 2-4 mm		370 kg			
	gravel 4-8 mm		564 kg			
	CEM I 52,5 R		408 kg			
	Fly-ash		157 kg			
	Superplast Chryso Premia 196		5.60 kg	(0.99% of pwd)		
	water		171 kg			
	specific mass		2355 kg/m ³			
wcf			0.420			
wpf			0.303			
batch volume			7 ltr			
strength				1 day	7 day	28 day
				Oct 18	Oct 24	Nov 14
		time cubes:				
		cube compr [MPa]	-	-	-	
		cube split [MPa]	-	-	-	
		time prisms:	12:30	16:30	12:05	
		prism bending tensile str [MPa]	7.1	8.1	9.9	
		mini prism cube compr [MPa]	39.6	64.4	78.5	
		mini prism cube compr [MPa]	41.7	62.6	81.6	
temperatures	room		- °C			
	aggregates		22.8 °C			
	cement + fly-ash		- °C			
	water		22.7 °C			
	fresh concrete directly after mixing		26.0 °C			
mixing procedure		aggregates + cement + fly-ash	20 sec	<i>used the Hobart bakery mixer</i>		
		add 50% of water + plastic then	40			
		add 50% of water then	90			
		scraping of mixer then	90			
			240 sec			
workability / rheology		slump flow [mm] / τ_o [Pa]	785	1.3	at t = 0:05	h:min
		slump time T50 [sec]	-		video	
		slump flow [mm] / τ_o [Pa]	700	2.3	at t = 0:45	h:min
		slump time T50	-		video	
		slump #1 [mm] / τ_o [Pa]	-		at t = -	h:min
		slump #2 [mm] / τ_o [Pa]	-		at t = -	h:min
		slump #3 [mm] / τ_o [Pa]	-		at t = -	h:min

batch

8 (continued)

general remarks
about the mixture:

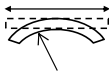
placing

video of placing placing time	mould 1 filled at	-	h:min	we did not cast any elements
	mould 2 filled at	-	h:min	
	mould 3 filled at	-	h:min	
	mould 4 filled at	-	h:min	

video of deformation deformation	mould 1 deformed at	-	h:min
	mould 2 deformed at	-	h:min
	mould 3 deformed at	-	h:min
	mould 4 deformed at	-	h:min



geometry		mould 1	mould 2	mould 3	mould 4	
	specimen length	-	-	-	-	mm
	specimen width	-	-	-	-	mm
	specimen height	-	-	-	-	mm
	radius Rx	-	-	-	-	m
	radius Ry	-	-	-	-	m



hardening

demoulding

inspection date n.a.

description of the batch *As there was no consistency in the mixtures obtained in the previous tests, it was decided to do just a test on the proportions of the mixture itself in a small volume. We weighed the contents for a small volume of concrete, 7 litre, which could be mixed in the smaller hobart mixer. The proportion of the plasticiser was kept to 1%. The mixture proved to be very fluid, self compacting and self levelling. The immediate slump flow was also satisfactory. However the slump flow after 45 minutes was quite high (700mm) and it appeared to segregate then. But it was seen that this mixture was better than the batches of 4,5,6 and 7 and easier to handle. So it was decided to repeat the same test the next day and check if the result would be consistent with this one.*

batch**9**

casting date

October 18, 2012

start mixing

11:00

mixture recipe
(per 1000 ltr)

sand 0.125-0.25 mm

sand 0.25-0.5 mm

sand 0.5-1.0 mm

gravel 1-2 mm

gravel 2-4 mm

gravel 4-8 mm

CEM I 52,5 R

Fly-ash

Superplast Chryso Premia 196

water

specific mass

wcf

wpf

mixture m_3

49 kg

126 kg

214 kg

290 kg

370 kg

564 kg

400 kg

160 kg

5.60 kg (1.00% of pwd)

171 kg2350 kg/m³

0.429

0.306

batch volume

7 ltr

strength



time cubes:

cube compr [MPa]

cube split [MPa]



time prisms:

prism bending tensile str [MPa]

mini prism cube compr [MPa]

mini prism cube compr [MPa]

1 day	7 day	28 day
Oct 19	Oct 25	Nov 15
-	-	-
-	-	-
11:50	16:00	12:05
7.5	9.7	9.4
40.5	67.3	91.2
44.7	68.9	91.2

temperatures

room

aggregates

cement + fly-ash

water

fresh concrete directly after mixing

- °C

22.5 °C

- °C

22.8 °C

28.2 °C

mixing procedure



aggregates + cement + fly-ash

add 50% of water + plastic then

add 50% of water then

scraping of mixer then

20 sec

40

90

90

240 sec

*used the Hobart
bakery mixer*workability /
rheologyslump flow [mm] / τ_o [Pa]

slump time T50 [sec]

slump flow [mm] / τ_o [Pa]

slump time T50

790

-

585

-

slump #1 [mm] / τ_o [Pa]slump #2 [mm] / τ_o [Pa]slump #3 [mm] / τ_o [Pa]

790

-

585

-

-

-

-

1.3 at t = 0:05 h:min

-

5.7 at t = 0:45 h:min

-

-

-

-

batch 9 (continued)

general remarks
about the mixture:

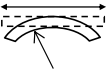
placing

video of placing placing time	mould 1 filled at	n.a.	h:min	<i>we did not cast any elements</i>
	mould 2 filled at	n.a.	h:min	
	mould 3 filled at	n.a.	h:min	
	mould 4 filled at	n.a.	h:min	

video of deformation deformation	mould 1 deformed at	n.a.	h:min
	mould 2 deformed at	n.a.	h:min
	mould 3 deformed at	n.a.	h:min
	mould 4 deformed at	n.a.	h:min



geometry		mould 1	mould 2	mould 3	mould 4	
	specimen length	n.a.	n.a.	n.a.	n.a.	mm
	specimen width	n.a.	n.a.	n.a.	n.a.	mm
	specimen height	n.a.	n.a.	n.a.	n.a.	mm
	radius Rx	n.a.	n.a.	n.a.	n.a.	m
	radius Ry	n.a.	n.a.	n.a.	n.a.	m



hardening

demoulding

inspection date n.a.

description of the batch *The same mixture as batch 8 yet was prepared. The mixture appeared to be similar to that of batch 8. The slump flow immediately also was satisfactory. The slump flow after 45 minutes was quite high but lesser than batch 8. Thus it was decided to use the same proportion for the next test for 100 litre for casting the elements*

batch**10**

casting date

October 19, 2012

start mixing

09:05

mixture recipe
(per 1000 ltr)

sand 0.125-0.25 mm

48 kg

sand 0.25-0.5 mm

128 kg

sand 0.5-1.0 mm

209 kg

gravel 1-2 mm

289 kg

gravel 2-4 mm

369 kg

gravel 4-8 mm

562 kg

CEM I 52,5 R**400 kg**

Fly-ash

160 kg

Superplast Chryso Premia 196

4.20 kg (0.75% of pwd)

water**172 kg**

specific mass

2340 kg/m³

wcf

0.430

wpcf

0.307

batch volume

100 ltr

strength



time cubes:

cube compr [MPa]

	3 day	7 day	28 day
	Oct 22	Oct 26	Nov 16
16:15	11:07	12:23	

58.9 66.4 71.1

cube split [MPa]

4.0 4.0 5.4

time prisms:



prism bending tensile str [MPa]

16:30 11:25 12:35

8.8 9.3 8.7

mini prism cube compr [MPa]

58.6 71.5

- prism off shape

mini prism cube compr [MPa]

63.3 79.1

- prism off shape

temperatures

room

22.5 °C

aggregates

24.0 °C

cement + fly-ash

23.7 °C

water

- °C

fresh concrete directly after mixing

- °C

mixing procedure



aggregates + cement + fly-ash

30 sec

add 90% of water

60

add 10% of water + plastic then

90

scraping of mixer then

30

210 sec

used the Eirich

mixer

modified mixing orderworkability /
rheologyslump flow [mm] / τ_o [Pa]

650

3.3

at t = 0:05 h:min

slump time T50 [sec]

-

video

Mueller M3

slump #1 [mm] / τ_o [Pa]

220

184

at t = 00:20 h:min

slump #2 [mm] / τ_o [Pa]

200

254

at t = 00:34 h:min

slump #3 [mm] / τ_o [Pa]

160

394

at t = 00:51 h:min

batch

10 (continued)

general remarks
about the mixture:

*modified mixing
order; better
workable*

placing

*some compaction
necessary*

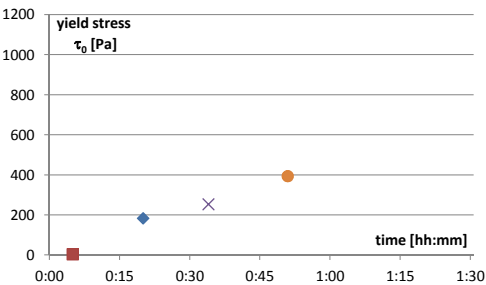


Figure: Development of yield stress in time based on the slump (flow) tests

video of placing
placing time

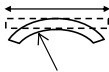
mould 1 filled at	0:03	h:min
mould 2 filled at	0:04	h:min
mould 3 filled at	0:06	h:min
mould 4 filled at	0:18	h:min

video of deformation
deformation



mould 1 deformed at	0:20	h:min
mould 2 deformed at	0:34	h:min
mould 3 deformed at	0:51	h:min
mould 4 deformed at	n.a.	h:min

geometry



	mould 1	mould 2	mould 3	mould 4	
specimen length	800	800	800	800	mm
specimen width	400	400	400	400	mm
specimen height	50	50	50	50	mm
radius Rx	1.5	1.5	1.5	∞	m
radius Ry	∞	∞	∞	∞	m

hardening

demoulding

inspection date

October 22, 2012

description of the batch

After advice of Dr. Gr ü newald the mixing procedure was modified. It appeared important to add the plasticiser after the cement absorbs water for the plasticiser to work effectively. Also the mixer now was wettened before pouring the ingredients, and also the slump cones and slump base plate were oiled.

Only 0.75% was added and the mixture was prepared with the changed mixing procedure. The mixture seemed fluid, self-compacting and self-leveling. However, it was segregating a bit and stabiliser was added to reduce the segregation. The mixture very workable, but not entirely self-leveling. It was easy to place and a little bit of compaction was necessary. The deformation was smooth. However surface cracks were visible immediately after deformation. This might be due to drying of the top surface, so we started to consequently cover the moulds with foil immediately after placing from this test on.

The elements had a good finish, except for some air bubbles and blobs of concrete sticking out due to the deterioration of the moulds. The cast surface had shrinkage cracks perpendicular to the direction of deformation, as observed immediately after deformation.

batch**11**

casting date

October 22, 2012

start mixing

13:30

mixture recipe
(per 1000 ltr)

sand 0.125-0.25 mm

48 kg

sand 0.25-0.5 mm

128 kg

sand 0.5-1.0 mm

209 kg

gravel 1-2 mm

289 kg

gravel 2-4 mm

370 kg

gravel 4-8 mm

562 kg

CEM I 52,5 R**400 kg**

Fly-ash

160 kg

Superplast Chryso Premia 196

3.64 kg

(0.65% of pwd)

water**172 kg**

specific mass

2342 kg/m³

wcf

0.430

wpf

0.307

batch volume

100 ltr

strength



time cubes:

cube compr [MPa]

	1 day Oct 23	7 day Oct 29	28 day Nov 19
time cubes:	16:15	10:17	11:15
cube compr [MPa]	47.5	67.0	76.8
cube split [MPa]	3.5	4.3	5.3
time prisms:	16:30	11:25	11:30
prism bending tensile str [MPa]	7.2	9.0	11.1
mini prism cube compr [MPa]	57.1	68.3	86.8
mini prism cube compr [MPa]	55.8	68.8	87.3

cube split [MPa]

time prisms:

prism bending tensile str [MPa]

mini prism cube compr [MPa]

mini prism cube compr [MPa]



temperatures

room

22.4 °C

aggregates

- °C

cement + fly-ash

- °C

water

23.1 °C

fresh concrete directly after mixing

27.7 °C

mixing procedure

aggregates + cement + fly-ash

30 sec

add 90% of water

60

add 10% of water + plastic then

90

scraping of mixer then

30

210 sec

*used the Eirich
mixer*workability /
rheologyslump flow [mm] / τ_o [Pa]

640

3.6

at t = 0:05 h:min

slump time T50 [sec]

11

video

slump flow [mm] / τ_o [Pa]

570

6.5

at t = 0:10 h:min

slump flow [mm] / τ_o [Pa]

610

4.6

00:15 h:min

slump #1 [mm] / τ_o [Pa]

185

Mueller M3

307

at t = 00:45 h:min

slump #2 [mm] / τ_o [Pa]

n.a.

at t = 01:00 h:min

slump #3 [mm] / τ_o [Pa]

n.a.

at t = 01:18 h:min

batch**11 (continued)**

general remarks
about the mixture:

Very workable mixture

placing

*not entirely self levelling
some compaction
necessary*

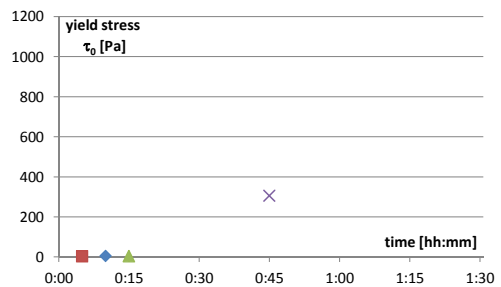


Figure: Development of yield stress in time
based on the slump (flow) tests

video of placing
placing time

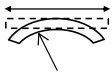
mould 1 filled at	0:05	h:min
mould 2 filled at	0:10	h:min
mould 3 filled at	0:14	h:min
mould 4 filled at	0:16	h:min

video of deformation
deformation



mould 1 deformed at	0:50	h:min	0:30 later than batch 10
mould 2 deformed at	1:00	h:min	0:26 later than batch 10
mould 3 deformed at	1:16	h:min	0:25 later than batch 10
mould 4 deformed at	n.a.	h:min	

geometry



	mould 1	mould 2	mould 3	mould 4	
specimen length	800	800	800	800	mm
specimen width	400	400	400	400	mm
specimen height	50	50	50	50	mm
radius Rx	1.5	1.5	1.5	∞	m
radius Ry	∞	∞	∞	∞	m

hardening

demoulding

inspection date

October 23, 2012

description of the batch

The percentage of plasticiser was reduced to .65%, to avoid the segregation observed during the previous mixture. The mixture was workable, self compacting, non-segregating but not entirely self-levelling. It was easy to place and a little bit of compaction was necessary. So, it was quite consistent with the previous mix. We didnt have enough concrete, strangely, to fill all sump cones and cubes.

The deformation of all the moulds were smooth. However surface cracks were visible immediatley after deformation.

The elements had a good finish, except for some air bubbles and blobs of concrete sticking out due to the deterioration of the moulds. The cast surface had shrinkage cracks perpendicular to the direction of deformation, as observed immediately after deformation.

batch**12**

casting date

October 30, 2012

start mixing

10:30

mixture recipe
(per 1000 ltr)

sand 0.125-0.25 mm

48 kg

sand 0.25-0.5 mm

128 kg

sand 0.5-1.0 mm

209 kg

gravel 1-2 mm

289 kg

gravel 2-4 mm

462 kg

gravel 4-8 mm

561 kg

CEM I 52,5 R**400 kg**

Fly-ash

160 kg

Superplast Chryso Premia 196

3.64 kg (0.65% of pwd)

water**172 kg**

specific mass

2433 kg/m³

wcf

0.430

wpcf

0.307

batch volume

80 ltr

strength



time cubes:

	1 day	7 day	28 day
	Oct 31	Nov 06	Nov 27
cube compr [MPa]	15:20	11:45	11:42
cube split [MPa]	45.4	65.69	75.4
	3.7	3.91	5.5

cube compr [MPa]

cube split [MPa]

time prisms:



prism bending tensile str [MPa]

mini prism cube compr [MPa]

mini prism cube compr [MPa]

temperatures

room

- °C

aggregates

- °C

cement + fly-ash

21.4 °C

water

22.3 °C

fresh concrete directly after mixing

25.3 °C

mixing procedure



aggregates + cement + fly-ash

30 sec

add 90% of water

60

add 10% of water + plastic then

90

scraping of mixer then

30

210 sec

*used the Eirich
mixer*workability /
rheologyslump flow [mm] / τ_o [Pa]

650

3.5

at t = 0:08 h:min

slump time T50 [sec]

10

Mueller M3

slump #1 [mm] / τ_o [Pa]

220

194

at t = 00:31 h:min

slump #2 [mm] / τ_o [Pa]

165

394

at t = 00:45 h:min

slump #3 [mm] / τ_o [Pa]

180

340

at t = 00:59 h:min

batch**12 (continued)**

general remarks
about the mixture:

Very workable mixture

placing

*cubes & prisms were
compacted using
vibration table*

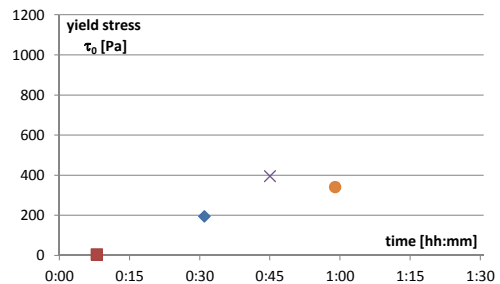


Figure: Development of yield stress in time
based on the slump (flow) tests

video of placing
placing time

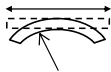
mould 1 filled at	00:12	h:min
mould 2 filled at	00:17	h:min
mould 3 filled at	00:19	h:min
mould 4 filled at	00:20	h:min

video of deformation
deformation



mould 1 deformed at	00:36	h:min
mould 2 deformed at	00:48	h:min
mould 3 deformed at	01:00	h:min
mould 4 deformed at	n.a.	h:min

geometry



	mould 1	mould 2	mould 3	mould 4	
specimen length	800	800	800	800	mm
specimen width	400	400	400	400	mm
specimen height	25	25	25	25	mm
radius Rx	1.5	1.5	1.5	∞	m
radius Ry	∞	∞	∞	∞	m

hardening

demoulding

inspection date

October 23, 2012

description of the batch

First series of 25mm thick elements. The exact mixture proportions as batch 11 was prepared. It was consistent with the previous mix- very workable, self- compacting but not entirely self leveling. The moulds were placed in reverse order, as the actuators were adjusted for deformation for moulds 2,3 and 4. Mould 1 was meant to be flat. Placement was easy. It was difficult to get uniform thickness of 25mm within the moulds of thickness 50mm. The moulds were covered with foil immediately after placing. No visible cracks were noticed immediately after deformation. It could be due to the effect of the foil, or because the strain caused by deformation for a thickness of 25mm panel is half of that for 50mm panel. Additional weights had to be placed on the moulds to get uniform curvature. The third slump cone collapsed while releasing the cone.

The elements had a smooth finish except for the effects of the deteriorated mould. No cracks visible.

batch**13**

casting date

October 31, 2012

start mixing

13:00

mixture recipe
(per 1000 ltr)

sand 0.125-0.25 mm

48 kg

sand 0.25-0.5 mm

128 kg

sand 0.5-1.0 mm

209 kg

gravel 1-2 mm

289 kg

gravel 2-4 mm

462 kg

gravel 4-8 mm

561 kg

CEM I 52,5 R**400 kg**

Fly-ash

160 kg

Superplast Chryso Premia 196

3.64 kg (0.65% of pwd)

water**172 kg**

specific mass

2433 kg/m³

wcf

0.430

wpcf

0.307

batch volume

80 ltr

strength



time cubes:

	1 day	7 day	28 day
	Nov 01	Nov 07	Nov 28
cube compr [MPa]	13:00	15:45	14:34
cube split [MPa]	42.9	73.8	83.9
	3.5	3.8	4.9
time prisms:	13:15	15:15	15:00
prism bending tensile str [MPa]	8.0	9.8	9.5
mini prism cube compr [MPa]	41.2	68.2	88.8
mini prism cube compr [MPa]	41.6	68.6	83.6

cube compr [MPa]

cube split [MPa]

time prisms:



prism bending tensile str [MPa]

mini prism cube compr [MPa]

mini prism cube compr [MPa]

temperatures

room

- °C

aggregates

- °C

cement + fly-ash

19.6 °C

water

20.6 °C

fresh concrete directly after mixing

22.9 °C

mixing procedure



aggregates + cement + fly-ash

30 sec

add 90% of water

60

add 10% of water + plastic then

90

scraping of mixer then

30

210 sec

*used the Eirich
mixer*workability /
rheologyslump flow [mm] / τ_o [Pa]

610

4.8

at t = 00:05 h:min

slump time T50 [sec]

Mueller M3

slump #1 [mm] / τ_o [Pa]

240

121

at t = 00:30 h:min

slump #2 [mm] / τ_o [Pa]

190

303

at t = 00:45 h:min

slump #3 [mm] / τ_o [Pa]

150

449

at t = 00:58 h:min

batch

13 (continued)

general remarks
about the mixture:

workable mixture

placing

reverse order
(mould 4 -> 1)

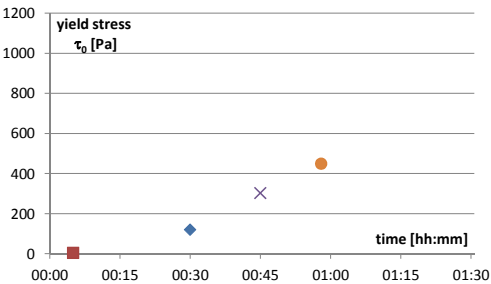


Figure: Development of yield stress in time based on the slump (flow) tests

video of placing
placing time

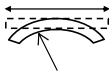
mould 1 filled at	00:30	h:min
mould 2 filled at	00:14	h:min
mould 3 filled at	00:17	h:min
mould 4 filled at	00:18	h:min

video of deformation
deformation



mould 1 deformed at	-	h:min
mould 2 deformed at	01:02	h:min
mould 3 deformed at	00:47	h:min
mould 4 deformed at	00:34	h:min

geometry



	mould 1	mould 2	mould 3	mould 4	
specimen length	800	800	800	800	mm
specimen width	400	400	400	400	mm
specimen height	25	25	25	25	mm
radius Rx	∞	-1.5	-1.5	-1.5	m
radius Ry	∞	∞	∞	∞	m

hardening

demoulding

inspection date

description of the batch

The first series of single curved negative curvature elements (thickness 25mm). The mixture was prepared with the same proportion as the previous one. The result was similar, though the slump flow was slightly lesser than the previous ones. Nevertheless, the workability was consistent. The placing was in reverse order as the last one. The moulds were covered with foil immediately after placing. No cracks seen after deformation. Additional weights had to be placed on the moulds to get uniform curvature. The third slump cone collapsed while releasing the cone.

The elements had a smooth finish except for the effects of the deteriorated mould. No cracks visible.

batch**14**

casting date

November 6, 2012

start mixing

09:00

mixture recipe
(per 1000 ltr)

sand 0.125-0.25 mm

48 kg

sand 0.25-0.5 mm

129 kg

sand 0.5-1.0 mm

209 kg

gravel 1-2 mm

290 kg

gravel 2-4 mm

373 kg

gravel 4-8 mm

562 kg

CEM I 52,5 R**400 kg**

Fly-ash

160 kg

Superplast Chryso Premia 196

3.92 kg

(0.70% of pwd)

water**172 kg**

specific mass

2348 kg/m³

wcf

0.430

wpcf

0.307

batch volume

107 ltr

strength



time cubes:

	1 day	7 day	28 day
	Nov 07	Nov 13	Dec 04
cube compr [MPa]	15:54	11:07	-
cube split [MPa]	51.1	70.6	-
time prisms:	15:20	11:35	15:38
prism bending tensile str [MPa]	7.5	9.3	10.6
mini prism cube compr [MPa]	50.7	75.9	84.5
mini prism cube compr [MPa]	48.3	78.5	82.5

cube compr [MPa]

15:54

11:07

-

cube split [MPa]

51.1

70.6

-

time prisms:

15:20

11:35

15:38



prism bending tensile str [MPa]

7.5

9.3

10.6

mini prism cube compr [MPa]

50.7

75.9

84.5

mini prism cube compr [MPa]

48.3

78.5

82.5

temperatures

room

- °C

aggregates

- °C

cement + fly-ash

22.4 °C

water

21.5 °C

fresh concrete directly after mixing

25.8 °C

mixing procedure



aggregates + cement + fly-ash

30 sec

used the Eirich

add 90% of water

60

mixer

add 10% of water + plastic then

90

scraping of mixer then

30

210 sec

workability /
rheologyslump flow [mm] / τ_o [Pa]

750

1.6

at t = 0:02 h:min

slump time T50 [sec]

3.75

slump flow [mm] / τ_o [Pa]

415

31.6

at t = 0:31 h:min

slump #1 [mm] / τ_o [Pa]

235

132

at t = 0:31 h:min

slump #2 [mm] / τ_o [Pa]

180

325

at t = 0:46 h:min

slump #3 [mm] / τ_o [Pa]

35

836

at t = 1:01 h:min

Mueller M3

batch

14 (continued)

general remarks
about the mixture:

very workable mixture

placing

reverse order
(mould 4 -> 1)

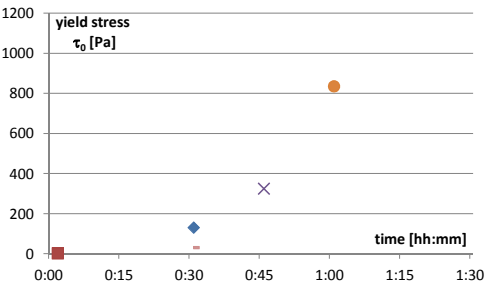


Figure: Development of yield stress in time based on the slump (flow) tests

video of placing
placing time

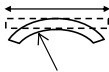
mould 1 filled at	0:26	h:min
mould 2 filled at	0:24	h:min
mould 3 filled at	0:20	h:min
mould 4 filled at	0:15	h:min

video of deformation
deformation



mould 1 deformed at	-	h:min
mould 2 deformed at	1:07	h:min
mould 3 deformed at	0:48	h:min
mould 4 deformed at	0:35	h:min

geometry



	mould 1	mould 2	mould 3	mould 4	
specimen length	800	800	800	800	mm
specimen width	400	400	400	400	mm
specimen height	50	50	50	50	mm
radius Rx	∞	-1.5	-1.5	-1.5	m
radius Ry	∞	∞	∞	∞	m

hardening

demoulding

inspection date

description of the batch

The proportion of the plasticiser was increased to 0.70%. The fluidity slightly increased, resulting in a slump flow of 700-800. The placing was in same order as the last one. The moulds were covered with foil immediately after placing. No cracks seen after deformation. 2 new slump cones are being used from this test onwards. The smaller slump cone is also being used.

The elements had a smooth finish except for the effects of the deteriorated mould. No cracks visible.

batch**15**

casting date

November 7, 2012

start mixing

13:00

mixture recipe
(per 1000 ltr)

sand 0.125-0.25 mm

48 kg

sand 0.25-0.5 mm

129 kg

sand 0.5-1.0 mm

209 kg

gravel 1-2 mm

291 kg

gravel 2-4 mm

373 kg

gravel 4-8 mm

564 kg

CEM I 52,5 R**400 kg**

Fly-ash

160 kg

Superplast Chryso Premia 196

3.92 kg (0.70% of pwd)

water**172 kg**

specific mass

2351 kg/m³

wcf

0.430

wpcf

0.307

batch volume

107.04 ltr

1000

strength



time cubes:

10:30

cube compr [MPa]

40.4

cube split [MPa]

3.3

time prisms:

11:05



prism bending tensile str [MPa]

5.6

mini prism cube compr [MPa]

36.4

mini prism cube compr [MPa]

37.6

temperatures

room

- °C

aggregates

- °C

cement + fly-ash

22.2 °C

water

20.8 °C

fresh concrete directly after mixing

25.6 °C

mixing procedure



aggregates + cement + fly-ash

30 sec

add 90% of water

60

add 10% of water + plastic then

90

scraping of mixer then

30

210 sec

*used the Eirich
mixer*workability /
rheologyslump flow [mm] / τ_o [Pa]

715

2.1

at t = 0:03 h:min

slump time T50 [sec]

-

Mueller M3

slump #1 [mm] / τ_o [Pa]

190

291

at t = 0:29 h:min

slump #2 [mm] / τ_o [Pa]

160

396

at t = 0:43 h:min

slump #3 [mm] / τ_o [Pa]

20

890

at t = 1:03 h:min

batch

15 (continued)

general remarks
about the mixture:

placing

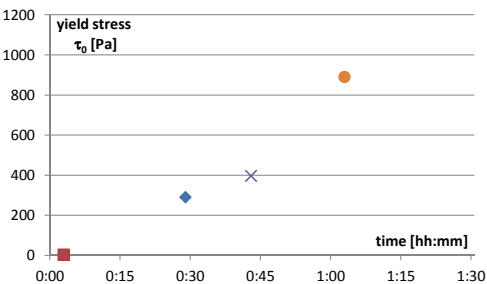


Figure: Development of yield stress in time based on the slump (flow) tests

video of placing
placing time

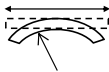
mould 1 filled at	h:min
mould 2 filled at	h:min
mould 3 filled at	h:min
mould 4 filled at	h:min

video of deformation
deformation



mould 1 deformed at	-	h:min
mould 2 deformed at	0:35	h:min
mould 3 deformed at	0:50	h:min
mould 4 deformed at	01:07	h:min

geometry



	mould 1	mould 2	mould 3	mould 4	
specimen length	800	800	800	800	mm
specimen width	400	400	400	400	mm
specimen height	50	50	50	50	mm
radius Rx	∞	-2.5	-1.5	-1.5	m
radius Ry	∞	-2.5	∞	∞	m

hardening

demoulding

inspection date

description of the batch

Prof. Vambersky and a student from Eindhoven were here to see the process. A first double curved element is tried. Mould 3 and 4 retain the same actuator position as the previous test. Mould 2 is adjusted to have a negative double curved panel of radius 2.5m (1.5m was tried out with just weights, which did not seem to work with the current width and stiffness of the lathes). The mixture proportions were exactly same as the previous test. It proved consistent with the previous one. All the moulds were filled within 20 minutes. The moulds were deformed starting from 2 and then till 4. The deformation of mould 2 was smooth. Additional weights were put in place as planned, though in the second row the mould still didnt touch the actuators at most places. There was a problem while deforming mould 3, the central actuator was not in place. So the deformation had disturbances many times before the problem was fixed. The deformation of mould 4 was smooth.

All elements were smooth except for the effects of the deterioration of the moulds. It was decided to make new moulds after this series.

batch**16**

casting date

November 27, 2012

start mixing

09:00

mixture recipe
(per 1000 ltr)

sand 0.125-0.25 mm

48 kg

sand 0.25-0.5 mm

129 kg

sand 0.5-1.0 mm

209 kg

gravel 1-2 mm

291 kg

gravel 2-4 mm

373 kg

gravel 4-8 mm

564 kg

CEM I 52,5 R**400 kg**

Fly-ash

160 kg

Superplast Chryso Premia 196

3.92 kg (0.70% of pwd)

water**172 kg**

specific mass

2351 kg/m³

wcf

0.430

wpcf

0.307

batch volume

107.04 ltr

1000

strength



time cubes:

	1 day	36 day	36 day
	Nov 28	Jan 02	Jan 02
cube compr [MPa]	14:39	09:19	09:26
cube split [MPa]	51.6	81.56	85.25
	3.3	3	5.77

cube compr [MPa]

cube split [MPa]

time prisms:

15:05 10:36 10:38



prism bending tensile str [MPa]

7.6 12.9 11.81

mini prism cube compr [MPa]

48.1 86.3 70.8

mini prism cube compr [MPa]

48.1 74.8 97.4

temperatures

room

- °C

aggregates

- °C

cement + fly-ash

22.3 °C

water

21.0 °C

fresh concrete directly after mixing

24.9 °C

mixing procedure



aggregates + cement + fly-ash

30 sec

add 90% of water

60

add 10% of water + plastic then

90

scraping of mixer then

30

210 sec

*used the Eirich
mixer*workability /
rheologyslump flow [mm] / τ_o [Pa]

730

1.9

at t = 0:09 h:min

slump time T50 [sec]

5

Mueller M3

slump #1 [mm] / τ_o [Pa]

170

361

at t = 0:45 h:min

slump #2 [mm] / τ_o [Pa]

40

819

at t = 1:01 h:min

slump #3 [mm] / τ_o [Pa]

190

291

at t = 1:15 h:min

batch**16 (continued)**

general remarks
about the mixture:

placing

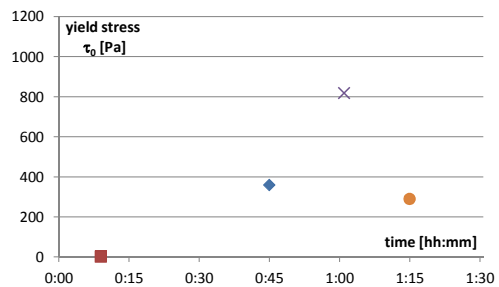


Figure: Development of yield stress in time
based on the slump (flow) tests

video of placing
placing time

mould 1 filled at	0:30	h:min
mould 2 filled at	0:25	h:min
mould 3 filled at	0:18	h:min
mould 4 filled at	0:14	h:min

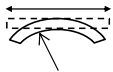
video of deformation
deformation



mould 1 deformed at	-	h:min
mould 2 deformed at	1:17	h:min
mould 3 deformed at	1:03	h:min
mould 4 deformed at	0:48	h:min

general problem with 2nd and 3rd rows

geometry



	mould 1	mould 2	mould 3	mould 4	
specimen length	800	800	800	800	mm
specimen width	400	400	400	400	mm
specimen height	50	50	50	50	mm
radius Rx	∞	-2.5	-2.5	-2.5	m
radius Ry	∞	-2.5	-2.5	-2.5	m

hardening

demoulding

inspection date

November 30, 2012

description of the batch

The first series of double curved elements and with new moulds. The new moulds consist of 3 moulds of silicone finish surface and 1 of polyurethane finish surface. The polyurethane mould was used for the flat elements. The mixture is prepared with same proportions as previous batch. The mixture is consistent with the previous results, though it stiffens faster. The polyurethane mould is oiled, to facilitate easy release. The moulds are placed in reverse order. The side pieces of the polyurethane mould started bulging out while placing the concrete, because the silicone sealant doesn't stick to polyurethane. Additional weights are placed along the edges to prevent it from bulging out. The deformation is also done in reverse order. The mould 4 has problems during deformation because one actuator which had come off the mdf top base. The deformation is smooth after that is fixed in place. However, the mould still didn't touch the actuators of second and third rows at most places. The third slump cone collapses during the test. The elements have a good shiny reflective finish. The polyurethane mould though gives a less glossy finish which appears to become lesser over time. The reflection of the lathes is visible over the surface. The elements have few air bubbles. The edges of the elements are straighter than the ones cast with the old moulds.

batch**17**

casting date

November 28, 2012

start mixing

12:30

mixture recipe
(per 1000 ltr)

sand 0.125-0.25 mm

48 kg

sand 0.25-0.5 mm

128 kg

sand 0.5-1.0 mm

209 kg

gravel 1-2 mm

289 kg

gravel 2-4 mm

462 kg

gravel 4-8 mm

561 kg

CEM I 52,5 R**400 kg**

Fly-ash

160 kg

Superplast Chryso Premia 196

3.92 kg (0.70% of pwd)

water**172 kg**

specific mass

2433 kg/m³

wcf

0.430

wpcf

0.307

batch volume

80 ltr

1000

strength



time cubes:

	1 day	35 day	35 day
	Nov 29	Jan 02	Jan 02
cube compr [MPa]	48.3	80.13	error
cube split [MPa]	3.5	5.04	5.81
time prisms:		10:46	10:48
prism bending tensile str [MPa]	7.1	10.2	10.35
mini prism cube compr [MPa]	37.3	92.9	92.6
mini prism cube compr [MPa]	47.8	91.6	82.2

cube compr [MPa]

cube split [MPa]

time prisms:



prism bending tensile str [MPa]

mini prism cube compr [MPa]

mini prism cube compr [MPa]

temperatures

room

- °C

aggregates

- °C

cement + fly-ash

22.1 °C

water

20.5 °C

fresh concrete directly after mixing

25.1 °C

mixing procedure



aggregates + cement + fly-ash

30 sec

add 90% of water

60

add 10% of water + plastic then

90

scraping of mixer then

30

210 sec

*used the Eirich
mixer*workability /
rheologyslump flow [mm] / τ_o [Pa]

685

2.7

at t = 0:10 h:min

slump time T50 [sec]

5.1

Mueller M3

slump #1 [mm] / τ_o [Pa]

215

212

at t = 0:30 h:min

slump #2 [mm] / τ_o [Pa]

175

358

at t = 0:46 h:min

slump #3 [mm] / τ_o [Pa]

85

686

at t = 0:59 h:min

batch

17 (continued)

general remarks
about the mixture:

placing

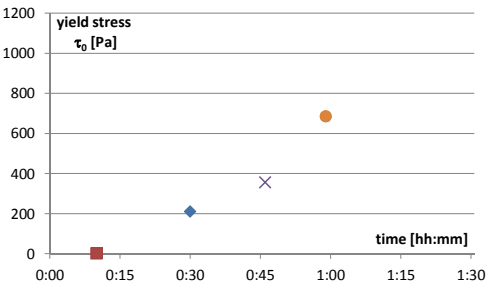


Figure: Development of yield stress in time based on the slump (flow) tests

video of placing
placing time

mould 1 filled at	0:21	h:min
mould 2 filled at	0:19	h:min
mould 3 filled at	0:16	h:min
mould 4 filled at	0:12	h:min

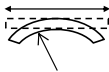
video of deformation
deformation



mould 1 deformed at	-	h:min
mould 2 deformed at	1:02	h:min
mould 3 deformed at	0:49	h:min
mould 4 deformed at	0:32	h:min

general problem with 2nd and 3rd rows

geometry



	mould 1	mould 2	mould 3	mould 4	
specimen length	800	800	800	800	mm
specimen width	400	400	400	400	mm
specimen height	25	25	25	25	mm
radius Rx	∞	-2.5	-2.5	-2.5	m
radius Ry	∞	-2.5	-2.5	-2.5	m

hardening

demoulding

inspection date

November 30, 2012

description of the batch

25mm thick double curved elements. The polyurethane mould is assembled again just 1.5 hours before the casting and weights are placed on the sides to prevent bulging. The mixture is prepared with same proportions as for the previous batch. The mixture is consistent with the previous results. All the moulds are oiled this time. The moulds are placed in reverse order. The deformation is also done in reverse order. All deformations are smooth this time. However, the mould still didnt touch the actuators of second and third rows at most places.

The elements have a good sniny reflective finish, slightly lesser than the previous batch. The polyurethane mould element has a less glossy finish. The reflection of the lathes is visible over the surface. The elements have few air bubbles. The edges of the elements are straigter than the ones cast with the old moulds.

batch**18**

casting date
start mixing

December 11, 2012
12:30

mixture recipe
(per 1000 ltr)

sand 0.125-0.25 mm	233 kg	
sand 0.25-0.5 mm	414 kg	
sand 0.5-1.0 mm	647 kg	
CEM I 52,5 R	570 kg	
Fly-ash	100 kg	
Betoflow D	100 kg	
Superplast Chryso Premia 196	4.56 kg	(0.59% of pwd)
water	225 kg	
wcf	0.395	
wpf	0.292	
specific mass	2293 kg/m ³	

mixture m₄

batch volume

107 ltr

strength



time cubes:

cube compr [MPa]

cube split [MPa]

time prisms:



prism bending tensile str [MPa]

mini prism cube compr [MPa]

mini prism cube compr [MPa]

1 day	3 day	28 day
Dec 12	Dec 14	Jan 08

48.3 58.23 90.4

3.5 4.03 5.2

7.1 7.3 10.6

37.3 55.3 88.6

47.8 59.1 90.7

temperatures

room

- °C

aggregates

- °C

cement + fly-ash

19.2 °C

water

19.8 °C

fresh concrete directly after mixing

- °C

mixing procedure



aggregates + cement + fly-ash

30 sec

add 90% of water

60

add 10% of water + plastic then

90

scraping of mixer then

30

210 sec

used the Eirich 08:35

mixer

workability /
rheology



slump flow [mm] / τ_o [Pa]

865

0.79

at t = 0:06 h:min

slump time T50 [sec]

3

mini-slump flow / τ_o

280

0.60

at t = 0:06 h:min

Mueller M3

(mini-slump 5 mm)



slump flow [mm] / τ_o [Pa]

650

3.28

at t = 0:24 h:min

slump flow [mm] / τ_o [Pa]

620

4.15

at t = 0:42 h:min

slump #3 [mm] / τ_o [Pa]

50

763

at t = 1:05 h:min

(mini-slump 0 mm)

batch

18 (continued)

general remarks
about the mixture:

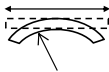
placing

video of placing
placing time

video of deformation
deformation



geometry



hardening

demoulding

inspection date

mould 1 filled at
mould 2 filled at
mould 3 filled at
mould 4 filled at

mould 1 deformed at
mould 2 deformed at
mould 3 deformed at
mould 4 deformed at

specimen length
specimen width
specimen height
radius Rx
radius Ry

November 30, 2012

description of the batch

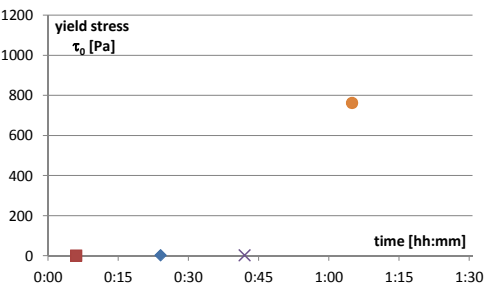


Figure: Development of yield stress in time
based on the slump (flow) tests

0:21 h:min
0:19 h:min
0:17 h:min
0:12 h:min

n.a. h:min
0:59 h:min
0:45 h:min
0:42 h:min

mould 1	mould 2	mould 3	mould 4	
800	800	800	800	mm
400	400	400	400	mm
50	50	25	25	mm
∞	-1.5	-2.5	-2.5	m
∞	∞	-2.5	-2.5	m

Appendix G

Set-up of BML Viscometer

Hardware revision and test parameters

By continuously registering the torque moment that the rotating concrete cylinder applies to the internal sensor cylinder ('beater'), the shear force in the fresh concrete mixture can be determined. The parameters that can be determined are the yield strength τ_0 and the plastic viscosity μ from the Bingham-equation 8.1 on page 126. Furthermore, the development of the yield strength in time can be measured, which says something about the thixotropy of the mixtures. By varying the rotation speed, a graph can be created in which the measured torque value is plotted against the rotation speed. By interpolating the data-points found at several shear rates, a line can be constructed that crosses the vertical axis at a value G , which value can be converted to the yield strength τ_0 . The inclination of the interpolation line H can be converted to the plastic viscosity μ . The conversion from G and H to τ_0 and μ is done with the use of kinematic and constitutive equations that describe the shear stress and shear speed distribution in the cylinder as a function of the geometry of the cylinders and the rotation speed. These equations are based on the Reiner-Rivling equation; this method is described in detail in Wallevik (2000, 2005).

For the purpose of the present research, the original machine was improved mechanically by replacing the old bearings, which showed significant corrosion. Furthermore the digital hardware of the BML needed repair and was connected to an up-to-date measuring card for the PC. The torque and rotation speed were recalibrated after this thorough mechanic and electronic revision. The new hardware had the disadvantage that the original control-software FreshWin for Windows 4.0, written by the manufacturer ConTec of the viscometer, could no longer be used, due to compatibility issues. As replacement of FreshWin, a custom measurement script was written in LUA, a script language for use within MP3, the new measurement control software. The mechanical and electronic revision and scripting was carried out by Stevin-lab technician Fred Schilperoort. The definition of the functionality of the scripts as well as post-processing of the measurement data in Excel was done by

Table G.1: Experimental set-up ConTec BML Viscometer

parameter	value
radius inner cylinder r_i [mm]	120
radius outer cylinder r_o [mm]	175
height inner cylinder h [mm]	200
max. rotation velocity [rps]	0.389
min. rotation velocity [rps]	0.026
number of measuring points	8
number of points per measurement	50 – 70
transient interval [s]	5 – 7
sampling rate [1/s]	10

the author. The parameters shown in Table G.1 were used during the measurements. A test measurement was carried out and is described below.

Test measurement

Wallevik and Wallevik (2011) suggest that typical Dutch SCC has a yield stress $\tau_0 \leq 10$ Pa and a plastic viscosity of around $\mu \approx 80$ Pa · s. A conventional (non self-compacting) concrete will have a yield stress in the range $500 \leq \tau_0 \leq 1000$ Pa, so an order of magnitude higher. This was compared to what was found in the present research for mixture m_3 . The procedure of post-processing the measuring data is shown in Figure G.1 on the facing page. It shows the linear regression of the marked data points in the torque measurement of mixture m_3 , measured briefly after mixing, so without setting time and without development of yield strength as a result of thixotropy. The regression results in $G = -0.22$ N · m and a $H = 12.8$ N · m · sec. Using the Reiner-Rivling equations G.1 and G.2, and filling in the correct geometrical properties of this specific BML container and beater, the following yield value τ_0 and plastic shear viscosity μ were found in the test run:

$$\begin{aligned} \tau_0 &= \frac{G}{4\pi h} \left(\frac{1}{r_i^2} - \frac{1}{r_o^2} \right) \frac{1}{\ln(r_o/r_i)} = \\ &= \frac{-0.22}{4\pi \cdot 0.200} \left(\frac{1}{0.120^2} - \frac{1}{0.175^2} \right) \frac{1}{\ln(0.175/0.120)} = -0.22 \times 38.8 = -8.5 \text{ Pa} \quad (\text{G.1}) \end{aligned}$$

$$\mu = \frac{H}{8\pi^2 h} \left(\frac{1}{r_i^2} - \frac{1}{r_o^2} \right) = \frac{12.8}{8\pi^2 \cdot 0.200} \left(\frac{1}{0.120^2} - \frac{1}{0.175^2} \right) = 12.8 \times 2.33 = 29.8 \text{ Pa} \cdot \text{s}. \quad (\text{G.2})$$

The negative yield value physically makes no sense and is due to the inaccuracies

of the combination translating a measured torque value to an assumed shear distribution and from this calculating the yield value. Using the same BML as in the present research, Grünewald (2004) also found negative yield values. In that research, for a series of 9 reference SCC's, yield values were measured between (rounded) -38 Pa and $+31 \text{ Pa}$ and plastic viscosities between $58 \text{ Pa} \cdot \text{s}$ and $98 \text{ Pa} \cdot \text{s}$.

From the measurements it can be concluded that the tested mixture shows little or no yield value, which means that without horizontal support the mixture can not stand in a column, like in a slump cone. The plastic viscosity is somewhat lower than expected. It was concluded that the BML viscometer can be used for the present research.

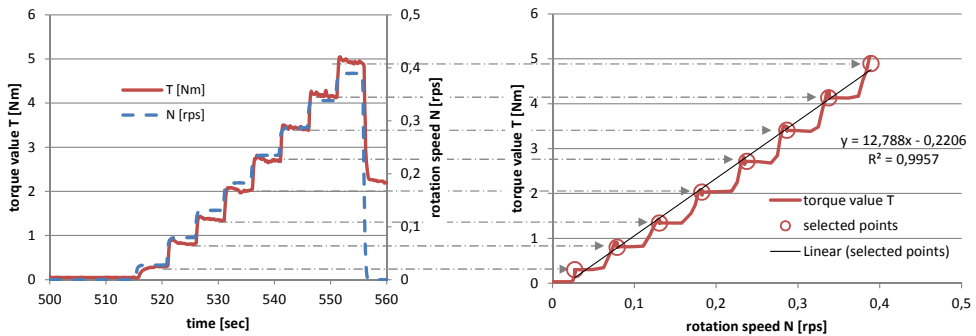


Figure G.1: Example of the interpretation of BML measurement data for a fresh SCC-mixture: in the left graph the measured torque value T is plotted on the left vertical axis against the time on the horizontal axis. It can be seen that after stepwise increase of rotation speed (dashed blue line), also the measured torque value (red drawn line) increases more or less stepwise: after each speed step-up the torque value initially shows a small peak, but then lowers to an equilibrium value, showing as 'plateaus' in the left graph. In the right hand graph then T is plotted again, but now against rotation speed N . The red circled points are selected from the plateaus in the left graph, each representing an equilibrium combination of N and T . By interpolating the points, the slope of the regression line graph can be determined, representing the H -value; the point where it crosses the vertical axis represents the G -value.

Appendix H

Brief review of theory of elasticity and plasticity

Kinematic relations analogue for solids and fluids

The kinematic equations used both in fluid and solid mechanics will be reviewed briefly here to show the analogy and differences between fluids and solids.

To describe the deformation of a volume of material, the same kinematic equations can be used both for solids and for fluids. Figure H.1 depicts the displacement of two points A and B in a deformable body or fluid volume between two moments in time $t = 0$ and $t = t_1$. The points A and B follow distinct paths of motion, not necessarily in a straight line. During this motion also the distance between the points may change. This illustrates that the spatial gradient of the displacement will not be zero during deformations. This is described as *strain*. The displacement vector \underline{u} is a function different for each coordinate location in the body (x, y, z) and possibly also different for each moment in time t and can be denoted as

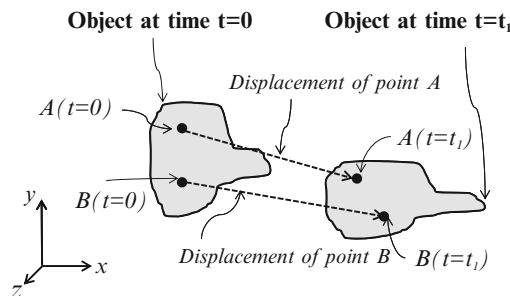


Figure H.1: Depiction of two points A and B in a deformable body, taken from Allen (2013)

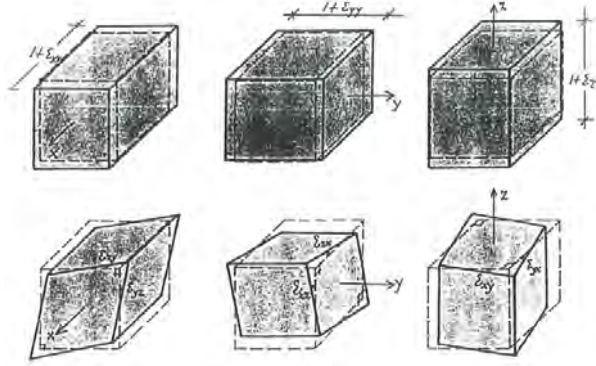


Figure H.2: Strains in six directions, sketches taken from Blaauwendraad (1984)

$$\underline{u} = \begin{pmatrix} u_x(x, y, z, t) \\ u_y(x, y, z, t) \\ u_z(x, y, z, t) \end{pmatrix}. \quad (\text{H.1})$$

The following definition of strains in a volume of material, both applicable for fluids and solids, are common (see Figure H.2):

$$\epsilon_{xx} = \frac{\partial u_x}{\partial x}, \epsilon_{yy} = \frac{\partial u_y}{\partial y}, \epsilon_{zz} = \frac{\partial u_z}{\partial z},$$

$$\epsilon_{xy} = \frac{1}{2} \left(\frac{\partial u_x}{\partial x} + \frac{\partial u_y}{\partial y} \right), \epsilon_{xz} = \frac{1}{2} \left(\frac{\partial u_x}{\partial x} + \frac{\partial u_z}{\partial z} \right), \epsilon_{yz} = \frac{1}{2} \left(\frac{\partial u_y}{\partial y} + \frac{\partial u_z}{\partial z} \right), \quad (\text{H.2})$$

in which ϵ_{xx} , ϵ_{yy} and ϵ_{zz} are the three normal strains in the three perpendicular directions and ϵ_{xy} , ϵ_{xz} and ϵ_{yz} are the three shear deformations leading to change of the 90° angles between the faces of the volume. The shear deformations are often denoted as total shear strains

$$\gamma_{xy} = 2\epsilon_{xy}, \gamma_{xz} = 2\epsilon_{xz}, \gamma_{yz} = 2\epsilon_{yz}. \quad (\text{H.3})$$

Both for solids and fluids, the strains can be split in a part that describes the *volume change*

$$\epsilon_0 = \frac{1}{3}(\epsilon_{xx} + \epsilon_{yy} + \epsilon_{zz}) \text{ or the isotropic strain } e = \epsilon_{xx} + \epsilon_{yy} + \epsilon_{zz} = 3\epsilon_0 \quad (\text{H.4})$$

and six parts that describes the *shape change*, known as the *deviator strains*

$$e_{xx} = \epsilon_{xx} - \epsilon_0, e_{yy} = \epsilon_{yy} - \epsilon_0, e_{zz} = \epsilon_{zz} - \epsilon_0, \gamma_{xy}, \gamma_{xz} \text{ and } \gamma_{yz}. \quad (\text{H.5})$$

This splitting in parts describing volume change and shape change has advantages in the further description of the relation between strains and stresses in the materials (Blaauwendraad, 1984), as will be shown below. The relation between deformation and stresses in a material are formed by the *constitutive* equations. On this point fluids and solids have both similarities and differences in their behaviour, so first the constitutive relations will now be described for solids.

Constitutive relations for solids

In many elastic solid materials, Hooke's law is applicable, describing a linear relation between isotropic stress and isotropic strain:

$$e = \frac{\sigma_0}{K}. \quad (\text{H.6})$$

In Hooke's law σ_0 is the isotropic stress in the material and K is the compression modulus, a material constant defined as

$$K = \frac{E}{3(1-2\nu)}. \quad (\text{H.7})$$

and in which E and ν are material properties. Similar relations can be given between deviator strains and deviator stresses:

$$e_{xx} = \frac{1}{2G}\sigma_{xx}, e_{yy} = \frac{1}{2G}\sigma_{yy} \text{ and } e_{zz} = \frac{1}{2G}\sigma_{zz} \quad (\text{H.8})$$

for the deviator normal stresses, and

$$\gamma = \frac{1}{G}\sigma_{yz}, \gamma_{zx} = \frac{1}{G}\sigma_{zx} \text{ and } \gamma_{xy} = \frac{1}{G}\sigma_{xy} \quad (\text{H.9})$$

for the deviator shear stresses, in which G is the shear modulus, defined as

$$G = \frac{E}{2(1+\nu)}. \quad (\text{H.10})$$

A different notation for the same constitutive equations is the Lamé-notation (Blaauwendraad, 1984):

$$\begin{aligned} \sigma_{xx} &= \lambda e + 2\mu\epsilon_{xx} & \sigma_{yz} &= 2\mu\epsilon_{yz} \\ \sigma_{yy} &= \lambda e + 2\mu\epsilon_{yy} & \sigma_{zx} &= 2\mu\epsilon_{zx} \\ \sigma_{zz} &= \lambda e + 2\mu\epsilon_{zz} & \sigma_{xy} &= 2\mu\epsilon_{xy} \end{aligned} \quad (\text{H.11})$$

where the Lamé-constants $\lambda = K - \frac{2}{3}G$ and $\mu = G$.

Constitutive relations for fluids

Under compression fluids and solids behave quite similar, although obviously under tension a fluid can only support a small amount of stress, depending on its molecular cohesion (Kundu and Cohen, 2008).

If the cause of the deformation, e.g. an external force, is removed, the material according to Hooke's law, will return to its original shape. For a fluid, however, it is known that after the cause of deformation is removed, the fluid will generally not return to the shape it initially had.

First we will look at the general equations

Yield criterions

Theory of *plasticity* of solids offers useful models to address the yielding of materials with almost-fluid, plastic characteristics. In the most general sense, all yield criteria can be seen as a function f of the six possible stress components (Kachanov, 1971; Blaauwendraad, 2004; Hosford, 2013):

$$f(\sigma_{xx}, \sigma_{yy}, \sigma_{zz}, \tau_{yz}, \tau_{zx}, \tau_{xy}) = C \quad (\text{H.12})$$

or, expressed in the three principle stresses, resulting in elimination of the shear terms:

$$f(\sigma_1, \sigma_2, \sigma_3) = C, \quad (\text{H.13})$$

where C is a material constant that defines yielding. This yield function f , is often depicted graphically as a yield contour in 2D or 3D (see for example Figure H.3): for all stress combinations that fall within the volume demarcated by this yield contour, where $f(\sigma_1, \sigma_2, \sigma_3) < C$, the material is unyielded, giving an elastic response. The contour itself, $f(\sigma_1, \sigma_2, \sigma_3) = C$, forms the collection of possible stress combinations that exactly lead to yield. Stress combinations outside the yield contour, $f(\sigma_1, \sigma_2, \sigma_3) > C$, can not exist, as the material does not physically allow that stress combination.

Literature on plasticity usually splits all stress and strain components in an *isotropic* part, that can be seen as the average 'hydrostatic' stress or strain in the material, and *deviatoric* parts, that is the remaining part of the stress or strain. Most literature states that shape change of a material is mainly the result of deviatoric strains, and that yielding therefore can be described as a function of the deviatoric stresses. In Figure H.3 this can be visualized as that part of the stress that deviates from the isotropic diagonal $\sigma_1 = \sigma_2 = \sigma_3$.

The deviatoric stress can consist of both normal stresses and shear stresses. Yield criteria found in literature use various combinations of normal and shear stresses as yield criterion:

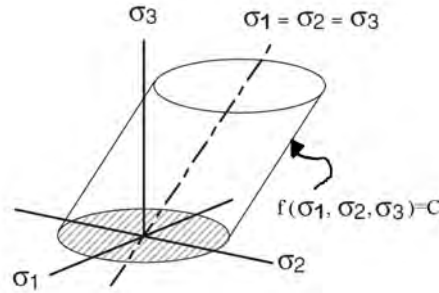


Figure H.3: Example of a yield contour in 3D, called a 'yield locus' (after Hosford, 2013)

Tresca proposed a simple yield criterion, stating that yielding occurs when the largest *shear stress* reaches a critical value. The largest shear stress can be related to the principle stresses (ordered $\sigma_1 > \sigma_2 > \sigma_3$) using Mohr's circle: $\tau_{max} = (\sigma_1 - \sigma_3)/2$. Tresca expressed his yield criterion as $(\sigma_1 - \sigma_3)/2 \leq k$ in which k is the shear yield strength (see Figure H.4). For an uniaxial tensile test resulting in a yield stress σ_{yield} , the relation between shear and tensile strength can be seen: $\sigma_1 = \sigma_2 = 0$ and $\sigma_3 = 2k = \sigma_{yield}$ leads to $\tau_{max} = \frac{1}{2}\sigma_{yield}$. This will later on prove a useful insight to compare the results of shear tests and tensile tests on fresh concrete. Note that the intermediate principle stress σ_2 does not play a role in Tresca's yield criterion.

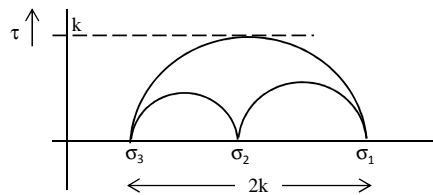


Figure H.4: Tresca's yield criterion shown with Mohr's circle (Blaauwendraad, 1984)

Bingham basically gives a similar one-parameter yield criterion based on *shear*: yield occurs if $\tau \geq \tau_0$. This criterion is usable for fluids and solids both. As stated earlier, the Bingham equation also says that the surplus of shear stress above the yield criterion is linearly coupled to the speed of deformation, the shear rate. The yield contour itself, though, is the same as for Tresca's criterion described above: $(\sigma_1 - \sigma_3)/2 \leq \tau_0$.

Von Mises stated that yielding also depends on the intermediate principle stress σ_2 . The criterion is formulated using the root-mean-square diameter of the three

Mohr's circles depicting the three principle stresses in the yield point: $\frac{1}{3}[(\sigma_2 - \sigma_3)^2 + (\sigma_3 - \sigma_1)^2 + (\sigma_1 - \sigma_2)^2] = C^2$. For an uniaxial tensile test resulting in a yield stress σ_{yield} , again the relation between shear and tensile strength can be seen: $\sigma_1 = \sigma_2 = 0$ and $\frac{1}{3}(\sigma_3^2 + \sigma_3^2) = \sigma_{yield}^2$ leads to $\tau_{max} = \frac{1}{\sqrt{3}}\sigma_{yield} \approx 0.58 \cdot \sigma_{yield}$, which is slightly higher than Tresca's yield shear stress.

Mohr-Coulomb is a yield criterion that was originally developed for soils, and is sometimes also used for concrete-like materials. Unlike the criterion discussed so far, it uses two material parameters instead of one: it states that the shear strength is consisting of a constant, called the cohesion c , and a variational part that is dependent on the normal stress σ and the angle of internal friction ϕ of the soil; the soil yields when $\tau \geq c + \sigma \cdot \tan \phi$. The cohesion c apparently is also a *shear* strength, which is important to remember, as the word is easily seen as an internal capacity of a material to take tensile stresses. It can be seen as an extended Tresca-criterion, extended with the term that makes the allowable shear grows with growing hydrostatic pressure.

It is concluded that the Bingham and Tresca yield criterions actually are identical, which is a useful finding for the present research.